Close Pairs of Galaxies and Merger Rate Evolution at Redshift Less Than 0.5

by

David Robert Patton
B.Math., University of Waterloo, 1992

A Dissertation Submitted in Partial Fulfillment of the
Requirements for the Degree of

DOCTOR OF PHILOSOPHY

in the Department of Physics and Astronomy

Supervisor: Dr. C. J. Pritchet

Abstract

New techniques are developed for relating the statistics of close galaxy pairs to the galaxy merger and accretion rates. Unlike the traditional pair fraction approach, these methods are shown to be robust to a number of selection effects related to the depth and completeness of the sample. These techniques are applied to the large, well-defined SSRS2 ($z \sim 0$) and CNOC2 ($0.1 \leq z \leq 0.55$) redshift surveys, yielding the first secure measurements of close pair statistics at low and moderate redshift. These results imply that the galaxy merger and accretion rates increase with redshift, approximately as $(1+z)^{2\pm1.5}$, for galaxies brighter than $M_B = -18$.

The CNOC2 survey is used to carry out a detailed comparison between close companions and field galaxies. Paired galaxies are found to be of slightly earlier spectral type, with a larger spread in properties. In particular, the spectral indices of close companions imply a more complex star formation history, as would be expected if galaxy interactions and mergers are prevalent.

Contents

List of Tables

List of Figures

Acknowledgements

There are many people and several organizations that I wish to thank for the role they played in this dissertation. This research has made use of data obtained from the Canada-France-Hawaii Telescope (CFHT), which is operated by the National Research Council of Canada, the Centre National de la Recherche Scientifique of France and the University of Hawaii. The Digitized Sky Survey images used in this research were obtained from the Canadian Astronomical Data Centre (CADC), which is operated by the National Research Council of Canada's Herzberg Institute of Astrophysics. Digitized Sky Survey images are based on photographic data of the National Geographic Society Palomar Observatory Sky Survey (NGS-POSS). The Digitized Sky Surveys were produced at the Space Telescope Science Institute under U.S. Government grant NAG W-2166.

I wish to thank all members of the SSRS2 collaboration for their work in compiling the SSRS2 survey. In particular, I am indebted to Ron Marzke and Luiz da Costa for the role they played in making the SSRS2 data available to me in a timely manner. Chapter 2 of this dissertation was based on the CNOC1 redshift survey, which provided the initial motivation for this dissertation. I am indebted to the many members of this collaboration for making these data available, and for their guidance in its interpretation. Chapters 4 and 5 made use of the CNOC2 Field Galaxy Redshift Survey. I am thankful

to everyone in this collaboration, for their tireless efforts in compiling the survey, for giving me the opportunity to gain valuable experience in observing and data reduction, and for their interest in my part of the project.

This work was supported in part by the Natural Sciences and Engineering Research Council of Canada, through research grants to R. G. Carlberg, H. K. C. Yee, and C. J. Pritchet, and a postgraduate scholarship to the author. Additional funding for the author was provided by a University of Victoria Fellowship, which arrived out of the blue at a most opportune time.

There are several individuals who contributed to my development as an astronomer. Howard Yee gave me the opportunity to gain valuable experience during the course of several CFHT observing runs. Huan Lin taught me about the subtleties of the luminosity function. Greg Wirth continues to be an invaluable colleague, mentor, and friend. Ron Marzke provided much of the scientific motivation for the new techniques that lie at the heart of this thesis. I have been fortunate to work with him, and to benefit from his sound advice and friendship. Ray Carlberg's unending enthusiasm for this project, and his support in furthering my career, were greatly appreciated. Finally, I am very much indebted to Chris Pritchet, my supervisor. Without his backing, financial and otherwise, this dissertation would not have been possible.

There are many friends I would like to acknowledge, for the roles they have played in the past years especially. To the many friends, past and present, with whom I have shared the hallowed halls of the Elliott fourth floor, I thank you. And not to forget Brigitte and Matt, who made my final year in Victoria one of the best. I feel fortunate to have met Gaby Canalizo

at Hale Pohaku, and her friendship has been one of the highlights of the past few years. I have been lucky to have had an exceptional group of friends back in Ontario, who have continued to be a big part of my life, despite the intervening miles. And finally, to Ravi, who has been a true friend over the years, through good times and bad, let me just say that I'm very glad that our paths crossed in Waterloo.

Finally, I would like to express my gratitude to my family. I can't imagine how I could possibly have completed this dissertation while retaining my sanity, without having that solid foundation at home. Dad, what can I say? Your constant encouragement and support, in good times and bad, has been a steadying wind in a sea of change. I feel even more fortunate now that June is a part of our family. Mark, you have been a great brother and friend over the years, and a constant source of strength. To Mary and Steve, I thank you both for standing by me these past years, and I look forward to being a part of your everyday lives. To Andrew and April, I have really valued your advice over the years, in matters related to career, family, and otherwise. The last few years of grad school brought a wonderful nephew and niece into my life. Brendan has put a smile on my face countless times. And Julia's blue eyes and charming smile won me over from the moment I first met her. They both reminded me of what is truly important and precious in life, at a time when I really needed it.

There is one final person I wish to thank - Helen Patton, my Mom. More than anyone else, she is the one I am grateful to. I am continually amazed at what she gave up in life to ensure that we kids were taken care of. She instilled a strong sense of commitment, patience, and perseverance in all four

of her children, both by the way she raised us, and by her example. Words cannot begin to express the pain I felt as I witnessed her battle against cancer. I cherish my last hour with her more than any other. This dissertation is dedicated, with love, to my Mom.

Chapter 1

Introduction

1.1 Galaxy Evolution

One of the most active fields of research in modern day astrophysics is the study of galaxy evolution. Individual galaxies and galaxy populations undergo a number of changes between the onset of galaxy formation and the present epoch. There is considerable debate as to the nature and cause of this evolution. As in other branches of science, there is a "nature versus nurture" question : are galaxy properties and distributions built in at the epoch of formation, or are they largely determined by the environments in which they reside? And, if environment is the dominant factor, which processes or mechanisms are driving this evolution?

There are a number of ways to investigate the different possibilities. The most obvious is to have a detailed look at the galaxy we live in, and try to piece together its life history. The relative proximity of sources within our Galaxy allows for in-depth investigations of stars, clusters and nebulae, at a level of detail which is not feasible for even our closest extra-galactic neigh-

bours. This approach is extremely useful for understanding many of the basic astronomical phenomena occurring in galaxies. However, it is difficult to use the results to form a working understanding of galaxies in general. While the Milky Way is a fairly ordinary spiral galaxy, observations of other galaxies have revealed an exceptionally diverse sample, ranging from massive giant elliptical galaxies to tiny star-forming dwarfs. A more global understanding of the formation and evolution of galaxies must incorporate this information, building a working model that can explain the wide-ranging properties of these galaxies. To this end, it is necessary to move outwards from our own Galaxy, carrying out studies of a representative sample of nearby galaxies. By studying how galaxy properties correlate with environment, one may gain valuable insight into the manner in which galaxies are transformed by their surroundings.

Investigations of the Milky Way and nearby galaxies, like endeavours in other areas of science, allow us to improve our understanding of the current state of affairs, and perhaps to use this knowledge to extrapolate back in time. This approach has proved to be very successful in astronomy, as in other fields. However, in this particular branch of science, we have the unique ability to look back in time, seeing the universe as it was at earlier epochs. This is made possible by the vast distances that separate us from distant galaxies, resulting in non-negligible light travel time. Advances in technology are now allowing us to study galaxies at lookback times comparable to the age of the Universe itself.

In this dissertation, we will focus on one particular class of galaxies: namely, those that are undergoing interactions with other galaxies. Some

of these galaxies are doomed to merge in a relatively short interval of time ($\lesssim$ 0.5 Gyr), resulting in a transformation of both member galaxies. We will carry out a detailed study of nearby interacting galaxies, using the Second Southern Sky Redshift Survey (hereafter SSRS2) to uncover clues as to the nature and importance of this class of galaxies at the present epoch. We will then compare our findings with distant galaxies catalogued in the Canadian Network of Observational Cosmology (hereafter CNOC) redshift surveys. Galaxies in these samples lie at a mean redshift of 0.33, corresponding to a lookback time of 3.2 Gyr in an Einstein-deSitter universe with H_0=70 km s^{-1}Mpc^{-1}. This is equivalent to seeing the universe when it was two thirds of its present age. In an attempt to understand how galaxy populations evolve, we will investigate how these galaxy aggregates differ from those at the present epoch.

Before embarking on these detailed studies, we provide a brief description of the physical processes involved in galaxy mergers and interactions (§ 1.2). We then summarize earlier studies of close pairs of galaxies (§ 1.3) and pair statistics (§ 1.4). The introduction closes with an overview of this dissertation.

1.2 Galaxy-Galaxy Mergers and Interactions

It seems clear that galaxy mergers or interactions may play a key role in the evolution of individual galaxies and galaxy populations at moderate redshift. In order to investigate this further, one should first understand something about the physics involved in these encounters. Also, we should look at how

this mechanism is expected to depend on environment. Finally, we should understand how this process will affect the observed properties of galaxies. Armed with this knowledge, we can predict the most favourable sites for mergers and interactions, and be aware of telltale signs of their presence.

1.2.1 How Merging Works

When two galaxies have a close encounter in space, a number of processes may be set into action. The gas in each system will likely be greatly affected, causing shock waves and compression of the gas. In the densest parts of these gas clouds, these compressions may cool rapidly and collapse, forming a new generation of stars. The pre-existing stars, however, will not be as greatly affected. Distances between stars are large with respect to the size of the stars themselves; hence, in a high speed collision of two galaxies, the stellar systems of each galaxy will pass right through each other, sustaining very little damage (Barnes et al. 1991).

Gravity is the dominant force driving galaxy-galaxy interactions. Since every star feels the gravitational pull of all the stars in its galaxy, along with all the stars in the nearby galaxy, this process is complex. As a result, N-body simulations are the most common method of investigating the dynamics of galaxy encounters. These simulations show that the *slowest* encounters are often the most disruptive. This is hardly surprising, since gravity has more time to work during slow encounters. When two galaxies are in close proximity, tidal forces become important, often creating tidal tails and bridges. During such an encounter, the total energy of the system is conserved. However, the orbital energy of the two galaxies is gradually con-

verted into internal motions within the galaxies themselves. This transfer of energy from galaxy motions to stellar motions is referred to as dynamical friction (Chandrasekhar 1943; Binney and Tremaine 1987). In some cases, depending on the relative velocities, orientation, and masses involved, this process may lead eventually to a merger of the two galaxies, leaving behind a single merger remnant. When a merger occurs between two galaxies of comparable mass (a major merger), the end product will usually look like an elliptical galaxy (e.g., Barnes 1988). Minor mergers will generally leave the larger galaxy intact. In many close encounters, a merger may not occur; however, the encounter may still have a noticeable effect on the galaxies involved. We will refer to these events as interactions, rather than mergers.

1.2.2 Where to Look for Mergers and Interactions

Environment

In our local neighbourhood, most galaxies do not appear to be undergoing major mergers. As a result, randomly-selected galaxies at low redshift provide a limited amount of information on such systems. In order to investigate this phenomenon, one must look in those environments most favourable to encounters. Naturally, the first requirement is for a high density of galaxies. This will optimize the rate of potential interactions. The most dense environments are found in the cores of rich clusters, compact groups, or close pairs of galaxies. The second requirement for interactions is low relative velocities. In this case, rich clusters are the worst place to look, since they have velocity dispersions on the order of 1000 km/s (e.g., Carlberg et al.

1996), while compact groups (e.g., Hickson et al. 1992) and close pairs (e.g., Charlton & Salpeter 1991) typically have velocity dispersions of < 400 km/s. Hence, the only nearby locations well-suited for studying the effects of galaxy interactions are close pairs and compact groups of galaxies.

Epoch

The local universe is arguably the *worst* place to look for signs of merger-related activity. There are a number of reasons to expect that the merger rate was significantly higher in the past. First, since the universe is expanding, the space density of galaxies was higher in the past. Theoretical models (e.g., Toomre 1977, Carlberg 1990) predict that mergers would have been much more frequent, even at fairly modest redshifts. Also, the effects of mergers and interactions on star-formation rates are expected to be greater, since galaxies were generally more gas-rich than they are at the present epoch. Observationally, these expectations appear to be validated by high resolution imaging of distant field galaxies. In addition, a number of studies of close pairs of galaxies at moderate redshift (e.g., Zepf and Koo 1989; Carlberg, Pritchet, and Infante 1994; Yee and Ellingson 1995) have attempted to measure the change in the merger rate with redshift; such studies consistently find a significant increase with redshift. Indirect evidence for an increase in interactions with redshift can also be inferred from studies of *IRAS* galaxies (Lonsdale et al. 1990), radio galaxies (e.g., Windhorst et al. 1995), and quasars (e.g., Bahcall et al. 1996). Hence, in some ways we are better off looking at distant samples of galaxies if we wish to determine the importance of merging in galaxy evolution. Within these distant samples, there are of

course a variety of environments which could be targeted. Here again, it would be wise to focus on those regimes in which mergers and interactions would be expected to be most prevalent. Once again, close pairs and compact groups will be the ideal place to look. In addition, as interactions are expected to be more common than at low redshift, loose groups (with velocity dispersions closer to that of compact groups than rich clusters) should also provide an environment conducive to galaxy encounters.

1.2.3 How to Detect Mergers and Interactions

There are a number of methods of detecting galaxy interactions or mergers. During interactions or the early stages of mergers, tidal features will often be present, especially in gas-rich systems. These are expected to be fairly short-lived, but may be detected with high quality imaging. At this stage, a strong burst of star formation may be triggered. This may be detected photometrically as a brightening and/or blueing of stellar light, due to the presence of young stars. Spectroscopically, a strong starburst may be detected by the presence of strong emission lines. While none of these effects alone provide unambiguous evidence for an ongoing merger or interaction, the combination of morphological, photometric, and spectral indicators can make a compelling case for such an event.

During a merger event, two galaxies will coalesce into a single entity. This stage may be accompanied by a massive starburst and/or AGN activity. As a result, a number of exotic phenomena may be observed. Heckman (1983) found that strongly interacting galaxies from the Arp Atlas (Arp 1966) were about eight times more likely to be radio loud than comparable isolated

galaxies. Detailed studies indicate that strong interactions and mergers of gas-rich spiral galaxies are the trigger for producing the most luminous infrared galaxies. The most extreme examples of these systems, known as ultra-luminous infrared galaxies (ULIRGs), seem to be associated with the actual merger of the two nuclei (Sanders and Mirabel 1996). While there is considerable debate regarding the relative importance of AGNs and starbursts in these systems (the "monsters versus babies" debate), it is clear that these systems are intimately connected with galaxy-galaxy mergers.

Shortly after a merger has taken place, the remnant will look distorted, with faint surface brightness tidal debris. At moderate redshift, these signs are very difficult to detect with ground based imaging; however, Mihos (1995) demonstrated that HST's WFPC2 is capable of detecting merger remnants up to 1 Gyr after the merger event, for galaxies at z=0.4. On a similar timescale, spectral indices can be used to identify E+A galaxies (Dressler and Gunn 1983). The combination of strong Balmer absorption and weak [OII] emission in these galaxies indicates that they have may have undergone a significant burst of star formation within the last Gyr. There is evidence for a strong connection between E+A galaxies and galaxy mergers or interactions (Liu and Kennicutt 1995; Zabludoff et al. 1996). Finally, it should be noted that merger-induced starbursts are often centrally concentrated, in both major (Mihos and Hernquist 1994) and minor mergers (Mihos and Hernquist 1996). This may be detected in merger remnants if the colours are bluest in the centre, which is opposite to the trend seen in normal elliptical galaxies (e.g., Peletier et al. 1990). Once again, several clues may be combined to unmask a merger remnant.

Throughout the remainder of this study, we will focus exclusively on close pairs of galaxies. However, it should be noted that the importance of mergers and interactions in clusters, loose groups, compact groups, and the remainder of the field population remains an open question.

1.3 Close Pairs of Galaxies

The study of close galaxy pairs began with Holmberg (1937), and has played a fundamental role in the study of galaxy interactions. A variety of catalogs (e.g., Karachentsev 1972, Charlton & Salpeter 1991) have been produced. While the definition of a "close pair" varies considerably from study to study, a reasonable definition would be that galaxy separations are comparable to the diameters of the galaxies themselves. Many galaxies in close pairs are found to be morphologically distorted by their nearby neighbours (e.g., Arp & Madore 1987). The resemblance of observed features such as tidal tails and bridges (e.g., Schweizer 1982) with those seen in N-body simulations (e.g., Barnes 1988) provides compelling evidence that gravitational interaction is the underlying driver of these processes. A number of groups have detected evidence of enhanced star formation activity in these galaxies, in both visible light (e.g., Kennicutt et al. 1987) and the far-infrared (e.g., Xu & Sulentic 1991). Spectroscopic studies also indicate a link between mergers and starbursts. For example, Liu & Kennicutt (1995) present clear evidence for both ongoing (via strong emission lines) and recent (with strong Balmer absorption) bursts in merging or strongly interacting systems.

While considerable progress has been made, many important questions

remain. The primary difficulty has been in relating these results to the global galaxy population. It is unclear how common these systems are, not only in the high redshift universe, but also at the present epoch. Moreover, the timescale of these processes is uncertain at present. Knowledge of this timescale is imperative if one wishes to determine the relative importance of these effects. For example, if mergers are very long-lived, then the relatively low frequency of present day mergers would imply that these processes do not drive galaxy evolution. If, on the other hand, mergers occur on a very short timescale, we would only expect to observe a small percentage of them at a given time. Thus, a small number of observed mergers would imply a much larger population of recent or imminent mergers.

1.4 Close Pair Statistics

Close pairs of galaxies provide an ideal laboratory for investigating galaxy-galaxy interactions and mergers. Of considerable interest is the manner in which galaxies cluster on these small scales. The galaxy-galaxy correlation function (hereafter CF) is the most widely used tool for probing galaxy clustering. The CF measures the excess clustering (above random) on different scales. It is generally used to investigate clustering on large scales, ranging from $\sim$ 100 h^{-1} kpc to $\sim$ 10 h^{-1} Mpc (here, the Hubble constant is given by H_0=100h km s^{-1}Mpc^{-1}). For the modest-sized galaxy samples currently available ($N \lesssim 10^4$), the correlation function ceases to be useful on smaller scales, since the number of pairs in a given separation bin becomes statistically insignificant. Hence, one must resort to an integrated measurement,

which combines all of the pairs on small scales. The close pair fraction, defined as the number of galaxies in pairs divided by the total number in the sample, provides one such measure. This statistic, and others that are very similar in nature, have been used as the primary indicators of small scale clustering.

The close pair fraction has been thought of as an elegant relative measure, because paired and field galaxies are subjected to many of the same selection effects. By computing the fraction of galaxies that lie in close pairs, the assumption is that many of these selection effects will cancel out, leaving a robust integrated measure of galaxy clustering. With this assumption, several authors have computed pair fractions for samples at low ($z \sim 0$) and moderate ($z \sim 0.3$) redshift, and used observed changes in the pair fraction to infer evolution in the galaxy merger rate.

Unfortunately, there is a serious conceptual problem with this approach. The primary difficulty lies in the assumption that the pair fraction depends exclusively on clustering. While this is true for the correlation function, the pair fraction has an additional dependence on the mean density of galaxies in the sample. Therefore, changes in the pair fraction may be due to any combination of changes in clustering and mean density. This dependence on mean density means that the pair fraction depends on the depth in luminosity to which a sample is probed. Moreover, observational selection effects that are related to the *apparent* density of galaxies, including flux limits and spectroscopic completeness, will distort the resulting measure of the pair fraction. This dependence on luminosity depth and selection effects has gone unrecognized or ignored in all published estimates of the pair fraction and

its evolution.

1.5 Dissertation Overview

This dissertation begins with the analysis of close pairs of galaxies in the CNOC1 redshift survey. This study [1] was completed in 1996, and published in 1997 (Patton et al. 1997). Following earlier attempts, the pair fraction was computed at $z \sim 0.3$, and compared with local estimates to infer evolution in the galaxy merger rate. In this study, new steps were taken to address issues of spectroscopic incompleteness. After accounting for inconsistencies in the correction for optical contamination and spectroscopic completeness in earlier studies, we found general consistency in the merger rate estimates gleaned from studies of close pairs. Since the publication of this paper, however, we have uncovered the conceptual problem with the pair fraction described above. In particular, we realize now that simple measurements of the pair fraction for flux-limited surveys are subjected to selection effects that have not been accounted for. Furthermore, without a robust determination of the limiting luminosity of different samples, additional uncertainties will be present when comparing pair fractions at different redshifts. Therefore, resulting estimates of merger rate evolution may be significantly biased, and the uncertainties underestimated. Nevertheless, this chapter represents an

[1] Chapter 2 is based exclusively on this paper by Patton et al. (1997). The co-authors of this paper are C. J. Pritchet, H. K. C. Yee, E. Ellingson, and R. G. Carlberg. These co-authors played a significant role in the acquisition and reduction of data as part of the CNOC1 collaboration. In addition, they contributed to some of the ideas that were incorporated into the analysis. Finally, C. J. Pritchet and H. K. C. Yee contributed to the classification of galaxy pairs (§ 2.9). The remainder of the analysis and all of the writing of this chapter was carried out by the author of this dissertation.

important first step, and sets the stage for the new techniques that form the core of this dissertation.

In Chapter 3, we begin from first principles, and devise two new pair statistics [2]. These statistics, denoted N_C and L_C, are related to the galaxy merger and accretion rates respectively. Both are pairwise statistics, and have a clearly stated dependence on mean density and clustering, as specified by the galaxy luminosity function (LF) and correlation function (CF) respectively. These statistics are tested using Monte Carlo simulations. Weighting schemes are introduced which allow these quantities to be computed for flux-limited samples, permitting the recovery of the intrinsic pair statistics built into the volume-limited simulations. These statistics are then applied to a large redshift survey at $z \sim 0$ (SSRS2), yielding the first secure measures of pair statistics at low redshift.

We extend this pair analysis to higher redshifts in Chapter 4, using the CNOC2 Field Galaxy Redshift Survey [3]. This sample spans the redshift range $0.1 \leq z \leq 0.55$, allowing us to measure pair statistics at a significant

[2]Chapter 3 is based on a paper that will be submitted to the Astrophysical Journal in June, 1999. The co-authors of this paper are R. G. Carlberg, R. O. Marzke, C. J. Pritchet, L. N. da Costa, and P. S. Pellegrini. Some of the ideas and techniques introduced in this chapter benefitted from discussions with the first three co-authors. In addition, R. G. Carlberg and R. O. Marzke participated in the pair classification experiment outlined in § 3.7. The remainder of the analysis and all of the writing of this chapter was carried out by the author of this dissertation.

[3]Chapter 4 is based on a paper that will be submitted to the Astrophysical Journal in the fall of 1999. The co-authors of this paper are C. J. Pritchet, R. G. Carlberg, R. O. Marzke, H. K. C. Yee, E. Ellingson, P. B. Hall, H. Lin, S. L. Morris, M. Sawicki, D. Schade, C. W. Shepherd, and G. D. Wirth. All authors participated in the acquisition and reduction of data as part of the CNOC2 collaboration. Some of the ideas and techniques introduced in this chapter benefitted from discussions with the first three co-authors. The remainder of the analysis and all of the writing of this chapter was carried out by the author of this dissertation.

lookback time. Before computing pair statistics, we take several precautions to ensure that our measurements will not be adversely affected by the differential effects of $k-$corrections and luminosity-dependent clustering. We then carefully correct for selection effects resulting from the flux limit, luminosity evolution, spectroscopic incompleteness, and boundary effects. After computing pair statistics at moderate redshift, we perform a direct comparison with the SSRS2 statistics from Chapter 3, using the relative abundance of close companions at different redshifts to generate measures of evolution in the galaxy merger and accretion rates. These results are then used to shed light on the relative importance of mergers to typical present-day galaxies.

In Chapter 5, we undertake a detailed comparison between galaxies in close pairs and the field, again using the CNOC2 sample [4]. After carefully identifying a control sample of field galaxies that is subjected to the same selection effects as galaxies in pairs, we carry out an extensive comparison of these two samples, focussing on the intrinsic properties of redshift, absolute magnitude, colours, and line indices. We then extend the analysis to search for trends in these properties with pair separation.

In the final chapter, we summarize the main results of this dissertation, highlighting the most important contributions we have made to the study of galaxy-galaxy interactions and mergers. We close with several suggestions as to how these results can be applied and extended in the future.

---

[4]Chapter 5 makes use of the CNOC2 Field Galaxy Redshift Survey. As a result, any publication that results from this chapter will have the following co-authors : C. J. Pritchet, R. G. Carlberg, R. O. Marzke, H. K. C. Yee, E. Ellingson, P. B. Hall, H. Lin, S. L. Morris, M. Sawicki, D. Schade, C. W. Shepherd, and G. D. Wirth. All authors participated in the acquisition and reduction of data as part of the CNOC2 collaboration. The analysis and writing of this chapter was carried out by the author of this dissertation.

Chapter 2

Close Pairs of Field Galaxies in the CNOC1 Redshift Survey

2.1 Introduction

Accumulating evidence indicates that galaxy populations have undergone significant evolution in the recent past. This initially became apparent with the excess number counts of faint blue galaxies (Tyson 1988). However, various redshift surveys (Broadhurst et al. 1988; Colless et al. 1990; Colless et al. 1993) showed the redshift distribution of faint galaxies to be indistinguishable from no-evolution model predictions. The picture that is emerging from recent observations is one in which the number density of L_* galaxies (i.e., relatively bright galaxies with characteristic luminosity L_*) was higher at moderate redshift (Lilly et al. 1995; Lin et al. 1997). This can be explained by the presence of star-bursting dwarf galaxies, which have since faded. At present, it is unclear what is driving this process. One possible explanation is galaxy-galaxy merging (Rocca-Volmerange and Guiderdoni 1990; Broadhurst et al. 1992; Carlberg and Charlot 1992). Merging is expected to make galax-

ies brighter and somewhat bluer, due to enhanced star formation (Larson and Tinsley 1978), and implies that galaxies were less massive in the past. However, the importance of merging in the observed evolution of galaxies remains an open question.

Galaxy merging affects a small fraction of galaxies at the present epoch. If the rate of merging remains constant, galaxy masses at z=1 will be reduced to about two thirds of their values at the present epoch for Ω=1 (Carlberg 1995). However, there are a number of reasons to believe that the merger rate was significantly higher in the past. First, since the universe is expanding, galaxies were closer together in the past, so naturally merging would have been more prevalent. Also, recent *Hubble Space Telescope* (*HST*) imaging of galaxies at moderate redshift (e.g., Griffiths et al., 1994; Driver et al., 1995; Glazebrook et al., 1995) reveals a relatively high proportion of galaxies which are morphologically anomalous, often exhibiting signs of interactions. Finally, a number of studies of close pairs of galaxies (e.g., Zepf and Koo, 1989; Carlberg, Pritchet, and Infante, 1995 [hereafter CPI]; Yee and Ellingson, 1995 [hereafter YE]) have attempted to measure the change in the merger rate with redshift; such studies consistently find a significant increase with redshift.

The CNOC (Canadian Network of Observational Cosmology) cluster redshift survey (hereafter CNOC1) was undertaken primarily to study galaxy clusters (Yee et al. 1996; Carlberg et al. 1996). However, a wealth of information on field galaxies was a natural by-product of the survey. This study uses the CNOC1 catalogs to investigate the properties of close pairs of field galaxies, and to place tighter constraints on the evolution of the merger

rate. The availability of large numbers of redshifts represents an important improvement over previous studies of close pairs.

In § 2.2, the CNOC1 observations will be briefly summarized. Section 2.3 describes the selection procedure used to identify an unbiased sample of field galaxies. The observed and physical pair fractions are determined in Sections 2.4 and 2.5 respectively, and the properties of galaxies which are paired and isolated are compared in § 2.6. The redshift dependence of the galaxy merger rate is calculated in § 2.7. The sample is divided up into redshift bins in § 2.8 to investigate possible trends with redshift. We focus on the subset of confirmed physical pairs in § 2.9. Finally, the results and ensuing implications are discussed in § 2.10. When necessary, we assume H_0=100 km/s/Mpc (h=1) and q_0=0.5 throughout.

2.2 Observations

Observations for the CNOC1 redshift survey were carried out using a multi-object spectrograph (MOS/SIS) at the Cassegrain focus of CFHT. The data catalogs consist of photometry (in Gunn g and r) in the regions of 16 rich clusters of galaxies, lying at redshifts of 0.18 – 0.55. Survey fields of up to 6 h^{-1} Mpc per cluster were covered, with the outer regions being dominated by the field population. Redshifts have been obtained for roughly half of the brighter galaxies, of which $\sim$ 50% are confirmed field galaxies; in the outer regions of the clusters, this fraction rises to $\sim$ 80%. For a complete description of the CNOC1 observational strategy and data reduction techniques, see Yee, Ellingson, and Carlberg (1996; hereafter YEC).

2.2.1 Photometric Data

The basic sample consists of a catalog of photometry in Gunn g and r, and is complete to a magnitude of r=23.0 (and fainter for most frames). For the purposes of this study, a uniform photometric limiting magnitude of r=23.0 is applied. The entire photometric survey is 100% complete to this limit, and most frames are complete to $r \sim 23.5$. Star-galaxy classification has been performed, and is considered to be *very* reliable as faint as $r \sim 22.5$. Misclassification (mostly of galaxies as stars) is $\lesssim 10\%$ at $r \sim 23.5$ for most images, which is fainter than the limiting magnitude used throughout this analysis. This gives us a catalog with 14831 galaxies covering ~ 0.66 deg^2.

2.2.2 Spectroscopic Data

The CNOC1 catalog contains redshifts for $\sim$ 2600 faint galaxies, of which roughly half are field galaxies. Redshifts and rough spectral classification were performed using the cross-correlation techniques described by Ellingson & Yee (1994). The spectroscopic completeness (defined as the fraction of objects with redshifts) varies from region to region, depending on the projected number density of cluster members and the number of MOS masks taken for a given field (ranging from 1−3). The cumulative spectroscopic completeness ranges from $\sim 50\%$ at r=21.5 to $\sim 17\%$ at r=23.0 (here cumulative refers to all galaxies brighter than the given apparent magnitude). Each redshift in the catalog has been assigned a "significance parameter" R, which is a measure of the strength of the redshift cross-correlation. We must consider two types of uncertainty in redshift measurements; identification error and ve-

locity error. The former arises when the wrong peak in the cross-correlation is selected, and can result in catastrophic redshift errors. Three quarters of the redshifts have either emission-line spectra with R > 5 or absorption-line spectra with R > 4; such redshifts are considered to be *very* secure ($\gtrsim$ 99% confidence, see YEC). The confidence level for the remaining objects drops to $\sim$ 95%. As an extra precaution against identification errors, all redshifts with R < 3 ($\sim$ 2% of the sample) are excluded from the analysis. This leaves us with redshifts for 2530 galaxies. Once a redshift has been identified, the uncertainty in velocity can be estimated in several ways. The most rigorous method is to use redundant observations; this yields a typical estimated uncertainty of $\sim$ 130 km/s. Redshift errors are discussed further in YEC.

2.3 Sample Identification

2.3.1 The Primary Redshift Sample

In order to study close pairs, we desire a sample of field galaxies (with measured redshifts) which is unbiased with respect to galaxy type and does not favour the identification of paired galaxies over isolated galaxies. The following sections describe the restrictions imposed to identify such a sample.

Excluding Cluster Members

Since we are interested in the close pair properties of *field* galaxies, we must first remove all cluster galaxies from the primary redshift sample. Eliminating known cluster members is a fairly straightforward procedure. For each cluster, a weighted mean redshift has been identified, along with correspond-

ing upper and lower redshift limits. These limits were derived by Carlberg et al. (1996), using a manually iterated procedure which depends on each cluster's measured velocity dispersion. A similar (but slightly less strict) constraint is to exclude all galaxies with velocities within 3000 km/s of each cluster's median velocity (the main results of this study are unchanged by imposing this criterion instead). After this restriction, we are left with a sample of 1257 field galaxies.

Excluding Field Galaxies with Potential Redshift Biases

In the original survey, band-limiting filters were used to reduce overlap of spectra, and hence to maximize the number of cluster redshifts obtained (see YEC). As a result, the limited spectral range associated with each filter imposes a restriction on the range of redshifts for which field galaxies can be consistently identified. Specifically, the lower limit is set by the ability to detect the [OII]3727Å line within 50Å of the blue edge of the spectra, while the upper limit reflects the redshift at which the 4000Å break is within 150Å of the red edge. The appropriate field redshift ranges can be found in Table 2 of YEC. All field galaxy redshifts within the appropriate redshift range are expected to be unbiased with respect to the redshift acquisition procedure, and hence are included in the primary sample. This leaves 797 field galaxies.

Excluding the Faintest Field Galaxies

The CNOC1 mask design algorithm selects proportionately fewer faint galaxies, in order to maximize the number of cluster galaxies obtained. In addi-

tion, fainter galaxies have spectra with lower signal-to-noise ratios, making it more difficult to extract reliable redshifts. To compensate for this, a magnitude selection function was measured, which estimates the spectroscopic completeness (the fraction of galaxies with measured redshifts) as a function of magnitude (see YEC). All galaxies with measured redshifts were assigned a weight, which is the inverse of the selection function for that magnitude, and for that particular region. To ensure that the primary field galaxy sample is unbiased, we wish to identify the range in apparent magnitude within which the spectroscopic completeness is at least 25%. Using the weights of all galaxies with measured redshifts, we determined this magnitude range for each field. As illustrated in Figure 2.1, this amounts to identifying a faint limiting magnitude only, since the completeness is greater than 25% for the brightest galaxies. All field galaxies which are fainter than this spectroscopic limiting magnitude are excluded from the primary sample.

Avoiding the Clusters

After all such restrictions have been made, we are left with an unbiased primary sample consisting of 572 field galaxies. However, there remains the danger of a given field galaxy being superimposed on the central region of a dense cluster of galaxies. In this case, the probability of a close companion being an optical superposition is greatly increased. To avoid this situation, we wish to exclude from the primary sample all field galaxies lying in regions which contain large numbers of cluster galaxies. This exclusion was carried out by computing the number density of galaxies around each field galaxy, within a somewhat arbitrarily-defined radius of $1'$. This radius was

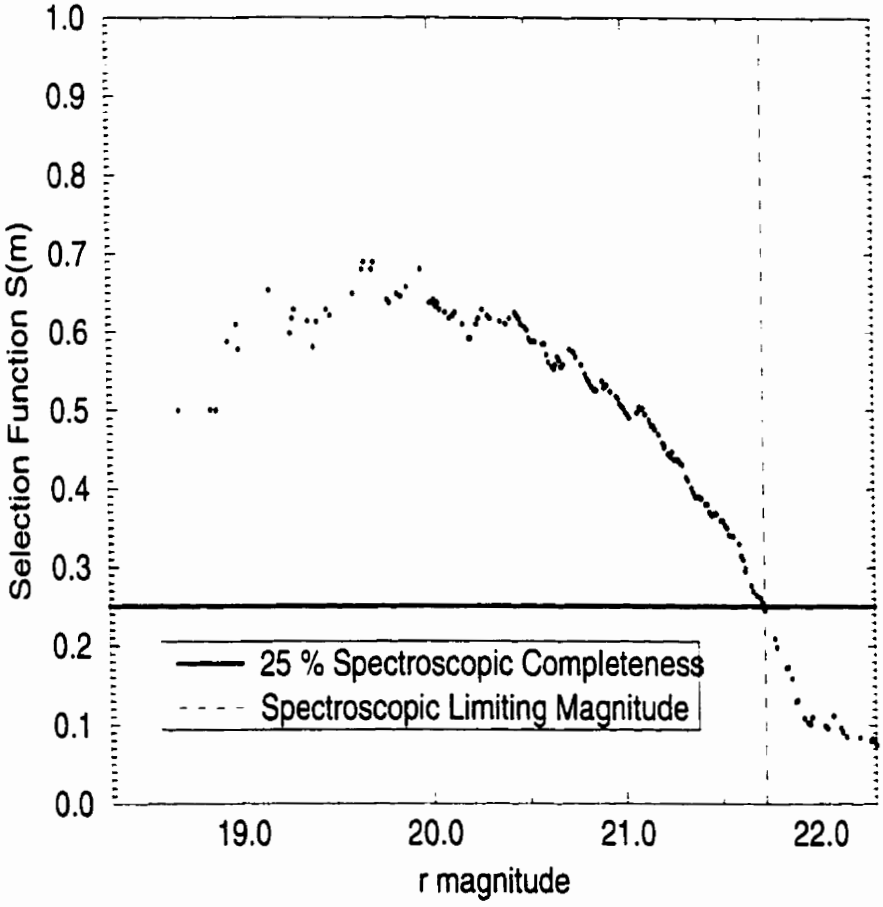

Figure 2.1: The selection function for all galaxies in the region of the cluster MS1621. The lines represent the restrictions imposed to ensure at least 25% spectroscopic completeness for each galaxy in the primary sample.

chosen to be large enough to minimize the influence of close ($< 20\ h^{-1}$ kpc) companions, while remaining small enough to detect local number density effects, such as the presence of the core of a cluster. It is desirable to use a faint limiting magnitude (e.g., r=23.0) to provide good statistics. However, to maximize sensitivity to the presence of cluster members, it is better to use a limiting magnitude which is closer to the typical absolute magnitude of cluster galaxies (M_*). For the CNOC1 clusters, M_* typically corresponds to $r \sim 20$, and the faintest is $r \sim 21.7$ (here, we have assumed $M_*(r)$=$-$20.6 mag for early-type galaxies from local galaxy luminosity functions (e.g., King & Ellis 1985). At fainter magnitudes, the slope of the cluster galaxy luminosity function flattens out relative to that of field galaxies, decreasing the fraction of cluster members. For this calculation only, a limiting magnitude of r=22.0 was selected. This includes an acceptable number of galaxies for computing the local number density, while being as close as possible to M_*.

A histogram of the number density in the region of all field galaxies is shown in Figure 2.2. This plot shows the existence of a high-density tail, which is expected to be those field galaxies lying in the central regions of clusters. A density threshold of 7 galaxies per square arcminute was selected, in order to eliminate most of the high-density tail while keeping the majority of galaxies having more typical local densities. In addition, all galaxies lying within 3′ of a cluster centre were excluded from the primary sample. All plots were checked by eye to ensure that: a) no primary galaxies remain in the central regions of clusters and b) no field galaxies lying far from the central regions are excluded from the primary sample. Using these criteria, 27 galaxies were excluded, leaving 545 galaxies in the primary sample.

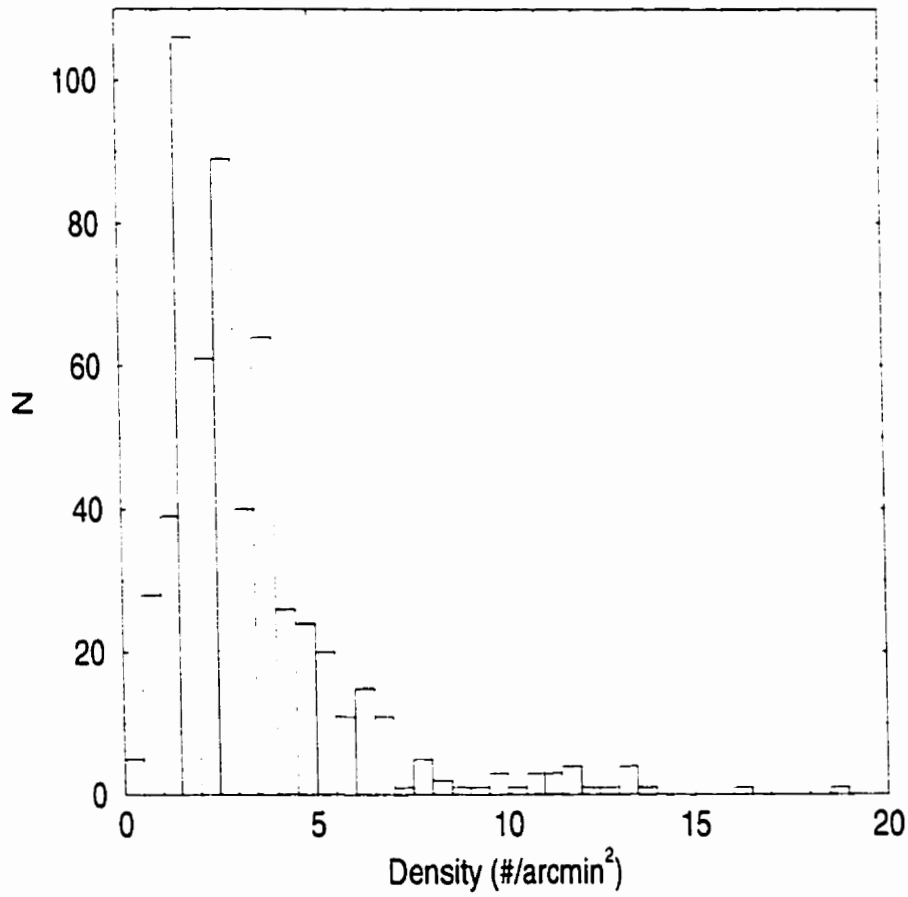

Figure 2.2: Histogram of the local number density of galaxies within a 1′ radius of each unbiased field galaxy, using a limiting magnitude of r=22.0.

2.3.2 The Secondary Sample

The initial task in a study of close pairs is to determine which galaxies have close companions. As with previous studies, we wish to look for companions which are comparable in luminosity to the primary sample, and to determine (where possible) which of these companions are physically associated. Therefore, we wish to identify a secondary sample, consisting of all galaxies (with or without redshifts) which are potential companions. In order to restrict the secondary sample to galaxies of similar luminosities, we need to impose the same restrictions in apparent magnitude as were earlier applied to the primary sample. Hence, we apply the spectroscopic limiting magnitudes derived in § 2.3.1 to all galaxies in the survey (with or without redshifts). The secondary sample is not distinct from the primary sample; rather, the primary sample is a subset of the secondary sample. There are 3739 galaxies in the secondary sample, of which roughly half (1972 galaxies) have redshifts.

2.4 The Observed Pair Fraction

In order to discuss the fraction of galaxies in close pairs, one must define what is meant by "close pair". For the purposes of this study, a close pair is defined as two galaxies with a projected separation of no more than 20 h^{-1} kpc. At this physical separation, dark galaxy halos and even visible disks will interact significantly (Carlberg 1995). N-body simulations indicate that these pairs will merge within $\sim$ 0.5 Gyr (e.g., Barnes 1988), as long as the galaxies have reasonably low relative velocities. For a galaxy with a known redshift, a projected separation D translates into an angular separation θ

using the equation

$$\theta = \frac{DH_0(1+z)^2}{2c\left(1+z-\sqrt{1+z}\right)} \tag{2.1}$$

(we assumed Ω_0=1 for these calculations; at z=0.33, θ would be $\sim$ 6% smaller for Ω_0=0.2). For redshifts of 0.18 $-$ 0.67 in the primary sample, D=20 h^{-1} kpc corresponds to separations (denoted by θ_{20}) of 10.″2 $-$ 5.″1, with a mean separation criterion of $\sim$ 7″.

To calculate the observed fraction of galaxies in close pairs, one simply counts the number of primary field galaxies which have companions within 20 h^{-1} kpc. Companions are selected from the secondary sample, and may or may not have redshifts. For the sample of 545 primary galaxies, 73 were found to have at least one close companion. A slight correction was made to take into account the fact that a small fraction of the search area is not covered by the survey (due to saturated stars, column bleeding, etc.). Using the number of companions observed (81), as compared with the number we would expect to have found if coverage had been complete (81.6), the expected number of galaxies with at least one companion is then 73.6, yielding a close pair fraction of 13.5 $\pm$ 1.6% (errors assume Poisson statistics).

2.4.1 Resolution Effects and the Angular Correlation Function

Seeing for the r images was typically $\sim$ 1″(FWHM). Hence, we are unable to resolve close pairs at or below this angular separation. To investigate empirically what effect this may have on the calculated pair fraction, we have plotted the number density of pairs versus angular separation for the entire

$r \leq 23.0$ sample in Figure 2.3a. Three features that stand out are: (a) at large ($\gtrsim 7''$) separations, the number density of pairs is roughly constant, as would be expected for a random distribution of galaxies; (b) there is a significant excess (over *random*) of close pairs at separations of a few arcseconds; and (c) there is a clear deficit of close pairs at separations $\lesssim 1\farcs5$.

While the excess over random is significant, an excess is expected from studies of the angular correlation function. This function, $\omega(\theta)$, measures the excess number of galaxies (over random) found at a given angular separation θ, and can be accurately represented by a power law of the form $\omega(\theta) = A_\omega \theta^{-\delta}$ (Peebles 1980). To estimate the expected $\omega(\theta)$ for our sample, we transform our magnitude limit to the F band, using the colour transformation of Windhorst et al. (1991) and the average colour ($g-r$=0.82) for our sample. Assuming the canonical value of δ=0.8 (Peebles 1980), the amplitude for our sample is estimated to be $A_\omega(1') = 0.056$, using the observed F band fits of Infante & Pritchet (1995). For comparison, we also use their results for δ=0.6 (the shallowest slope found), which gives $A_\omega(1')$=0.062. We can then compute the expected pair number density, since $\sigma_{exp}(\theta) = [1 + \omega(\theta)]\sigma_{av}$. Here, $\sigma_{exp}(\theta)$ is the expected pair number density at separation θ, while σ_{av} is the average number density of galaxies. Note that σ_{av} was computed using the observed counts at separations of $1'$, and dividing by $1 + \omega(1')$. That is, the observed and predicted pair densities are normalized to agree at θ=$1'$. The predicted relations are plotted in Figure 2.3a, and we can see that the observed excess is roughly consistent with what is expected from the angular correlation function. The expected $\omega(\theta)$ is derived from a pure field sample; what effect do the superimposed CNOC1 cluster galaxies have on this? To

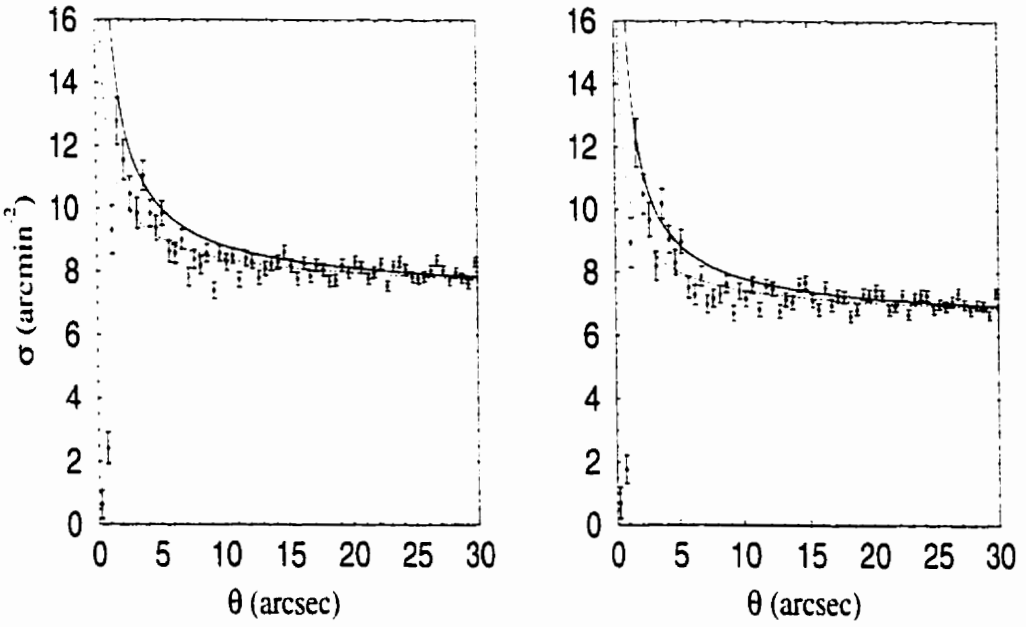

Figure 2.3: Histogram of the pair number density, binned in annular rings of width 0.″5. The lines represents the pair number density predicted using the F band angular correlation function from Infante & Pritchet (1995), with δ=0.8 (*solid line*) and δ=0.6 (*dotted line*). Note the absence of pairs at very small angular separations, due to the limited resolution of the observations. (*a*) All galaxies brighter than r=23.0. (*b*) All galaxies brighter than r=23.0, excluding known cluster members.

address this issue, the analysis was repeated after excluding all known cluster members from the sample. As seen in Figure 2.3b, the agreement is similar, and indicates that the cluster galaxies do not strongly influence the observed relation.

We conclude that the observed number density of pairs is consistent with the extrapolation of the angular correlation function to small scales. We note that, while Woods, Fahlman, & Richer (1995) find no excess over random in their photometric survey of faint pairs, their result appears to be consistent with the excess found in this study. Our Figure 2.3 shows that our results are clearly not consistent with no excess over random. The deficit of close pairs at very small scales is confirmed, however, and is clearly due to resolution effects. To compensate for this effect, a minimum search radius of $1''$ was implemented when computing the observed pair fraction. None of the primary field galaxies have observed companions within this radius; hence, the observed pair fraction remains the same as above. We are unable to correct for unresolved companions; however, by extrapolating $\omega(\theta)$ to the smallest scales, we would expect companions closer than $\sim 1''$ to contribute $\lesssim 5\%$ to the observed pair fraction. This estimate is consistent with the *HST* pairs study by Burkey et al. (1994), who found that only 1 out of their 25 close pairs had a projected separation of $< 1''$. This effect is sufficiently small (compared with the uncertainty in the measured pair fraction) that we have chosen to ignore it.

2.4.2 Sampling Effects

When using an incomplete redshift survey to calculate the close pair fraction, one must sample paired galaxies fairly, or else correct for unfair sampling. Although the CNOC1 survey is designed to compensate for pair-distribution selection effects (see YEC), we will demonstrate a method of determining if pairs are *in fact* sampled fairly. In addition, this method will enable us to estimate the observed pair fraction in a sample which is not fairly sampled.

We begin with an idealized sample in which all redshifts are known. Then, by modelling the redshift selection procedure, one can compute what the observed pair properties of the sample would be. Suppose we start with a sample of N galaxies, of which a fraction x lie in apparent close pairs. We model the redshift selection as a two-step procedure. First, let S be the probability of obtaining a redshift for an isolated galaxy or the first galaxy in a close pair. Then, let R be the probability of obtaining a redshift for the second galaxy in a pair, assuming a redshift has already be obtained for the first. If pair selection is fair, $R{=}S$. Now, let us also assume that, for all galaxies for which redshifts are obtained, a fraction P will be members of the primary sample (i.e. lying in the redshift range of interest). Knowing these properties, we can determine what the actual observed sample will look like. The observable properties we will use are as follows: np_1 is the number of primary galaxies which have companions with measured redshifts, np_0 is the number of primary galaxies which have companions without redshifts, n_0 is the number of primary galaxies which are isolated, and nnz is the number of galaxies without redshifts. By applying the selection procedure, it follows

that

$$np_1 = NxSRP, \tag{2.2}$$

$$np_0 = \frac{1}{2}NxS\,(2 - R - S)\,P, \tag{2.3}$$

$$n_0 = N\,(1 - x)\,SP, \tag{2.4}$$

$$nnz = \frac{1}{2}NxS\,(S - R) + N\,(1 - S). \tag{2.5}$$

We now have four independent equations, with four input parameters (S, R, P, x) and four resultant observed quantities (np_1, np_0, n_0, nnz). For a real sample, we can retrieve the input parameters by solving this system of equations in terms of the observable quantities. The solution is as follows:

$$A = N\,(np_1 + np_0 + n_0),$$

$$B = n_0\,(nnz - 3N) - 2N\,(np_1 + np_0),$$

$$C = (N - nnz)\,(np_1 + 2np_0 + 2n_0),$$

$$S = \frac{-B - \sqrt{B^2 - 4AC}}{2A}, \tag{2.6}$$

$$R = \frac{np_1\,(2 - S)}{np_1 + 2np_0}, \tag{2.7}$$

$$P = \frac{n_0}{N\,(1 - x)\,S}, \tag{2.8}$$

$$x = \frac{np_1 + 2np_0}{(2 - S)\,n_0 + np_1 + 2np_0}. \tag{2.9}$$

We now apply this technique to our sample, in order to determine the input parameters. However, for a real sample, we have the complicating effect that galaxies may be found in multiple systems. That is, a primary galaxy may have more than one companion. For our sample, there are 65

primary galaxies with one companion, and 8 with two companions. We take this effect into account by using the fraction of companions with measured redshifts to calculate np_1 and np_0. There are 49 companions with redshifts and 32 without; hence, $np_1 = 44.2$ and $np_0 = 28.8$, for a total of 73 paired primary galaxies. The number of isolated primary galaxies (n_0) is 472, giving a total of 545 primary galaxies. For a pure field sample, nnz and N are easy to determine. With the CNOC1 survey, we must keep in mind that primary galaxies are selected so as to avoid cluster centres - hence, only a subset of the area is truly surveyed for primary galaxies. Instead, we compute an effective N (and effective nnz), by determining the ratio of primary galaxies to total number of galaxies (and total number without redshifts) in the neighbourhood of each of the primary galaxies. An annulus with inner radius of $1'$ and outer radius of $1'.5$ was used, which is representative of the sample as a whole. The total number of galaxies within these annuli is 3108, of which 1329 have no redshifts and 781 are members of the primary sample. This leads to N=2169 and nnz=927.

Using equations 2.6– 2.9, we find : S=57.1%, R=62.1%, P=43.9%, and x=13.1%. What does this mean? First of all, S and R agree closely. If we define the pair sampling rate to be R/S, we find a value of 109%. This implies that galaxies in pairs are sampled in the same way as other galaxies, demonstrating that the mask design algorithm of YEC successfully compensates for pair selection bias. Also, x is in fact the observed pair fraction for all galaxies in the sample. Strictly speaking, this is not the same as the observed pair fraction for primary galaxies, but it should be fairly similar, since non-primary galaxies cover a similar (but larger) range

in redshift. After correcting for incomplete area coverage (see § 2.4), we find an observed pair fraction of 13.2%, in excellent agreement with the result found earlier in § 2.4.

2.5 The Physical Pair Fraction

2.5.1 Companions With Measured Redshifts

A total of 81 companions were found, of which 49 have redshifts. However, a significant fraction of these companions could be optical superpositions. We can use the available redshifts to weed out some apparent companions which lie at significantly different redshifts from the primary galaxies. The aim here is to exclude only those galaxies which cannot be physically associated with the primary. Fortunately, choosing an appropriate cutoff turns out to be quite simple. For all possible pairs with 2 redshifts, 2 quantities were calculated: projected separation D (in h^{-1} kpc), and rest-frame velocity difference ΔV (in km/s). Projected separation is calculated with equation 2.1, using the angular separation and average redshift for the pair. These quantities are plotted in Figure 2.4a, for large ranges of D and ΔV. Points lying in the lower portion of the plot represent pairs of galaxies which are apparently close together on the sky. Of these, only those with relatively low velocity differences may in fact be physically close. From the plot, there is an obvious population of close (D $< 20\ h^{-1}$ kpc) physical pairs, all of which have $\Delta V <$ 600 km/s; these are shown more clearly in Figure 2.4b. The remaining pairs have $\Delta V > 4000$ km/s (note that velocity errors are at most 150 km/s, and are typically $\sim$ 130 km/s). Using a pair velocity criterion of 1000 km/s, we

find that 22 companions (with measured redshifts) are not physically associated with the corresponding primary galaxy. Hence, 55% of the companions with redshifts are deemed to be physically associated. If we had redshifts for all galaxies in the sample, this would allow us to eliminate all optical companions.

2.5.2 Companions Without Redshifts

Even without a redshift, one can glean some information about a galaxy's distance from its colour. Specifically, at any given redshift, there is a limit to how red normal galaxies are expected to be, the reddest being those of E/S0 morphological types. Any galaxies which are significantly redder than this can safely be assumed to lie at a higher redshift. Recall that the E/S0 envelope gets progressively redder with increasing redshift (cf. Koo and Kron, 1992). This is also strikingly apparent in the colour-redshift distribution of the field galaxies in this study (see Figure 2.5). For a given field galaxy at redshift z, we assume that all companions lying more than 0.15 magnitudes redward of the $E/S0$ sequence must lie at higher redshift. Note that once again we wish to eliminate only those galaxies which cannot be physically related, so it is best to make a conservative cut only. It turns out that none of the companions are eliminated using this restriction. However, in a larger and deeper redshift sample, this technique could be used to eliminate a significant number of optical companions.

We are left with 32 companions without redshifts. Without additional information about these galaxies, we cannot determine which companions are physically associated on a galaxy-by-galaxy basis. However, we can correct

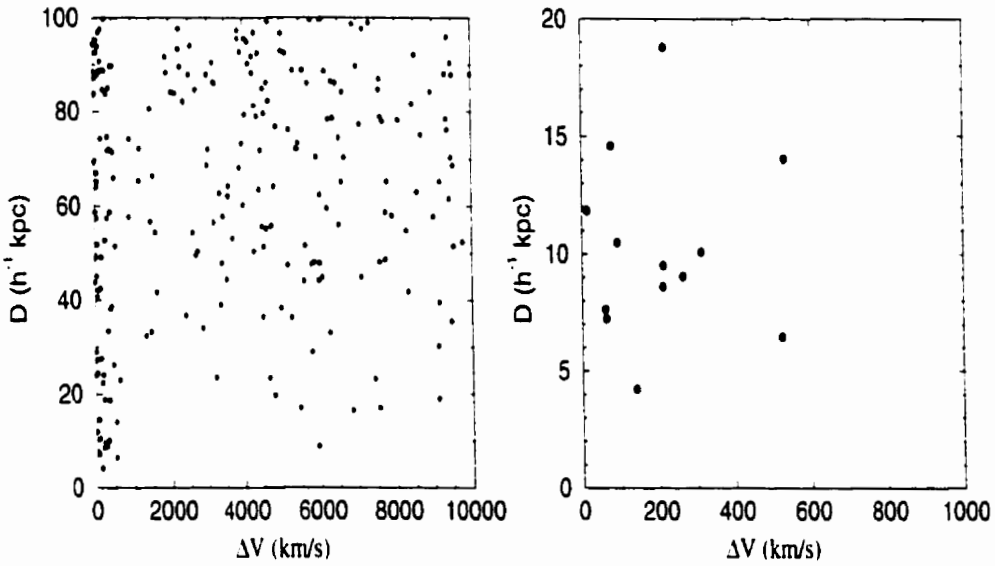

Figure 2.4: Projected separation (D) versus rest-frame velocity difference (ΔV) for galaxy pairs with 2 redshifts. Points with small projected separations and small velocity differences represent pairs which are physically associated. $\Omega_0 = 1$ was assumed for this calculation. (*a*) Pairs with two redshifts satisfying $\Delta V < 10000$ km/s and D < 100 h^{-1} kpc. (*b*) The subset of close physical pairs of primary galaxies.

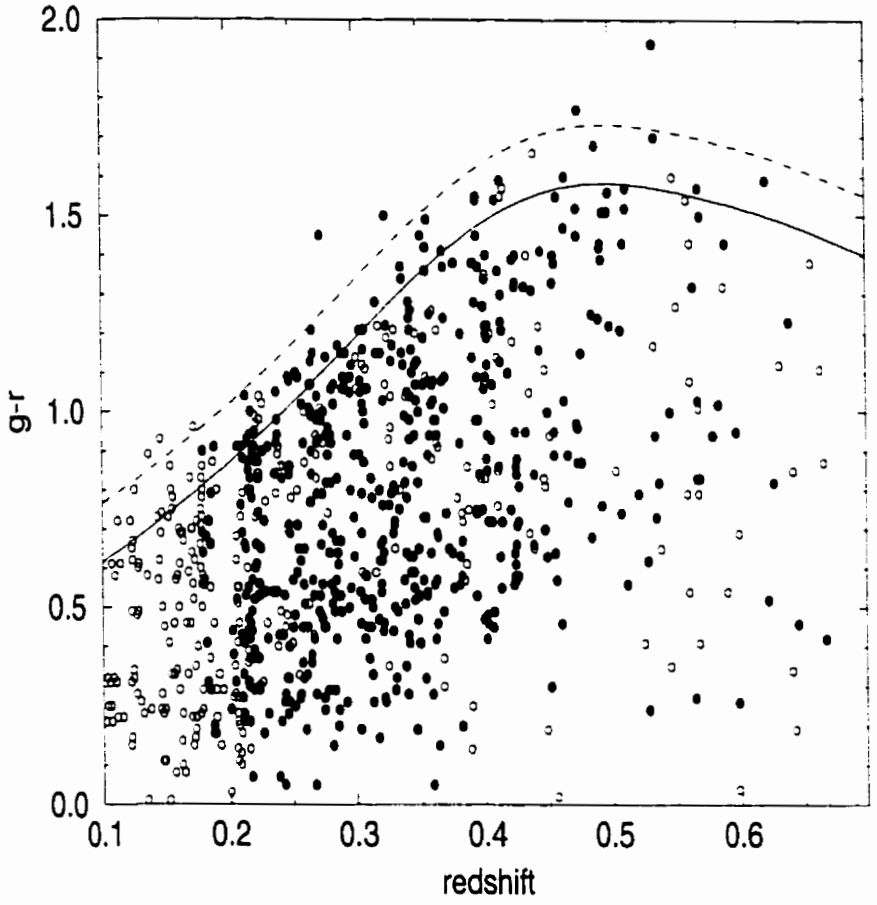

Figure 2.5: The determination of a colour cutoff. For a given primary galaxy at redshift z, all companions without redshifts which lie more than 0.15 magnitudes redward of the E/S0 sequence are assumed to lie at larger redshift. Hence, any such companions are expected to be unrelated. The non-evolving E/S0 sequence (*solid line*) was determined by convolving the filters with a typical E/S0 galaxy spectrum from Coleman, Wu, and Weedman (1980). The dashed line lies 0.15 magnitudes redward of the E/S0 sequence. Filled symbols represent field galaxies from the primary sample; open symbols represent field galaxies which are not part of the primary sample.

for this effect statistically, by comparing the number density of the remaining companions with the background density of galaxies without redshifts. That is, we can calculate the number of companions expected (on average) in a random distribution, and compare it with the number actually found. To estimate the number of random companions expected, the average number density of galaxies (without redshifts) near each galaxy was computed. Once again, we use the colour cutoff. This was done using an annulus with an outer radius of 1.'5 arcmin and an inner radius of twice θ_{20} (typically $\sim$ 15″). The outer radius was chosen to be large enough to sample properly the local region around the galaxy, but small enough to minimize the effects of cluster density gradients. The inner radius was chosen to be large enough to avoid the influence of the galaxy and its close companions on the number density. The number of random companions expected for a given galaxy was computed by multiplying the number density by the effective search area. Owing to the resolution effects described earlier, we use annuli with inner radii of 1″ and outer radii of θ_{20}. Any excess over random was then attributed to the presence of physically associated companions.

The total number of random companions (without redshifts) expected is 16.8 $\pm$ 0.4, as compared with 32 found. This optical fraction (53%) is consistent with that found for companions with measured redshifts (45%), demonstrating that the statistical correction for optical companions is reliable (in fact, we expect the optical fraction to be slightly higher for companions without redshifts, since galaxies outside the primary redshift limits are less likely to have redshifts). It follows that the overall fraction of companions (with or without redshifts) which are physical is 52.2 $\pm$ 8.6%. Therefore, the

fraction of galaxies which are in close *physical* pairs is 7.1 ± 1.4%.

2.6 Properties of Galaxies in Close Pairs

In order to investigate the properties of galaxies in close pairs, we wish to compare the "paired" galaxies (those in the primary sample with companions of comparable luminosity) with galaxies which are not in pairs. For this part of the analysis, a "paired" galaxy is defined as one which has at least one companion which may be physically associated. Hence, known optical companions will be discarded. In identifying an isolated sample, we note that some galaxies have companions which are too faint to be included in the secondary sample. If we include these galaxies in the sample of galaxies not in pairs, we may be smearing out any observed property differences. Instead, we define the "isolated" sample to be those galaxies in the primary sample which have no companions brighter than the limiting magnitude of the entire sample (r=23.0). Galaxies with faint companions only (hereafter designated "paired [faint]") will be included in the ensuing analysis for completeness, but we will focus on comparing the paired and isolated samples.

A compilation of the mean properties of paired and isolated galaxies is given in Table 2.1 and 2.2. In Table 2.1, we compare mean redshift ($< z >$), observed colour ($< g-r >$), the fraction of galaxies with emission-line spectra (Em), and the fraction colour-classified as Scd+Im galaxies. In Table 2.2, we present mean rest-frame ($< g - r >$) colour, r-band apparent ($< r >$) and absolute ($< M_r >$) magnitude, and [OII] rest-frame equivalent width (EW). Each of these properties is defined and discussed in detail in the sections that

Table 2.1: Average Properties of Paired and Field Galaxies : I

Galaxy Sample	N	$< z >$	Observed $< g - r >$	*Em* Fraction	*Scd + Im* Fraction
Paired	55	0.325± 0.012	0.80 ±0.06	29.1± 7.3%	36.4± 8.1%
Paired (faint)	97	0.322± 0.011	0.83 ±0.04	25.8± 5.2%	33.0± 5.8%
Isolated	393	0.335± 0.005	0.78 ±0.02	32.3± 2.9%	39.2± 3.2%
Paired (phys)	27	0.344± 0.017	0.96 ±0.10	22.2± 9.1%	29.6±10.5%
Paired (no z)	28	0.306± 0.015	0.65 ±0.06	35.7±11.3%	42.9±12.4%
Comp. (phys)	27	0.344± 0.017	0.98 ±0.09	18.5± 8.3%	25.9± 9.8%
Comp. (no z)	32	...	0.73 ±0.06	...	...

follow. Errors quoted are errors in the mean, with the exception of the Em and Scd+Im fractions, for which Poisson statistics are assumed.

As it is possible to have samples with similar mean properties but different overall distributions, we carry out Kolmogorov-Smirnov (K-S) tests to determine if paired and isolated galaxies have statistically significant differences. The results of these tests are presented in Tables 2.3 and 2.4. The K-S test statistic, expressed as a percentage, indicates the significance level for the hypothesis that two sets of data are drawn from the same distribution. A small significance level indicates that two distributions have significantly different cumulative distribution functions.

2.6.1 Redshifts

Of primary interest is the redshift distribution of the two samples. YE found that the average redshifts of their paired and isolated samples were identical

Table 2.2: Average Properties of Paired and Field Galaxies : II

Galaxy Sample	N	Rest-Frame $< g-r >$	$< r >$	$< M_r >$	[OII]EW (Å)
Paired	55	0.26±0.03	20.28± 0.12	−19.47± 0.09	10.9± 2.0
Paired (faint)	97	0.29±0.02	20.00± 0.08	−19.68± 0.06	10.5± 1.5
Isolated	393	0.25±0.01	20.37± 0.04	−19.43± 0.03	11.6± 0.8
Paired (phys)	27	0.31±0.05	20.47± 0.19	−19.36± 0.15	8.5± 2.5
Paired (no z)	28	0.22±0.03	20.09± 0.15	−19.58± 0.10	13.0± 3.1
Comp. (phys)	27	0.33±0.04	20.41± 0.19	−19.73± 0.15	8.5± 2.5
Comp. (no z)	32	...	20.54± 0.15	...	...

Table 2.3: K−S Tests for Paired/Isolated Galaxy Properties : I

Redshift Range	N Paired	N Isolated	z	Observed $< g-r >$	Spectral Type	Colour Type
0.18−0.67	55	393	67	57	>99	>99
0.18−0.67	97(faint)	393	15	79	89	36
0.18−0.30	23	165	27	88	>99	93
0.30−0.45	26	178	37	49	98	83

Table 2.4: K−S Tests for Paired/Isolated Galaxy Properties : II

Redshift Range	N Paired	N Isolated	Rest-Frame $< g-r >$	r	$< M_r >$	[OII]EW (Å)
0.18−0.67	55	393	65	83	77	77
0.18−0.67	97(faint)	393	13	0.00	0.38	76
0.18−0.30	23	165	78	38	26	75
0.30−0.45	26	178	31	>99	97	35

to within $\Delta z/z \lesssim 0.1$, implying that both populations have similar characteristic luminosities. With about 5 times as many redshifts, we can place even tighter constraints on this relation. The average redshift for our paired sample is statistically equivalent to that of the isolated sample. We conclude that the average redshifts of the two samples are identical to within $\Delta z/z \lesssim 0.05$. A K-S test and the visual appearance of the redshift histograms (see Figure 2.6) are consistent with this conclusion.

2.6.2 Galaxy Classification

Each field galaxy was classified using its $g-r$ colour and redshift. The basic method was to use a fit to the colour k-corrections of YEC, who convolved typical galaxy spectra from Coleman, Wu, and Weedman (1980; hereafter CWW) with the filters used in the observations. The colour-redshift relations corresponding to elliptical, Sbc, Scd, and Im galaxies are plotted in Figure 2.7. Each primary galaxy's location on this plot was used to estimate the most appropriate type classification by using the sequence with the closest colour at the galaxy's redshift. The relative proportions of early and late-type galaxies were determined for both the paired and isolated samples. The fraction of late-type (Scd+Im) galaxies is slightly lower for the paired sample, but the difference is not statistically significant. The corresponding K-S test result is consistent with this conclusion.

We can perform an independent check on this result, using the spectral classification given in the CNOC1 catalogs. Each galaxy has been assigned a spectral type based on the template giving the highest redshift cross-correlation value. Galaxies are identified as either early-type, Sbc,

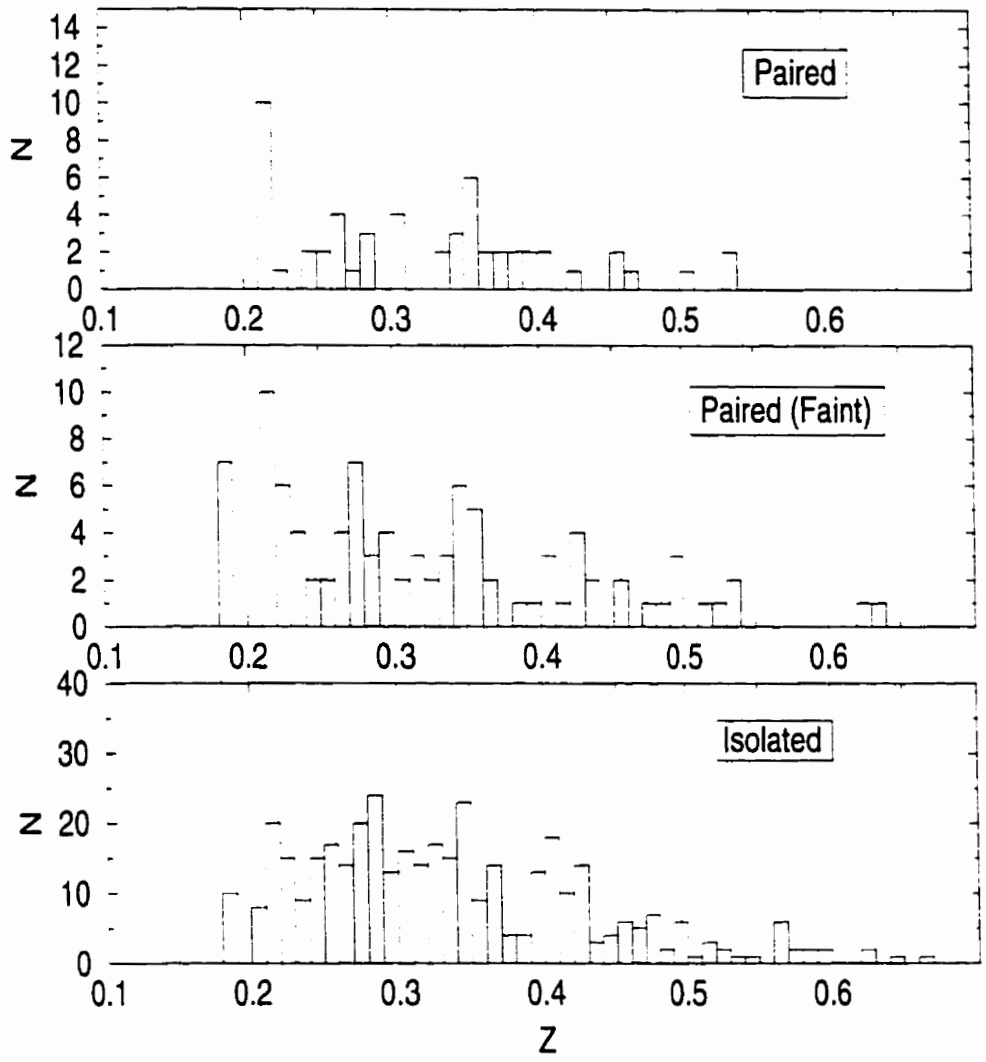

Figure 2.6: Histograms of redshifts for the paired and isolated samples. Paired galaxies have at least one companion of comparable luminosity. Paired (faint) galaxies have at least one companion brighter than r=23.0, but none of comparable luminosity. Isolated galaxies have no companions brighter than r=23.0.

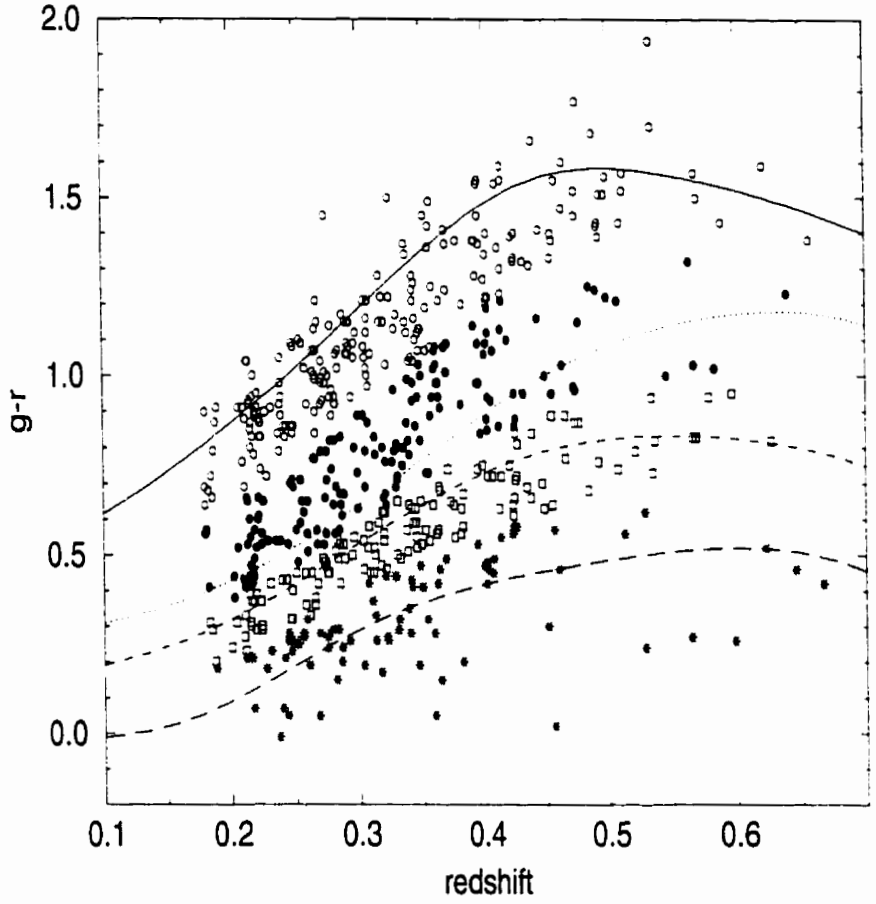

Figure 2.7: The colour classification of galaxies in the primary sample. Classification was determined based on the observed $g - r$ colours and redshifts. The lines represent the colours of non-evolving galaxies derived by YEC by convolving Gunn filter responses with the standard typical galaxy spectra of CWW. The different galaxy sequences and corresponding classifications are: E (*solid line, open circles*), Sbc (*dotted line, filled circles*), Scd (*dashed line, open squares*), and Im (*long-dashed line, stars*).

or emission-line galaxies. This determination is independent of colour, and hence provides a good comparison with the classifications determined above. We find that the fraction of emission-line galaxies is slightly lower for the paired sample, but again the difference is not significant, as demonstrated by the K-S test. Hence, neither spectral nor colour classification reveals any measurable differences between paired and isolated galaxies.

2.6.3 Colours

Since we might expect galaxies in close pairs to have different colours than other galaxies, we compare the observed colour distributions of the two sets of data. The mean $g - r$ colours were found to agree quite closely, and a K-S test confirms this. This result has also been found by CPI and YE, among others. It is more instructive to compare the *rest-frame* colours of the two samples. Using the spectral classifications from above, each galaxy's colour was k-corrected, by interpolating in colour between the closest typical galaxy sequences. We find that the mean rest-frame colours are nearly identical, with a very slight trend toward paired galaxies being redder. No apparent difference in the distribution of rest-frame colours is apparent from the histograms (Figure 2.8) or the K-S test. Therefore, we find no measurable differences between the k-corrected colours of paired and isolated galaxies. Mean rest-frame colour differences of $\mid \Delta(g - r) \mid \gtrsim 0.1$ magnitudes can be ruled out at the 3σ level.

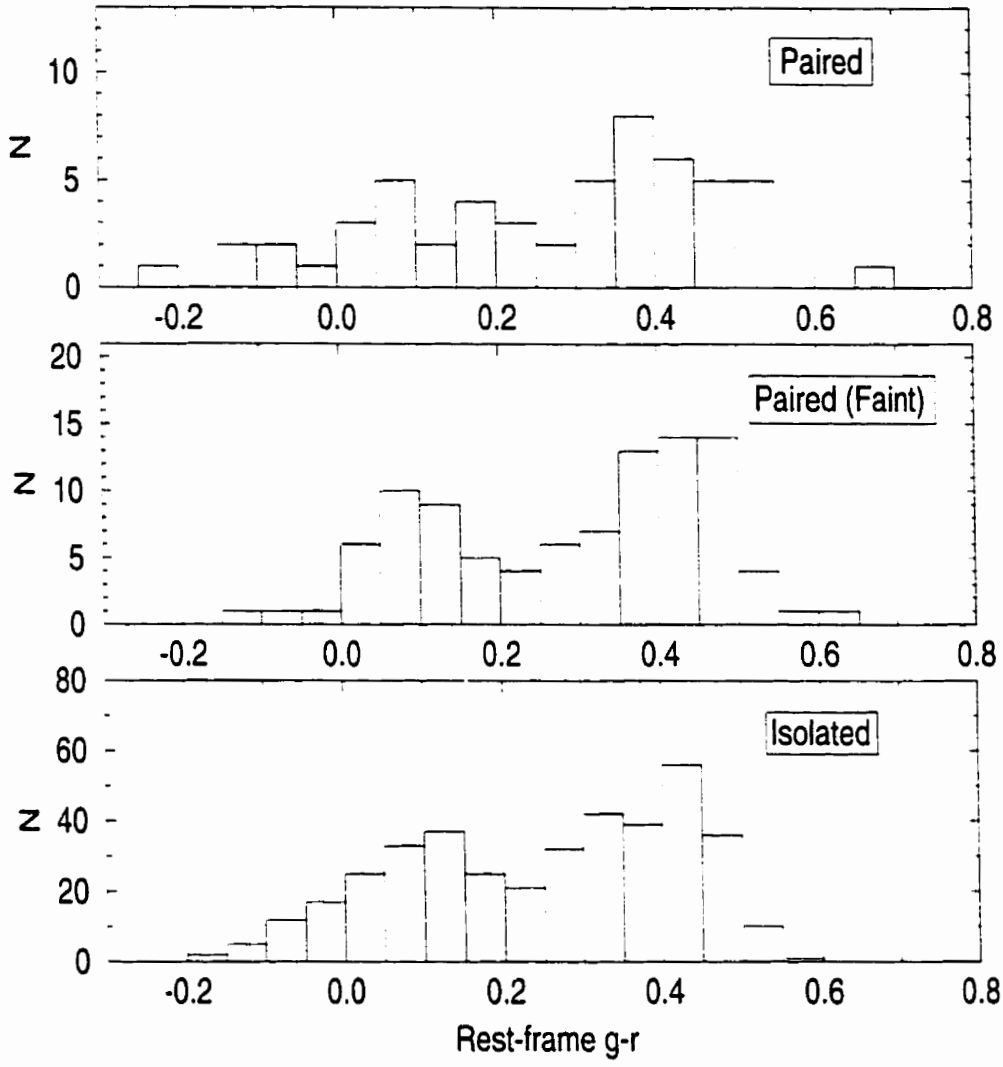

Figure 2.8: Histograms of rest-frame $g-r$ colours for the paired and isolated samples. Rest-frame colours were derived using $g-r$ k-corrections from YEC (using spectra of CWW). Paired galaxies have at least one companion of comparable luminosity. Paired (faint) galaxies have at least one companion brighter than r=23.0, but none of comparable luminosity. Isolated galaxies have no companions brighter than r=23.0.

2.6.4 Luminosities

The apparent magnitude distributions of the two samples are also very similar. However, it is preferable to compare intrinsic luminosities. Therefore, we compute the absolute magnitude for each galaxy. Since we are looking only at relative luminosities, the results will not be sensitive to the choice of cosmological parameters. The k-correction in r for each galaxy was extracted from the CNOC1 database. These k-corrections were derived using the data of Sebok (1986) for Gunn r, and depend only on the galaxy's redshift and colour. The average k-correction for the paired sample (0.27 mag) is identical to that for the isolated sample.

The resulting mean absolute magnitude of paired galaxies was found to be nearly identical to that of the isolated sample. This is confirmed with a K-S test (see Figure 2.9 also). A similar finding was made by YE. However, there is an indication that galaxies in the paired (faint) sample are significantly more luminous than galaxies with no companions (isolated). This result is confirmed with a K-S test. The difference can be attributed to an inherent bias in selecting galaxies for the paired (faint) sample. Primary galaxies which are brighter in apparent magnitude will be more likely to have faint physical companions detected than will apparently fainter galaxies. This selection effect comes into play only when the apparent magnitude limit for companions is extended deeper than that for the primary sample, and hence does not affect the paired sample.

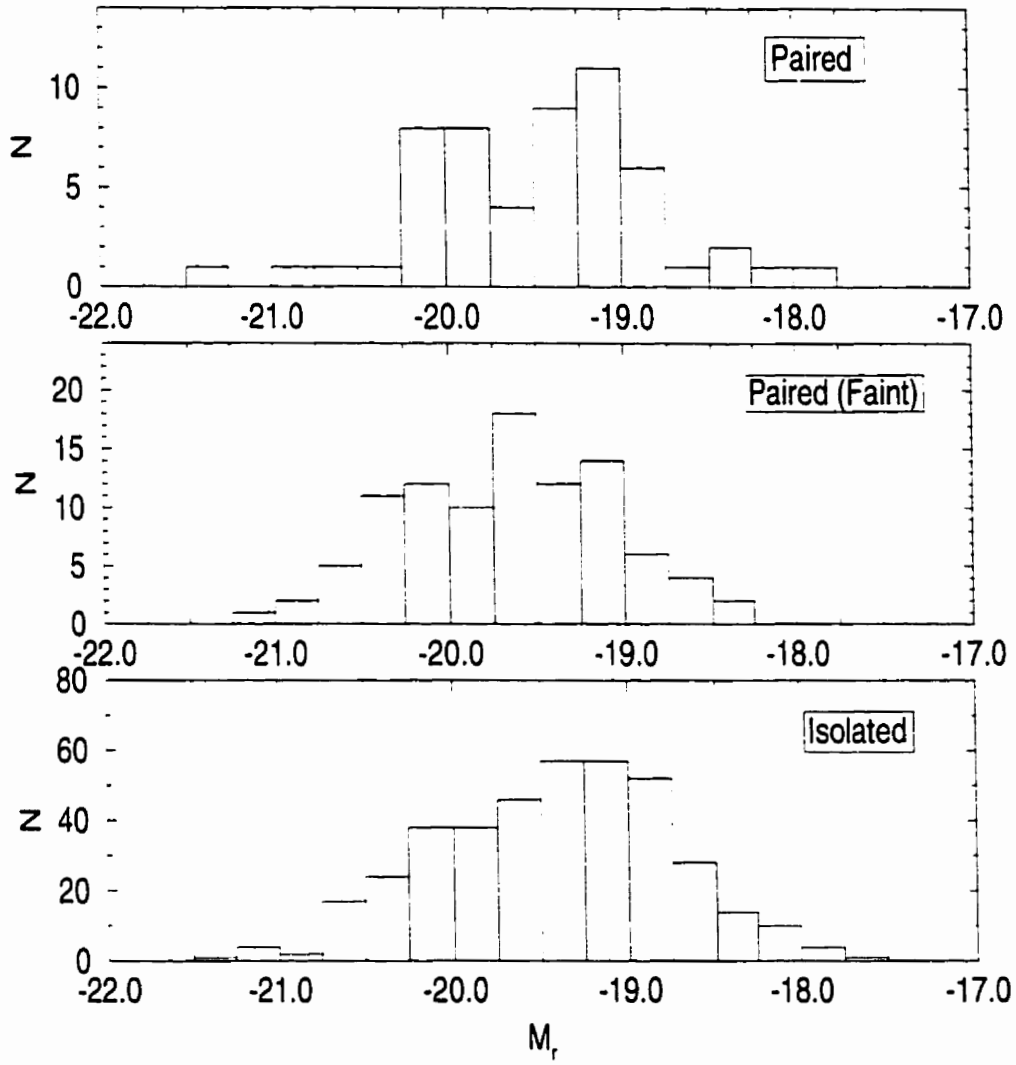

Figure 2.9: Histograms of absolute r magnitudes for the paired and isolated samples. Determination of M_r uses r band k-corrections derived from Sebok (1986) by YEC, and assumes h=1. Paired galaxies have at least one companion of comparable luminosity. Paired (faint) galaxies have at least one companion brighter than r=23.0, but none of comparable luminosity. Isolated galaxies have no companions brighter than r=23.0.

2.6.5 [OII]3727Å Equivalent Widths

One of the best indicators of current star formation is the presence of spectral emission lines such as [OII]3727Å. Using a local sample of galaxies, Liu and Kennicutt (1995) found that the mean [OII] equivalent width was 19Å for merging galaxies, as compared with 11Å for the complete sample. We used the procedure outlined in Abraham et al. (1996) to measure the [OII] rest-frame equivalent widths of all the CNOC1 galaxies. We were able to determine equivalent widths for 81% of the primary sample. Typical errors are estimated to be $\lesssim 20\%$. The mean [OII] equivalent width is found to be the same for paired and isolated galaxies. K-S tests and the visual appearance of the histograms (Figure 2.10) confirm this finding. CPI found a similar result.

2.6.6 Properties within Sub-samples

The paired galaxy sample can be divided into two subsets : those which have at least one confirmed companion ("paired [phys]", based on velocity criterion of § 2.5.1), and those for which the companions have photometric information only ("paired [no z]"). All pairs in the former sample are physical (although not necessarily merging) and therefore would be expected to exhibit greater mean property differences from the isolated sample if merging affects galaxy properties significantly. The observed properties of these two samples (see Tables 2.1 and 2.2) are found to be statistically equivalent to the isolated sample, strengthening the earlier conclusions. One might also ask how the properties of the companions themselves compare with the

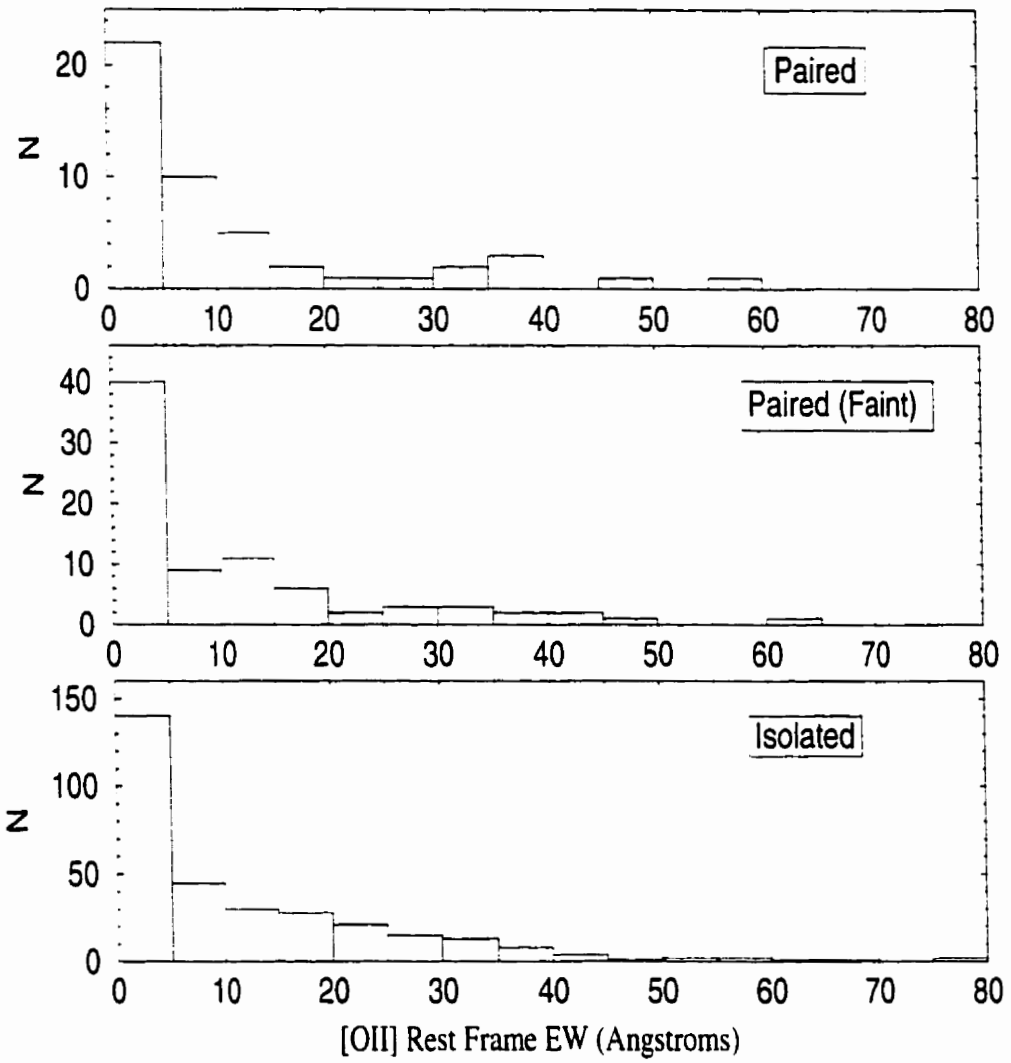

Figure 2.10: Histograms of [OII] rest-frame equivalent widths for the paired and isolated samples. Paired galaxies have at least one companion of comparable luminosity. Paired (faint) galaxies have at least one companion brighter than r=23.0, but none of comparable luminosity. Isolated galaxies have no companions brighter than r=23.0.

paired and isolated galaxies in the primary sample. Because of the nature of our sample selection (see Section 2.3), most of the companions which have redshifts are also part of the paired primary sample; therefore the mean properties are very similar. The mean apparent magnitude and colour of the companions without redshifts are also found to be statistically equivalent to that of the isolated galaxies in the primary sample. To summarize, there are no observed differences in the overall properties of galaxies which have close companions of comparable luminosity and galaxies with no companions brighter than r=23.0.

2.7 The Galaxy Merger Rate

As mentioned earlier, the average redshift of the sample is 0.33, which gives us some leverage in investigating the redshift dependence of the merger rate. For comparison, we will use a low redshift sample which is derived from the UGC catalog (Nilson 1973). We select all galaxies with measured diameters of at least 1′ in both B and R, to a (statistically complete) limiting magnitude of B=14.5. Within this sample, the average redshift (for galaxies with measured redshifts) is 0.0076. At this distance, a physical separation of 20 h^{-1} kpc corresponds to an angular separation of 184″. We find that 130 out of 3058 galaxies have companions within this radius, yielding a close pair fraction of 4.3 $\pm$ 0.4%. Since optical companions are negligible at these bright magnitudes (see CPI), we take this to be the fraction of galaxies in close physical pairs. We note, however, that this estimate is approximate in nature. While the internal error in the local pair fraction is small, the

systematic errors may be fairly large. A more complete redshift sample with well-defined selection effects is needed to improve this estimate.

Before comparing the two samples, we must ensure that the pair fraction does not depend strongly on the luminosities of the galaxies involved. For the nearby sample, B=14.5 corresponds to an average absolute limiting magnitude of M_B=−17.3 (based on the average redshift). The CNOC1 primary field sample has an average apparent limiting magnitude of r=21.3, which corresponds to B=23.1 using the Gunn colour transformation of Windhorst et al. (1991) and the average colour ($g - r$=0.79) of the primary galaxies. The average B k-correction (k_B=1.0) was estimated using the mean redshift (z=0.33), the colour classification fractions determined in Section 2.6.2, and the k-corrections of Frei & Gunn (1994). This results in an average absolute limiting magnitude of $M_B = -18.1$, which is roughly one magnitude brighter than the low-redshift sample. It has been shown by YE that the UGC pair fraction remains basically unchanged over a range of $\sim$ 2 mag brighter than $B = 14.5$; hence, we conclude that the two samples are of comparable luminosity, and the pair fractions derived should not be sensitive to the particular magnitude limits used.

We need to determine the fraction of galaxies in each sample which are likely to merge. While those in close physical pairs are likely candidates, some may be moving at such high relative velocities that they are unlikely to merge. Using dynamical arguments, CPI argue that, at the present epoch, pairs with relative velocities less than 350 km/s are likely to merge. They estimate this fraction to be $\sim$ 50%. For a pairwise velocity evolving as $(1+z)^{-1}$ (see CPI), this increases to a fraction of 66% at z=0.33. There are

13 close physical pairs of primary galaxies in our distant sample for which redshifts are available for both members. In this sample, 11 out of 13 pairs (85 ± 26%) have ΔV <350 km/s, which is consistent with the assumed pairwise velocity. Using the close pair fraction determined earlier in this section, we conclude that the local merging fraction is 2.1 ± 0.2%. It follows that, with 7.1 ±1.4% of our distant sample in close physical pairs, the merging fraction at z=0.33 is $4.7 \pm 0.9\%$. If we assume the functional form of $(1+z)^m$ for the increase of the merger rate with redshift (Carlberg 1990), we find m = 2.8 ±0.9.

This value is consistent with the merger rate of CPI, who found m = 3.4 ± 1.0 using the same method (and the same low redshift sample). We note, however, that they overestimated the local pair fraction by underestimating its mean redshift. After correcting for this, we find $m = 4.0 \pm 1.0$ for their sample. Our merger rate is significantly lower than that obtained using the physical pair fraction found by YE, which translates into $m \sim 5.0 \pm 1.5$ using our parameterization of the merger rate with redshift. Their sample is the largest pair redshift survey next to ours; hence, it is important to find out what is causing this discrepancy. One major difficulty with the YE redshift sample is that pairs are known to be under-selected. This effect was accounted for by randomly discarding redshifts in each two redshift pair, and then correcting for this. Their result was tested using the method outlined in § 2.4.2. For the observed quantities, we use their original sample (before redshifts were discarded). Using $np_1 = 7.2$, $np_0 = 9.8$, $n_0 = 90$, $nnz = 200$, and $N = 376$, we find S = 47%, R = 41%, P = 61%, and x = 16.3%. The pair sampling (R/S) is 87%. YE estimate that ~ 55% of their observed pairs

are physical. This leads to a physical pair fraction of 8.9 $\pm$ 3.9%, which is considerably lower than the 15.5 $\pm$ 6.6% reported in their study. This revised pair fraction leads to a merger rate of $m = 3.4 \pm 1.9$, which is consistent with our result.

Using *HST* images, Burkey et al. (1994) derived m $\sim$ 2.5 $\pm$ 0.5, which would appear to agree with our merger rate. However, they parameterized the evolution of the merger rate in a different way (by taking the merger rate to be the z-derivative of the pair counts). If we use their pair fraction with our method, we find $m = 4.5 \pm 0.5$, which is significantly higher than our result. However, YE point out that the pair fraction of 34 $\pm$ 9% used by Burkey et al. (1994) is approximately twice as large as the *physical* pair fraction (due to optical pairs). After taking this into account, and using our parameterization of the merger rate evolution, we find m $\sim$ 2.9 for the Burkey et al. (1994) sample, in agreement with our result.

2.8 Redshift-binned Samples

An additional test of the validity of the preceding results is to divide the sample into redshift bins. The idea here is to look for redshift dependence in various properties, and also to have independent samples to look for common trends. We wish to have redshift bins which are small enough to avoid properties varying with redshift and large enough to ensure good statistics. Hence, we designate the following two samples : $0.18 < z < 0.30$ and $0.30 < z < 0.45$. This spans all primary field galaxies with $z \leq 0.45$, and avoids the sparsely populated high redshift regime (see Figure 2.6). Both samples

Table 2.5: Average Properties in Redshift−Binned Samples : I

Redshift Range	Galaxy Sample	N	Observed $< g-r >$	Em Fraction	$Scd + Im$ Fraction
0.18−0.30	Paired	23	0.59 ±0.06	30.4±11.5%	34.8±12.3%
0.18−0.30	Paired (faint)	49	0.67 ±0.04	14.3± 5.4%	24.5± 7.1%
0.18−0.30	Isolated	165	0.64 ±0.02	26.7± 4.0%	34.5± 0.4.6%
0.30−0.45	Paired	26	0.87 ±0.08	23.1± 0.9.4%	38.5±12.2%
0.30−0.45	Paired (faint)	35	0.96 ±0.06	34.3± 0.9.9%	37.1±10.3%
0.30−0.45	Isolated	178	0.83 ±0.02	33.1± 4.3%	43.3± 4.9%

have $\sim$ 240 field galaxies, allowing for good statistics. Note that both bins cover lookback time intervals of $\sim$ 0.68 h^{-1} Gyr (assuming Ω_0=1), which each correspond to $\sim$ 10% of the age of the universe for that model. The results of the following comparisons of various properties are summarized in Tables 2.5 and 2.6.

2.8.1 Galaxy Properties

For each sample, there is no measurable difference between the observed or rest-frame colours of paired and isolated galaxies. This is consistent with the findings of YE, who used similar redshift bins. In the low redshift bin, paired galaxies are slightly more luminous on average, but the difference is at the one sigma level. The mean absolute magnitudes are statistically equivalent in the high redshift bin. No significant differences were found in the classifications of paired and isolated galaxies in either redshift bin (note that very high K-S test significance levels are the result of the discrete

Table 2.6: Average Properties in Redshift−Binned Samples : II

Redshift Range	Galaxy Sample	Rest-Frame $< g-r >$	$< M_r >$	[OII]EW (Å)
0.18−0.30	Paired	0.26±0.04	−19.49± 0.16	11.1± 3.2
0.18−0.30	Paired (faint)	0.30±0.03	−19.60± 0.09	10.1± 2.0
0.18−0.30	Isolated	0.28±0.01	−19.30± 0.06	10.9± 1.4
0.30−0.45	Paired	0.24±0.04	−19.53± 0.13	10.6± 3.0
0.30−0.45	Paired (faint)	0.28±0.03	−19.75± 0.09	11.2± 2.8
0.30−0.45	Isolated	0.23±0.01	−19.54± 0.05	12.9± 1.2

classification systems). YE, on the other hand, found a larger emission line fraction in their high-redshift pair sample, but the difference was at the one sigma level.

2.8.2 Pair Fractions

As with the entire sample, we wish to investigate the pair fraction. However, by using the same apparent magnitude criteria as before, we encounter the problem that the low redshift sample will contain intrinsically fainter companions than the high redshift sample, rendering a direct comparison invalid. In order to compare the two redshift bins, we instead impose different limiting magnitudes, to sample galaxies of comparable luminosity. For this comparison, we relax the constraint that the secondary samples be drawn from populations of similar luminosity as the primary sample. For the high redshift bin, we impose the faintest magnitude limit possible - r=23.0. We can estimate the absolute magnitude of the faintest companions detectable in this bin by using z=0.45 and the average k-correction of 0.27 mag, yield-

ing M_r=−18.1. For the low redshift bin, the average k-correction is 0.19 mag. In order that the faintest companions in the low redshift bin also have M_r=−18.1, it follows that we must impose an apparent magnitude limit of r=22.0. Since all primary galaxies are brighter than this, we can do this without reducing the size of the primary sample.

Using the two defined samples, the pair fractions were determined. The fraction of galaxies in close physical pairs for the low redshift bin is 10.2 ±3.2%, as compared with 11.3 ±3.5% for the high redshift bin. The pair fractions for the redshift binned samples are larger than the fraction derived earlier for the entire sample, but this is to be expected since fainter companions have been included. A more suitable comparison is the merging fraction, found to be 6.3 ±2.0% for the low redshift bin, as opposed to 7.6 ±2.4% for the high redshift bin. In principle, these two independent quantities can be used to measure the merger rate evolution; however, the small numbers of galaxies makes this measurement (m = 2.1 ± 5.2) nearly meaningless for our sample. However, larger redshift surveys will be able to place tighter constraints on the redshift dependence of the merger rate using this approach.

2.9 Properties of Close Physical Pairs

In the following section, we will focus on close pairs in which both galaxies are members of the primary sample. In addition, we will concentrate only on those pairs in which the galaxies are physically associated (based on the relative velocity criterion outlined in § 2.5.1). These pairs are the best candidates for systems undergoing mergers or interactions. Images of the 13 pairs

satisfying these criteria are displayed in Figure 2.11.

Close inspection of these images reveals clear evidence of ongoing interactions in some pairs. While the image quality is not sufficient to perform detailed morphological classifications of each galaxy, it is adequate to separate the pairs in the following three categories : interacting (int), possibly interacting (int?), or not interacting (no). Pair classification was carried out by DRP, CJP, and HKCY, with no prior knowledge of any other properties of the pairs or member galaxies. In all cases, at least two of us agreed on the classification, and there was no disagreement by more than one class. The majority classification was adopted in each case.

The pair identification number, rest-frame velocity difference, projected separation, and image classification for each pair is listed in Table 2.7. In addition, Table 2.8 provides the CNOC1 identification number, rest-frame colour, spectral classification, and [OII] rest-frame equivalent width for each galaxy in these close physical pairs. It is immediately apparent that the four pairs classified as interacting (int) are very blue, with exceptionally strong emission lines. In addition, all four pairs have low (< 150 km/s) relative velocities. Since each of these measures is determined independently, this suggests that these pairs are in the process of merging. Such strong evidence of merging is surprising in the light of earlier analysis on the mean properties of this sample. That is, while the mean properties of these galaxies are indistinguishable from the field, a subset of the pairs do exhibit significantly different properties. This shows that indications of mergers are being swamped by non-merging pairs in our sample of close pairs.

We clearly have not identified all galaxies in the sample which are cur-

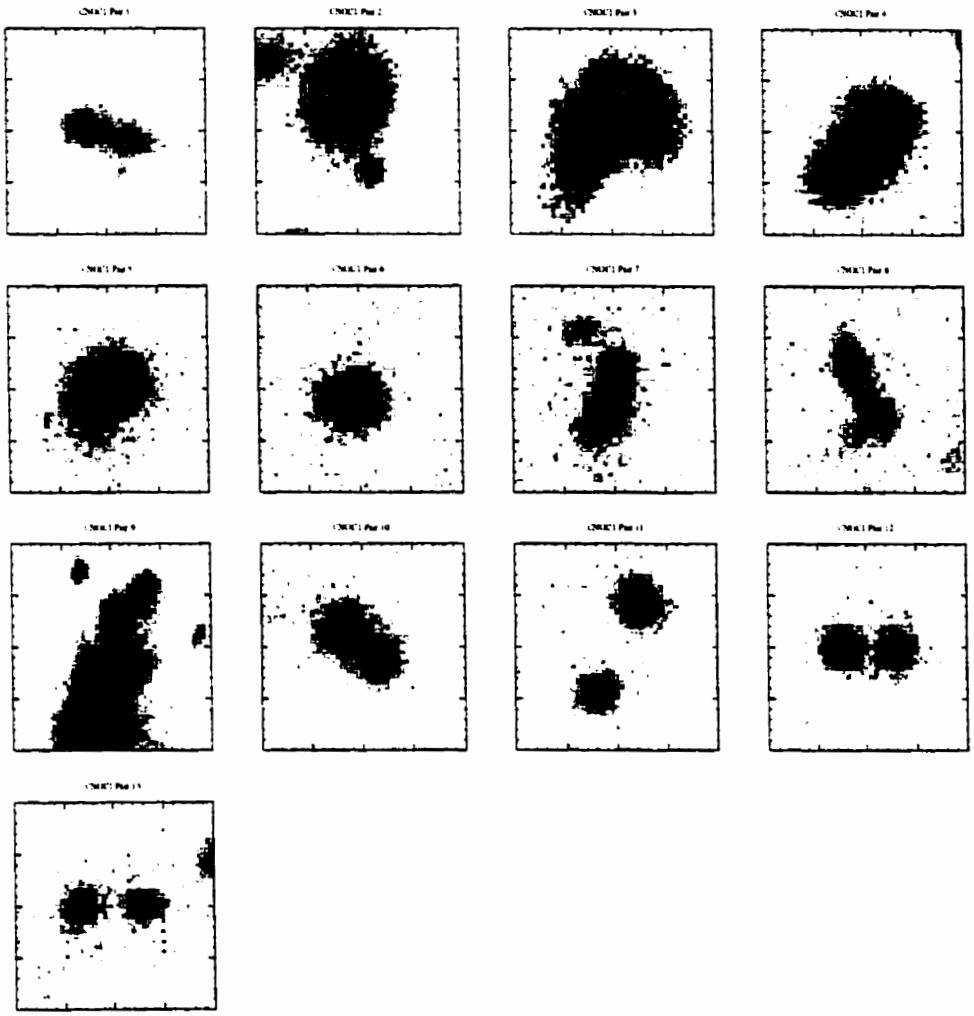

Figure 2.11: Mosaic of images for 13 close *physical* pairs in which both galaxies are primary field galaxies. North is up and east is to the left. Each image is 40 pixels square, corresponding to $\sim 12\farcs5$ on a side. Pair identifications correspond to those found in Tables 2.7 and 2.8. The physical projected pair separation ranges from 4 h^{-1} kpc (Pair 6) to 19 h^{-1} kpc (Pair 11). The typical FWHM is $\sim 1\farcs0$, and is fairly constant from image to image.

Table 2.7: Properties of Close Physical Pairs

Pair ID	Redshift $< z >$	ΔV km/s	Separation (h^{-1} kpc)	Image Class.
1	0.46	91	10.5	int?
2	0.31	530	14.0	no
3	0.22	311	10.1	int?
4	0.22	61	7.7	int
5	0.35	522	6.5	int?
6	0.38	140	4.2	int
7	0.34	63	7.2	int
8	0.36	15	11.8	int
9	0.34	263	9.1	int?
10	0.40	211	8.6	int?
11	0.37	216	18.8	no
12	0.27	212	9.5	int?
13	0.53	78	14.6	no

Table 2.8: Properties of Galaxies in Close Physical Pairs

Pair ID	CNOC1 Galaxy ID	Rest−Frame $g-r$	Spectral Class	[OII] EW (Å)
1	E0015: 1560	0.41	Em?	<5
	E0015: 1558	0.41	Em	12.3
2	E0302: 741	0.46	no	<5
	E0302: 726	0.42	no	8.9
3	E0839: 130289	0.51	no	<5
	E0839: 130282	0.47	no	11.9
4	E0839: 130451	0.31	Em?	5.3
	E0839: 130460	0.09	Em	13.1
5	E1224: 1635	0.47	no	<5
	E1224: 1632	0.51	no	<5
6	E1512: 202223	0.11	Em?	13.4
	E1512: 202227	-0.13	Em?	13.8
7	E1512: 200400	-0.07	Em?	8.4
	E1512: 200408	0.15	Em	35.3
8	E1512: 201709	-0.20	Em	45.4
	E1512: 201721	-0.08	Em	21.2
9	E1621: 102127	0.38	no	<5
	E1621: 102139	0.35	no	<5
10	E1621: 301135	0.44	no	<5
	E1621: 301126	0.50	no	<5
11	E1621: 300268	0.36	Em?	<5
	E1621: 300251	0.48	no	<5
12	E1621: 301023	0.53	no	...
	E1621: 301020	0.38	no	...
13	E1621: 300307	0.65	no	...
	E1621: 300306	0.54	no	<5

rently affected by mergers. First of all, there are some merging pairs which would be missed by our approach. Galaxies with very close ($< 1''$) companions may appear as isolated galaxies on our images. Also, some galaxies may have close companions which fall below the magnitude limit imposed in our study. In both cases, even if these companions are relatively small, it is possible that minor mergers may trigger strong starburst activity (Mihos and Hernquist 1994). Secondly, there are probably isolated galaxies in the field that have recently undergone mergers, and no longer have detectable companions nearby. These galaxies will obviously be missed in a study of close pairs. They may be identified as merger remnants if they have distorted appearances. However, as demonstrated by Mihos (1995), morphological signs of interactions are relatively short-lived, and can be difficult to detect at these redshifts. The presence of emission lines (such as [OII]) can be used independently to detect on-going merger-induced starbursts, while other spectral indices (e.g. $H\delta$) serve as useful diagnostics of recent starburst activity (see Couch & Sharples 1987). Furthermore, AGB light resulting from a starburst may last for several Gyr after a merger (Silva and Bothun 1995). Finally, we note that some mergers may not produce any obvious signs that a merger is taking place. This is particularly true for mergers of early-type galaxies, which will not produce either a strong starburst or clear morphological signs of interaction.

2.10 Discussion

Using a redshift-selected sample of field galaxies with $< z > \sim 0.33$, we find that roughly 7% have close physical companions of comparable luminosity. This is a factor of 1.7 higher than the physical pair fraction found locally. The mean properties of these paired galaxies are found to be indistinguishable from those of isolated galaxies. Upon dividing the sample into two independent sets based on redshift, we find a similar result. The only trend we find, although not statistically significant, is for paired galaxies to be (on average) slightly redder, more luminous, and of earlier type-classification than galaxies with no close companions. These results are consistent with evidence that early-type galaxies are more clustered than late-type galaxies (Roberts and Haynes 1994). For example, Loveday et al. (1995) find that early-type galaxies are clustered more strongly than late-type galaxies by a factor of $3.5 - 5.5$ locally, while Neuschaefer et al. (1995) find a similar effect in a sample with an average redshift of $z \sim 0.5$.

Upon examining the images of the 13 pairs which are known to be physically associated (based on similar redshifts), we find that the galaxies in pairs which are classified as interacting (based on their appearances) do exhibit very different properties. These pairs all have low relative velocities, and their galaxies have very blue rest-frame colours and spectra with strong emission lines. This is the first clear evidence (at this redshift) that paired galaxies have significantly different properties than field galaxies in general. This implies that mergers are responsible for at least some of the starbursting activity seen in samples of faint field galaxies. There are two ways to im-

prove on this result. First, a larger and more complete redshift sample will increase the yield of close physical pairs. Secondly, high resolution images would allow for improved detection of signs of interactions in these pairs.

We can use the information in Figure 2.4b to make a rough estimate of the mean dynamical friction timescale for the close physical pairs in our sample. Following Binney & Tremaine (1987), we can estimate the time needed for a companion to merge. Taking projected separations and relative velocities from Table 4, and assuming conservative values for the Coulomb logarithm ($\ln\Lambda \sim 3$) and galaxy mass-to-light ratio ($M/L \sim 5$), we find a mean timescale of ~ 150 Myr. Strictly speaking, this technique doesn't apply to mergers between galaxies of comparable mass (the typical mass ratio is 2:1 for these pairs); however, it confirms the assumption that the timescales involved are short. An alternative approach is to use the method outlined by Charlton and Salpeter (1991) for mergers between galaxies of comparable mass. Assuming the inward drift due to dynamical friction is independent of separation (once halos overlap appreciably), and adopting a typical number of decay orbits (3) based on N-body calculations, we find a mean dynamical friction timescale of ~ 400 Myr. Again, while this method is approximate in nature, it indicates that these close physical pairs should merge quickly, as expected.

The merger rate is estimated to increase with redshift as $(1+z)^m$, with $m = 2.8 \pm 0.9$. We demonstrate that our determination of the increase in the merger rate with redshift is consistent with earlier determinations using close pairs, and provides one of the strongest constraints to date. The observed increase in the merger rate with redshift implies that the average galaxy mass

at $z \sim 0.33$ was substantially lower than at the present epoch. Our observed value of m is consistent with the theoretical value of $m = 2.5$, derived by Toomre (1977) using binding energies of bound pairs. Carlberg (1990) estimated that m $\simeq 4.51\Omega^{0.42}$, for Ω near 1 and a CDM-like cosmology. This implies that our result is consistent with a low density universe, as found in several recent studies (e.g., Carlberg et al. 1996). Our result is also consistent with merging being the cause of the observed evolution in co-moving luminosity density found by Lilly et al. (1996). For blue wavelengths, they find luminosity density $\propto (1+z)^{2.3\pm0.5}$ for Ω_0=0.1 and q_0=0.05 (luminosity density $\propto (1+z)^{2.7\pm0.5}$ for Ω_0=1 and q_0=0.5). They attribute this evolution to a rapid decline in the global star formation rate since $z \sim 1$.

There are several obvious ways of improving on the results of this study. A larger and more complete set of redshifts would decrease the swamping effect of unrelated optical pairs, and reduce the uncertainty in estimating the merger rate and differences in various properties. Secondly, additional spectral features and colours may prove to be better diagnostics of on-going or recent mergers. Finally, a significant short-coming of this type of study is simply a lack of resolution. High resolution imaging would allow close faint companions to be identified, purifying the pair sample. In addition, improved morphological indications of ongoing mergers or disruptions would help to identify merger candidates. Quantitative determinations of morphology of individual galaxies would also allow the competing effects of mergers and the morphology-density relation to be disentangled more easily.

Chapter 3

New Techniques for Relating Dynamically Close Galaxy Pairs to Merger and Accretion Rates : Application to the SSRS2 Redshift Survey

3.1 Introduction

Studies of galaxy evolution have revealed surprisingly recent changes in galaxy populations. Comparisons of present day galaxies with those at moderate ($z \sim 0.5$) and high ($z \sim 3$) redshift have uncovered trends which are often dramatic, and may trace galaxies to the time at which they were first assembled into recognizable entities. These discoveries have shed new light on the formation of galaxies, and have provided clues as to the nature of their evolution. At $z < 1$, the picture that is emerging is one in which early type galaxies evolve slowly and passively, while late type galaxies become more numerous with increasing redshift (e.g., Lin et al. 1999). At higher redshifts,

deep surveys such as the Hubble Deep Field (Williams et al. 1996) indicate an increase in the cosmic star formation rate out to $z \sim 2$ (e.g., Madau, Pozzetti, and Dickinson 1998).

While considerable progress has been made in the observational description of galaxy evolution, important questions remain regarding the physical processes driving this evolution. Mechanisms that have been postulated include galaxy-galaxy mergers, luminosity-dependent luminosity evolution, and the existence of a new population of galaxies that has faded by the present epoch (see reviews by Koo and Kron 1992; Ellis 1997). In this chapter, we will investigate the relative importance of mergers in the evolution of field galaxies. Mergers transform the mass function of galaxies, marking a progression from small galaxies to larger ones. In addition, mergers can completely disrupt their constituent galaxies, changing gas-rich spiral galaxies into quiescent ellipticals (e.g., Toomre and Toomre 1972). During a collision, a merging system may also go through a dramatic transition, with the possible onset of triggered star formation and/or accretion onto a central black hole (see review by Barnes and Hernquist 1992).

It is clear that mergers do occur, even during the relatively quiet present epoch. However, the frequency of these events, and the distribution of masses involved, has yet to be accurately established. This is true at both low and high redshift. Furthermore, while a number of attempts have been made, a secure measurement of evolution in the galaxy merger rate remains elusive, and a comparable measure of the accretion rate has yet to be attempted.

In this study, we introduce a new approach for relating dynamically close galaxy pairs to merger and accretion rates. These new techniques yield ro-

bust measurements for disparate samples, thereby allowing meaningful comparisons of mergers at low and high redshift. In addition, these pair statistics can be adapted to a variety of redshift samples, and to studies of both major and minor mergers. We apply these techniques to a large sample of galaxies at low redshift (SSRS2), providing a much needed local benchmark for comparison with samples at higher redshift. In Chapter 4, we will apply these techniques to a large sample of galaxies at moderate redshift (CNOC2; $0.1 \leq z \leq 0.5$), yielding a secure estimate for the rate of evolution in the galaxy merger and accretion rates.

An overview of earlier pair studies, and a discussion of their limitations and shortcomings, are given in the next section. The SSRS2 data are described in § 3.3. Section 3.4 discusses the connection between close pairs and the merger and accretion rates, while § 3.5 introduces new statistics for relating these quantities. Section 3.6 describes how these statistics can be applied to flux-limited surveys in a robust manner. A pair classification experiment is presented in § 3.7, giving empirical justification for our close pair criteria. Pair statistics are then computed for the SSRS2 survey in § 3.8. The results are compared with earlier studies, and with measurements on larger scales, in § 3.9. Conclusions are given in the final section. Throughout this chapter, we assume a Hubble constant of $H_0 = 100h$ km s^{-1} Mpc^{-1}, and q_0=0.1. Where convenient, we set h=1.

3.2 Background

Every estimate of evolution in the merger and/or accretion rate begins with the definition of a merger statistic. Ideally, this statistic should be independent of selection effects such as optical contamination due to unrelated foreground/background galaxies, redshift incompleteness, redshift-dependent changes in minimum luminosity resulting from flux limits, contamination due to non-merging systems, k-corrections, and luminosity evolution. In addition, it should be straightforward to relate the statistic to the global galaxy population, and to measurements on larger scales. The statistic should then be applied to large, well-defined samples from low to high redshift, yielding secure estimates of how the merger and/or accretion rates vary with redshift.

Within the past decade, there have been a number of attempts to estimate evolution in the galaxy merger rate using close pairs of galaxies (e.g. Zepf and Koo 1989; Burkey et al. 1994; Carlberg, Pritchet,and Infante 1994; Woods, Fahlman, and Richer 1995; Yee and Ellingson 1995; Le Fèvre et al. 1999; Chapter 2). The statistic that has been most commonly employed is the traditional pair fraction, which gives the fraction of galaxies with suitably close physical companions. This statistic is assumed to be proportional to the galaxy merger rate. The local (low-redshift) pair fraction was estimated in Chapter 2, using a flux-limited ($B \leq 14.5$) sample of galaxies from the UGC catalog (Nilson 1973). Using pairs with projected physical separations of less than 20 h^{-1} kpc, the local pair fraction was estimated to be $4.3 \pm 0.4\%$. This result was shown to be consistent with the local pair fraction estimates of Carlberg et al. (1994) and Yee & Ellingson (1995), both of whom also

used the UGC catalog. The pair fraction has been measured for samples of galaxies at moderate redshift ($z \sim 0.5$), yielding published estimates ranging from approximately 0% (Woods et al. 1995) to 34% $\pm$ 9% (Burkey et al. 1994). Evolution in the galaxy merger rate is often parameterized as $(1+z)^m$. Close pair studies have yielded a wide variety of results, spanning the range $0 \lesssim m \lesssim 5$. There are several reasons for the large spread in results. First, different methods have been used to relate the pair fraction to the merger rate. In addition, some estimates have been found to suffer from biases due to optical contamination or redshift completeness. In Chapter 2, we demonstrated that, after taking all of these effects into account, most results are broadly consistent with our estimate of m=2.8 $\pm$ 0.9, made using the largest redshift sample (545 galaxies) to date.

While this convergence seems promising, all of these results have suffered from a number of very significant difficulties. The central (and most serious) problem has been the comparison between low and moderate redshift samples. Low-z samples have been poorly defined, due to a lack of suitable redshift surveys. In addition, the pair fraction depends on both the clustering and mean density of galaxies. The latter is very sensitive to the limiting absolute magnitude of galaxies, leading to severe redshift-dependent biases when using flux-limited galaxy samples. These biases have not been taken into account in the computation of pair fractions, or in the comparison between samples at different redshifts.

While these problems are the most serious, there are several other areas of concern. A lack of redshift information has meant dealing with optical contamination due to unrelated foreground and background galaxies. More-

over, while one can statistically correct for this contamination, it is still not possible to discern low velocity companions from those that are physically associated but unbound, unless additional redshift information is available. Finally, there is no direct connection between the pair fraction and the galaxy correlation function (CF) and luminosity function (LF), making the results more difficult to interpret.

To address these issues, we have developed a novel approach to measuring pair statistics. We will introduce new statistics that overcome many of the afflictions of the traditional pair fraction. We will then apply these statistics to a large, well-defined sample of galaxies at low redshift.

3.3 Data

The Second Southern Sky Redshift Survey (da Costa et al. 1998; hereafter SSRS2) consists of 5426 galaxies with $m_B \leq 15.5$, in two regions spanning a total of 1.69 steradians in the southern celestial hemisphere. The first region, denoted SSRS2 South, has boundaries $-40° \leq \delta \leq -2.5°$ and $b_{II} \leq -40°$. The second region, SSRS2 North, is a more recent addition, and is bounded by $\delta \leq 0°$ and $b_{II} \geq 35°$. Galaxies were selected primarily from the list of non-stellar objects in the *Hubble Space Telescope* Guide Star Catalog, with positions accurate to $\sim 1''$ and photometry with an rms scatter of ~ 0.3 magnitudes (Alonso et al. 1993, Alonso et al. 1994). The sample now includes redshifts for all galaxies brighter than $m_B \leq 15.5$. We correct all velocities to the local group barycentre using Equation 6 from Courteau and van den Bergh (1999). We restrict our analysis to the redshift range $0.005 \leq$

$z \leq 0.05$. This eliminates nearby galaxies, for which recession velocities are dominated by peculiar velocities, giving poor distance estimates. We also avoid the sparsely sampled high redshift regime. This leaves us with a well-defined sample of 4852 galaxies.

3.4 The Galaxy Merger and Accretion Rates

3.4.1 Definitions

The primary goal of earlier close pair studies has been to determine how the galaxy merger rate evolves with redshift. The merger rate affects the mass function of galaxies, and may also be connected to the cosmic star formation rate. Before attempting to measure the merger rate, it is important to begin with a clear definition of a merger and a merger rate. Here, we refer to mergers between two galaxies which are both above some minimum mass or luminosity. If this minimum corresponds roughly to a typical bright galaxy (L_*), this criterion can be thought of as selecting so-called major mergers. We consider two merger rate definitions. First, it is of interest to determine the number of mergers that a typical galaxy will undergo per unit time. In this case, the relevant rate may be termed the galaxy merger rate (hereafter $\mathcal{R}_{\rm mg}$). A related quantity is the total number of mergers taking place per unit time per unit co-moving volume. We will refer to this as the volume merger rate (hereafter $\mathcal{R}_{{\rm mg}_V}$). Clearly, $\mathcal{R}_{{\rm mg}_V} = n_0 \mathcal{R}_{\rm mg}$, where n_0 is the co-moving number density of galaxies.

While both of these merger rates provide useful measures of galaxy interactions, they have their limitations. As one probes to faint luminosities,

one will find an increasing number of faint companions; hence, the number of inferred mergers will increase in turn. For all realistic LFs, this statistic will become dominated by dwarf galaxies. In addition, it is of interest to determine how the mass of galaxies will change due to mergers. To address these issues, we will also investigate the rate at which mass is being accreted onto a typical galaxy. This quantity, the total mass accreted per galaxy per unit time, will be referred to as the galaxy accretion rate (hereafter $\mathcal{R}_{ac}$). This is related to the rate of mass accretion per unit co-moving volume ($\mathcal{R}_{acV}$) by $\mathcal{R}_{acV} = n_0 \mathcal{R}_{ac}$. The mass (or luminosity) dependence of the accretion rate means that it will be dominated by relatively massive (or luminous) galaxies, with dwarfs playing a very minor role unless the mass function is very steep.

3.4.2 Observable Quantities

In order to determine $\mathcal{R}_{mg}$ observationally, one may begin by identifying systems which are destined to merge. By combining information about the number of these systems and the timescale on which they will undergo mergers, one can estimate an overall merger rate. Specifically, if one identifies N_m ongoing mergers per galaxy, and if the average merging timescale for these systems is T_{mg}, then $\mathcal{R}_{mg} = N_m/T_{mg}$. If the mass involved in these mergers (per galaxy) is M_m, then $\mathcal{R}_{ac} = M_m/T_{mg}$.

In practice, direct measurement of these quantities is a daunting task. It is difficult to determine if a given system will merge; furthermore, estimating the merger timescale for individual systems is challenging with the limited information generally available. However, if one simply wishes to determine how the merger rate is *changing* with redshift, then the task is more man-

ageable. If one has the same definition of a merger in all samples under consideration, then it is reasonable to assume that the merger timescale is the same for these samples. In this case, we are left with the task of measuring quantities which are directly proportional to the number or mass of mergers per galaxy or per unit co-moving volume. If one wishes to consider luminosity instead of mass, the relation between mass and luminosity must either be the same at all epochs, or understood well enough to correct for the differences.

We have considered several quantities that fit this description. All involve the identification of close physical associations of galaxies. A "close companion" is defined as a neighbour which will merge within a relatively short period of time ($T_{\rm mg} \ll t_H$), which allows an estimate of the instantaneous merger/accretion rate. If a galaxy is destined to undergo a merger in the very near future, it must have a companion close at hand. One might attempt to estimate the number of mergers taking place within a sample of galaxies. For example, a close pair of galaxies would be considered one merger, while a close triple would lead to two mergers, etc. Owing to the difficulty of determining with certainty which systems are undergoing mergers, we will not use this approach. One alternative is to estimate the number of galaxies with one or more close companions, otherwise known as the pair fraction. One drawback of this approach is that close triples or higher order N-tuples complicate the analysis, since they are related to higher orders of the correlation function. This also makes it difficult to correct for the flux-limited nature of most redshift surveys. As a result, we choose to steer clear of this method also.

In this study, we choose instead to use the *number and luminosity of close companions* per galaxy. The number of close companions per galaxy, hereafter N_c, is similar in nature to the pair fraction. In fact, they are identical in a volume-limited sample with no triples or higher order N-tuples. However, N_c will prove to be much more robust and versatile. We assume that N_c is directly proportional to the number of mergers per galaxy, such that $N_m = kN_c$ (k is a constant). This pairwise statistic is preferable to the number of mergers per galaxy or the fraction of galaxies in merging systems, in that it is related, in a direct and straightforward manner, to the galaxy two-point CF and the LF (see Section 3.5). We note that it is not necessary that there be a one-to-one correspondence between companions and mergers, as long as the correspondence is the same, on average, in all samples under consideration.

Using this approach to estimate the number of mergers per galaxy, the merger rate is then given by $\mathcal{R}_{\rm mg} = kN_c/T_{\rm mg}$. The actual value of k depends on the merging systems under consideration. If one identifies a pure set of galaxy pairs, each definitely undergoing a merger, then each pair, consisting of 2 companions, would lead to one merger, giving k=0.5. For a pair sample which includes some triples and perhaps higher order N-tuples, $k < 0.5$. If the merging sample under investigation contains some systems which are not truly merging (for instance, close pairs with hyperbolic orbits), then k will also be reduced. While k clearly varies with the type of merging system used, the key is for k to be the same for all samples under consideration.

We take a similar approach with the accretion rate. We again use close companions, and in this case we simply add up the luminosity in companions,

per galaxy (L_c). Defining the mean companion mass-to-light ratio as Υ, it follows that $M_m = \Upsilon L_c$ and $\mathcal{R}_{ac} = \Upsilon L_c / T_{mg}$. When comparing different samples, any significant differences in Υ must accounted for.

3.4.3 A Simple Model of Mass Function Evolution Due to Mergers

In order to motivate further the need for merger rate measurements, and to set the stage for future work relating pair statistics to the mass and luminosity function, we develop a simple model which relates these important quantities. Suppose the galaxy mass function is given by $\phi(M,t)$. This function gives the number density of galaxies of mass M at time t, per unit mass. The model that follows can also be expressed in terms of luminosity or absolute magnitude, rather than mass.

We begin by assuming that all changes in the mass function are due to mergers. While this is clearly simplistic, this model will serve to demonstrate the effects that various merger rates can have on the mass function. In order to relate the mass function to the observable luminosity function, we further assume that mergers do not induce star formation. Again, this is clearly an oversimplification; however, this simple case will still provide a useful lower limit on the relative contribution of mergers to LF evolution. Finally, we assume that merging is a binary process.

Following Bahcall and Tremaine (1988), we consider how $\phi(M,t)$ evolves as the universe ages from time t to time $t + \Delta t$. Each merger will remove two galaxies from the mass function, and produce one new galaxy. Let $\Delta\phi(M,\Delta t)_{out}$ represent the decrease in the mass function due to galaxies

removed by mergers, while $\Delta\phi(M,\Delta t)_{\rm in}$ gives the increase due to the remnants produced by these mergers. Evolution in the mass function can then be given by

$$\phi(M,t+\Delta t) = \phi(M,t) - \Delta\phi(M,\Delta t)_{\rm out} + \Delta\phi(M,\Delta t)_{\rm in}. \qquad (3.1)$$

We model this function by considering all galaxy pairs, along with an expression for the merging likelihood of each. Let $p(M,M',\Delta t)$ denote the probability that a galaxy of mass M will merge with a galaxy of mass M' in time interval Δt. In order to estimate $\Delta\phi(M,\Delta t)_{\rm out}$, we need to take all galaxies of mass M, and integrate over all companions, yielding

$$\Delta\phi(M,\Delta t)_{\rm out} = \int_0^\infty \phi(M,t)\phi(M',t)p(M,M',\Delta t)dM'. \qquad (3.2)$$

We devise a comparable expression for $\Delta\phi(M,\Delta t)_{\rm in}$ by integrating over all pairs with end−products of mass M. This is achieved by considering all pairs with component of mass $M-M'$ and M', such that

$$\Delta\phi(M,\Delta t)_{\rm in} = \int_0^\infty \phi(M-M',t)\phi(M',t)p(M-M',M',\Delta t)dM'. \qquad (3.3)$$

We can also express Equation 3.1 in terms of the pair statistics outlined in Section 3.4.2. If one considers close companions of mass $M' \leq \infty$ next to primary galaxies of mass M, the volume merger rate can be expressed as $\mathcal{R}_{{\rm mg}_V}(M)$, yielding

$$\Delta\phi(M,\Delta t)_{\rm out} = \mathcal{R}_{{\rm mg}_V}(M)\Delta t. \qquad (3.4)$$

Similarly, if one defines a merger remnant statistic, $\mathcal{R}_{{\rm mr}_V}(M)$, to be the comoving number density of merger remnants per unit time corresponding to

these same mergers, then

$$\Delta\phi(M, \Delta t)_{\rm in} = \mathcal{R}_{\rm mrv}(M)\Delta t. \tag{3.5}$$

Therefore, it is possible, in principle, to use pair statistics to measure the evolution in the mass or luminosity function due to mergers. However, current pair samples are too small to permit useful pair statistics for different mass combinations. In addition, present day observations of close pairs are not of sufficient detail to determine the proportion of pairs that will result in mergers (factor k in previous section). Moreover, timescale estimates for these mergers are not known with any degree of certainty. Hence, useful observations of mass function evolution due to mergers will have to wait for improved pair samples and detailed estimates of merger timescales.

3.5 A New Approach to Measuring Pair Statistics

In this section, we outline the procedure for measuring the mean number (N_c) and luminosity (L_c) of close companions around a sample of galaxies with measured redshifts. We begin by defining these statistics in real space, demonstrating how they are related to the galaxy LF and CF. We then show how these statistics can be applied in redshift space.

3.5.1 Pair Statistics in Real Space

In this study, we will measure pair statistics for a complete low-redshift sample of galaxies (SSRS2). However, we wish to make these statistics applicable

to a wide variety of redshift samples. We would like this method to be useful for studies of minor mergers, where one is interested in faint companions around bright galaxies. In addition, these techniques should be adaptable to redshift samples with varying degrees of completeness (that is, with redshifts not necessarily available for every galaxy). Therefore, in the following analysis, we treat host galaxies and companions differently.

Consider a primary sample of N_1 host galaxies with absolute magnitudes $M \leq M_1$, lying in some volume V. Suppose this volume also contains a secondary sample of N_2 galaxies with $M \leq M_2$. In the general case, the primary and secondary samples may have galaxies in common. This includes the special case in which the two samples are identical. If $M_1 \approx M_2$, this will tend to probe major mergers. If M_2 is chosen to be significantly fainter than M_1, this will allow for the study of minor mergers. We assume here that both samples are complete to the given absolute magnitude limits; in Section 3.6, we extend the analysis from volume-limited samples to those that are flux-limited.

We wish to determine the mean number and luminosity of companions (in the secondary sample) for galaxies in the primary sample. In real space, we define a close companion to be one that lies at a true physical separation of $r \leq r^{\max}$, where $r^{\max}$ is some appropriate maximum physical separation. To compute the observed mean number (N_c) and luminosity (L_c) of companions, we simply add up the number (N_{c_i}) and luminosity (L_{c_i}) of companions for each of the N_1 galaxies in the primary sample, and then compute the mean.

Therefore,

$$N_c(M \leq M_2) = \sum_{i=1}^{N_1} N_{c_i}/N_1 \tag{3.6}$$

and

$$L_c(M \leq M_2) = \sum_{i=1}^{N_1} L_{c_i}/N_1. \tag{3.7}$$

We can also estimate what these statistics should be, given detailed knowledge of the galaxy two-point CF ξ and the LF $\phi(M)$. This is necessary if one wishes to relate these pair statistics to measurements on larger scales. Consider a galaxy in the primary sample with absolute magnitude M_i at redshift z_i. We would first like to estimate the number and luminosity of companions lying in a shell at physical distance (*proper* co-ordinates) $r \leq r_{ij} \leq r + dr$ of this primary galaxy. To make this estimate, we need to know the mean density of galaxies (related to the LF), and the expected overdensity in the volume of interest (given by the CF). The mean physical number density of galaxies at redshift z_i in the secondary sample, with absolute magnitudes $M \leq M_j \leq M + dM$, is given by

$$n_2(z_i, M)dM = (1 + z_i)^3 \phi(M, z_i)dM, \tag{3.8}$$

where $\phi(M, z_i)$ is the differential galaxy LF, which specifies the *co-moving* number density of galaxies at redshift z_i, in units of $h^3\mathrm{Mpc}^{-3}\mathrm{mag}^{-1}$. The actual density of objects in the region of interest is determined by multiplying the mean density by $(1+\xi)$, where ξ is the overdensity given by the two-point CF (Peebles 1980). In general, ξ depends on the pair separation r, the mean redshift z_i, the absolute magnitude of each galaxy (M_i, M_j), and the orbits involved, specified by components parallel ($v_\parallel$) and perpendicular ($v_\perp$)

to the line of sight. It follows that the mean number of companions with $M \leq M_j \leq M + dM$ and $r \leq r_{ij} \leq r + dr$ is given by

$$N_{c_i}(z_i, M_i, M, r, v_\perp, v_\parallel) dM dr = n_2(z_i, M) dM [1 + \xi(r, z_i, M_i, M, v_\perp, v_\parallel)] 4\pi r^2 dr. \quad (3.9)$$

We must now integrate this expression for all companions with $M \leq M_2$ and $r \leq r^{\max}$. Integration over the LF yields

$$n_2(z_i, M \leq M_2) = (1 + z_i)^3 \int_{-\infty}^{M_2} \phi(M, z_i) dM. \quad (3.10)$$

Integration over the CF is non-trivial, because of the complex nature of $\xi(r, z_i, M_i, M, v_\perp, v_\parallel)$. With redshift samples that are currently available, it is not possible to measure this dependence accurately for the systems of interest. Hence, we must make three important assumptions at this stage. First, we assume that ξ is independent of luminosity. Later in the chapter, we demonstrate empirically that this is a reasonable assumption, provided one selects a sample with appropriate ranges in absolute magnitude (see Section 3.6.1). Secondly, we assume that the distribution of velocities is isotropic. If one averages over a reasonable number of pairs, this is bound to be true, and therefore ξ is independent of $v_\perp$ and $v_\parallel$. Finally, we assume that the form of the CF, as measured on large scales, can be extrapolated to the small scales of interest here. This assumption applies only to the method of relating pairs to large scale measures, and not to the actual measurement of pair statistics.

It is now straightforward to integrate Equation 3.9. The mean number of companions with $M \leq M_2$ and $r \leq r^{\max}$ for a primary galaxy at redshift

z_i is given by

$$N_{c_i}(z_i, M \leq M_2, r \leq r^{\max}) = n_2(z_i, M \leq M_2) \int_0^{r^{\max}} [1 + \xi(r, z_i)] 4\pi r^2 dr \quad (3.11)$$

We derive an analogous expression for the mean luminosity in companions. The integrated luminosity density is given by

$$j_2(z_i, M \leq M_2) = (1 + z_i)^3 \int_{-\infty}^{M_2} \phi(M, z_i) L(M) dM, \quad (3.12)$$

where

$$L(M) = 10^{-0.4(M - M_\odot)} L_\odot. \quad (3.13)$$

Therefore,

$$L_{c_i}(z_i, M \leq M_2, r \leq r^{\max}) = j_2(z_i, M \leq M_2) \int_0^{r^{\max}} [1 + \xi(r, z_i)] 4\pi r^2 dr \quad (3.14)$$

Given measurements of the CF on large scales, it is then straightforward to integrate these equations to arrive at predicted values of N_{c_i} and L_{c_i}.

It is important to note that these statistics are directly dependent on M_2, which affects the mean density of galaxies in the secondary sample. This is different from statistics such as the correlation function, which are independent of density. Hence, this serves as a reminder that we must exercise caution when choosing our samples, to ensure that differences in the pair statistics (and hence in the merger and accretion rates) are not simply due to apparent density differences resulting from selection effects. In addition, note that the choice of M_1 has no density-related effects on N_c and L_c.

3.5.2 Dynamical Pairs in Redshift Space

While it is preferable to identify companions based on their true physical pair separation, this is clearly not feasible when dealing with data from red-

shift surveys. In the absence of independent distance measurements for each galaxy, one must resort to identifying companions in redshift space. In this section, we outline a straightforward approach for measuring our new pair statistics in redshift space. We then attempt to relate these statistics to their counterparts in real space.

For any given pair of galaxies in redshift space, one can compute two basic properties which describe the intrinsic pair separation : the projected physical separation (hereafter r_p) and the rest-frame relative velocity along the line of sight (hereafter Δv). For a pair of galaxies with redshifts z_i (primary galaxy) and z_j (secondary), with angular separation θ, these quantities are given by $r_p = \theta d_A(z_i)$ and $\Delta v = c|z_j - z_i|/(1 + z_i)$, where $d_A(z_i)$ is the angular diameter distance at redshift z_i. Note that r_p gives the projected separation at the redshift of the primary galaxy.

We define a close companion as one in which the separation (both projected and line-of-sight) is less than some appropriate separation, such that $r_p \leq r_p^{max}$ and $\Delta v \leq \Delta v^{max}$. The line-of-sight criterion depends on both the physical line-of-sight separation and the line-of-sight peculiar velocity of the companion. It is of course not possible to determine the relative contributions of these components without distance information. However, for the small companion separations we will be concerned with, the peculiar velocity component is likely to be dominant in most cases. Hence, this criterion serves primarily to identify companions with low peculiar velocities. While this is fundamentally different from the pure separation criterion used in real space, it too will serve to identify companions with the highest likelihood of undergoing imminent mergers. Using this definition of a close companion, it

is straightforward to compute N_c and L_c, using Equations 3.6 and 3.7. Thus, the complexities of redshift space do not greatly complicate the computation of these pair statistics.

As in real space, we wish to relate these statistics to measurements on larger scales, given reasonable assumptions about the LF and CF. The situation is more complicated in redshift space, and therefore involves additional assumptions. We stress, however, that these assumptions apply only to the method of relating pair statistics to large scale measures, and not to the measured pair statistics themselves. To outline an algorithm for generating these predictions, we follow the approach of the previous section. We begin by modifying Equations 3.11 and 3.14, integrating over the new pair volume defined in redshift space. In order to do this, we use the two dimensional correlation function in redshift space, $\xi_2(r_p, r_v, z)$, giving

$$N_{c_i}(z_i, M \leq M_2, r_p \leq r_p^{\max}, |r_v| \leq r_v^{\max}) = n_2(z_i, M \leq M_2) \int_{-r_v^{\max}}^{r_v^{\max}} \int_0^{r_p^{\max}} [1 + \xi_2(r_p, r_v, z_i)] 2\pi r_p dr_p dr_v \qquad (3.15)$$

and

$$L_{c_i}(z_i, M \leq M_2, r_p \leq r_p^{\max}, |r_v| \leq r_v^{\max}) = j_2(z_i, M \leq M_2) \int_{-r_v^{\max}}^{r_v^{\max}} \int_0^{r_p^{\max}} [1 + \xi_2(r_p, r_v, z_i)] 2\pi r_p dr_p dr_v. \qquad (3.16)$$

The two dimensional correlation function is the convolution of the velocity distribution in the redshift direction, $F(v_z)$, with the spatial correlation function $\xi(r, z)$, given by

$$\xi_2(x_p, x_v, z) = \int_{-\infty}^{\infty} \xi(\sqrt{x_p^2 + y^2}, z) F(H(z)[y - x_v]) dy. \qquad (3.17)$$

Here, $H(z)$ is the Hubble constant at redshift z, given by $H(z) = H_0(1 + z)\sqrt{1 + \Omega_0 z}$. We have ignored the effect of infall velocities, which must be taken into account at larger radii but is an acceptable approximation for small separations. If the form of the CF and LF are known, it is straightforward to integrate Equations 3.15 and 3.16, yielding predictions of N_c and L_c.

3.5.3 Physical Pairs in Redshift Space

It is not always possible to have precise redshifts for all galaxies of interest in a sample. A common scenario with redshift surveys is to have redshifts available for a subset of galaxies identified in a flux-limited photometric sample. The photometric sample used to select galaxies for follow-up spectroscopy probes to fainter apparent magnitudes than the spectroscopic sample. In addition, the spectroscopic sample may be incomplete, even at the bright end of the sample. In this section, we will describe the procedure for applying pair statistics to this class of samples.

Suppose the primary sample is defined as all galaxies in the spectroscopic sample with absolute magnitudes $M \leq M_1$. The secondary sample consists of all galaxies lying in the photometric sample, regardless of whether or not they have measured redshifts. Once again, there may be some overlap between the primary and secondary samples. We must now identify close pairs. For each primary-secondary pair, we can compute r_p in precisely the same manner as before (see previous section), since we need only the redshift of the primary galaxy and the angular separation of the pair. However, we are no longer able to compute the relative velocity along the line of sight, since this requires redshifts for both members of the pair. Thus, we do

not have enough information to identify close dynamical pairs. However, it is still possible to determine, in a statistical manner, how many physically associated companions are present. This is done by comparing the number (or luminosity) of observed companions with the number (or luminosity) expected in a random distribution.

As stressed in Section 3.5.1, pair statistics depend on the minimum luminosity M_2 imposed on the secondary sample. While we are now unable to compute the actual luminosity for galaxies in the secondary sample, we must still impose M_2 if the ensuing pair statistics are to be meaningful. To do this, we make use of the fact that all physical companions must lie at approximately the same redshift as the primary galaxy under consideration. Therefore, M_2 corresponds to a limiting *apparent* magnitude m_2 at redshift z_i, such that

$$m_2 = M_2(z_i) - 5\log h + 25 + 5\log d_L(z_i) + k(z_i), \qquad (3.18)$$

where $d_L(z_i)$ is the luminosity distance at redshift z_i, and $k(z_i)$ is the k-correction.

To begin, one finds all observed close companions with $m \leq m_2(z_i)$, using only the r_p criterion. This results in the quantities $N_c^{\rm D}$ and $L_c^{\rm D}$, where the "D" superscript denote companions found in the data sample. One must then estimate the number ($N_c^{\rm R}$) and luminosity ($L_c^{\rm R}$) of companions expected at random. The final pair statistics for close physical companions are then given by $N_c = N_c^{\rm D} - N_c^{\rm R}$ and $L_c = L_c^{\rm D} - L_c^{\rm R}$.

We will now describe how to predict these statistics using the known LF and CF. This is relatively straightforward, since the excess ξ given by the

CF is determined by the relative proportions of real and random companions. The pair statistics are once again integrals over the two dimensional CF in redshift space, as specified by Equations 3.15 and 3.16. In the "$1 + \xi$" term, the first part gives the random contribution, while the second gives the excess over random. Thus, these pair statistics give the true density of companions, rather than the "excess" density. This is intentional, since mergers will occur even in an uncorrelated, randomly distributed sample of galaxies. At the small separations of interest, usually less than 1% of the correlation length, the difference between the mean density and the mean overdensity is less than about 0.01% in real space. For practical measurements in redshift space, where $r_v = \Delta v H(z)^{-1}$ is of order the correlation length, the background contribution is substantially larger than real space, but still amounts to less than 1%. Thus, for the close pairs considered in this study, it is reasonable to ignore the contribution that random companions make to the sample of physical companions. That is, we take $1 + \xi \approx \xi$. This allows us to relate the predictions to the measured pair statistics set out above. In principle, Equations 3.15 and 3.16 can be integrated over the range $-\infty < r_v < \infty$ to obtain predictions of N_c and L_c.

3.5.4 Application to Volume-limited Monte Carlo Simulations

To illustrate the concepts introduced so far, and to emphasize how these statistics depend on M_2, we apply these techniques to volume-limited Monte Carlo simulations, which mimic the global distribution of galaxies in the SSRS2 North and South catalogs. Using q_0=0.5, galaxies are distributed

randomly within the co-moving volume enclosed by $0.005 \leq z \leq 0.05$ and the SSRS2 boundaries on the sky (see Section 3.3). All peculiar velocities are set to zero. To create a volume limited sample, we impose a minimum luminosity of $M_B=-16$, and assign luminosities using the SSRS2 LF (Marzke et al. 1998), which has Schechter function parameters $M_* - 5\log h=-19.43$, $\alpha=-1.12$, and $\phi_* = 0.0128\ h^3\mathrm{Mpc}^{-3}\mathrm{mag}^{-1}$. An arbitrarily large number of galaxies can be generated, which is of great assistance when looking for small systematic effects. We produce 16000 galaxies in the South, and 8070 in the North; this gives the same density of galaxies in both regions.

Using these simulations, we compute N_c and L_c. For comparison, we will also compute pair statistics that are representative of the traditional pair fraction. We define a statistic f_p, which is directly comparable to N_C, but will not be corrected for flux-limit biases. For volume limited samples, $f_p=N_c$. As these galaxies are distributed randomly (as opposed to real galaxies which are clustered), close pairs are relatively rare. To ensure a reasonable yield of pairs, we use a pair definition of $r_p^{\mathrm{max}}=1\ h^{-1}$ Mpc and $\Delta v^{\mathrm{max}}=1000$ km/s. We note that there are no peculiar velocities in these simulations; hence, the Δv^{max} criterion provides upper and lower limits on the line-of-sight distance to companions. Also, recall from the preceding section that the choice of M_1 has no effect on the pair statistics if clustering is independent of luminosity. Hence, we choose $M_1=M_2$, which maximizes the size of the primary sample, and therefore minimizes the errors in N_c and L_c.

With these assumptions, we compute pair statistics for a range of choices of M_2. Errors are computed using the Jackknife technique. For this resampling method, partial standard deviations, δ_i, are computed for each ob-

ject by taking the difference between the quantity being measured, f, and the same quantity with the i^{th} galaxy removed from the sample, f_i, such that $\delta_i = f - f_i$. For a sample of N galaxies, the variance is given by $[(N-1)/N \sum_i \delta_i^2]^{1/2}$ (Efron 1981; Efron & Tibshirani 1986). Results are given in Figure 3.1. All three statistics continue to increase as M_2 becomes fainter. f_p is identical to N_C, as required for these volume-limited simulations. N_c and f_p diverge at faint magnitudes, while L_c is seen to converge. This behaviour is a direct consequence of the shape of the LF; N_c converges for $\alpha > -1$, while L_c converges for $\alpha > -2$. The existence and magnitude of these trends clearly demonstrate the need to specify M_2 when measuring pair statistics.

3.6 Application to Flux Limited Samples

The preceding section gives a prescription for computing pair statistics in volume-limited samples. Using this approach, it is straightforward to compare pair statistics in different volume-limited samples. However, redshift surveys are generally flux-limited. By defining a volume-limited sample within such a survey, one must discard a large proportion of the data. In this section, we will outline how these pair statistics can be applied to flux-limited surveys.

Pair statistics necessarily depend on both clustering and mean density, as shown by Equations 3.15 and 3.16. In a flux-limited sample, both clustering and mean density will vary throughout the sample. We will use these equations to account for redshift-dependent density variations, and we will

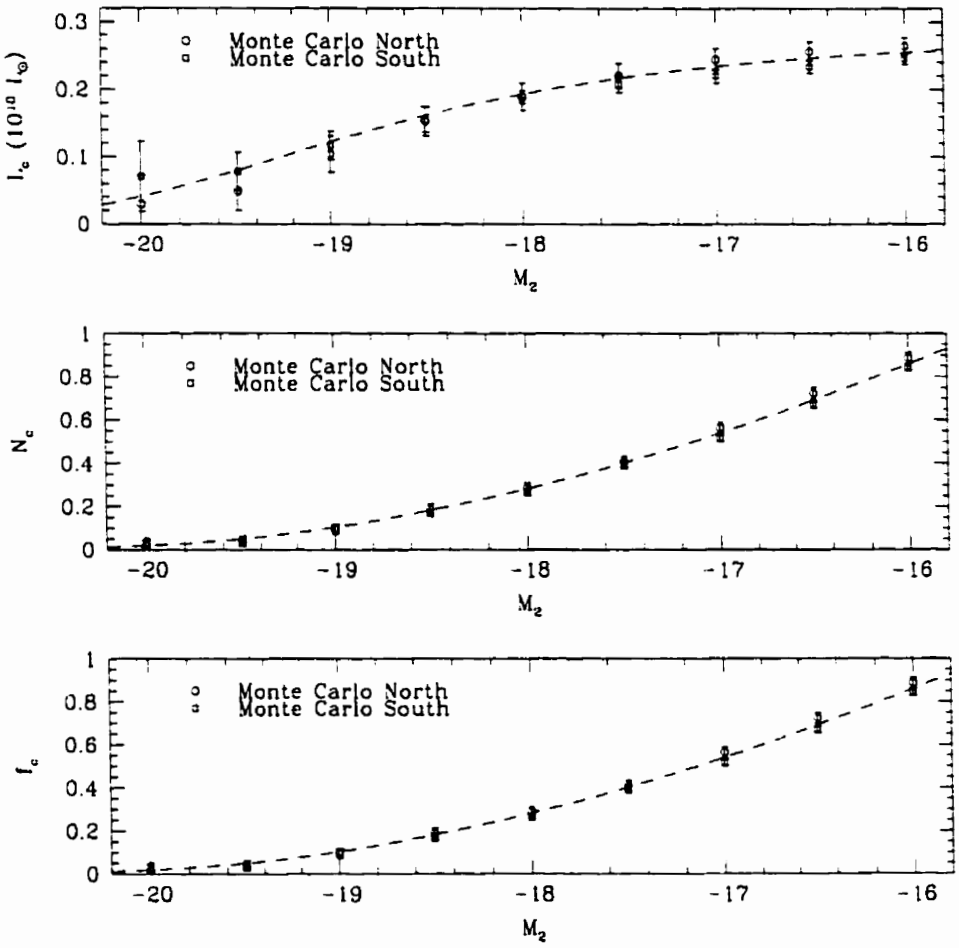

Figure 3.1: Pair statistics are computed for the volume-limited Monte Carlo simulations. Three pair statistics (f_p, N_c, and L_c) are given, for a range of choices of M_2, with M_1=M_2. Error bars are computed using the Jackknife technique. The dashed lines are the relations predicted using the input SSRS2 luminosity function, and normalized to match the data at M_2=−16.

demonstrate how to minimize the effects of clustering differences. These techniques will then be tested with Monte Carlo simulations.

3.6.1 Dependence on Clustering

By removing the fixed luminosity limit, the overall distribution of galaxy luminosities will vary with redshift within the sample, and the mean luminosity of the sample will differ from the volume limited sample. However, galaxy clustering is known to be luminosity dependent. Measures of the galaxy correlation function (e.g., Loveday et al. 1995, Willmer et al. 1998), power spectrum (e.g., Vogeley 1993), and counts in cells (Benoist et al. 1996) all find that luminous galaxies ($L > L_*$) are more clustered than sub-L_* galaxies, typically by a factor of ~ 2. This increase in clustering may be particularly strong (factor ~ 4) for very luminous galaxies ($M_B < -21$). Clearly, this cannot be ignored when computing pair statistics. In principle, this could be incorporated into the measurement of these pair statistics. However, available pair samples are too small to measure this dependence. We choose instead to minimize the effects of luminosity-dependent clustering by avoiding the extremes. First, we impose a maximum redshift $z_{\rm max}$ on the sample. This constraint eliminates the high redshift end of the sample, which includes only intrinsically bright galaxies. Secondly, we exclude all galaxies below some minimum luminosity $M_{\rm faint}$; this removes the most extreme low luminosity galaxies. Having reduced the effects of luminosity segregation, we then assume that the remaining differences will not have a significant effect on the measured pair statistics. In Section 3.8.3, we use the SSRS2 sample to verify this assumption empirically.

3.6.2 Dependence on Limiting Absolute Magnitude

In Section 3.5, we demonstrated that these pair statistics are meaningful only if one specifies the minimum luminosity of the primary and secondary samples. For a flux limited sample, however, the minimum luminosity of the sample increases with redshift. One must therefore decide on a representative minimum luminosity, and account for differences between the desired minimum luminosity and the minimum imposed by the apparent magnitude limit of the sample. If the LF is known, this can be achieved by weighting each galaxy appropriately. In this section, we outline a weighting scheme which makes this correction.

Weighting of Secondary Sample

Consider a flux−limited sample in which host galaxies are placed at a variety of redshifts. Those at low redshift will have the greatest probability of having close companions that lie above the flux limit, since the flux limit corresponds to an intrinsic luminosity that is fainter than that for galaxies at higher redshift. If we wish to avoid an inherent bias in the pair statistics, we must correct for this effect. Furthermore, we have demonstrated the importance of specifying a limiting absolute magnitude for companions (M_2) when computing pair statistics. Therefore, we must attempt to correct the pair statistics to the values that would have been achieved for a volume−limited secondary sample with $M \leq M_2$. Qualitatively, this correction should assign greater importance (or weight) to the more rare companions found at the high redshift end of the flux−limited sample. To make this correction as rig-

orous as possible, we will use the galaxy LF. By integrating the LF down to a given absolute magnitude, one can obtain an estimate of the mean number or luminosity density of galaxies in the sample. By performing this integration at a range of redshifts, and imposing a limiting absolute magnitude that corresponds to the flux−limit of the survey, it is possible to quantify how the mean density is affected by the flux−limit. This information can be used to remove this unwanted bias from the pair statistics.

We assign a weight to each galaxy in the secondary sample, which renormalizes the sample to the density corresponding to $M \leq M_2$. We must first determine $M_{\rm lim}(z_i)$, which gives the limiting absolute magnitude allowed at redshift z_i. At most redshifts, this is imposed by the limiting apparent magnitude m, such that $M_{\rm lim}(z_i) = m - 5\log d_L(z) - 25 - k(z)$. At the low redshift end of the sample, however, $M_{\rm faint}$ (defined in § 3.6.1) will take over. That is, the limiting absolute magnitude used for identifying galaxies in the secondary sample is given by

$$M_{\rm lim}(z_i) = \max[M_{\rm faint}, m - 5\log d_L(z) - 25 - k(z)]. \qquad (3.19)$$

The selection function, denoted $S(z)$, is defined as the ratio of densities in flux-limited versus volume-limited samples. This function, given in terms of number density ($S_N(z)$) and luminosity density ($S_L(z)$), is as follows :

$$S_N(z_i) = \frac{\int_{-\infty}^{M_{\rm lim}(z_i)} \phi(M)dM}{\int_{-\infty}^{M_2} \phi(M)dM} \qquad (3.20)$$

$$S_L(z_i) = \frac{\int_{-\infty}^{M_{\rm lim}(z_i)} \phi(M)L(M)dM}{\int_{-\infty}^{M_2} \phi(M)L(M)dM}, \qquad (3.21)$$

where $L(M)$ is defined in Equation 3.13. In order to recover the correct pair statistics, each companion must be assigned weights $w_{N2}(z_i) = 1/S_N(z_i)$ and

$w_{L2}(z_i) = 1/S_L(z_i)$. The total number and luminosity of close companions for the i^{th} primary galaxy, computed by summing over the j galaxies satisfying the "close companion" criteria, is given by $N_{c_i} = \sum_j w_{N2}(z_j)$ and $L_{c_i} = \sum_j w_{L2}(z_j)L_j$ respectively. By applying this weighting scheme to all galaxies in the secondary sample, we will retrieve pair statistics that correspond to a volume–limited sample with $M \leq M_2$.

Weighting of Primary Sample

The above weighting scheme ensures that the number and luminosity of companions found around each primary galaxy is normalized to M_2. However, these estimates are obviously better for galaxies at the low redshift end of the primary sample, since they will have the largest number of *observed* companions. Recall that N_c and L_c are quantities that are averaged over a sample of primary galaxies. In order to minimize the errors in these statistics, we assign weights to the primary galaxies (denoted $w_{N1}(z_i)$ and $w_{L1}(z_i)$) which are inversely proportional to the square of their uncertainty. If the observed number and luminosity of companions around the i^{th} primary galaxy are given by $N_i(obs)$ and $L_i(obs)$ respectively, and if we assume that the uncertainties are determined by Poisson counting statistics, then $N_{c_i} = w_{N2}(z_i)N_i(obs) \pm w_{N2}(z_i)\sqrt{N_i(obs)}$ and $L_{c_i} = w_{L2}(z_i)L_i(obs) \pm w_{L2}(z_i)\sqrt{L_i(obs)}$. On average, these quantities will be related to expectation values $< N_c >$ and $< L_c >$ by $< N_c >= w_{N2}(z_i)N_i(obs)$ and $< L_c >= w_{L2}(z_i)L_i(obs)$. Combining these relations yields

$$w_{N1}(z_i) = \frac{1}{N_i(obs)w_{N2}(z_i)^2} = \frac{1}{< N_c > w_{N2}(z_i)} \propto w_{N2}(z_i)^{-1} \qquad (3.22)$$

$$w_{L1}(z_i) = \frac{1}{L_i(obs)w_{L2}(z_i)^2} = \frac{1}{< L_c > w_{L2}(z_i)} \propto w_{L2}(z_i)^{-1} \qquad (3.23)$$

That is, the optimal weighting is the reciprocal of the weighting scheme used for companions. Therefore, weights $w_{N1}(z_i) = S_N(z_i)$ and $w_{L1}(z_i) = S_L(z_i)$ should be assigned to primary galaxies. The pair statistics are then computed as follows :

$$N_c = \frac{\sum_i w_{N1}(z_i)N_{c_i}}{\sum_i w_{N1}(z_i)} \qquad (3.24)$$

$$L_c = \frac{\sum_i w_{L1}(z_i)L_{c_i}}{\sum_i w_{L1}(z_i)}. \qquad (3.25)$$

It is worth noting that, for a close pair, both galaxies will lie at roughly the same redshift, meaning that $w_1(z_i) \times w_2(z_j) \approx 1$. We choose not to make this approximation, in order to keep these relations valid for pairs that are not close, and to allow for future application to pairs with additional selection weights. However, we stress that, with or without this approximation, the primary weights in the denominator provide an overall correction for the flux limit, unlike the traditional pair fraction. Note also that, for a volume-limited sample, weights for all galaxies in the primary and secondary samples are equal, reducing these equations to $N_c = \sum N_{c_i}/N_1$ and $L_c = \sum L_{c_i}/N_1$, as defined in Section 3.5.1.

Boundary Effects

A small correction must be made to these weights if a primary galaxy lies close to a part of the sky that is not covered by the survey. This will happen if a galaxy lies close to the boundaries on the sky, or close to the minimum

or maximum redshift allowed. If this is the case, it is possible that close companions will be missed, leading to an underestimate of the pair statistics. Therefore, we must account for these effects.

First, we consider galaxies lying close to the survey boundaries on the sky, as defined in Section 3.3. For each galaxy in the primary sample, we compute the fraction of sky with $r_p^{\rm min} \leq r_p \leq r_p^{\rm max}$ that lies within the survey boundaries. This fraction will be denoted f_b. For SSRS2, our usual choices of $r_p^{\rm min}$ and $r_p^{\rm max}$ (see § 3.7) make this a very small effect, with f_b=1 for 99.75% of galaxies in the primary sample. Having measured f_b for each galaxy in the primary sample, we must incorporate this into the measurement of the pair statistics. The first task is to ensure that we correct the number of companions to match what would be expected if coverage was complete. We do this by assigning each companion a boundary weight $w_{b_2} = 1/f_b$, where f_b is associated with its host galaxy from the primary sample. By multiplying each companion by its boundary weight, we will recover the correct number of companions. We must also adjust weights for the primary galaxies. Following the method described in the previous section, we wish to give less weight to galaxies that are likely to have fewer observed companions. Therefore, each primary galaxy is assigned a boundary weight $w_{b_1} = f_b$.

We now consider galaxies which lie near the survey boundaries along the line of sight. If a primary galaxy lies close to the minimum or maximum redshift allowed, it is possible that we will miss companions because they lie just across this redshift boundary. In order to account correctly for this effect, one would need to model the velocity distribution of companions. As this requires several assumptions, we choose instead to exclude all companions

that lie between a primary galaxy and its nearest redshift boundary, provided the boundary lies within $\Delta v^{\max}$ of the primary galaxy. To account for this exclusion, we assume that the velocity distribution is symmetric along the line of sight. Thus, as we will miss half of the companions for these galaxies, we assign a weight of $w_{2_v}=2$ to any companions found in the direction opposite to the boundary. We must also consider how to weight the primary galaxies themselves. Clearly, primary galaxies close to the redshift boundaries will be expected to have half as many *observed* companions as other primary galaxies. To minimize the errors in computing the pair statistics, we assign these primary galaxies weights $w_{v_1}=0.5$.

To summarize, weights for companions in the secondary sample are given by

$$w_{N_2} = S_N(z_i)^{-1} w_{b_2} w_{v_2}, \tag{3.26}$$

$$w_{L_2} = S_L(z_i)^{-1} w_{b_2} w_{v_2}, \tag{3.27}$$

while primary galaxies are assigned weights

$$w_{N_1} = S_N(z_i) w_{b_1} w_{v_1}, \tag{3.28}$$

$$w_{L_1} = S_L(z_i) w_{b_1} w_{v_1}. \tag{3.29}$$

3.6.3 Confirmation Using Monte Carlo Simulations

We will now perform a test to see if this weighting scheme achieves the desired effects. To do this, we will use flux-limited Monte Carlo simulations, for which the intrinsic density and clustering are fixed. Therefore, the *intrinsic* pair statistics do not depend on redshift or luminosity. If the secondary sample

weights are correct, the measured pair statistics will be the same everywhere (within the measurement errors), regardless of redshift or luminosity. We will also check to see if the weights for the primary sample are correct. If they are, the errors on the pair statistics will be minimized, as desired.

The flux-limited Monte Carlo simulations were generated in a similar manner to the simulations described in Section 3.5.4; however, a limiting apparent magnitude of $m_B \leq 15.5$ was imposed. Sample sizes of 8000 (South) and 4035 (North) were used, providing a good match to the overall density in SSRS2. The resulting simulations are similar to SSRS2 in all respects, except for the absence of clustering. We have already established how the pair statistics depend on the choice of M_1 and M_2. In the following analysis, we choose $M_2{=}M_1{=}-19$. In Section 3.6.1, we outlined reasons for imposing a minimum luminosity ($M_{\rm faint}$) and maximum redshift ($z_{\rm max}$). Here, we demonstrate how these parameters affect N_c and L_c. For comparison, we will also compute f_p, for which $w_{N_1}{=}w_{N_1}{=}1$. This will provide some insight into the behaviour of the traditional (uncorrected) pair fraction.

These tests are most straightforward if the intrinsic pair statistics are the same everywhere in the enclosed volume. This is not quite true for these simulations, however. Galaxies are distributed randomly within the enclosed *co-moving* volume. As a result, the physical density varies with redshift as $(1+z)^3$. In addition, the volume element encompassed by the line-of-sight pair criterion Δv varies with redshift as $(1{+}z)^{-3/2}$ for $q_0{=}0.5$. In order to have the simulations mimic a sample with universal pair statistics, we normalize the sample for these effects by weighting each galaxy by $(1+z)^{-3/2}$. We stress that this is done only for the Monte Carlo simulations. One should

not apply either of these corrections to real redshift data.

In Figure 3.2, the pair statistics are computed for a range of $M_{\rm faint}$. It is clear that both N_c and L_c are independent of this choice, within the errors. This verifies that we have correctly accounted for the biases introduced by the apparent magnitude limit. In contrast, f_p is seen to have a strong dependence on $M_{\rm faint}$. As expected, f_p increases as $M_{\rm faint}$ becomes fainter, due to the increase in sample density. We stress that this does not happen with N_c and L_c because both statistics are corrected to a fixed limiting absolute magnitude (M_2).

It is also important to verify that N_c and L_c do not depend on redshift. As expected, Figure 3.3 shows that both N_c and L_c are independent of the choice of $z_{\rm max}$. On the other hand, f_p decreases with redshift. This is expected, since the high redshift end of an apparent magnitude sample has the lowest apparent density.

Finally, we demonstrate that the weighting scheme used for the primary sample (§ 3.6.2) does in fact minimize errors in N_c and L_c. Recall that the weighting used was the reciprocal of the weights for the secondary sample. Here we will assume that $w_{N1} \propto w_{N2}(z_i)^x$ and $w_{L1} \propto w_{L2}(z_i)^x$. In Section 3.6.2, justification was given for setting $x=-1$. Here, we will allow x to vary, in order to investigate empirically which value minimizes the errors. Special cases of interest are $x=0$ (no weighting) and $x=1$ (same weighting as *secondary* sample). The results are given in Figure 3.4. The relative errors in N_c and L_c reach a minimum at $x \sim -1$, as expected. Errors are $\sim 40\%$ larger if no weighting is used ($x=0$). For $x=1$, errors are much larger, increasing by nearly a factor of 5. While errors increase dramatically for $x \geq 0$,

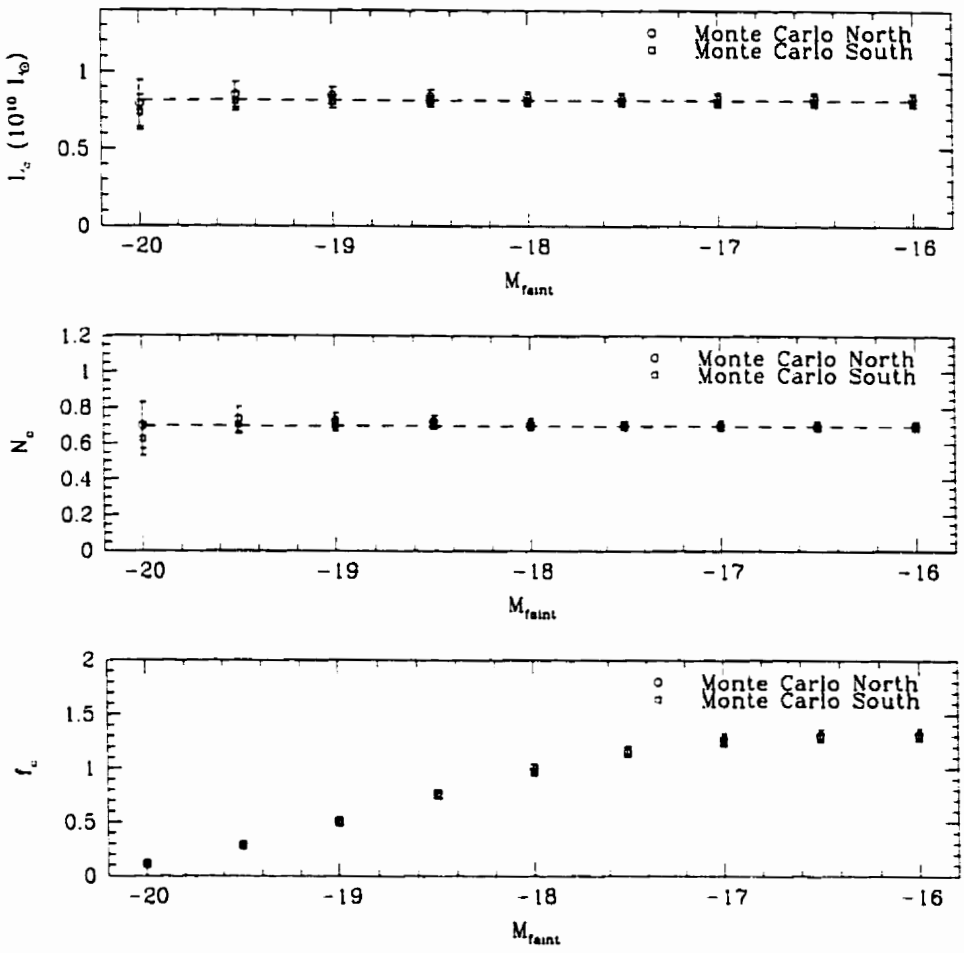

Figure 3.2: Pair statistics are computed for the flux-limited Monte Carlo simulations. Three pair statistics (f_p, N_c, and L_c) are given, for a range of choices of minimum luminosity $M_{\rm faint}$, with M_2=M_1=-19. Error bars are computed using the Jackknife technique. f_p exhibits a systematic increase with $M_{\rm faint}$. This is a consequence of not correcting for the corresponding increase in mean galaxy number density. This bias is taken into account when computing N_c and L_c. The horizontal dashed lines match the data at M_{faint}=-16, and demonstrate that N_c and L_c do not depend on M_{faint}.

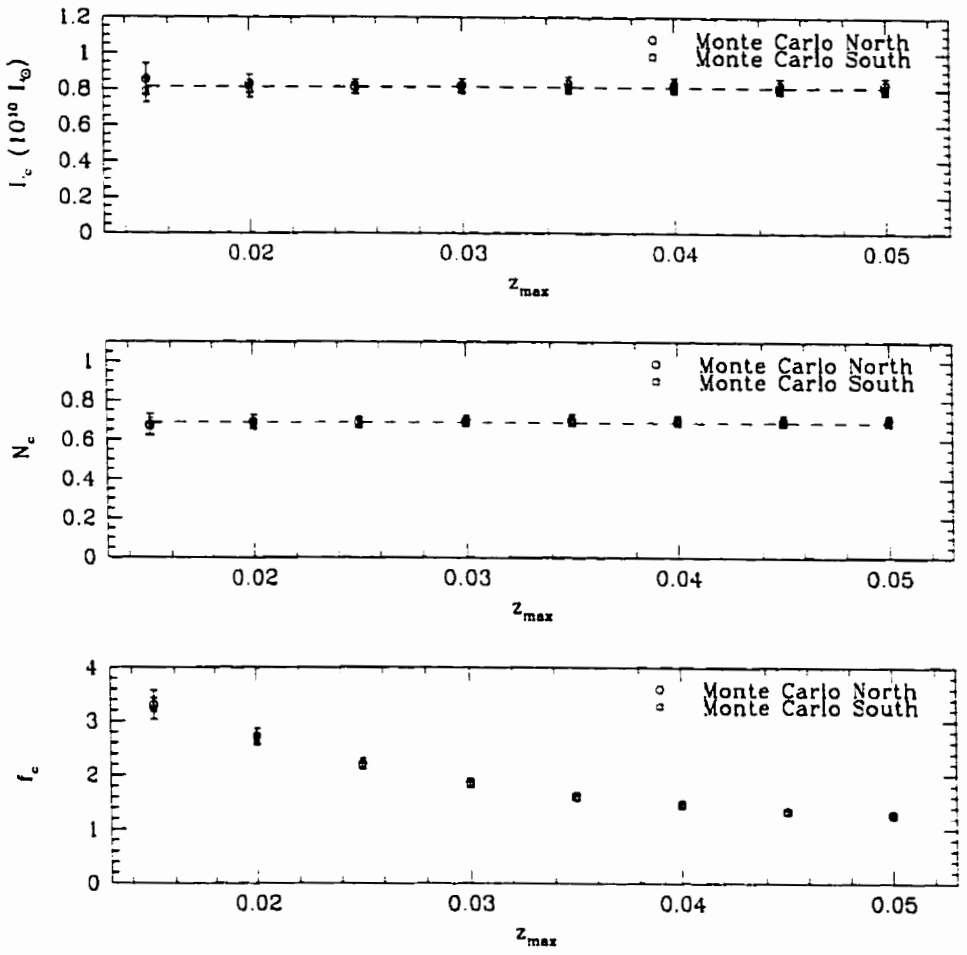

Figure 3.3: Pair statistics are computed for the flux-limited Monte Carlo simulations. Three pair statistics (f_p, N_c, and L_c) are given, for a range of choices of maximum redshift (z_{max}). Error bars are computed using the Jackknife technique. f_p exhibits a systematic and unwanted decrease with z_{max}. This is due to the apparent decrease in mean density with redshift, for this flux-limited sample. This bias is taken into account when computing N_c and L_c. The horizontal dashed lines match the data at z_{max}=0.05, and demonstrate that N_c and L_c do not depend on z_{max}.

they change slowly around $x = -1$. Clearly, $x = -1$ is an excellent choice.

3.7 A Pair Classification Experiment

The first step in applying these techniques to a real survey of galaxies is to decide on a useful close pair definition. This involves imposing a maximum projected physical separation ($r_p^{\max}$) and, if possible, a maximum line-of-sight rest-frame velocity difference ($\Delta v^{\max}$). The limits should be chosen so as to extract information on mergers in an optimal manner. This involves a compromise between the number and merging likelihood of pairs. While one should focus on companions which are most likely to be involved in mergers, a very stringent pair definition may yield a small and statistically insignificant sample.

In previous close pair studies, the convention has been to set $r_p^{\max} = 20$ h^{-1} kpc. Pairs with separations of $r_p \leq 20$ h^{-1} kpc are expected to merge within 0.5 Gyr (e.g., Barnes 1988; Chapter 2). We note, however, that timescale estimates are approximate in nature, and have yet to be verified. In earlier work, it has not been possible to apply a velocity criterion, since redshift samples have been too small to yield useful pair statistics using only galaxies with measured redshifts. Instead, all physical companions have been used, with statistical correction for optical contamination (Chapter 2). With a complete redshift sample, we can improve on this. This can be seen by inspecting a plot of r_p versus Δv for the SSRS2 pairs, given in Figure 3.5. By imposing a velocity criterion, we can eliminate optical contamination; furthermore, we are able to concentrate on the physical pairs with the lowest

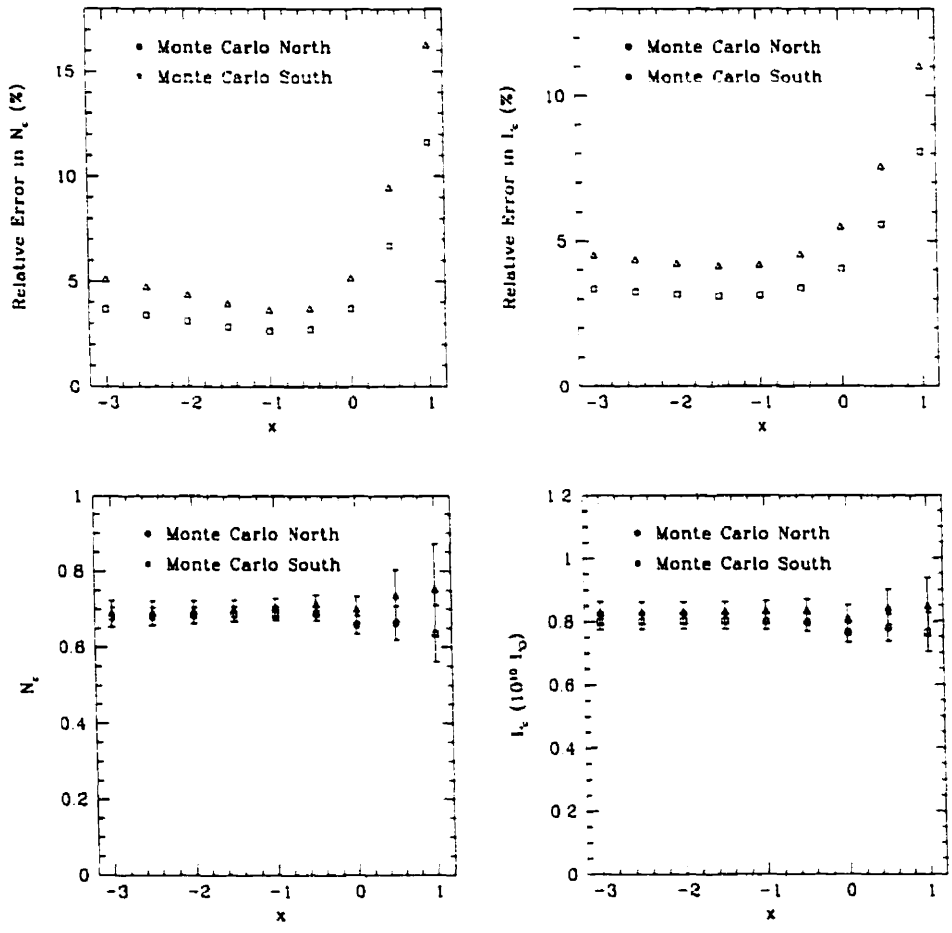

Figure 3.4: Pair statistics are computed for a range of possible weighting schemes for primary galaxies. Error bars are computed using the Jackknife technique.

relative velocities, and hence the greatest likelihood of merging.

We can now use our large sample of low-z pairs to shed new light on these issues. We will use images of these pairs in an attempt to determine how signs of interactions are related to pair separation. We begin by finding all 255 SSRS2 pairs with $r_p \leq 100\ h^{-1}$ kpc, computing r_p and Δv for each. Images for these pairs were extracted from the Digitized Sky Survey. Interactions were immediately apparent in some of these pairs, and the images were deemed to be of sufficient quality that a visual classification scheme would be useful. An interaction classification parameter (I_c) was devised, where I_c=0 indicates that a given pair is "definitely not interacting", and I_c=10 indicates "definitely interacting". In order to avoid a built-in bias, the classifier is not given the computed values of r_p and Δv. The classifier uses all visible information available (tidal tails and bridges, distortions/asymmetries in member galaxies, apparent proximity, etc.). Classifications were performed by three of us (DRP, ROM, RGC), and the median classification was determined for each system. The results are presented in Figure 3.6.

There are several important features in this plot. First, there is a clear correlation between I_c and r_p, with closer pairs exhibiting stronger signs of interactions. There are several interacting pairs with $r_p \sim 50\ h^{-1}$ kpc. While these separations are fairly large, it is not surprising that there would be some early-stage mergers with these separations (e.g., Barton, Bromley, & Geller 1998). An excellent example of this phenomenon is the striking tail-bridge system Arp 295a/b (cf. Hibbard and van Gorkum 1996), which has r_p = 95 h^{-1} kpc. However, these systems clearly do not dominate; almost all pairs with large separations have very low interaction classifications. The

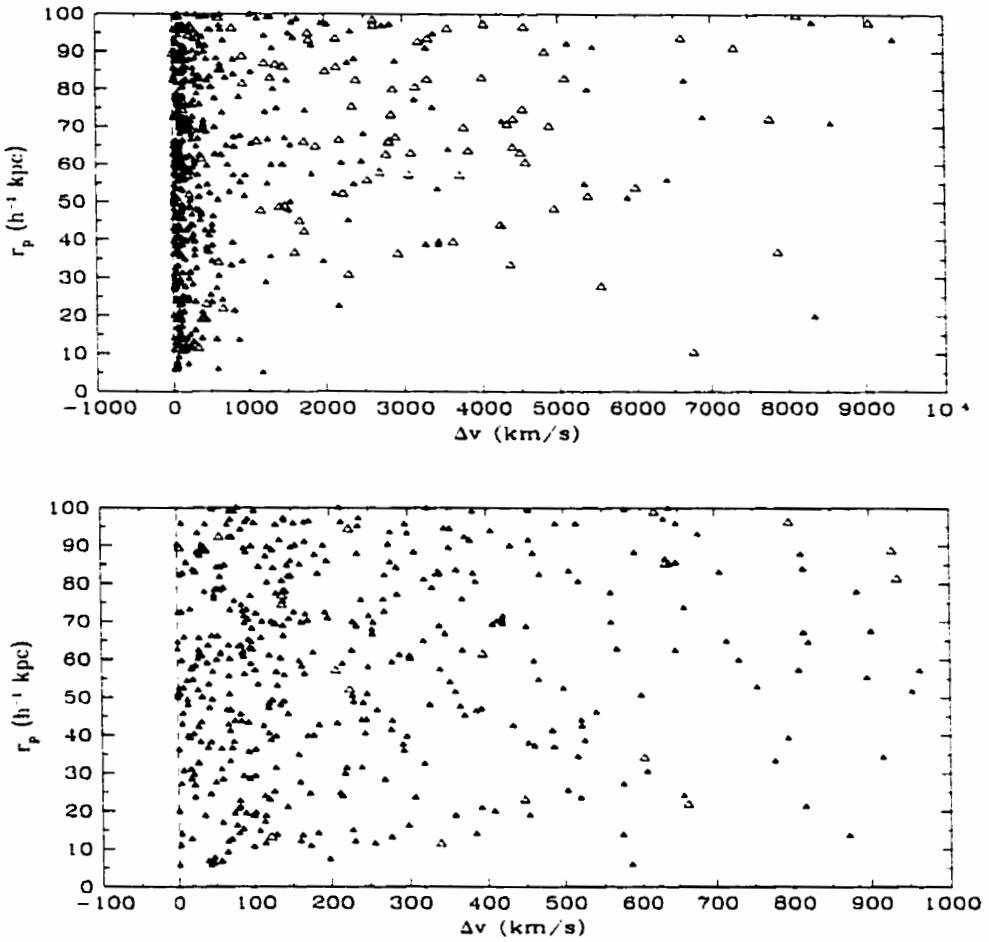

Figure 3.5: Projected separation (r_p) is plotted versus rest-frame velocity difference (Δv) for all pairs with $r_p \leq 100\ h^{-1}$ kpc. Pairs were identified by looking for close companions (real or random) around primary galaxies in the SSRS2 survey. Filled triangles represent real companions found in the SSRS2 survey. Open triangles denote random companions found in the Monte Carlo simulations. Note that the density of the simulations was matched to the real data sample when generating this plot, ensuring a fair comparison. The upper plot gives a wide range in velocity differences, demonstrating how the number of companions in excess of random becomes negligible beyond $\sim$ 1000 km/s. The lower plot is a zoomed-in version of the upper plot, giving a better feel for the distribution of physical pairs.

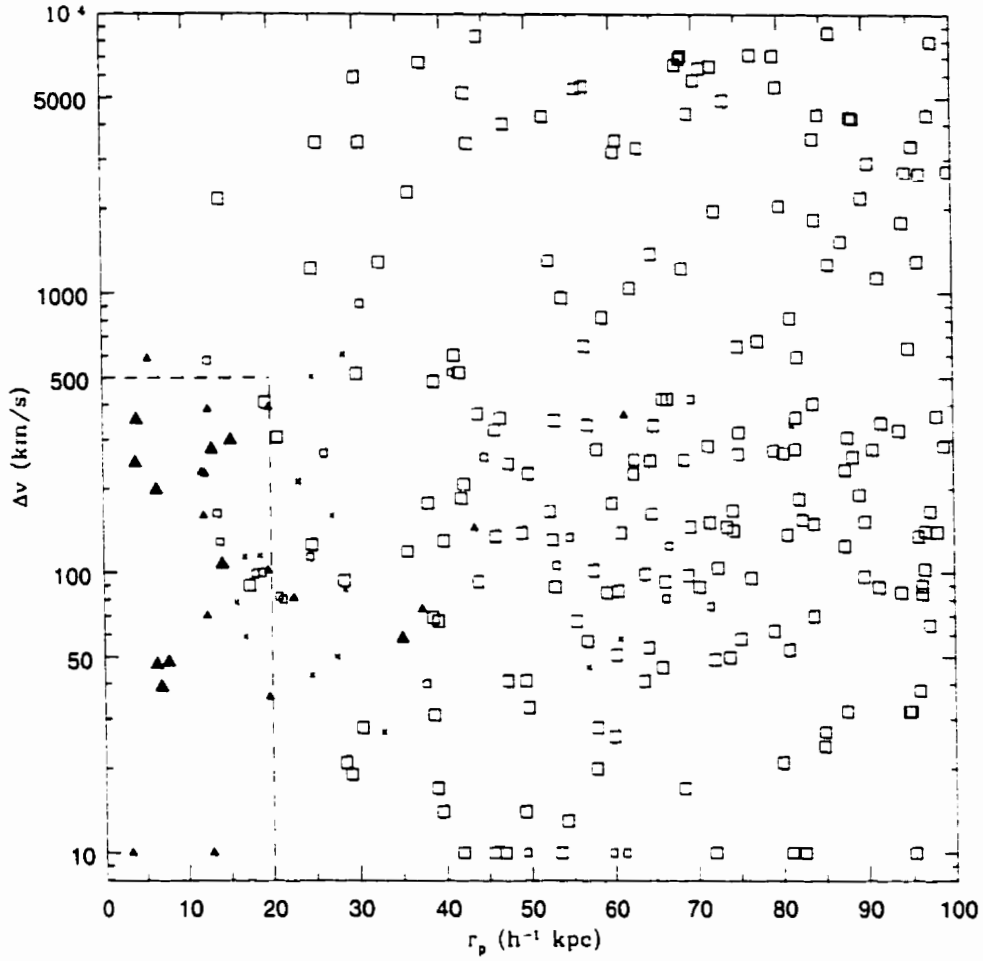

Figure 3.6: Pair interaction classification (I_c) is plotted as a function of projected physical separation (r_p) and line-of-sight rest-frame velocity difference (Δv), for 255 unique SSRS2 pairs with $r_p < 100\ h^{-1}$ kpc. Symbols are defined as follows : I_c=0,1 (large open squares), I_c=2,3 (small open squares), I_c=4−6 (crosses), I_c=7,8 (small filled triangles), and I_c=9,10 (large filled triangles). High I_c indicates increased likelihood of interaction. For plotting convenience, pairs with $\Delta v < 10$ km/s are assigned $\Delta v = 10$ km/s. The dashed line marks the close pair criteria (r_p=20 h^{-1} kpc and Δv=500 km/s) used for computing pair statistics.

majority of pairs showing clear signs of interactions/mergers have $r_p \lesssim 20$ h^{-1} kpc .

There is also a clear connection with Δv. Pairs with $\Delta v > 600$ km/s do not exhibit signs of interactions, with 61/63 (97%) classified as $I_c \leq 1$. This indicates that interactions are most likely to be seen in low velocity pairs, as expected. We note, however, that there are very few optical pairs (i.e., small r_p and large Δv) in this low redshift sample. At higher redshift, increased optical contamination may lead to difficulties in identifying interacting systems when the galaxies are close enough to have overlapping isophotes. Clearly, it is necessary to have redshift information for both members of each pair if one is to exclude these close optical pairs.

After close inspection of Figure 3.6, we decided on close pair criteria of $r_p^{\max} = 20\ h^{-1}$ kpc and $\Delta v^{\max} = 500$ km/s. A mosaic of some of these pairs is given in Figure 3.7. In this regime, 31% (9/29) exhibit convincing evidence for interactions ($I_c \geq 9$), while 69% (20/29) show some indication of interactions ($I_c \geq 6$). Furthermore, the vast majority (9/10) of pairs with clear signs of interactions ($I_c \geq 9$) are found in this regime. These criteria appear to identify a sample of pairs which are likely to be undergoing mergers; moreover, the resulting sample includes most of the systems classified as interacting.

We also impose an inner boundary of $r_p = 5\ h^{-1}$ kpc. This limit is chosen so as to avoid the confusion that is often present on the smallest scales. In this regime, it is often difficult to distinguish between small galaxies and sub-galactic units, particularly in merging systems. While we are omitting the most likely merger candidates, those at separations $< 5\ h^{-1}$ kpc are

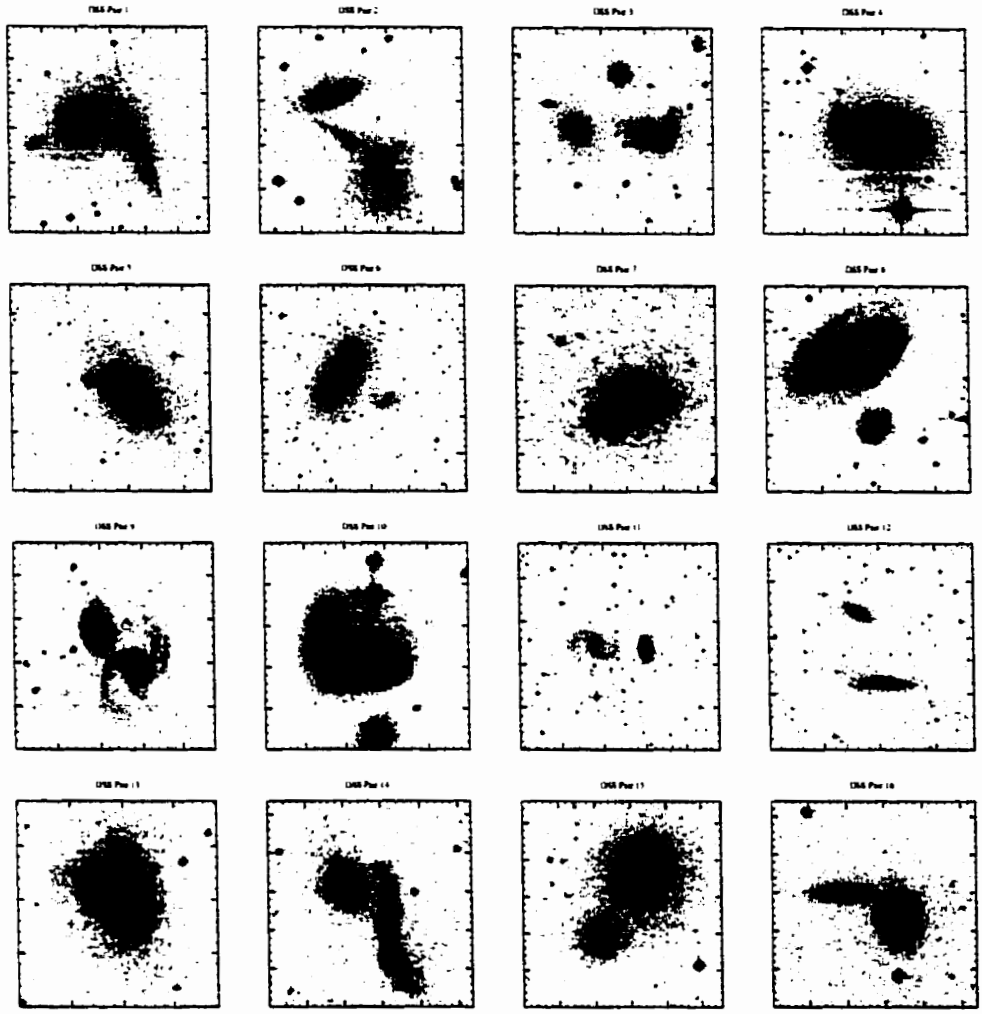

Figure 3.7: A mosaic of images is given for the 38 close ($5\ h^{-1}$ kpc $< r_p \leq 20\ h^{-1}$ kpc) dynamical ($\Delta V < 500$ km/s) pairs or triples satisfying the criteria used for computing pair statistics. These images were obtained from the Digitized Sky Survey. Each image is $50\ h^{-1}$ kpc on a side, corresponding to angular sizes of $1.5' - 10'$.

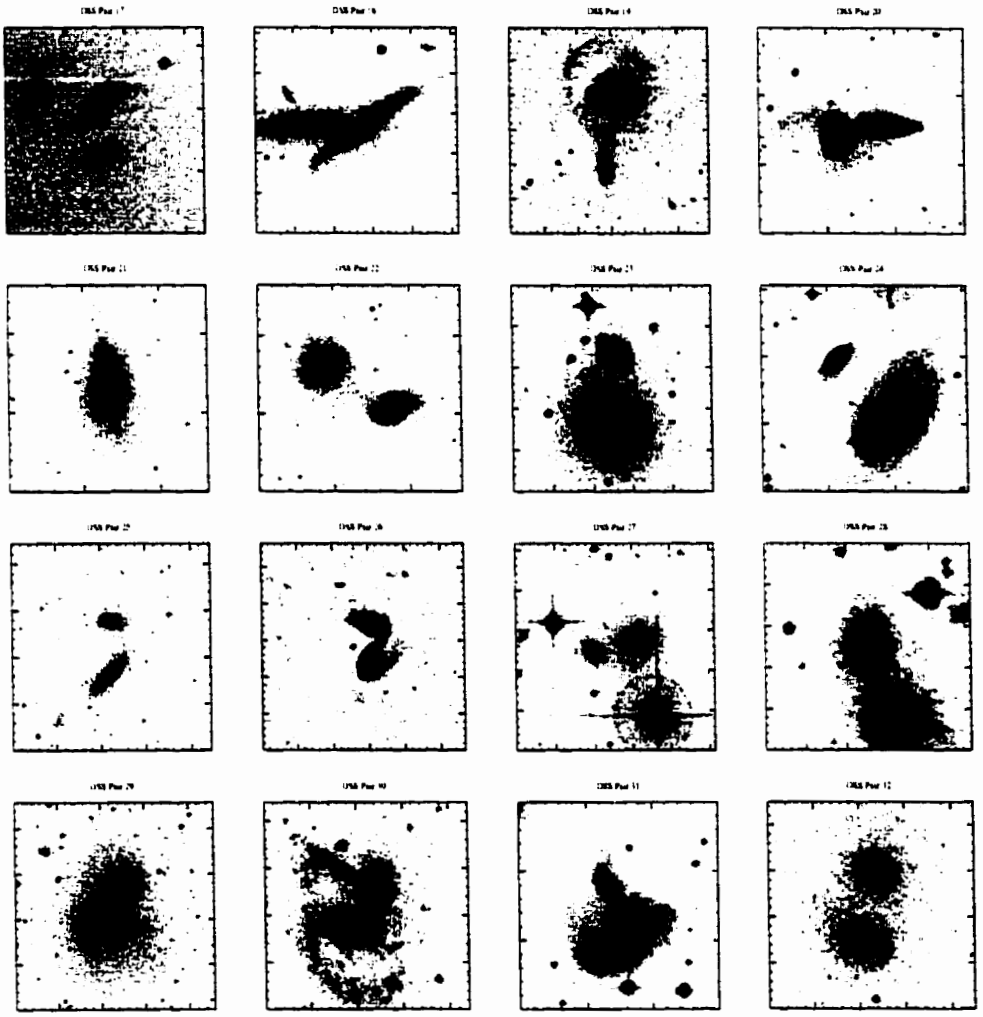

Figure 3.7: Continued

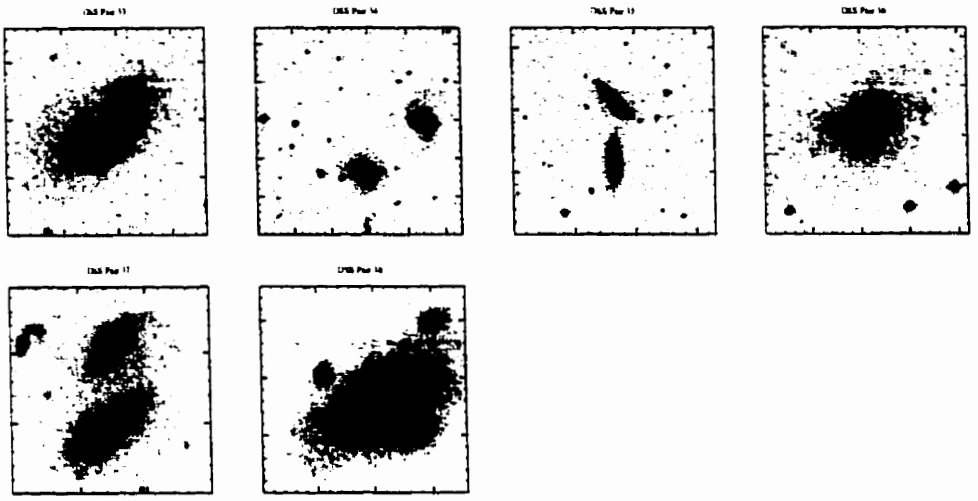

Figure 3.7: Continued

not expected to account for more than $\sim$ 5% of the companions within 20 h^{-1} kpc . This expectation, which has yet to be verified, is based both on pair counts in *HST* imaging (Burkey et al. 1994) and on inward extrapolation of the correlation function (Chapter 2). While this inner boundary will lead to a slight decrease in N_c and L_c, it should have no significant effect on estimates of merger/accretion rate evolution, provided the same restriction is applied to comparison samples at other redshifts.

3.8 Application to SSRS2

In the preceding sections, we have outlined techniques for measuring pair statistics in a wide variety of samples. We have demonstrated a robust method of applying this approach to flux-limited samples, accounting for redshift-dependent density changes and minimizing differences in clustering. We have also selected pair definitions that identify the most probable imminent mergers. We will now apply these techniques to the SSRS2 survey. As this is a complete redshift survey, redshifts are available for all close companions; hence, for the first time, we will measure pair statistics using only close *dynamical* pairs. After making reasonable choices of $M_{\rm faint}$ and $z_{\rm max}$, we compute N_c and L_c for the SSRS2 survey.

3.8.1 Defining Survey Parameters

In Section 3.6.1, we emphasized the importance of applying a minimum luminosity ($M_{\rm faint}$) and maximum redshift ($z_{\rm max}$) to minimize bias due to luminosity-dependent clustering. For SSRS2, we set $M_{\rm faint}=-17$, which re-

sults in the exclusion of intrinsically faint galaxies at $z \lesssim 0.01$. We choose z_{max}=0.04, which serves to exclude the high redshift end of the sample, where all galaxies are brighter than $M_B \sim -20$. This pruning of the sample is illustrated in Figure 3.8. These parameters allow us to retain 90% of the sample. The final results are insensitive to these particular choices (see Section 3.8.3).

We must also choose limiting absolute magnitudes for the primary and secondary samples. The mean limiting absolute magnitude of the primary sample, weighted according to Section 3.6.2, is $M_B = -17.8$. For convenience, we set $M_2(B) = -18.0$ (we will compute pair statistics for $-19 \leq M_2(B) \leq -17$ in the following section). For reference, we note that this corresponds to m_B=15.5 at z=0.017. As we are dealing with a complete redshift sample, we set $M_1(B) = M_2(B)$ in order to use all of the available information.

3.8.2 SSRS2 Pair Statistics

Using these parameters, we identified all close companions in SSRS2. The North sample yielded 23 companions, and 54 were found in the South, giving a total of 77. We emphasize that it is *companions* that are counted, rather than pairs; hence, if both members of a pair fall within the primary sample, the pair will usually yield 2 companions. A histogram of companion absolute magnitudes is given in Figure 3.9. This plot shows that 90% of the companions we observe in our flux limited sample fall in the range $-21 \leq M_B \leq -18$. Hence, very luminous or faint companions do not dominate the sample. Tables 3.1 and 3.2 give complete lists of close aggregates (pairs and triples) for SSRS2 North and South respectively. These systems contain all companions used in the computation of pair statistics. These tables list system identi-

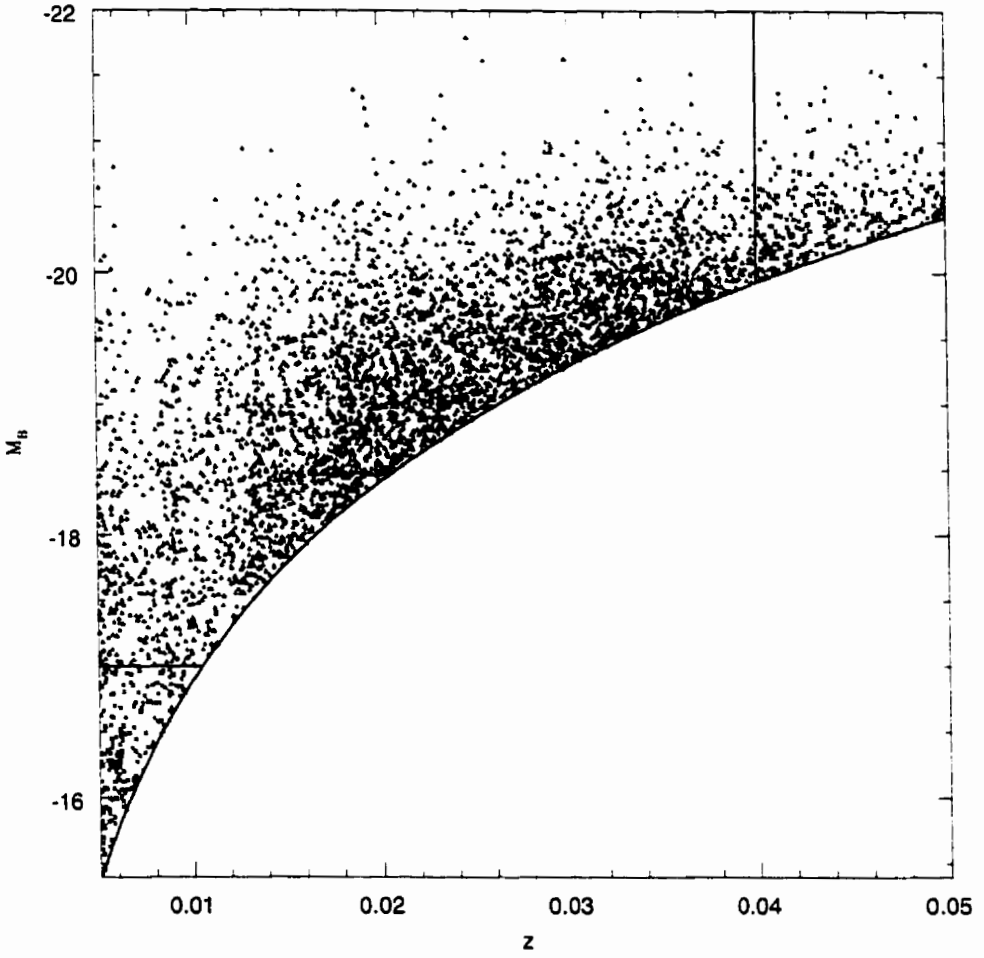

Figure 3.8: $B-$band absolute magnitude is plotted versus redshift for all SSRS2 galaxies with $m_B \leq 15.5$ and $0.005 \leq z \leq 0.05$. The curved line marks the boundary imposed by this apparent magnitude limit. The horizontal line indicates the minimum luminosity imposed ($M_{\rm faint}=-17$), while the vertical line represents the maximum redshift allowed ($z_{max}=0.04$). Galaxies satisfying all of these criteria (and hence used in the calculation of N_c and L_c) are marked with triangles; the remainder are indicated with crosses.

Table 3.1: SSRS2 North : Close Pairs and Triples

ID	N	r_p	Δv	RA(1950.0)	DEC(1950.0)	cz
1	2	12.7	385	12:23:39.7	-07:24:21	5183
2	2	19.8	392	12:39:42.8	-05:30:33	6604
3	2	18.1	357	12:49:52.3	-15:14:45	4539
4	2	13.0	183	12:50:31.4	-08:55:47	4149
5	3	11.4	42	13:01:21.2	-11:13:39	2965
6	2	14.0	227	13:17:00.1	-27:09:24	1835
7	2	6.5	198	13:23:14.6	-26:24:59	9596
8	2	18.1	99	13:30:31.8	-15:52:26	5813
9	2	12.5	70	13:32:37.2	-10:37:55	6550
10	2	15.7	298	13:57:36.5	-23:03:54	10592
11	2	12.8	4	14:01:52.3	-24:35:25	2117
12	2	18.4	89	14:10:41.5	-02:56:41	1664

fier (ID), number of members, r_p (h^{-1} kpc), Δv (km/s), RA (1950.0), DEC (1950.0), and recession velocity (km/s). DSS images for these systems were given earlier in Figure 3.7.

Using this sample of companions, the pair statistics were computed. The results are given in Table 3.3. Errors were computed using the Jackknife technique. Results from the two subsamples were combined, weighting by Jackknife errors, to give $N_c = 0.0227 \pm 0.0054$ and $L_c = 0.0235 \pm 0.0061 \times 10^{10}\ h^2 L_\odot$ at z=0.016. Results from the two subsamples agree within the quoted 1σ errors.

To facilitate future comparison with other samples, we also generate pair statistics spanning the range $-19 \leq M_2(B) \leq -17$ (see Table 3.4). We note, however, that while we account for changes in number and luminosity

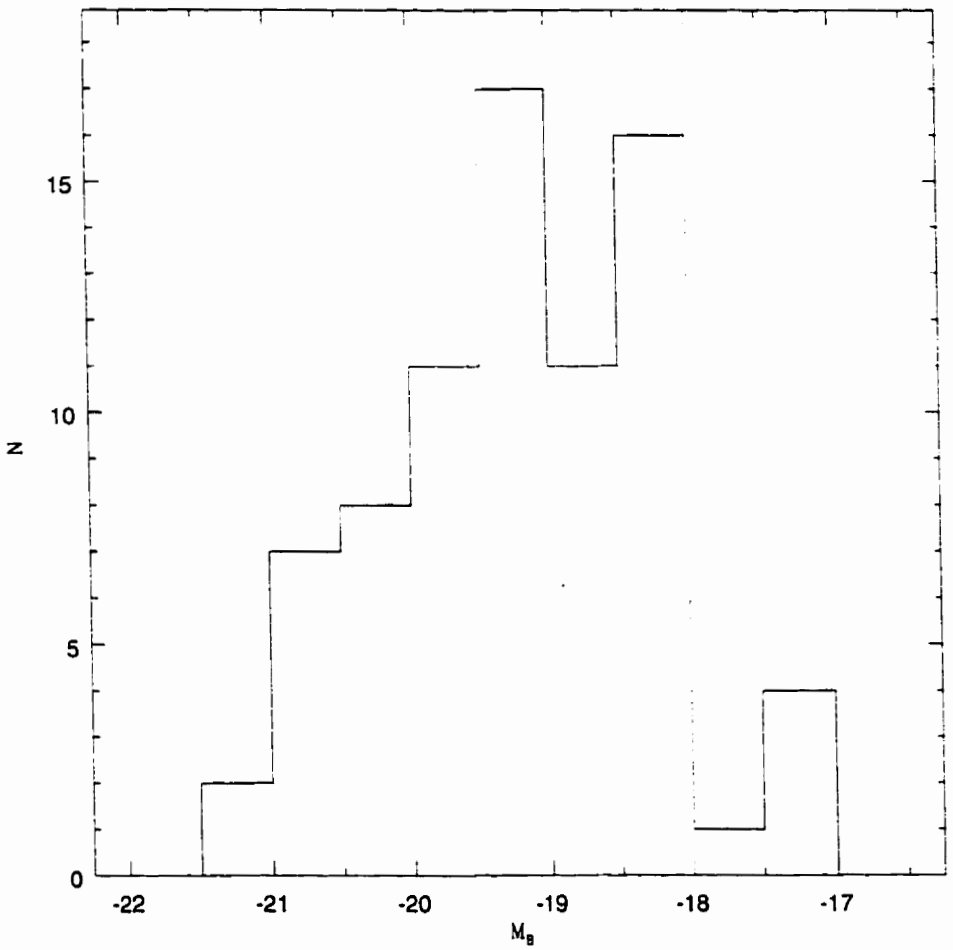

Figure 3.9: An absolute magnitude histogram is given for the 77 companions used in the pair statistics.

Table 3.2: SSRS2 South : Close Pairs and Triples

ID	N	r_p	Δv	RA(1950.0)	DEC(1950.0)	cz
13	2	7.8	48	00:13:51.2	-06:35:57	8070
14	2	13.7	276	00:56:52.5	-05:04:07	5771
15	2	18.9	100	01:06:26.0	-28:51:25	5522
16	2	14.1	163	01:10:01.2	-04:24:30	5723
17	2	12.4	160	01:13:05.7	-06:51:23	6365
18	2	12.4	229	01:16:22.5	-17:04:00	6002
19	2	16.8	114	01:34:10.7	-37:35:09	5171
20	2	10.7	173	02:06:55.3	-10:22:13	4143
21	2	6.9	39	02:26:44.0	-11:03:15	4695
22	2	19.6	102	02:55:45.2	-10:33:21	4647
23	2	16.0	78	03:04:11.5	-39:13:15	6188
24	2	19.2	115	03:08:51.0	-09:06:01	4020
25	2	12.9	18	03:22:17.8	-03:12:17	2764
26	3	7.8	61	04:13:09.8	-28:36:32	5450
27	2	10.8	256	04:29:34.7	-29:51:29	4032
28	3	19.7	227	21:08:47.2	-23:22:03	10682
29	2	10.8	99	21:59:10.7	-32:13:26	2674
30	2	11.9	66	22:03:22.9	-28:11:55	7042
31	2	11.5	114	22:06:17.6	-28:03:03	6943
32	2	16.8	59	22:19:05.8	-25:50:09	6904
33	2	14.2	107	22:52:34.7	-34:09:30	8700
34	2	19.6	36	22:55:33.0	-04:02:30	3828
35	2	14.0	129	22:57:31.1	-13:05:22	3115
36	2	6.5	47	23:00:35.1	-09:15:38	7360
37	2	19.4	409	23:23:42.7	-39:29:48	10759
38	2	15.5	86	23:45:09.7	-28:24:56	8700

Table 3.3: SSRS2 Pair Statistics

Sample	N	N_{comp}	$\bar{z}$	N_c	$L_c(10^{10}h^2L_\odot)$
SSRS2 North	1546	23	0.015	0.0174± 0.0073	0.0165± 0.0080
SSRS2 South	2672	54	0.017	0.0292± 0.0081	0.0331± 0.0093
SSRS2 (N+S)	4218	77	0.016	0.0227± 0.0054	0.0235± 0.0061

density over this luminosity range (using LF weights described in Section 3.6), there is no correction for changes in clustering. Hence, our statistics should be considered most appropriate for $M_2(B)=-18$, and more approximate in nature at brighter and fainter levels. The results in Table 3.4 indicate that N_c increases by a factor of 5 between $M_2(B)=-19$ and $M_2(B)=-17$, resulting solely from an increase in mean number density. The change in L_c is less pronounced, with an increase by a factor of 2 over the same luminosity range. These substantial changes in both statistics emphasize the need to specify M_2 when computing pair statistics and comparing results from different samples. In addition, the smaller change in L_c is indicative of the benefits of using a luminosity statistic such as L_c, which is more likely to converge as one goes to fainter luminosities (see Section 3.5.4). L_c will always converge faster than N_c, thereby reducing the sensitivity to M_2. Furthermore, it is possible to retrieve most of the relevant luminosity information without probing to extremely faint levels. For example, for the SSRS2 LF, 70% of the total integrated luminosity density is sampled by probing down to $M_B=-18$. To first order, the same will be true for L_c. Going 2 magnitudes fainter would increase the completeness to 95%. While we are currently unable to apply

pair statistics down to these faint limits, this will be pursued when deeper surveys become available.

3.8.3 Sensitivity of Results to Survey Parameters

In this section, we explore the effects of choosing different survey parameters. Earlier in this study, we demonstrated that N_c and L_c are insensitive to the choice of $M_{\rm faint}$ and $z_{\rm max}$, provided clustering is independent of luminosity. Here, we test this hypothesis empirically.

First, we compute the pair statistics for a range in $M_{\rm faint}$. Figure 3.10 demonstrates an apparent trend of decreasing pair statistics with fainter $M_{\rm faint}$. This trend, however, is significant only for the brightest galaxies ($M_{\rm faint} \lesssim -19$). This is consistent with the findings of Willmer et al. (1998), who measure an increase in clustering for bright galaxies in SSRS2, on scales of $r_p > 1\ h^{-1}$ Mpc. For fainter $M_{\rm faint}$, there is no significant dependence. The pair statistics vary by $\sim 5\%$ over the range $-17.5 \leq M_{\rm faint} \leq -16.5$, which is well within the error bars. Therefore, we conclude that our choice of $M_{\rm faint}$=-17 has a negligible effect on N_c and L_c. This implies that, to first order, clustering is independent of luminosity within this sample.

Similarly, N_c and L_c are computed for a range of $z_{\rm max}$. Results are given in Figure 3.11. There is no large dependence on $z_{\rm max}$, as expected. The pair statistics change by $\sim 5\%$ over the range $0.035 \leq z_{\rm max} \leq 0.045$; again, this is well within the quoted errors. We conclude that our particular choice of $z_{\rm max}$ (0.04) has a negligible effect on N_c and L_c.

Finally, we investigate how the pair statistics depend on our particular choices of $r_p^{\rm max}$ and $\Delta v^{\rm max}$, which comprise our definition of a close compan-

Table 3.4: SSRS2 Pair Statistics for Various Choices of $M_2(B)$

M_2	N_c	$L_c(10^{10}h^2L_\odot)$
-19.0	0.0083± 0.0020	0.0148± 0.0038
-18.9	0.0094± 0.0022	0.0158± 0.0041
-18.8	0.0105± 0.0025	0.0168± 0.0043
-18.7	0.0118± 0.0028	0.0178± 0.0046
-18.6	0.0131± 0.0031	0.0187± 0.0048
-18.5	0.0146± 0.0035	0.0196± 0.0051
-18.4	0.0160± 0.0038	0.0204± 0.0053
-18.3	0.0176± 0.0042	0.0213± 0.0055
-18.2	0.0192± 0.0046	0.0221± 0.0057
-18.1	0.0209± 0.0050	0.0228± 0.0059
-18.0	0.0227± 0.0054	0.0235± 0.0061
-17.9	0.0245± 0.0058	0.0242± 0.0062
-17.8	0.0264± 0.0063	0.0248± 0.0064
-17.7	0.0284± 0.0068	0.0254± 0.0066
-17.6	0.0304± 0.0072	0.0260± 0.0067
-17.5	0.0325± 0.0077	0.0265± 0.0068
-17.4	0.0346± 0.0082	0.0270± 0.0070
-17.3	0.0368± 0.0088	0.0275± 0.0071
-17.2	0.0390± 0.0093	0.0279± 0.0072
-17.1	0.0413± 0.0098	0.0283± 0.0073
-17.0	0.0437± 0.0104	0.0287± 0.0074

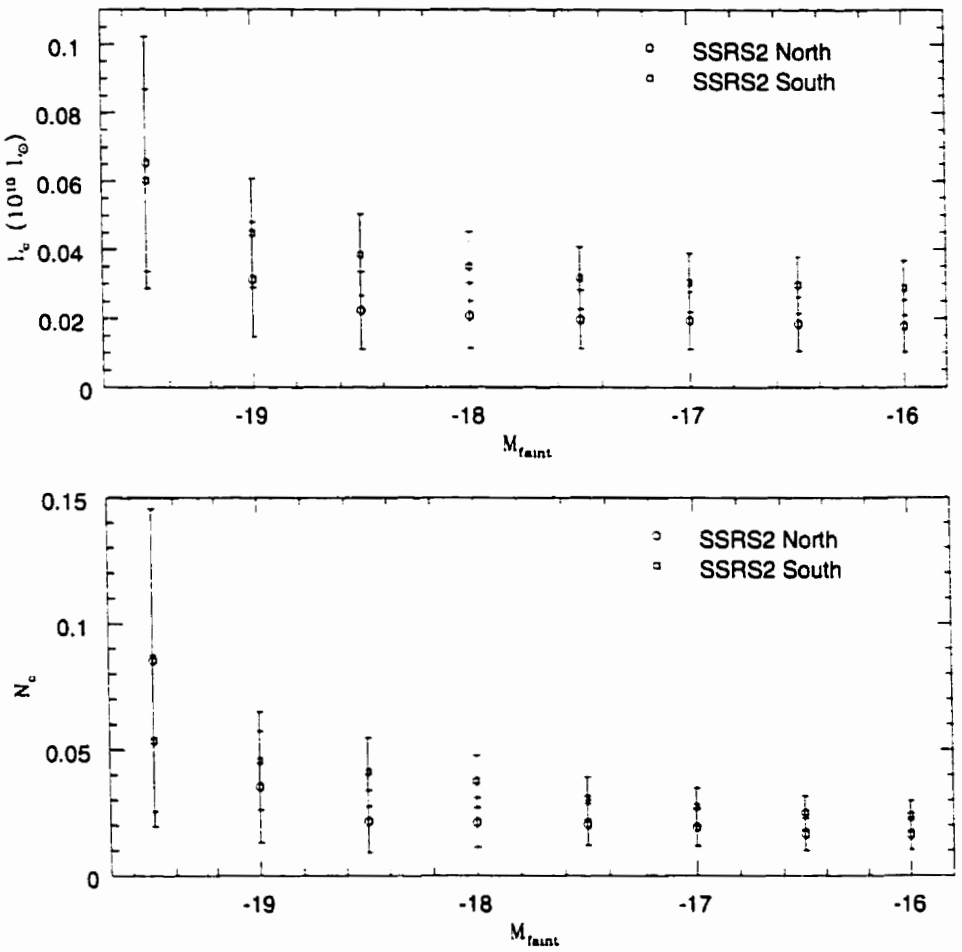

Figure 3.10: Pair statistics are computed for SSRS2 North and South. N_c and L_c are given, for a range in minimum luminosity $M_{\rm faint}$, with $M_2{=}M_1{=}{-}18$. Error bars are computed using the Jackknife technique. Both N_c and L_c appear to be independent of $M_{\rm faint}$, within the errors, over the range $-18 \leq M_{\rm faint} \leq -16$. This implies that, to first order, clustering is independent of luminosity in this regime.

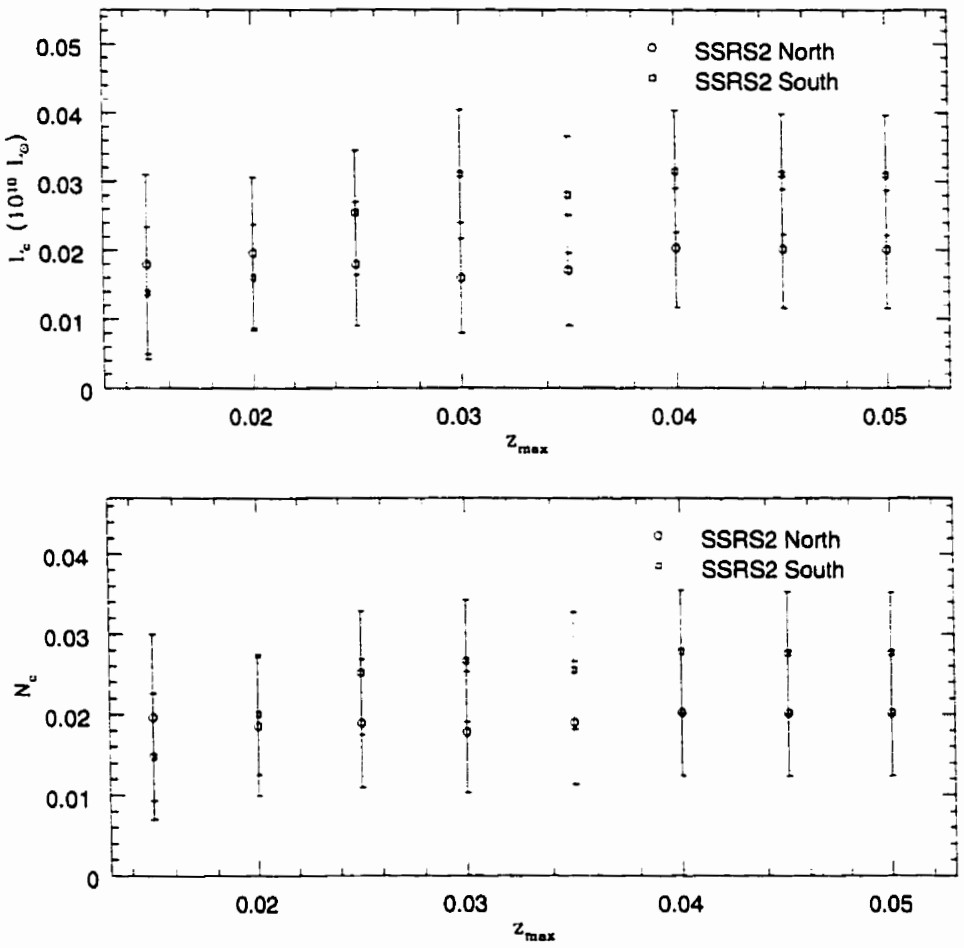

Figure 3.11: Pair statistics are computed for SSRS2 North and South. N_c, and L_c are given, for a range of choices of maximum redshift (z_{max}). Error bars are computed using the Jackknife technique. Both statistics appear to be independent of z_{max}, within the errors.

ion. First, we compute pair statistics for 10 h^{-1} kpc$\leq r_p^{max} \leq 100h^{-1}$ kpc, with $\Delta v^{max} = 500$ km/s. Results are given in Figure 3.12. This plot indicates a smooth increase in both statistics with r_p^{max}. This trend is expected from measurements of the galaxy CF. The CF is commonly expressed as a power law of the form $\xi(r,z) = (r_0/r)^{\gamma}$, with γ=1.8 (Davis and Peebles 1983). Integration over this function yields pair statistics that vary as $r_p^{3-\gamma} \approx r_p^{1.2}$, which is in good agreement with the trend found in Figure 3.12. From this plot, it also appears likely that there are systematic differences between the two subsamples. This is hardly surprising, since there are known differences in density between the subsamples, and it is likely that there are non-negligible differences in clustering as well. This cosmic variance is not currently measurable on the smaller scales ($r_p \leq 20\ h^{-1}$ kpc) relevant to our main pair statistics. Hence, we choose to ignore these differences for now. However, these field-to-field variations are certain to add some systematic error to our quoted pair statistics.

We also compute pair statistics for a range in Δv^{max}. This is done first for $r_p^{max} = 20\ h^{-1}$ kpc, showing the relative contributions at different velocities to the main pair statistics quoted in this chapter. We also compute statistics using $r_p^{max} = 100\ h^{-1}$ kpc, in order to improve the statistics. Results are given in Figure 3.13. Several important conclusions may be drawn from this plot. First, at small velocities ($\Delta v^{max} \lesssim 700$ km/s), both pair statistics increase with Δv^{max}, as expected. This simply indicates that one continues to find additional companions as the velocity threshold increases. Secondly, it appears that our choice of Δv^{max} was a good one. The $r_p \leq 20\ h^{-1}$ kpc pair statistics increase very little beyond $\Delta v^{max} = 500$ km/s, while the contami-

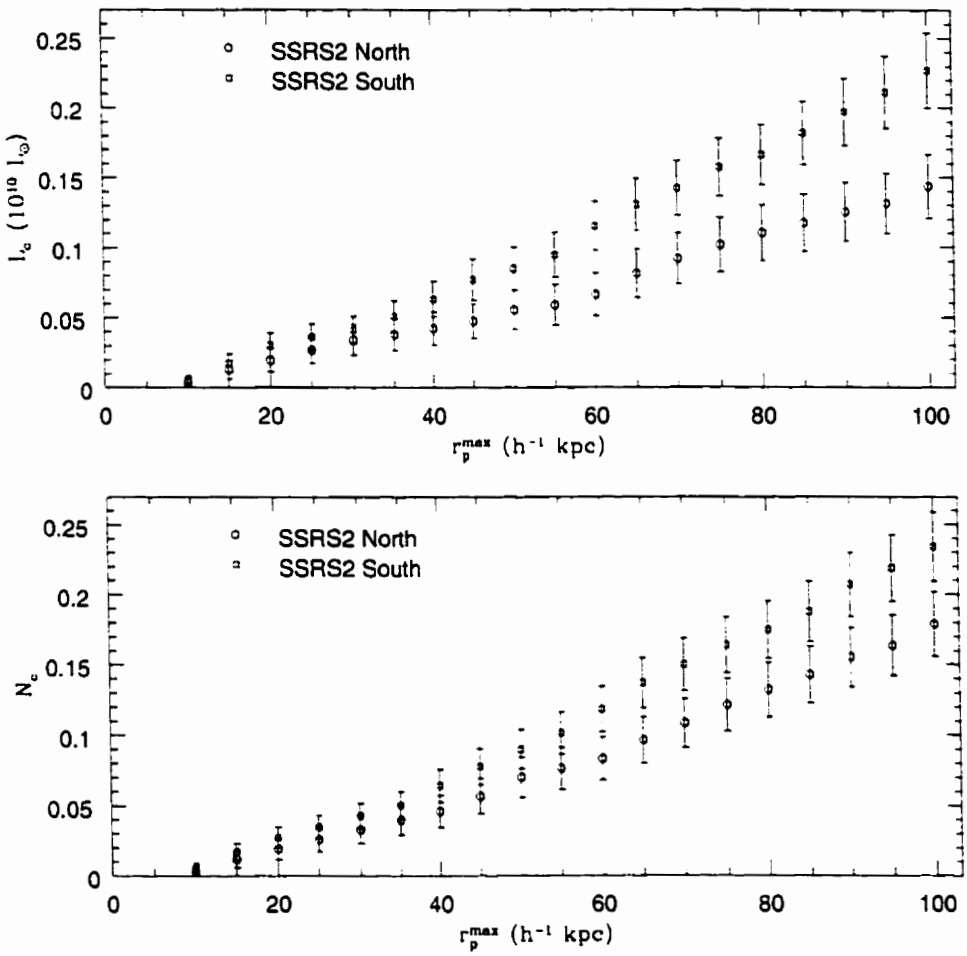

Figure 3.12: Pair statistics are computed for $\Delta v \leq 500$ km/s, for a range of maximum projected separations (r_p^{max}). A minimum projected separation of $r_p = 5\ h^{-1}$ kpc is applied in each case. Error bars are computed using the Jackknife technique. Both N_C and L_C are cumulative statistics; hence, measurements in successive bins are not independent.

nation due to non−merging pairs would continue to increase (see Figure 3.5). Moreover, as both pair statistics flatten out at around $\Delta v^{\max} = 500$ km/s, small differences in the velocity distributions of different samples should not result in large differences in their pair statistics. Finally, for $r_p^{\max} \leq 100$ h^{-1} kpc, the pair statistics continue to increase out to ~ 2000 km/s. This indicates an increase in velocity dispersion at these larger separations. This provides additional confirmation that one is less likely to find low−velocity pairs at larger separations, thereby implying that mergers should also be less probable.

3.9 Discussion

3.9.1 Comparison with Earlier Estimates of the Local Pair Fraction

All published estimates of the local pair fraction have been hindered by small sample sizes and a lack of redshifts. In addition, as demonstrated throughout this chapter, the traditional pair fraction is not a robust statistic, particularly when applied to flux-limited surveys. The new statistics introduced in this chapter, along with careful accounting for selection effects such as the flux limit, yield the first secure measures of pair statistics at low redshift. Therefore, strictly speaking, the results in this chapter cannot be compared directly with earlier pair statistics. However, it is possible to check for general consistency in results, and we will attempt to do so.

In Chapter 2, we estimated the local pair fraction to be $4.3 \pm 0.4\%$, using the UGC catalog. This estimate was based on a flux limited sample with

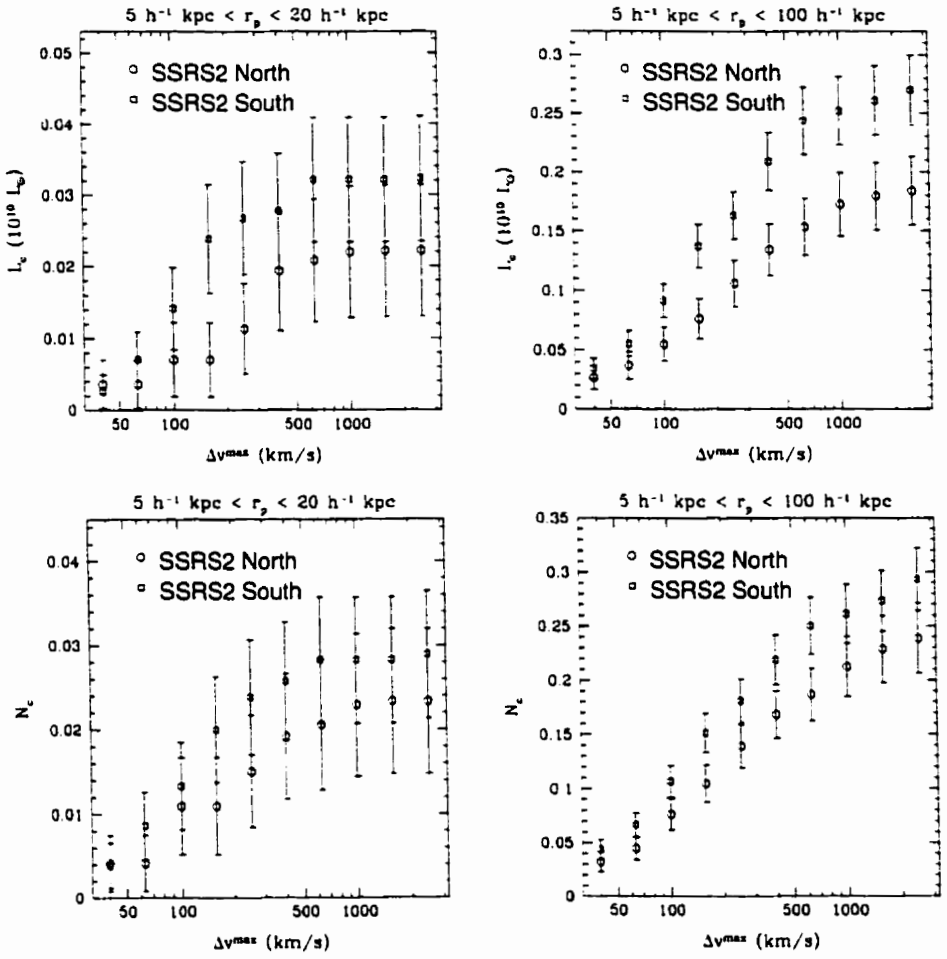

Figure 3.13: Pair statistics are computed for $\Delta v \leq 500$ km/s, for a range of projected separations. Error bars are computed using the Jackknife technique. Both N_C and L_C are cumulative statistics; hence, measurements in successive bins are not independent.

$B \leq 14.5$, and a mean redshift of z=0.0076. This corresponds roughly to an average limiting absolute magnitude of M_B=−17.3. Loosely speaking, this is analogous to M_2. The pair definition used in this estimate was $r_p \leq 20$ h^{-1} kpc, with no Δv criterion. N_c may be interpreted as an approximation to the traditional pair fraction, provided the relative proportion of triples is small. We recompute the SSRS2 pair statistics, using $\Delta v^{\rm max}$=1000 km/s in an attempt to match the results that would be found using no Δv criterion (see Figure 3.13). We find $N_c = 0.026 \pm 0.006$. This implies a local pair fraction of 2.6 ± 0.6%. This value is somewhat smaller than the earlier result, with larger errors. We strongly emphasize that, while these results are broadly consistent, we would not expect excellent agreement, due to the improved techniques used in this study.

3.9.2 The Merger Fraction at $z \sim 0$

Now that we have computed N_c and L_c, we would like to ascertain how they relate to the global galaxy population. These numbers provide information about the prevalence of mergers at the present epoch. Recall that N_C and L_C use companions with 5 h^{-1} kpc $\leq r_p \leq$ 20 h^{-1} kpc and $\Delta v \leq$ 500 km/s. These criteria are useful for identifying galaxies with a relatively high incidence of ongoing interactions (§ 3.7). While these galaxies appear to be good merger candidates, we have not assumed that they will all merge. In fact, due to the smearing effects of redshift along the line of sight, some of these companions are certain to lie at separations considerably larger than 20 h^{-1} kpc, implying that they probably will not merge on the short timescales of interest here. In order to transform from N_C (and L_C) to an estimate of the incidence

of mergers, we must determine what fraction of our close companions have true 3-dimensional physical separations of $r < 20\ h^{-1}$ kpc. This quantity, which we refer to as f_{3D}, has been estimated by Yee and Ellingson (1995). Using the spatial correlation function of the form $r^{-\gamma}$, with γ=1.8, they find f_{3D}=0.55. Arguments based on the pairwise velocity dispersion and theoretical estimates of the critical velocity necessary for merging ((Carlberg 1999)) also yield $f_{3D}\approx$0.5. We will take f_{3D}=0.5 to be the best estimate currently available.

We can now estimate the merger fraction (f_{mg}) at the present epoch. In this study, we have found N_C=0.0227$\pm$0.0054. As most companions are found in pairs, rather than triplets or higher order N-tuples, this is comparable to the fraction of galaxies in close pairs. From our estimate of f_{3D}, we infer that half of these galaxies are in merging systems, yielding $f_{mg} \approx 0.011$. This implies that approximately 1.1% of $M_B \leq -18$ galaxies are undergoing mergers at the present epoch. We stress here that this result applies only to galaxies above the specified limiting absolute magnitude. Probing to fainter luminosities would cause f_{mg} to increase substantially. In addition, this result applies only to the close companions defined in this analysis. Clearly, by modifying this definition (and therefore changing the typical merger timescale under consideration), the merger fraction would also be certain to change.

3.9.3 The Merger Timescale

We now have an idea of how prevalent ongoing mergers are at the present epoch. In order to relate this result to the overall importance of mergers, we must estimate the merger timescale (T_{mg}). We will use the properties of

our SSRS2 pairs to estimate the mean dynamical friction timescale for pairs in our sample. Following Binney and Tremaine (1987), we assume circular orbits and a dark matter density profile given by $\rho(r) \propto r^{-2}$. The dynamical friction timescale $T_{\rm fric}$ (in Gyr) is given by

$$T_{\rm fric} = \frac{2.64 \times 10^5 r^2 v_c}{M \ln \Lambda}, \tag{3.30}$$

where r is the initial physical pair separation in kpc, v_c is the circular velocity in km/s, M is the mass ($M_\odot$), and $\ln \Lambda$ is the Coulomb logarithm. We estimate r and v_c using the pairs in Tables 3.1 and 3.2. The mean projected separation is $r_p \sim 14h^{-1}$ kpc. As our procedure already includes a correction from projected separation (r_p) to 3-dimensional separation (r), we take $r = r_p$. Assuming h=0.7, this leads to $\bar{r} \sim 20$ kpc. The mean line of sight velocity difference is $\Delta v \sim 150$ km/s. We assume the velocity distribution is isotropic, which implies that $v_c = \sqrt{3}\Delta v \sim 260$ km/s. The mean absolute magnitude of companions is $M_B \sim -19$ (see Figure 3.9). We assume a representative estimate of the galaxy mass-to-light ratio of $M/L \sim 5$, yielding a mean mass of $M \sim 3 \times 10^{10} M_\odot$. Finally, Dubinski, Mihos, and Hernquist (1999) estimate $\ln \Lambda \sim 2$, which fits the orbital decay of equal mass mergers seen in simulations. Using Equation 3.30, we find $T_{\rm fric} \sim 0.5$ Gyr. We caution that this estimate is an approximation, and is averaged over systems with a wide range in merger timescales. Nevertheless, we will take $T_{\rm mg} = 0.5$ Gyr as being representative of the merger timescale for the pairs in our sample.

3.9.4 The Cumulative Effect of Mergers Since $z \sim 1$

Now that we have estimated the present epoch merger fraction and the merger timescale, we will attempt to ascertain what fraction of present galaxies have undergone mergers in the past. These galaxies can be classified as merger remnants; hence, we will refer to this fraction as the remnant fraction ($f_{\rm rem}$). We begin by imagining the state of affairs at a lookback time of $t = T_{\rm mg}$. Suppose the merger fraction at the corresponding redshift is given by $f_{\rm mg}(z)$. In the time interval between then and the present, a fraction $f_{\rm mg}(z)$ of galaxies will undergo mergers, yielding $0.5 f_{\rm mg}(z)$ merger remnants. Therefore, the remnant fraction at the present epoch is given by

$$f_{\rm rem} = 1 - \frac{1 - f_{\rm mg}(z)}{1 - 0.5 f_{\rm mg}(z)}. \tag{3.31}$$

Similarly, if we extend this to a lookback time of $NT_{\rm mg}$, where N is an integer, then the remnant fraction is given by

$$f_{\rm rem} = 1 - \prod_{j=1}^{N} \frac{1 - f_{\rm mg}(z_j)}{1 - 0.5 f_{\rm mg}(z_j)}, \tag{3.32}$$

where z_j corresponds to a lookback time of $t = jT_{\rm mg}$. We now make the simple assumption that the merger rate does not change with time. In this case, our present epoch estimate of the merger fraction holds at all redshifts, giving $f_{\rm mg}(z)$=0.011. In order to convert between redshift and lookback time, we must specify a cosmological model. We assume a Hubble constant of h=0.7. For simplicity, we assume q_0=0.5. Therefore, $z = (1 - 3H_0 t/2)^{-2/3} - 1$. Using our merger timescale estimate of $T_{\rm mg}$=0.5 Gyr, we can now investigate the cumulative effect of mergers. With the chosen cosmology, z=1 corresponds to a

lookback time of $\sim$ 6 Gyr, or $12T_{\rm mg}$ (N=12). With this lookback time, Equation 3.32 yields $f_{\rm rem}$=0.066. This implies that $\sim$ 6.6% of galaxies brighter than M_B=$-$18 have undergone mergers since $z \sim 1$.

If the mergers taking place in our sample produce elliptical galaxies, it is worthwhile comparing the remnant fraction to the elliptical fraction (cf. Toomre 1977). The elliptical fraction for bright field galaxies is generally found to be about 10% (e.g., Dressler 1980, Postman and Geller 1984). This result is broadly consistent with the remnant fraction found in this chapter.

While our estimate of the remnant fraction is based on our statistically secure measurement of N_C, it also relies on fairly crude assumptions regarding the merger fraction and merger timescale. In particular, the merger rate has been assumed to be constant. There is no physical basis for this assumption; in fact, a number of studies have predicted a rise in the merger rate with redshift. If this is true, we will have underestimated the remnant fraction, and the relative importance of mergers. In the following chapter, we will address this issue by investigating how the merger rate changes with redshift.

3.10 Conclusions

We have introduced two new pair statistics, N_c and L_c, which are shown to be related to the galaxy merger and accretion rates respectively. Using Monte Carlo simulations, these statistics are found to be robust to the redshift-dependent density changes inherent in flux limited samples; this represents a very significant improvement over all previous estimators. In addition, we provide a clear prescription for relating N_c and L_c to the galaxy CF and LF,

enabling straightforward comparison with measurements on larger scales.

These statistics are applied to the SSRS2 survey, providing the first statistically sound measurements of pair statistics at low redshift. For an effective limiting absolute magnitude of $M_2(B)=-18$, we find $N_c = 0.0227 \pm 0.0052$ at $z=0.016$, implying that $\sim 2\%$ of these galaxies have companions within a projected physical separation of 5 h^{-1} kpc $\leq r_p \leq 20$ h^{-1} kpc and 500 km/s along the line of sight. If this pair statistic remains fixed with redshift, simple assumptions imply that $\sim 6.6\%$ of present day galaxies brighter than $M_B=-18$ have undergone mergers since $z=1$. For our luminosity statistic, we find $L_c = 0.0248 \pm 0.0060 \times 10^{10}\ h^2 L_\odot$. This statistic gives the mean luminosity in companions, per galaxy. Both of these statistics will serve as local benchmarks in ongoing and future studies aimed at detecting redshift evolution in the galaxy merger and accretion rates.

It is our hope that these techniques will be applied to a wide range of future redshift surveys. As we have demonstrated, one must carefully account for differences in sampling effects between pairs and field galaxies. This will be of increased importance when applying pair statistics at higher redshift, as k-corrections, luminosity evolution, band-shifting effects, and spectroscopic completeness have to be properly accounted for. The general approach outlined in this chapter indicates the steps that must be taken to allow for a fair comparison between disparate surveys at low and high redshift. These techniques are applicable to redshift surveys with varying degrees of completeness, and are also adaptable to redshift surveys with additional photometric information, such as photometric redshifts, or even simply photometric identifications. Finally, this approach can be used for

detailed studies of both major and minor mergers.

Chapter 4

Dynamically Close Galaxy Pairs in the CNOC2 Field Galaxy Redshift Survey: Evolution in the Galaxy Merger Rate at $z < 0.5$

4.1 Introduction

In the preceding chapter, we outlined new techniques for measuring pair statistics. These methods were tested extensively, and found to be amenable to robust comparisons of pair statistics at different redshifts. This novel approach was applied to the large, well-defined SSRS2 survey, yielding the first secure estimates of pair statistics at low redshift ($z \sim 0$). In this chapter, we will apply these techniques to the CNOC2 Field Galaxy Redshift Survey (hereafter CNOC2). This large, well-defined sample of galaxies at moderate redshift ($0.1 \leq z \leq 0.55$) will be used to establish how pair statistics evolve with redshift. This will allow us to infer changes in the galaxy merger and

accretion rates.

In Sections 4.2 and 4.3, we describe the CNOC2 survey, and summarize the CNOC2 luminosity function (LF) results of Lin et al. (1999). An overview of the basic methods for computing pair statistics in given in Section 4.4. We then discuss how galaxies are selected for the primary and secondary samples required for the pairs analysis. A detailed treatment of selection effects is given in § 4.6, accounting for flux limits, luminosity evolution, spectroscopic incompleteness, and boundary effects. CNOC2 pair statistics are presented in Section 4.7, and used to measure evolution in the galaxy merger and accretion rates (§ 4.8). Results are discussed in the final section.

4.2 CNOC2 Observations

The CNOC2 Field Galaxy Redshift Survey consists of redshifts for $\sim$ 5000 field galaxies spanning the redshift range $0.1 \leq z \leq 0.55$. The observational technique is similar to that used in the CNOC1 Cluster Redshift Survey (Yee et al. 1996). A detailed description of the CNOC2 observations and data reduction methods will be given by Yee et al. (1999; see also Yee et al. 1997). Here, we give a brief overview of the survey, focussing on aspects relevant to this study.

4.2.1 Survey Overview

The CNOC2 survey covers 4 well-separated patches on the sky, each subtending ~ 0.4 deg^2. These patches have been assigned names based on their

equatorial coordinates (B1950.0), as follows : 0223+00, 0920+37, 1447+09, and 2148-05. Each patch consists of a contiguous L-shaped region with a central block (see Figure 1 of Yee et al. 1997). These patches were chosen to avoid bright stars, known low-redshift clusters, and other bright objects at low redshift. Data were acquired during 7 observing runs at the Canada-France-Hawaii Telescope (CFHT), between February 1995 and May 1998. All imaging and spectroscopic data were obtained with CFHT's Multi-Object Spectrograph (MOS). A total of 74 MOS fields were used, each of size $\sim 9' \times 8'$.

4.2.2 Photometry

Images of all patches were obtained in Kron-Cousins R_C and I_C, and Johnson U, B, and V, using MOS in imaging mode. Exposure times range from 6 to 15 minutes. Object detection, star-galaxy classification, and photometry were carried out using an improved version of the Picture Processing Package (Yee 1991; Yee, Ellingson, and Carlberg 1996). We correct our photometry for extinction from the Milky Way (see Lin et al. 1999). In this study, we will use observations in R_C and B, which have average 5σ detection limits of 24.0 and 24.6 respectively. The primary spectroscopic sample is chosen in the R_C band, and we adopt R_C=21.5 as the nominal spectroscopic completeness limit.

4.2.3 Spectroscopy

Spectra were obtained using the B300 grism, providing a resolution of $\sim$ 15Å. A band-limiting filter was used to enable stacking of spectra, increasing the

size of our redshift sample. The wavelength coverage of this filter is 4400Å to 6300Å. This allows for the identification of important spectral features in galaxies of all spectral types, over the redshift range $0.1 \leq z \leq 0.55$. Redshift measurements were performed using cross-correlation techniques, yielding rms velocity errors of approximately 100 km/s.

For reasons of observational efficiency, we did not attempt to obtain spectra for the complete sample of galaxies with $R_C \leq 21.5$. Instead, two multi-slit masks were used for each field, yielding a total of 80−90 redshifts in most cases. The cumulative redshift sampling rate, defined as the fraction of $R_C \leq 21.5$ galaxies with measured redshifts, is about 50%. The differential redshift sampling rate, which gives the sampling rate at a given apparent magnitude, is highest at bright magnitudes, and decreases to $\sim 20\%$ at R_C=21.5. We have carefully accounted for selection effects that results from the spectroscopic incompleteness of our sample. Discussion of these corrections is deferred to Sections 4.6.3 and 4.6.4.

4.3 The CNOC2 B−Band Luminosity Function

In order to apply pair statistics to a flux-limited sample, rather than a volume limited sample, it is necessary to correct the statistics to some fiducial limiting absolute magnitude (see Chapter 3). We will use the galaxy luminosity function (LF) to make this correction. Lin et al. (1999) have carried out a detailed study of the CNOC2 LF, introducing a convenient parameterization of luminosity and number density evolution. Here, we summarize the results

briefly.

The differential galaxy LF, denoted $\phi(M)$, gives the co-moving number density of galaxies of absolute magnitude M. We adopt the usual Schechter (1976) parameterization of this function,

$$\phi(M) = (0.4 \ln 10)\phi^*[10^{0.4(M^*-M)}]^{1+\alpha} \exp[-10^{0.4(M^*-M)}], \qquad (4.1)$$

with characteristic absolute magnitude M^*, faint-end slope α, and normalization ϕ^*. Numerous studies have revealed significant evolution in the galaxy LF, even at the fairly modest redshifts of concern here (see Ellis 1997 for a review). Hence, the LF parameters will, in general, vary with redshift. This evolution can be parameterized as follows :

$$\begin{aligned} M^*(z) &= M^*(0.3) - Q(z - 0.3) \\ \alpha(z) &= \alpha(0) \\ \phi^*(z) &= \phi^*(0)10^{0.4Pz} . \end{aligned} \qquad (4.2)$$

Here, Q provides a linear fit to M^* or luminosity evolution, while P models density evolution. Lin et al. (1999) used 5−colour photometry ($UBVR_CI_C$) to classify galaxies according to their spectral energy distributions (SED's). Treating early, intermediate, and late-type galaxies separately, they computed the galaxy LF in the rest-frame B_{AB}, R_C, and U bandpasses. We summarize their results for the B_{AB} LF (h=1) in Table 4.1. As we are concerned only with the global field population, we will combine LF's for the three SED types. In order to compare with B-band pair statistics at low redshift, we will transform from B_{AB} using the relation $B = B_{AB} + 0.14$ (Fukugita et al. 1995).

Table 4.1: CNOC2 B_{AB} LF Parameters

Sample	$M^*(z{=}0.3)$	α	$\phi^*(z{=}0)$	P	Q
		$q_0 = 0.5$			
Early	-19.06	0.08	0.0203	-1.07	1.58
Intermediate	-19.38	-0.53	0.0090	0.73	0.90
Late	-19.26	-1.23	0.0072	3.08	0.18
		$q_0 = 0.1$			
Early	-19.19	0.08	0.0197	-1.79	2.00
Intermediate	-19.51	-0.53	0.0087	0.00	1.32
Late	-19.38	-1.23	0.0071	2.34	0.61

4.4 Basic Method

In the previous chapter, we outlined new techniques for measuring pair statistics. These techniques were used to compute pair statistics at low redshift, providing the local benchmark for measuring evolution in the galaxy merger and accretion rates. In this section, we outline the key results from this earlier work, setting the stage for our analysis of CNOC2 pairs.

1) Close pairs of galaxies provide the best available means of estimating the galaxy merger rate, and its evolution with time. Traditional close pair statistics provide an integrated measure of galaxy clustering on small scales, and are often assumed to be largely independent of selection effects such as sampling depth and completeness. However, these statistics, like the merger rate, necessarily depend on both clustering and limiting absolute magnitude (or minimum mass). In order to account for the latter, one must specify a limiting absolute magnitude (or mass) when computing pair statistics. Fur-

thermore, when comparing the pair statistics of different samples, one must ensure that this limit is the same for all samples.

2) When applying pair statistics to flux-limited surveys, it is necessary to select a limiting absolute magnitude which is representative of the sample. One must then correct the pair statistics for the change in sampling depth with redshift. A number of pair statistics are not well suited to making these corrections. This includes the fraction of galaxies in pairs, and nearest neighbour statistics. Pairwise statistics are the most straightforward to apply correctly.

3) Two robust pair statistics were introduced. The number of close companions per galaxy, hereafter called N_c, is directly related to the galaxy merger rate. The luminosity in companions per galaxy, designated L_c, is directly related to the mass accretion rate. These statistics are applied to primary and secondary samples of galaxies, where one searches for companions (in the secondary sample) close to host galaxies (primary sample). A weighting scheme was introduced, allowing these statistics to be computed for a flux-limited sample. These weights recover correctly the equivalent volume-limited pair statistics (verified with Monte Carlo simulations) and minimize the uncertainty in the measured pair statistics.

4) Pairs in redshift space can be uniquely specified by their projected physical separation (r_p) and rest-frame line-of-sight velocity difference (Δv). A useful definition of a close companion that is likely to merge in a short timescale ($T_{\rm mg} \lesssim 0.5$ Gyr) is 5 h^{-1} kpc$< r_p \leq 20\ h^{-1}$ kpc and $\Delta v \leq 500$ km/s. These choices make sense from a theoretical standpoint; furthermore, we now have empirical evidence to support the assumption that these are

good merger candidates. At least half of all SSRS2 pairs satisfying these criteria exhibit clear morphological signs of on-going interactions.

5) Pair statistics were computed for the SSRS2 survey, which consists of 5426 galaxies at $z \sim 0$. Primary and secondary samples are drawn from the same set of galaxies, with $M_B \leq -18$. Using close ($5\ h^{-1}$ kpc $\leq r_p \leq 20\ h^{-1}$ kpc) dynamical ($\Delta v \leq 500$ km/s) pairs and $M_2(B)=-18$, pair statistics are as follows : $N_c(M_B \leq -18) = 0.0227 \pm 0.0054$ and $L_c(M_B \leq -18) = 0.0235 \pm 0.0061 \times 10^{10}\ h^2 L_\odot$ at z=0.016. These are the first secure measurements of pair statistics at low redshift.

4.5 Sample Selection

We will now apply these techniques to the CNOC2 survey. In this section, we outline our approach for identifying a well-defined sample of galaxies to be used in the pairs analysis. We begin by describing our choice of a flux-limited sample that is not biased towards different galaxy SED types. We then prune the sample in order to minimize the effects of luminosity-dependent clustering on the pair statistics.

4.5.1 Flux Limit

As with earlier studies, we choose to use a flux-limited sample. Galaxies were originally selected for follow-up spectroscopy based on their R_C-band apparent magnitudes. As described in Section 4.2, the nominal spectroscopic completeness limit for CNOC2 is R_C=21.5. We adopt this as our initial flux limit. It is important to note that the observed R_C-band corresponds to

rest-frame B-band at z=0.5. Thus, we are selecting these galaxies based on their flux in the optical part of the spectrum. While we have selected galaxies based on their R_C-band flux, we are actually more interested in their luminosity in the rest-frame $B-$band. The primary reason for this choice is to enable us to perform a direct comparison with the low$-$redshift $B-$band pair statistics from the SSRS2 survey. Our $B-$band photometry will be used to measure galaxy luminosities, for use in the pair statistics. In Figure 4.1, $B-$band luminosity is plotted versus redshift for all CNOC2 galaxies above the initial flux limit ($R_C \leq 21.5$) and $0.1 \leq z \leq 0.55$. We will continue to refer to this figure as we impose more restrictions on this initial sample.

4.5.2 Estimating k-corrections

Interpretation of galaxy fluxes is complicated by band-shifting effects when redshifts are significantly larger than zero. A galaxy's spectrum will be shifting redward, with the observed wavelength of each feature being a factor of $(1 + z)$ larger than the true rest-frame wavelength. For a spectrum that is not flat and featureless, this will alter the flux observed in a given spectral range, such as that spanned by a broadband filter. While these effects are negligible for low-redshift samples such as SSRS2, they must be accounted for in the moderate-z CNOC2 survey under consideration here. In order to compensate for these effects, one needs to know the redshift and spectral energy distribution (SED) of each galaxy, along with the characteristics of the broadband filters being used. We have computed $B-$band k-corrections (hereafter k_B), which are used to correct the observed apparent magnitudes

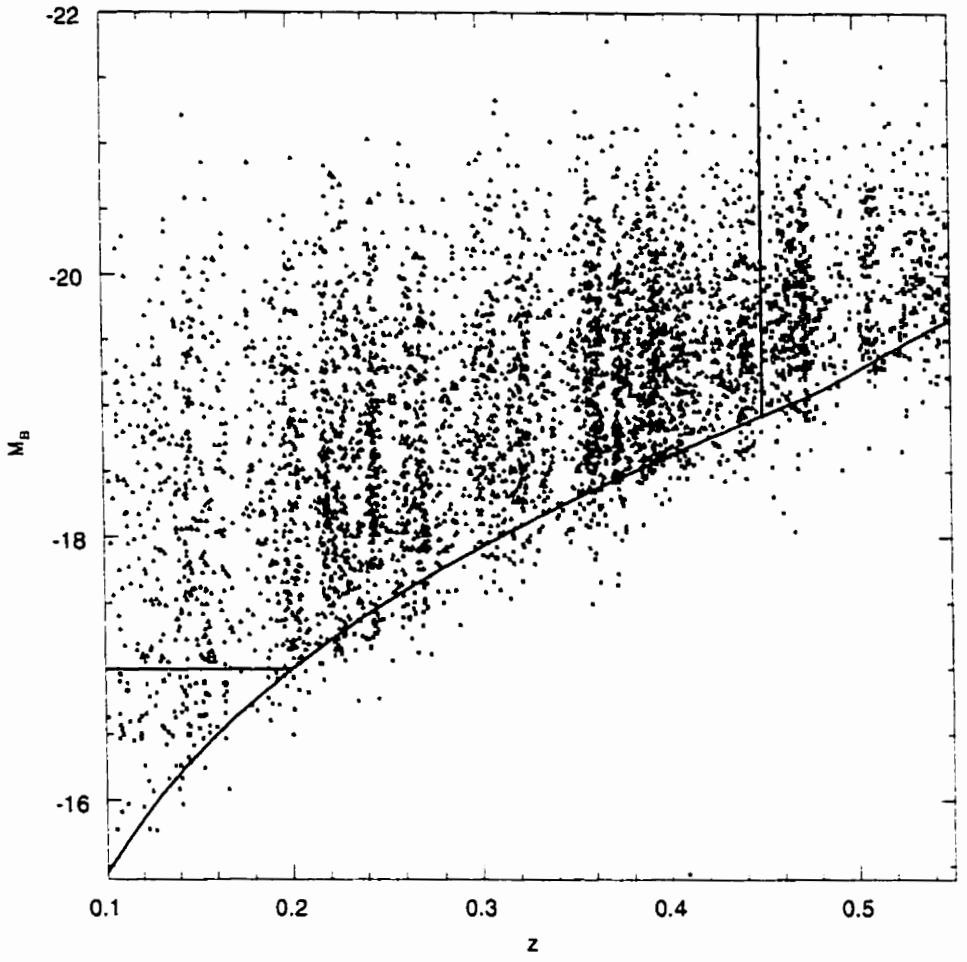

Figure 4.1: $B-$band absolute magnitude is plotted versus redshift for all CNOC2 galaxies with $R_C \leq$=21.5 and $0.1 \leq z \leq 0.55$. The curved line gives the limit imposed by the limiting apparent magnitude, assuming the maximum k-correction ($k_{R_C toB}$) at redshift z. The vertical line marks the maximum redshift (z_{max}= 0.45) allowed. The horizontal line gives the faintest absolute magnitude permitted (M_{faint}= -17). Galaxies satisfying all of these criteria (and hence used in the calculation of N_c and L_c) are marked with triangles; the remainder are indicated with crosses.

to the desired rest frame magnitudes. These k-corrections are computed by first fitting our 5−colour photometry ($UBVR_CI_C$) to the SED models of Coleman, Wu, and Weedman (1980). After interpolating to obtain an SED type, the interpolated SED is then used to derive the k-correction.

Having computed k-corrections for each galaxy, we must consider how these k-corrections will affect the initial flux limit imposed on the sample. As these k-corrections vary for galaxies with different SED's, we run the risk of preferentially selecting galaxies of a particular spectral type. This applies to galaxies that lie close to the flux limit. To avoid this bias, we will choose a more conservative limit, to ensure that galaxies of all spectral types will be observable. First, we compute the maximum k-correction at each redshift. This is done by using the k-corrections of Coleman, Wu and Weedman (1980), for 4 different SED types (E/S0, Sbc, Scd, and Im). At each redshift, we select the SED type with the largest k-correction. This is shown in Figure 4.2. At $z \lesssim 0.47$, the E/S0 spectral type has the maximum k-correction, while the Im spectral type takes over at higher redshift (k-corrections are nearly identical for all galaxy types at $z \sim 0.48$). This gives us a function, denoted $k^{\max}_{R_C \to B}(z)$, which provides a good estimate of the maximum k-correction at all redshifts of interest.

We now combine this function with the chosen flux-limit (R_C=21.5) to set the limiting absolute magnitude as a function of redshift. This is given by the following expression

$$M_{\rm lim}(z_i) = m - 5\log d_L(z) - 25 - k^{\max}_{R_C \to B}(z). \qquad (4.3)$$

This relation is shown in Figure 4.1. This constraint ensures that galaxies of

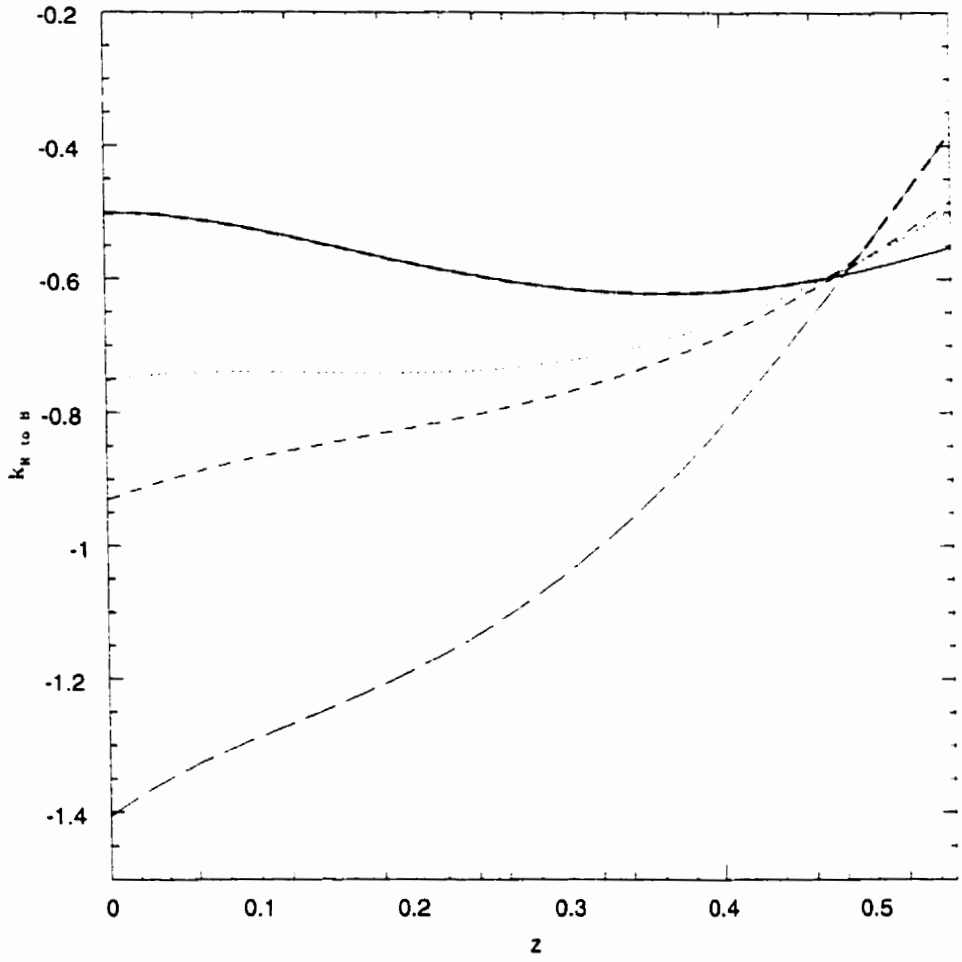

Figure 4.2: Model k-corrections from Coleman, Wu, and Weedman (1980) are given for 4 galaxy types. Lines are as follows : E/S0 (solid line), Sbc (dotted line), Scd (dashed line), and Im (long−dashed line). The maximum k-correction (k_{max}) is marked with a thick dashed line.

all spectral types will have an equal probability of falling within our sample.

4.5.3 Minimizing the Luminosity Dependence of Clustering

As discussed in Chapter 3, it is prudent to constrain a flux−limited sample in both redshift and absolute magnitude, in order to minimize the bias that may be introduced by luminosity−dependent clustering. They demonstrated empirically that this approach is generally successfully in recovering a sample that is free of strong luminosity dependence. We begin by imposing a maximum redshift of $z_{\rm max}$= 0.45. This eliminates the high redshift end of the sample, where all galaxies are intrinsically quite luminous ($M_B < -19$). We also impose a limiting absolute magnitude of $M_{\rm faint}(B)$=−17. This eliminates the subset of galaxies that is intrinsically the most faint, and affects galaxies only at $z < 0.2$. These two constraints are shown in Figure 4.1. Our final sample consists of 3434 galaxies which satisfy all of the criteria outlined in this section.

4.5.4 Choosing M_1 and M_2

The final step is to identify primary and secondary samples. As reviewed in Section 4.4, the general approach is to search for companions in the secondary sample that are close to host galaxies in the primary sample. When computing pair statistics, it is critical that one impose a representative limiting absolute magnitude M_2 for companions. This is straightforward for a volume-limited sample. For a flux-limited sample such as CNOC2, one must instead select a representative limiting absolute magnitude, and then correct

the pair statistics to this limit. The mean limiting absolute magnitude of the sample, computed using weights described in the following section, is $M_B=-17.7$. For convenience, we select $M_2(B)=-18$. This is identical to the limit chosen in Chapter 3 for the SSRS2 sample, enabling us to make a direct comparison between our CNOC2 pair statistics ($z \sim 0.3$) and the SSRS2 pair statistics ($z \sim 0$). We must also choose a limiting absolute magnitude for the primary sample (M_1). In order to maximize the number of pairs observed, we set $M_1=M_2$.

4.6 Accounting For Selection Effects

In Chapter 3, we devised a simple weighting scheme to apply when measuring pair statistics for a flux-limited redshift survey. We will generalize this approach to account for several additional selection effects present in CNOC2. There are two key points to consider. First, companions should be weighted so as to renormalize correctly the number of companions to that expected for a volume-limited sample with $M \leq M_2$. Secondly, one should apply weights to galaxies in the primary sample (so-called host galaxies) so as to give larger weights to galaxies that are likely to have larger numbers of *observed* companions. By choosing these weights appropriately, one will minimize the measurement error in the pair statistics. In the following sections, we will apply this methodology to several selection effects that are present in our sample. We will treat each selection effect separately at first, showing how they relate to the weights of galaxies in the primary (w_1) and secondary (w_2) samples. Where necessary, we will distinguish between weights appli-

cable specifically to N_C (w_{N_1}, w_{N_2}) and L_C (w_{L_1}, w_{L_2}). In Section 4.6.6, we summarize and combine these weights to give expressions for the final weights used in the pairs analysis.

4.6.1 Correcting for the Flux Limit

We must first determine $M_{\rm lim}(z_i)$, which gives the limiting absolute magnitude allowed at redshift z_i. At most redshifts, this is imposed by the limiting apparent magnitude m, such that $M_{\rm lim}(z_i) = m - 5\log d_L(z) - 25$. At the low redshift end of the sample, however, $M_{\rm faint}$ (defined in § 4.5.3) will take over. That is, the limiting absolute magnitude used for identifying galaxies in the secondary sample is given by

$$M_{\rm lim}(z_i) = \max[M_{\rm faint}, m - 5\log d_L(z) - 25]. \tag{4.4}$$

When relating a flux-limited sample to its volume-limited counterpart, it is possible to transform between the two, provided the LF is known. The selection function, denoted $S(z)$, is defined as the density of galaxies expected in the flux-limited sample, divided by the density of galaxies expected in the volume-limited sample. We will use this function to derive appropriate weights for our pair statistics. As shown in Chapter 3, these weights concern the density of galaxies in the secondary sample only ($M \leq M_2$). The form of the selection function, given for both number density ($S_N(z)$) and luminosity density ($S_L(z)$), is as follows :

$$S_N(z_i) = \frac{\int_{-\infty}^{M_{\rm lim}(z_i)} \phi(M)dM}{\int_{-\infty}^{M_2} \phi(M)dM}, \tag{4.5}$$

$$S_L(z_i) = \frac{\int_{-\infty}^{M_{\rm lim}(z_i)} \phi(M)LdM}{\int_{-\infty}^{M_2} \phi(M)LdM}. \tag{4.6}$$

In order to recover pair statistics that are applicable to a secondary sample with $M \leq M_2$, one should apply weights $w_{N_2}(z_i) \propto 1/S_N(z_i)$ and $w_{L_2}(z_i) \propto 1/S_L(z_i)$ to all companions at redshift z_i. Errors in the pair statistics are minimized by applying weights to galaxies in the primary sample that are the reciprocal of the secondary weights (see Chapter 3). Thus, $w_{N_1}(z_i) \propto S_N(z_i)$ and $w_{L_1}(z_i) \propto S_L(z_i)$.

4.6.2 Luminosity Evolution

The preceding section relies on the implicit assumption that the mass-to-light ratio (M/L) of galaxies is the same at all redshifts. That is, by choosing a limiting absolute magnitude (M_2) that does not change with redshift, we are assuming that this corresponds to a fixed minimum mass. This assumption does not hold over the sizable redshift range ($0.1 \leq z \leq 0.55$) explored here. While there is considerable controversy in the literature as to how and why galaxies evolve over this redshift range, it is certain that some evolution does take place (Lin et al. 1999). At the very least, galaxies will evolve passively, as a result of the normal aging of its stellar population. The net effect appears to be a gradual fading of optical light with time. Therefore, mean galaxy luminosities will increase with redshift, at least over the range of redshift under consideration here.

This luminosity evolution can lead to a significant bias in our pair statistics. By using a fixed M_2, the apparent number and luminosity density of galaxies would appear to increase with redshift, even if galaxy masses did not change. Thus, we would be probing further down the mass function at higher redshift. However, as we have stressed earlier in this study, pair

statistics will continue to increase as one probes deeper. Therefore, without correction, this effect would lead to an apparent increase in pair statistics with redshift, even if there is no change in the galaxy distribution. This is a very important issue, and it has not been addressed in any pairs study to date.

At present, we are unable to measure the amount of brightening for individual galaxies in our sample. Thus, we are not able to make a rigorous correction for this bias. However, a detailed study of LF evolution within the CNOC2 sample (Lin et al. 1999) has provided some useful indications of the global trends that are present. In Section 4.3, we provided an overview of the results from this analysis. Of particular interest is the modelling of M^* evolution, given by the parameter Q. We will take M^* to be representative of the mean luminosity of CNOC2 galaxies. Thus, a galaxy at redshift z will be assumed to be brightened by Qz magnitudes. The mean value of this parameter, averaged over all SED types, is $Q \sim 1$. We assume Q=1 throughout the remainder of this analysis, unless specified otherwise. However, for clarity, Q is given explicitly in the equations that follow.

We must now incorporate this luminosity evolution into the measurement of pair statistics. The most straightforward approach is to simply modify M_2 when computing the selection function. Recall from the previous section that the selection function is used to generate weights, which in turn correct pair statistics for the varying minimum luminosity of a flux-limited redshift survey. We will incorporate Q into the selection function, such that the pair statistics will be normalized to a fixed evolution-corrected limiting absolute magnitude. To do this, the selection function will be modified for a sample

with a limiting absolute magnitude of $M_2 + Qz$, rather than the fixed M_2 described earlier. Therefore, Equations 4.5 and 4.6 must be rewritten, as follows :

$$S_N(z_i) = \frac{\int_{-\infty}^{M_{\rm lim}(z_i)} \phi(M)dM}{\int_{-\infty}^{M_2-Qz_i} \phi(M)dM}, \tag{4.7}$$

$$S_L(z_i) = \frac{\int_{-\infty}^{M_{\rm lim}(z_i)} \phi(M)LdM}{\int_{-\infty}^{M_2-Qz_i} \phi(M)LdM}. \tag{4.8}$$

To provide an intuitive feel for this correction, we give a simple example. Suppose we compute pair statistics for M_2=$-$18 at z=0, and wish to make a direct comparison with a sample at z=0.3. Assuming Qz=0.3 magnitudes of luminosity evolution, we should normalize to $-$18.3 at z=0.3. This will increase $S_N(z_i)$ and $S_L(z_i)$, and will translate into a decrease in N_C and L_C. In Section 4.8.3, we will discuss the impact of this correction on the main results of this study.

4.6.3 Overall Spectroscopic Completeness

The CNOC2 survey, like many other redshift surveys, is not spectroscopically complete. This incompleteness must be taken into account when computing pair statistics. To understand why this is necessary, suppose we randomly acquired redshifts for some fraction x of all galaxies. In this case, for any given primary galaxy, we would detect a fraction x of its close companions. Thus, the pair statistics (N_C and L_C) would be underestimated by a factor of $1/x$. Clearly this effect is very significant if the sampling is sparse. This is the case for CNOC2, so we must carefully account for these effects.

If galaxies were chosen at random for followup spectroscopy, this procedure would be very straightforward. One would compute the cumulative

redshift sampling rate (§ 4.2.3), and assign each galaxy a weight equal to the reciprocal of this number. For CNOC2, however, galaxies are not chosen completely at random. Fortunately, the selection effects are well-understood, allowing for an accurate modelling of the selection process. This incompleteness is primarily a function of apparent magnitude. This effect is mainly a consequence of differences in the signal-to-noise ratio for objects of different brightness, and the distribution of apparent magnitudes for objects selected in the mask design process. A secondary correction is made to account for a dependence in colour. This selection effect arises from the varying strength of spectral features in galaxies of different spectral types. Selection weights have been computed to account for dependence on both apparent magnitude (w_m) and colour (w_c). The reader is referred to Yee, Ellingson, and Carlberg (1996) and Lin et al. (1999) for a more thorough discussion of these selection weights. For this study, we combine these weights to arrive at a spectroscopic weight for each galaxy, denoted w_z, where $w_z = w_m w_c$.

We must now decide how to apply these weights to the pair statistics. As mentioned above, one must apply these weights to each close companion, in order to compensate for the underestimate in N_C and L_C. Thus, $w_2 \propto w_z$. When applying weights to primary galaxies, the idea is to give increased weight to galaxies which are likely to have larger numbers of observed companions. In this case, the spectroscopic weight of a primary galaxy does not tell us whether we are more or less likely to find observed companions. This is because there is no direct correlation between the spectroscopic weights of two galaxies in a close pair (the two members may have completely different apparent magnitudes and colours). Therefore, we choose not to apply these

spectroscopic weights to galaxies in the primary sample.

4.6.4 Spectroscopic Completeness at Small Separations

We have accounted for the overall spectroscopic incompleteness as a function of apparent magnitude and colour. We now investigate if there is any dependence on pair separation. Recall that we use two masks per field when acquiring spectra (see § 4.2.3). While this increases the overall completeness of the survey, it also allows for a better handling of objects in close pairs. If two objects are close together on the sky, it is usually not possible to place a slits on both objects simultaneously. Hence, if a single mask is used, these objects will be systematically underselected. Our mask design program compensates for this effect by giving preference to these objects on the second mask (Yee, Ellingson, and Carlberg 1996). Here, we will check to see how well this algorithm has worked, to ensure that any remaining bias in the spectroscopic selection of pairs is accounted for.

We begin by identifying two samples of galaxies. The first contains all CNOC2 galaxies with $R_C \leq 21.5$, and will be referred to as the photometric sample. We then identify a spectroscopic sample, which consists of all galaxies in the photometric sample with measured redshifts in the range $0.1 \leq z \leq 0.55$. We will use the ratio of galaxies in these two samples to measure spectroscopic completeness.

We wish to determine how the spectroscopic completeness varies as a function of angular pair separation θ. We begin by measuring θ for all pairs in the photometric sample. These pairs will be referred to as p-p pairs. Similarly, we find all z-z pairs in the spectroscopic sample. We assign these

pairs to bins of angular size 5″, for separations less than 5′. If paired galaxies are selected fairly, the number of z-z pairs (hereafter N_{zz}) is related to the number of p-p pairs (N_{pp}) as follows :

$$N_{zz}(\theta) = f_z^2 N_{pp}(\theta), \tag{4.9}$$

where f_z is the mean spectroscopic completeness on large scales. We compute $N_{zz}(\theta)/N_{pp}(\theta)$ for the full CNOC2 sample, and compute error bars using the Jackknife technique. The results are given in the lower panel of Figure 4.3.

It is immediately apparent that there is a significant and systematic decrease in spectroscopic completeness at small separations. This deficit is noticeable at $\sim$ 3′, and increases fairly smoothly down to $\approx$ 10″. A sharp drop is seen below 10″. These results clearly indicate that our mask design algorithm does not completely compensate for pair selection effects. Without correction, this would lead to a very significant underestimate in the pair statistics measured in this study. Most of our close pairs lie at $\theta \leq 10''$, where the deficit is greatest.

We will correct for this effect by modelling the incompleteness and using this to generate weights for removing the bias. As the clear trend on large scales does not continue below θ=10″, we will treat these regimes separately. At $\theta \leq 10''$, the error bars become too large to detect any significant trends. Hence, we use a fixed value of N_{zz}/N_{pp}=0.14. For $\theta > 10''$, we fit an exponential function to the data. In order to ensure convergence with measurements on large scales, this function is constrained to asymptotically approach f_z^2=0.1838 at $\theta \sim 300''$. After smoothing the data, this fitting

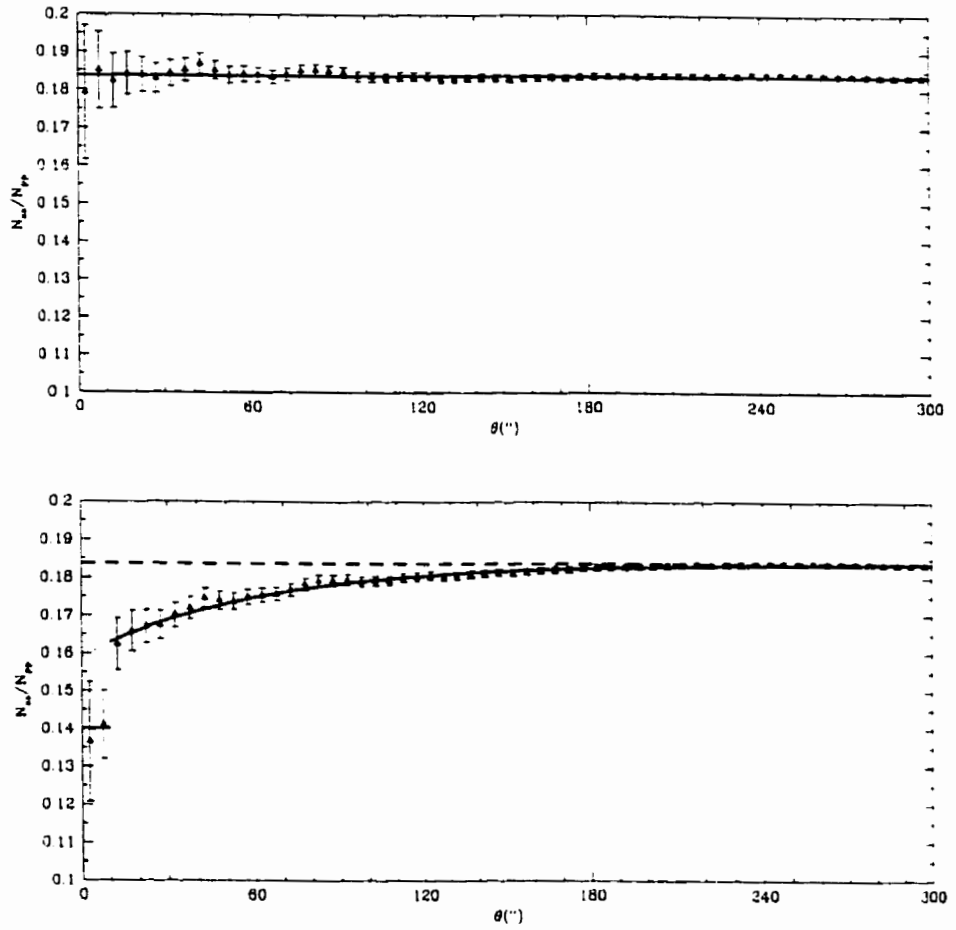

Figure 4.3: Spectroscopic completeness is computed for a range of angular pair separations. (a) In the lower plot, we compute the ratio of spectroscopic pairs (N_{zz}) to photometric pairs (N_{pp}), for a range of angular separations. With fair selection, $N_{zz}/N_{pp} = f_z^2 \approx 0.1838$ (dashed line). Error bars are computed using the Jackknife technique. We model the incompleteness with a power law at $\theta > 10''$. The dotted line indicates that this provides an inadequate fit at $\theta \leq 10''$; hence, we take N_{zz}/N_{pp}=0.14. This combined fit is marked with a thick solid line. (b) The observed spectroscopic completeness is corrected using weights from the smoothed fit, and plotted in the upper panel. The horizontal solid line gives f_z^2=0.1838.

scheme yields the following expression :

$$g(\theta) = \begin{cases} 0.14 & \theta \leq 10'', \\ (f_0^2 - f_z^2)\mathrm{e}^{-a\theta} + f_z^2 & \theta > 10'', \end{cases} \tag{4.10}$$

where f_0^2=0.159 and a=0.0169. This function gives a good match to the data and is shown in the lower panel of Figure 4.3.

Using this functional fit, we are able to estimate the deficit in spectroscopic completeness as a function of angular separation. To remove this deficit, we assign each member of the pair a weight, denoted w_θ, that is inversely proportional to the deficit. That is, $w_\theta = \sqrt{f_z^2/g(\theta)}$ (recall that, if pairs are selected fairly, $g(\theta) = f_z^2$). We repeat the measurement of spectroscopic completeness using these weights, and plot the results in the upper panel of Figure 4.3. The corrected measurements of N_{zz}/N_{pp} are consistent at all separations less than 5′, within the errors. Thus, this weighting scheme successfully removes the bias due to decreased spectroscopic completeness on small scales.

We must now incorporate these weights (w_θ) into the measurement of pair statistics. The first task is to ensure that we apply weights to the secondary sample such that the correct number or luminosity of companions will be recovered. Clearly, for each companion at separation θ, one should apply weight $w_{2_\theta} = w_\theta$. For the close companions found in this study, $\bar{\theta} = 5''.0$, yielding $\bar{w_{2_\theta}} = 1.15$. The net effect of these weights is to increase the observed pair statistics by $\approx 15\%$. We must also consider the primary sample. Weights should be assigned only if there is a known effect on the likelihood of finding observed companions. The decreased spectroscopic completeness on small scales applies only to observed companions at known separations.

Therefore, all primary galaxies should be treated equally. As a result, we do not apply w_θ weights to galaxies in the primary sample. This is consistent with the weighting scheme used in Figure 4.3.

4.6.5 Boundary Effects

Some of the galaxies in the primary sample lie close to the edge of the field (on the sky), or within $\Delta v^{\rm max}$ of the redshift limits. In addition, a number of galaxies lie close to bright stars; consequently, some of the surrounding regions may be hidden from view. Each of these factors will contribute to an underestimate of the pair statistics.

For CNOC2, we have generated field area maps which mark out the edges of each patch, and indicate which regions are blocked by bright stars. For each galaxy in the primary sample, we compute the fraction of the sky within $r_p^{\rm min} \leq r_p \leq r_p^{\rm max}$ that lies within these survey boundaries, where $r_p^{\rm min}$ and $r_p^{\rm max}$ denoted the minimum and maximum projected separation used to define close companions. This fraction will be denoted f_b. For CNOC2, our usual choices of $r_p^{\rm min}$ and $r_p^{\rm max}$ (see § 4.4) lead to $f_b = 1$ for 94.7% of the galaxies in the primary sample. For the remainder, most have f_b close to 1, with a total of only 0.2% having $f_b < 0.5$. Each companion is assigned a boundary weight $w_{b_2} = 1/f_b$, where f_b is associated with its host galaxy from the primary sample. By multiplying each companion by its boundary weight, we will recover the correct number of companions. To minimize errors, primary galaxies are assigned weights $w_{b_1} = f_b$.

We now consider galaxies which lie near the survey boundaries along the line of sight. We follow the approach laid out in Section 3.6.2. That

is, we exclude all companions that lie between a primary galaxy and its nearest redshift boundary, provided the boundary lies within $\Delta v^{\max}$ of the primary galaxy. We assign a weight of w_{2_v}=2 to any companions found in the direction opposite to the boundary. To minimize the errors in computing the pair statistics, the corresponding primary galaxies are assigned weights w_{v_1}=0.5.

4.6.6 Combining Weights

To summarize, weights for companions in the secondary sample are given by :

$$w_{N_2} = S_N(z_i)^{-1} w_{z_2} w_{2_\theta} w_{b_2} w_{v_2}, \tag{4.11}$$

$$w_{L_2} = S_L(z_i)^{-1} w_{z_2} w_{2_\theta} w_{b_2} w_{v_2}, \tag{4.12}$$

where $S_N(z)$ and $S_L(z)$ are given by Equations 4.7 and 4.8 respectively (and not Equations 4.5 and 4.6). For the primary sample, the corresponding expressions are as follows :

$$w_{N_1} = S_N(z_i) w_{b_1} w_{v_1}, \tag{4.13}$$

$$w_{L_1} = S_L(z_i) w_{b_1} w_{v_1}. \tag{4.14}$$

The total number and luminosity of close companions for the i^{th} primary galaxy, computed by summing over the j galaxies satisfying the close companion criteria, is given by $N_{c_i} = \sum_j w_{N2}(z_j)$ and $L_{c_i} = \sum_j w_{L2}(z_j) L_j$ respectively. The mean number and luminosity of close companions is then computed by summing over all galaxies in the primary sample, using weights

w_{N1} and w_{L1}, yielding

$$N_c = \frac{\sum_i w_{N1}(z_i) N_{c_i}}{\sum_i w_{N1}(z_i)} \tag{4.15}$$

$$L_c = \frac{\sum_i w_{L1}(z_i) L_{c_i}}{\sum_i w_{L1}(z_i)}. \tag{4.16}$$

4.7 CNOC2 Pair Statistics

We have now set out an approach for measuring pair statistics for the CNOC2 survey. We define a close companion to be one with a projected physical separation of $5\ h^{-1}$ kpc $\leq r_p \leq 20\ h^{-1}$ kpc and a rest-frame line-of-sight velocity difference of $\Delta v \leq 500$ km/s. Using this definition, and the survey parameters set out above, we find a total of 88 close companions in CNOC2. When using the same limiting absolute magnitude for the primary and secondary samples (i.e., M_1=M_2) as we have done here, a given galaxy pair usually contributes two companions. For CNOC2, this is the case for all of our pairs; furthermore, no triples are found. Thus, our 88 close companions are found in 44 unique pairs. The basic properties of these pairs are listed in Tables 4.2–4.5. A histogram of companion absolute magnitudes is given in Figure 4.4. We also present a mosaic of R_C–band images for these systems in Figure 4.5. Some of these pairs exhibit clear signs of interactions; however, in most cases, the poor resolution of these ground based images renders classification uncertain at best.

Table 4.2: CNOC2 0223+00 Close Pairs

ID	N	r_p	Δv	RA(1950.0)	DEC(1950.0)	$\bar{z}$
1	2	18.3	103	00:00:48.9	-00:16:05	0.13339
2	2	8.3	399	00:00:10.0	+00:06:55	0.19578
3	2	13.2	232	00:00:41.1	-00:11:26	0.26693
4	2	12.7	133	00:00:54.6	-00:00:29	0.35090
5	2	6.0	318	00:02:36.1	-00:22:15	0.27009
6	2	6.7	273	00:00:37.3	+00:03:08	0.40391
7	2	6.6	63	00:00:13.1	-00:05:57	0.38407
8	2	6.0	162	00:00:14.2	+00:11:52	0.29829
9	2	19.1	189	00:00:07.4	+00:28:36	0.27099
10	2	12.8	76	00:00:28.7	-00:11:20	0.26747
11	2	11.5	264	00:00:14.3	+00:15:19	0.40769
12	2	11.1	76	00:01:01.8	-00:17:20	0.14997
13	2	16.6	9	00:00:00.2	-00:01:29	0.26799
14	2	19.4	189	00:00:04.5	+00:12:57	0.30031
15	2	7.4	62	00:00:14.3	+00:22:30	0.39882
16	2	5.5	101	00:00:10.1	+00:19:41	0.39666

Using this sample of companions, the pair statistics were computed for each of the 4 CNOC2 patches. Errors were computed using the Jackknife technique. These results are given in Table 4.6. Results from the 4 patches were combined, weighting by Jackknife errors, to give $N_c = 0.0342 \pm 0.0077$ and $L_c = 0.0367 \pm 0.0093 \times 10^{10}\ h^2 L_\odot$ at z=0.271. Results from all 4 patches are consistent with these mean values, within the quoted 1σ errors. We now investigate how sensitive these results are to the particular parameters selected in this study.

Table 4.3: CNOC2 0920+37 Close Pairs

ID	N	r_p	Δv	RA(1950.0)	DEC(1950.0)	$\bar{z}$
17	2	18.2	423	00:00:13.0	-00:00:21	0.19171
18	2	18.1	2	00:00:10.2	+00:39:08	0.24652
19	2	5.4	284	00:00:41.9	+00:03:08	0.24645
20	2	13.1	193	00:00:04.0	+00:26:31	0.13640
21	2	13.8	360	00:00:16.8	+00:00:31	0.19029
22	2	6.0	50	00:00:27.4	+00:01:53	0.39017
23	2	5.5	87	00:01:12.2	-00:14:28	0.24452
24	2	7.4	29	00:00:13.1	+00:06:09	0.32471
25	2	8.7	198	00:01:02.8	-00:18:20	0.39208
26	2	17.3	10	00:02:07.6	-00:24:02	0.44085
27	2	12.8	196	00:00:07.3	+00:38:60	0.20778

Table 4.4: CNOC2 1447+09 Close Pairs

ID	N	r_p	Δv	RA(1950.0)	DEC(1950.0)	$\bar{z}$
28	2	9.6	5	00:00:46.9	-00:11:50	0.14608
29	2	18.1	404	00:00:41.4	-00:11:40	0.26193
30	2	18.4	43	00:01:15.0	-00:11:55	0.19365
31	2	12.1	212	00:00:07.7	-00:10:49	0.27244
32	2	6.5	184	00:00:10.7	-00:16:11	0.26968
33	2	19.5	94	00:00:05.2	+00:02:32	0.21406
34	2	5.9	138	00:00:15.7	+00:30:25	0.34926
35	2	16.2	171	00:00:27.1	+00:03:37	0.36420
36	2	12.0	111	00:01:23.9	-00:12:35	0.32429
37	2	11.7	41	00:00:31.2	-00:03:42	0.32469

Table 4.5: CNOC2 2148-05 Close Pairs

ID	N	r_p	Δv	RA(1950.0)	DEC(1950.0)	$\bar{z}$
38	2	19.8	249	00:00:09.0	+00:45:30	0.15447
39	2	6.6	107	00:01:59.8	-00:25:21	0.31239
40	2	18.4	115	00:00:22.4	-00:05:24	0.14462
41	2	16.9	48	00:00:07.2	+00:15:44	0.19767
42	2	16.8	143	00:00:01.4	+00:48:14	0.40839
43	2	7.9	6	00:00:42.6	+00:03:59	0.42589
44	2	7.3	15	00:00:11.8	-00:19:11	0.39884

Table 4.6: CNOC2 Pair Statistics

Sample	N	N_{comp}	$\bar{z}$	N_c	$L_c(10^{10}h^2L_\odot)$
0223	988	32	0.287	0.0512± 0.0187	0.0508± 0.0210
0920	911	22	0.272	0.0296± 0.0128	0.0326± 0.0159
1447	757	20	0.271	0.0335± 0.0149	0.0362± 0.0182
2148	866	14	0.253	0.0294± 0.0170	0.0307± 0.0206
CNOC2	3522	88	0.271	0.0342± 0.0077	0.0367± 0.0093

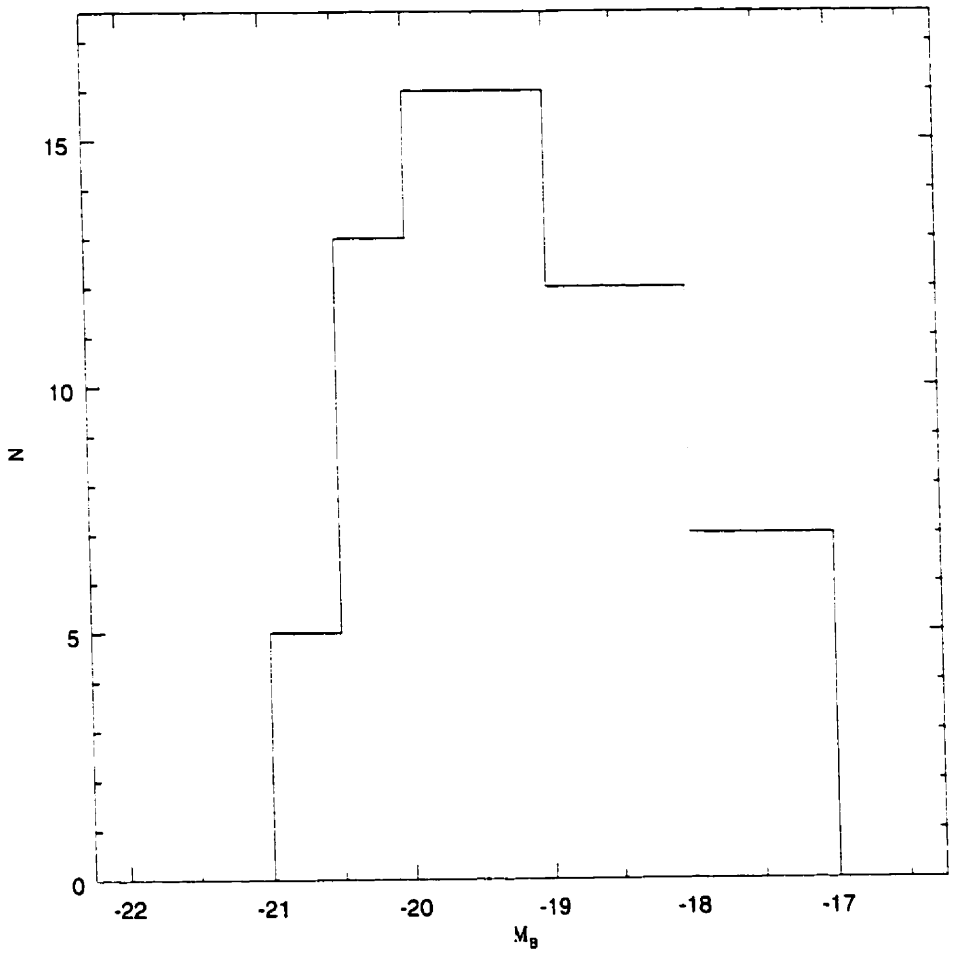

Figure 4.4: An absolute magnitude histogram is given for the 88 companions used in the pair statistics.

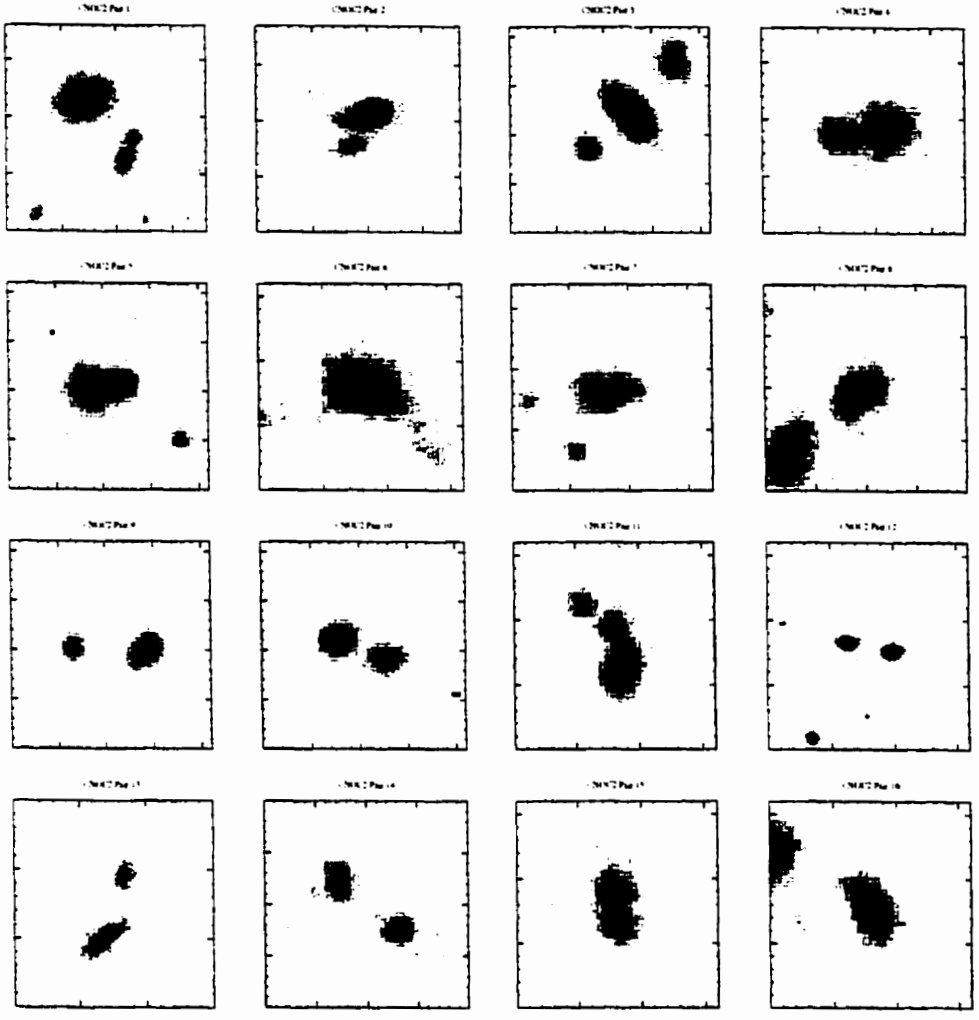

Figure 4.5: A mosaic of images is given for the 44 close ($5\ h^{-1}$ kpc $< r_p \leq 20$ h^{-1} kpc) dynamical ($\Delta V < 500$ km/s) pairs or triples satisfying the criterion used for computing pair statistics. These R_C-band images were obtained using the CFHT MOS. Each image is $50\ h^{-1}$ kpc on a side, corresponding to typical angular sizes of $\sim 20''$.

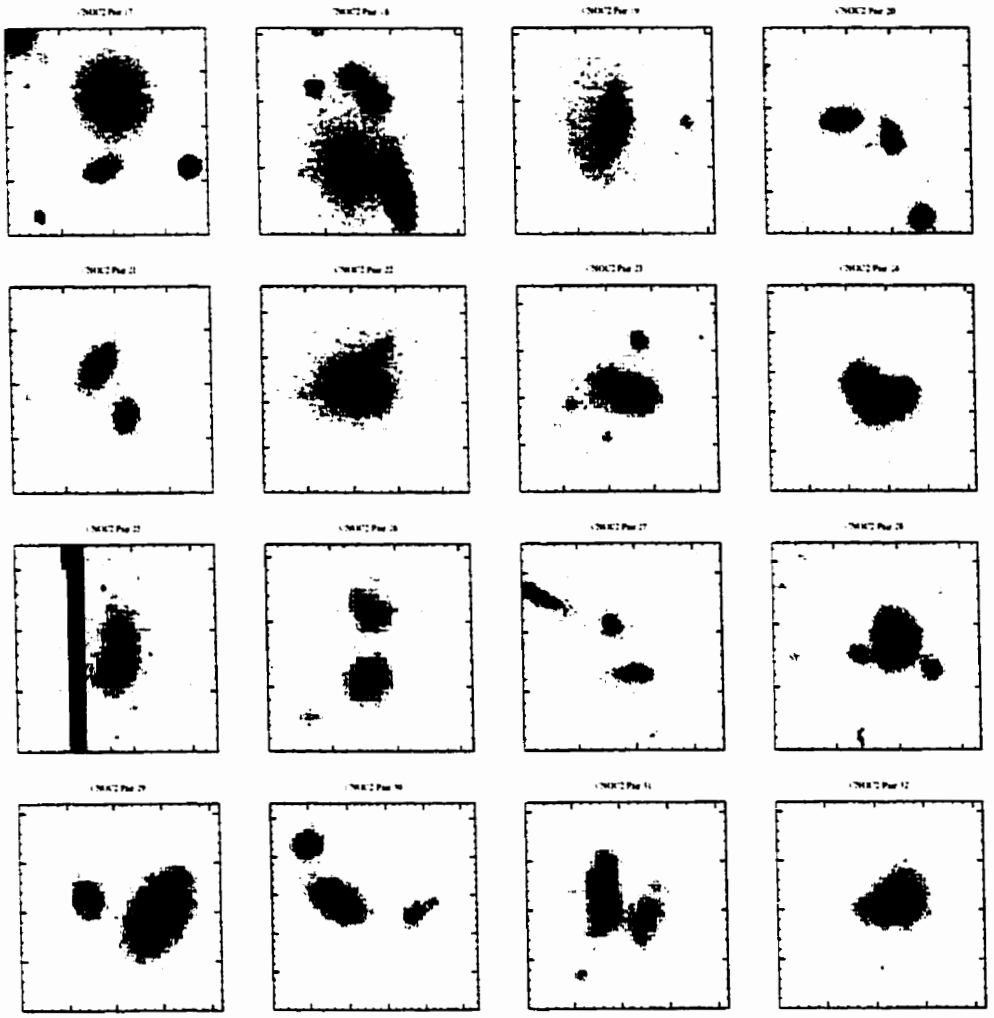

Figure 4.3: Continued

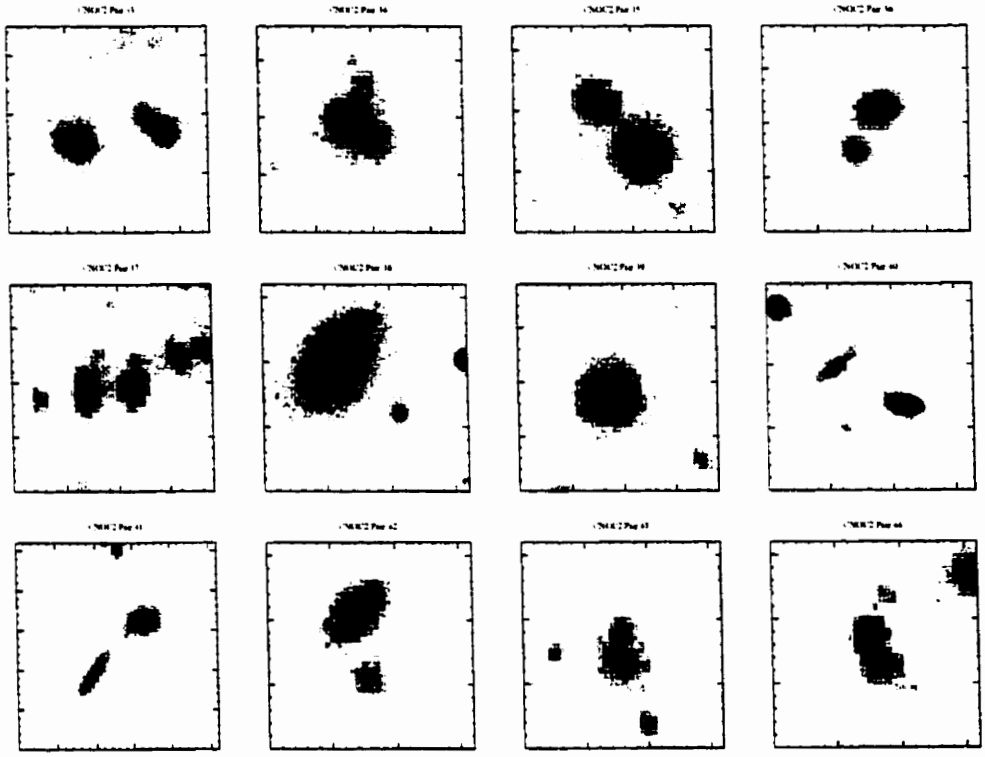

Figure 4.3: Continued

4.7.1 Dependence on M_2

We have stressed the importance of specifying a limiting absolute magnitude M_2 for companions, when computing pair statistics. For this study, we have selected $M_2(B)=-18$ as being representative of our sample (see § 4.5.4). It is useful to see how our results change with different choices of this important parameter. We now compute our pair statistics for $-19 \leq M_2 \leq -17$. The results, after combining all 4 patches, are given in Table 4.7.

Pair statistics are expected to increase as M_2 becomes fainter, and this is seen in Table 4.7. N_C increases by a factor of ~ 5 between $M_2=-19$ and $M_2=-17$. L_C is less sensitive to M_2, changing by a factor of ~ 2 over the same range. In both cases, the changes are due solely to the increase in mean number or luminosity density, resulting from integrating deeper into the LF. These results are very similar to what was found for SSRS2, and the same conclusions apply.

4.7.2 Dependence on $r_p^{\max}$

Close companions are required to have projected separations less than $r_p^{\max}$, where $r_p^{\max} = 20\ h^{-1}$ kpc. While this maximum separation is thought to be ideal for isolating good merger candidates, it is useful to see how the pair statistics behave at larger separations. With this in mind, we compute pair statistics for 10 h^{-1} kpc$\leq r_p^{\max} \leq$ 100 h^{-1} kpc, with $\Delta v^{\max} = 500$ km/s. Results are given in Figure 4.4. This plot indicates a smooth increase in both statistics with $r_p^{\max}$. This trend is expected from measurements of the galaxy CF. The CF is commonly expressed as a power law of the form

Table 4.7: CNOC2 Pair Statistics for Various Choices of $M_2(B)$

M_2	N_c	$L_c(10^{10}h^2L_\odot)$
-19.0	0.0129± 0.0029	0.0230± 0.0058
-18.9	0.0146± 0.0033	0.0247± 0.0062
-18.8	0.0165± 0.0037	0.0263± 0.0066
-18.7	0.0184± 0.0041	0.0279± 0.0070
-18.6	0.0205± 0.0046	0.0294± 0.0074
-18.5	0.0226± 0.0051	0.0308± 0.0078
-18.4	0.0248± 0.0056	0.0321± 0.0081
-18.3	0.0271± 0.0061	0.0334± 0.0084
-18.2	0.0294± 0.0066	0.0346± 0.0087
-18.1	0.0318± 0.0071	0.0357± 0.0090
-18.0	0.0342± 0.0077	0.0367± 0.0093
-17.9	0.0367± 0.0082	0.0377± 0.0095
-17.8	0.0393± 0.0088	0.0386± 0.0098
-17.7	0.0419± 0.0094	0.0394± 0.0100
-17.6	0.0445± 0.0100	0.0402± 0.0102
-17.5	0.0472± 0.0106	0.0409± 0.0104
-17.4	0.0500± 0.0112	0.0416± 0.0105
-17.3	0.0527± 0.0119	0.0422± 0.0107
-17.2	0.0556± 0.0125	0.0428± 0.0108
-17.1	0.0585± 0.0131	0.0434± 0.0110
-17.0	0.0614± 0.0138	0.0439± 0.0111

$\xi(r,z) = (r_0/r)^\gamma$, with γ=1.8 (Davis and Peebles 1983). Integration over this function yields pair statistics that vary as $r_p^{3-\gamma} \approx r_p^{1.2}$, which is in good agreement with the trend found in Figure 4.4.

4.7.3 Dependence on $\Delta v^{\max}$

We also compute pair statistics for a range in $\Delta v^{\max}$. This is done first for $r_p^{\max} = 20\ h^{-1}$ kpc, showing the relative contributions at different velocities to the mean pair statistics quoted in this study. We also compute statistics using $r_p^{\max} = 100\ h^{-1}$ kpc, in order to improve the statistics. Results are given in Figure 4.5. Several important conclusions may be drawn from this plot. First, at small velocities ($\Delta v^{\max} \lesssim 700$ km/s), both pair statistics increase with $\Delta v^{\max}$, as expected. This simply indicates that one continues to find additional companions as the velocity threshold increases. Secondly, it appears that our choice of $\Delta v^{\max}$ was a good one. The $r_p \leq 20\ h^{-1}$ kpc pair statistics increase very little beyond $\Delta v^{\max} = 500$ km/s, while the contamination due to non−merging pairs would continue to increase. Moreover, as both pair statistics flatten out at around $\Delta v^{\max} = 500$ km/s, small differences in the velocity distributions of different samples should not result in large differences in their pair statistics. Finally, for $r_p^{\max} \leq 100\ h^{-1}$ kpc, the pair statistics continue to increase out to $\sim$ 2000 km/s. This indicates an increase in velocity dispersion at these larger separations. This provides additional confirmation that one is less likely to find low−velocity pairs at larger separations, thereby implying that mergers should also be less probable.

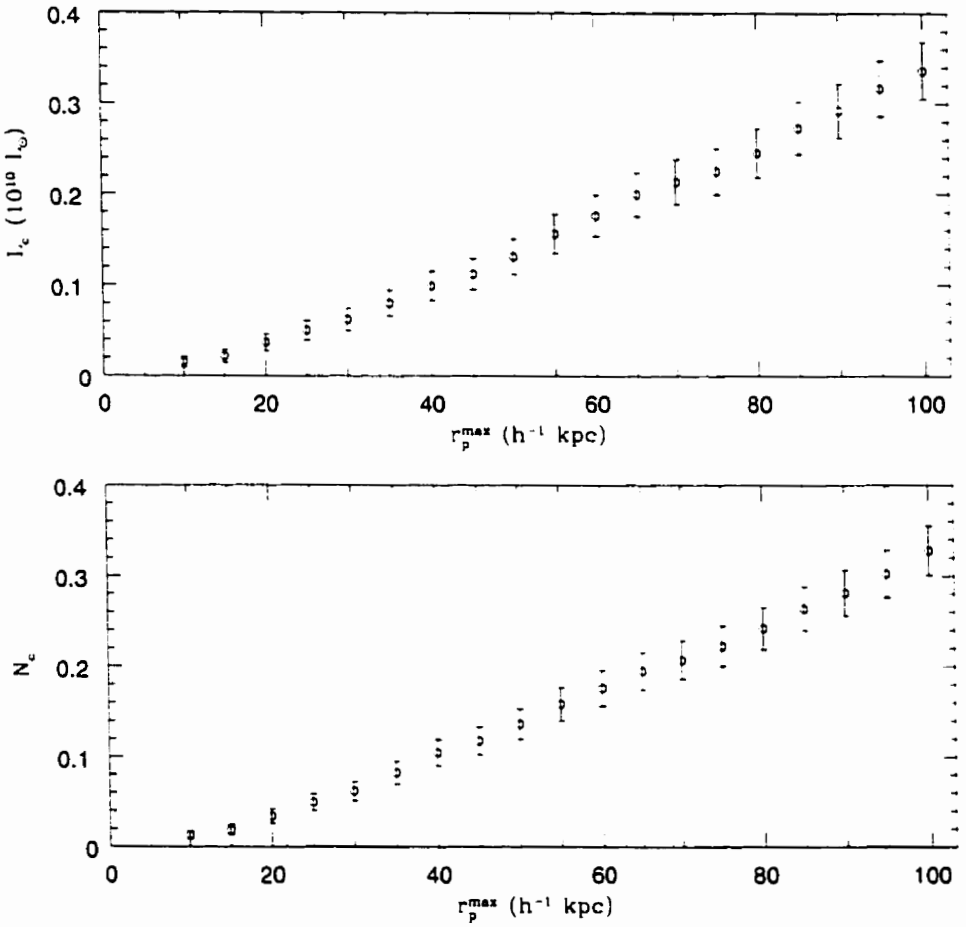

Figure 4.4: Pair statistics are computed for $\Delta v \leq 500$ km/s, for a range of maximum projected separations (r_p^{max}). A minimum projected separation of $r_p = 5\ h^{-1}$ kpc is applied in each case. Error bars are computed using the Jackknife technique. Both N_C and L_C are cumulative statistics; hence, measurements in successive bins are not independent.

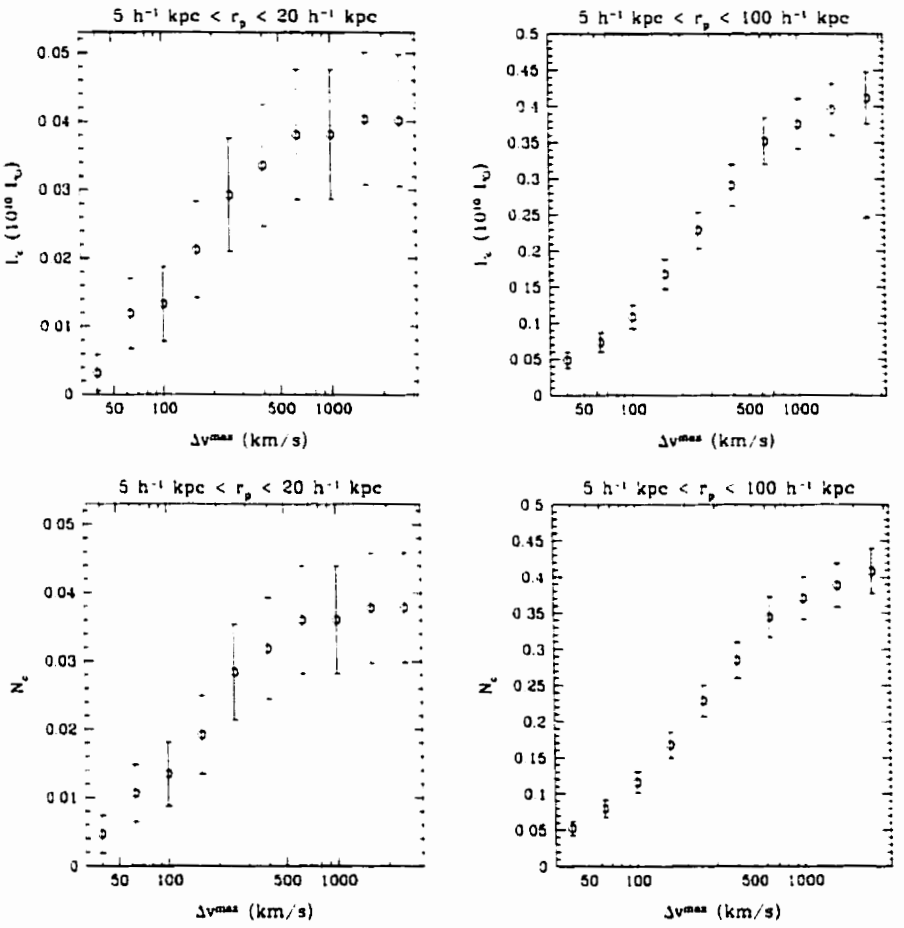

Figure 4.5: Pair statistics are computed for $\Delta v \leq 500$ km/s, for a range of projected separations. Error bars are computed using the Jackknife technique. Both N_C and L_C are cumulative statistics; hence, measurements in successive bins are not independent.

4.8 Merger Rate Evolution

Having computed pair statistics at moderate redshift, we are now in a position to say something about the change in these statistics since the present epoch. We will use our measurements from Chapter 3 to infer evolution in the galaxy merger and accretion rates from $z \sim 0$ to $z \sim 0.5$. We begin by justifying a direct comparison of these two samples. After estimating the evolution in the merger and accretion rates, we will explore the sensitivity of our results to various assumptions that have been made in this analysis.

4.8.1 Validity of Comparison

Throughout this study, we have stressed the importance of making careful measurements of pair statistics, to avoid various biases that may adversely affect the results. Here, we review the important issues that must be addressed before comparing pair statistics for different samples.

First of all, one must ensure that the definition of a close companion is identical in all samples. When comparing samples at different redshifts, one must be cautious of definitions that may have redshift-dependent biases present. For example, earlier pair studies have had to correct for optical contamination due to unrelated foreground or background galaxies. While this contamination can be accounted for, the degree of contamination increases systematically with redshift; hence, it is clearly preferable to avoid this correction, if possible. For both SSRS2 and CNOC2, we have used the same definition of a close companion. Our dynamical definition is unaffected by optical contamination, or other redshift-dependent biases. The only remain-

ing factor that may cause our definition to change with redshift is the choice of cosmology. That is, if our choice of cosmological parameters is not correct, there will be a redshift-dependent change in the projected physical separation used to identify close companions. In Section 4.8.5, we explore the effects that different choices of cosmological parameters have on our estimates of merger rate evolution.

There are two passband effects that must be considered when comparing different samples. First, one must obviously compute pair statistics in the same passband. For both SSRS2 and CNOC2, we compute pair statistics in the rest-frame $B-$band. It is also important to *select* galaxies at approximately the same rest-frame wavelength. If this is not done, any differences in the resulting pair statistics may simply be artifacts of the selection process. The SSRS2 sample was selected in the B-band. The CNOC2 sample was instead selected in the observed R_C passband. However, because of the band-shifting effects of redshift, these are actually quite similar. We note that observed R_C is roughly equivalent to rest-frame B at $z \sim 0.5$. Thus, SSRS2 and CNOC2 are selected at comparable rest-frame wavelengths.

We have strongly emphasized the need to specify a limiting absolute magnitude M_2 for computing pair statistics. When comparing different samples, it is critical that this correspond to the same intrinsic luminosity in all samples. For SSRS2, we selected $M_2(B)=-18$. For CNOC2, we have chosen the same limiting absolute magnitude. However, we have also incorporated a correction for luminosity evolution (see Section 4.6.2). This helps to ensure that we are probing down to the same minimum mass at all redshifts.

4.8.2 Redshift Evolution

Having demonstrated that it is reasonable to compare our SSRS2 and CNOC2 pair statistics, we now proceed with the analysis. SSRS2 pair statistics were summarized in Section 4.4. CNOC2 pair statistics were given in Table 4.6. Pair statistics for both SSRS2 and CNOC2 are plotted in Figure 4.6. Recall that N_C is related to the galaxy merger rate, while L_C depends on the accretion rate. Following the convention in this field, we choose to parameterize evolution in the galaxy merger rate by $(1+z)^{m_N}$, where m_N is determined by changes in N_C with redshift. Similarly, we take the accretion rate to evolve as $(1+z)^{m_L}$. We find $m_N = 1.83 \pm 1.47$ and $m_L = 1.99 \pm 1.62$. These relations are plotted in Figure 4.6. As an additional test, we divide our sample into two independent redshift bins, and measure the pair statistics in each. The results are given in Figure 4.7, and are found to be consistent with the merger rate estimates made using the full sample.

4.8.3 Dependence on the Degree of Luminosity Evolution

In Section 4.6.2, we described the detrimental effects that luminosity evolution can have on the measurement of pair statistics. We outlined our approach for removing this effect, using the Q parameter derived from measurements of the CNOC2 LF. When computing pair statistics, we have taken Q=1, which assumes an average of z magnitudes of luminosity evolution at redshift z. To see how this assumption affects our results, we recompute the pair statistics, using Q=0 (no evolution) and Q=2 ($2z$ magnitudes of evolu-

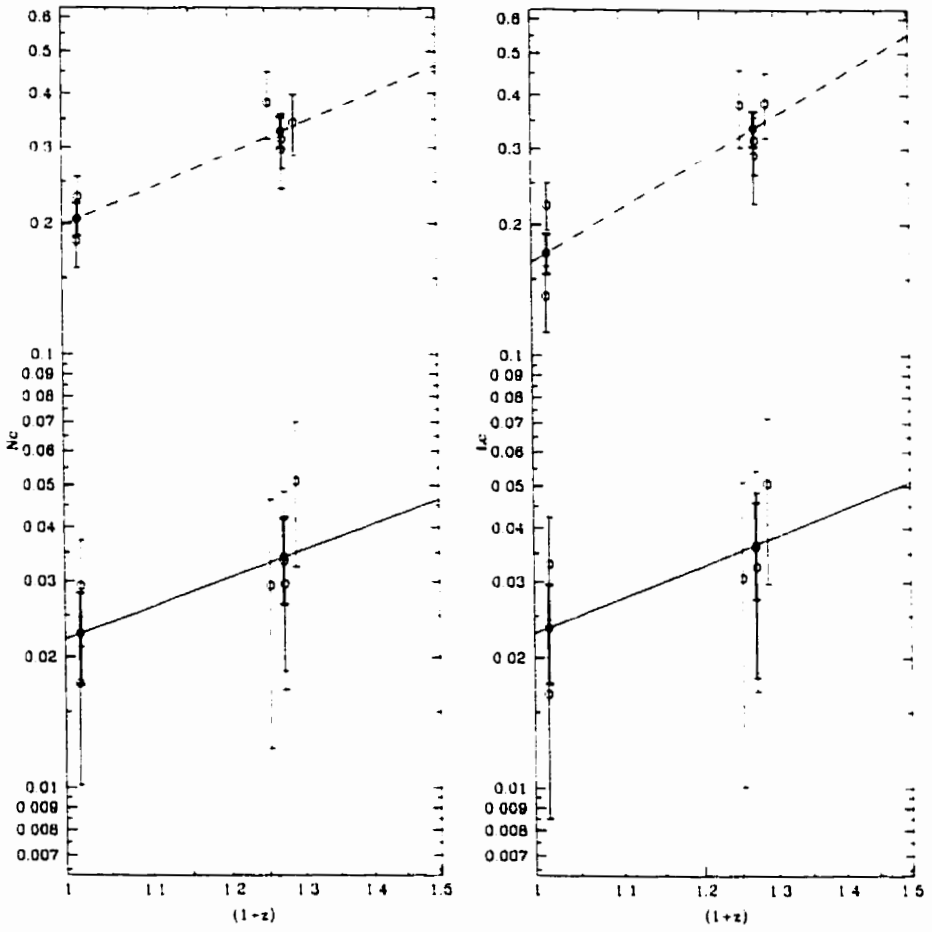

Figure 4.6: Pair statistics (N_c and L_c) are given for SSRS2 ($z \approx 0.016$) and CNOC2 ($z \approx 0.27$). Those in the lower half of the plot are computed using $r_p^{\max}$=20 h^{-1} kpc, while those in the upper half use $r_p^{\max}$=100 h^{-1} kpc. Open symbols denote statistics for survey sub−samples; filled circles (with thicker error bars) represent combined results (SSRS2, CNOC2). Lines indicate evolution varying as $(1+z)^m$. Solid lines ($r_p^{\max}$=20 h^{-1} kpc) correspond to m_N=1.83 and m_L=1.99, while dashed lines ($r_p^{\max}$=100 h^{-1} kpc) give m_N=2.09 and m_L=2.98.

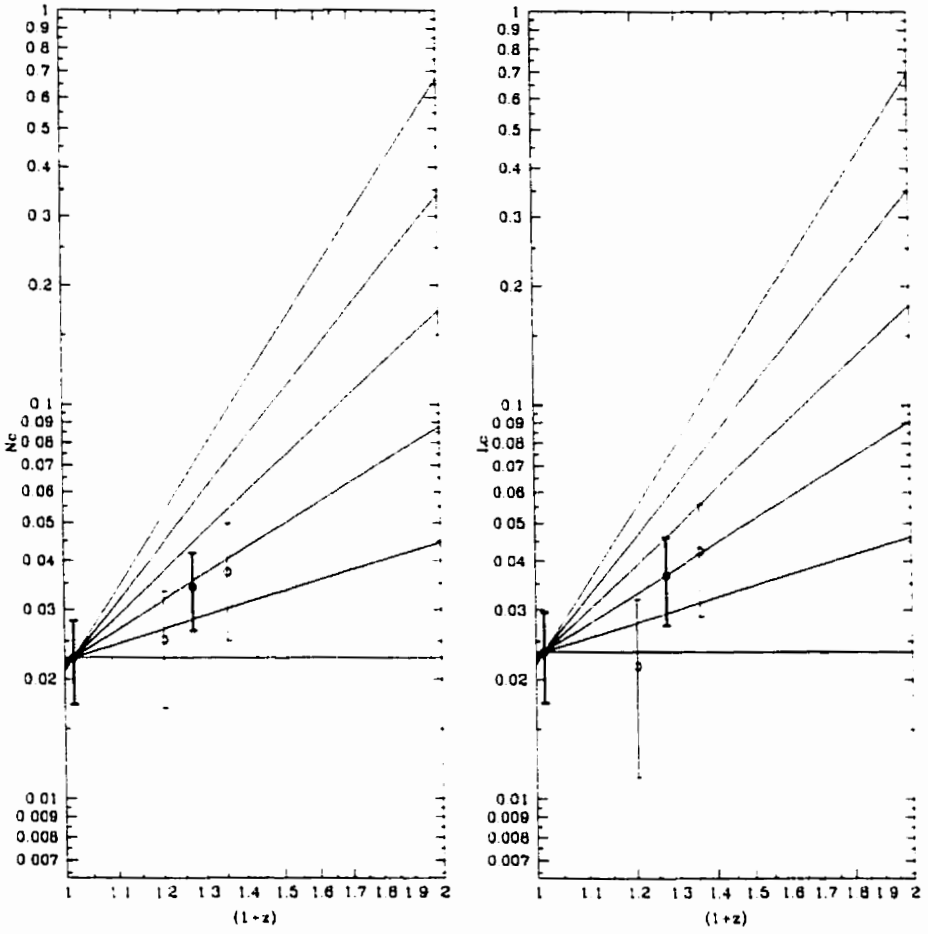

Figure 4.7: Pair statistics (N_c and L_c) are given for SSRS2 ($z \approx 0.016$) and CNOC2 ($z \approx 0.27$). In both cases, solid symbols indicate mean statistics for the survey. Open symbols represent statistics measured for the lower ($0.1 \leq z \leq 0.27$) and upper ($0.27 \leq z \leq 0.45$) redshift ranges of CNOC2. Errors bars are computed using the Jackknife technique. Lines indicate evolution varying as $(1+z)^m$, ranging from m=0 (horizontal line) to m=5 (uppermost line).

tion at redshift z). The former is clearly an underestimate, as it is certain that some evolution takes place. The latter invokes more evolution than is seen in studies of the LF, but nevertheless provides a useful upper limit.

For Q=0, we find $m_N = 2.61 \pm 1.50$ and $m_L = 2.31 \pm 1.65$. Thus, if we do not account for luminosity evolution, we infer a stronger increase in the merger and accretion rates with redshift. For Q=2, we find $m_N = 0.93 \pm 1.43$ and $m_L = 1.57 \pm 1.58$. As expected, this decreases our estimates of m_N and m_L. The effect is strongest for N_C, which is quite sensitive to the limiting absolute magnitude (see § 4.7.1). The magnitude of this effect demonstrates the importance of taking this into account when computing N_C. Our luminosity statistic, L_C, is less affected; in fact, our general conclusions regarding m_L are unchanged for reasonable choices of Q.

4.8.4 Dependence on $r_p^{\rm max}$ and $\Delta v^{\rm max}$

In this section, we examine the sensitivity of our merger rate estimates to our particular definition of a close companion. In Figure 4.4, we demonstrated a smooth increase in N_C and L_C with increasing $r_p^{\rm max}$. This trend was also apparent for SSRS2. The similarity and smoothness of these relations indicates that our particular choice of $r_p^{\rm max}$ should not have a strong effect on our merger rate estimates. It is difficult to say conclusively how our estimates would change on smaller scales, since the small number of pairs results in large measurement uncertainties. However, it is reasonable to probe out to slightly larger scales to see how this affects our merger rate estimates. As an example, we use $r_p^{\rm max}$=100 h^{-1} kpc, which probes reasonably small scales, and yet is dominated by companions beyond 20 h^{-1} kpc. We recompute

pair statistics for both SSRS2 and CNOC2, and find $m_N = 2.09 \pm 0.53$ and $m_L = 2.98 \pm 0.63$. These results are given in Figure 4.6, and are consistent with the measurements given in Section 4.8.2.

Following the same approach, we now investigate the effects of changing $\Delta v^{\max}$. Referring to Figure 4.5, we note that the CNOC2 pair statistics flatten out beyond $\sim$ 500 km/s. The same effect was seen with SSRS2. As a check, we recompute pair statistics for both surveys, using $\Delta v^{\max} =$ 1000 km/s. We find $m_N = 1.43 \pm 1.41$ and $m_L = 1.61 \pm 1.56$. Again, these results are consistent with the estimates given earlier. We conclude that our inferred evolution in the galaxy merger and accretion rates is not overly sensitive to our particular definition of a close companion.

4.8.5 Dependence on q_0

The choice of q_0 will affect the computed value of r_p for each pair. For our low redshift sample ($z < 0.05$), q_0 does not have a significant effect. At moderate redshift, the effect is quite noticeable, and will therefore affect our estimates of m_N and m_L. At z=0.33, r_p will be $\sim$ 6% smaller for q_0=0.5. The choice of q_0 also affects measurement of the galaxy LF, which is needed for measuring pair statistics for this flux-limited sample. Lin et al. (1999) have measured the CNOC2 LF for both q_0=0.1 and q_0=0.5 (see Table 4.1). We recompute our pair statistics using q_0=0.5, finding $m_N = 2.22 \pm 1.40$ and $m_L = 1.84 \pm 1.61$. Thus, we find a slight increase in merger rate evolution, and a slight decrease in accretion rate evolution. This effect is quite small at the modest redshifts under consideration here, but will become more of an issue as pair studies are extended to higher redshifts.

4.9 Discussion

4.9.1 Summary of New Results

We have used the CNOC2 redshift survey to compute secure measurements of close pair statistics at $z \sim 0.27$. These are the first measurements at $z > 0$ that use only dynamically confirmed pairs ($\Delta v < 500$ km/s). Moreover, we have carefully accounted for a number of selection effects that have affected earlier estimates. In particular, we have accounted for the dependence on the limiting absolute magnitude of companions; without this crucial step, it is very dangerous to compare pair statistics from different surveys. This is also the first study to include an explicit correction for the redshift-dependent bias introduced by luminosity evolution. Following the techniques outlined in the previous chapter, we have computed pair statistics using the number and luminosity of companions. N_C gives the number of close companions per galaxy, while L_C measures the luminosity in close companions, per galaxy. We find $N_c(M_B \leq -18) = 0.0342 \pm 0.0077$ and $L_c(M_B \leq -18) = 0.0367 \pm 0.0093 \times 10^{10}\ h^2 L_\odot$ at z=0.271. We then compare these quantities with their low redshift counterparts, as presented in the preceding chapter. Changes in N_C and L_C with redshift allow us to infer evolution in the galaxy merger and accretion rates. Parameterizing this evolution as $(1+z)^m$, we find we find $m_N = 1.83 \pm 1.47$ and $m_L = 1.99 \pm 1.62$.

4.9.2 Comparison With Earlier Studies

As with earlier close pair studies, we have arrived at an estimate of the rate at which the galaxy merger rate changes with redshift. As reviewed in Chapter

2, these studies have yielded a wide variety of results in the past. Using a consistent transformation between the pair fraction and merger rate (§ 2.7), results vary from $m \sim 0$ (Woods et al. 1995) to $m \sim 5$ (Zepf and Koo 1989; Yee and Ellingson 1995). After accounting for various discrepancies due to optical contamination and spectroscopic completeness, these results were shown to be roughly consistent with the value of $m = 2.8 \pm 0.9$ derived in Chapter 2. However, as we have stressed throughout this chapter, one must be very careful when comparing samples of close pairs at different redshifts. If differences exist in the limiting absolute magnitudes of the samples, or if there are systematic differences in the way galaxies and pairs are selected, the comparison is necessarily rendered invalid. In our judgement, there are no currently available merger rate estimates that satisfy these important criteria. This includes several earlier works by these authors (Carlberg, Pritchet, and Infante 1994; Yee and Ellingson 1995), along with the merger rate results given in Chapter 2. Thus, rather than compare our results with these earlier findings, we will take our new results to supersede these earlier estimates.

It is worth noting that, in spite of two large redshift samples, the resulting uncertainties in our merger rate estimates are still quite large. In fact, our errors are larger than those estimated in Chapter 2, which were made using a sample that is a tenth of the size of CNOC2. There are a number of reasons for this somewhat surprising result. The primary difference in our pair sample is that we have required all pairs to have redshifts for both members. This yields results that are on a much more secure footing than earlier studies which incorporated the use of companions with and without redshifts. We have purified our pair sample further by requiring $\Delta v \leq 500$

km/s. We have also restricted our sample in redshift and luminosity, in order to minimize the detrimental effects of luminosity-dependent clustering. All of these effects have made our sample more secure, but have greatly reduced the size of our sample. Finally, we have computed errors using the Jackknife technique, which is well-suited to the weighted pair statistics used in this study. These errors were found to be larger than the Poisson statistics used in earlier studies, by a factor of $\approx \sqrt{2}$. The reason for this difference lies in a subtle but important detail regarding the application of Poisson statistics to pairs. The number of *independent* objects being counted is the number of pairs, rather than the number of galaxies in pairs. In Chapter 2, as in earlier studies, this was not recognized, leading to uncertainties that were underestimated by a factor of $\sqrt{2}$.

4.9.3 Implications

In order to interpret our merger rate estimates, it is useful to consider several simple scenarios. First, for a universe with fixed co-moving density and no clustering, the physical density increases as $(1+z)^3$. As our pair statistics measure the number and luminosity of companions within a fixed physical volume (determined by $r_p^{\max}$ and $\Delta v^{\max}$), they would be expected to increase at the same rate. Of course, there is likely to be evolution in the co-moving number density of galaxies, as indicated from studies of the galaxy LF. These changes will translate, on average, into comparable changes in pair statistics. We must also consider the effects of clustering on the evolution of the merger rate. The scenario outlined above includes no clustering, and hence is not representative of the real universe. In order to incorporate clustering, we refer

to the galaxy correlation function (CF), which provides a convenient parameterization of clustering. The galaxy correlation function, and its evolution with redshift, is traditionally parameterized as follows :

$$\xi(r,z) = \xi(r,0)(1+z)^{-(3+\epsilon)}, \tag{4.17}$$

where

$$\xi(r,0) = \left(\frac{r}{r_0}\right)^{-\gamma}. \tag{4.18}$$

Our pair statistics are proportional to the mean physical density, which varies as $(1+z)^3$, multiplied by an integral over the CF, which varies as $(1+z)^{-(3+\epsilon)}$. Thus, $N_C \propto (1+z)^{-\epsilon}$ (L_C has the same dependence). Suppose we require that clustering remain fixed in proper (physical) coordinates. This corresponds to ϵ=0. In this case, the physical density of companions will not evolve. That is, we would expect to find m_N=m_L=0. Similarly, we consider a scenario in which the clustering is fixed in co-moving coordinates. In this case, $\epsilon = \gamma - 3$. Measurements of the CF routinely give $\gamma = 1.8$ (Davis and Peebles 1983). This gives pair statistics that vary as $(1+z)^{1.2}$. Finally, we consider measurements of the evolution of clustering. Carlberg et al. (1998) have used the CNOC2 survey to measure how clustering evolves. They find $\epsilon = -0.6 \pm 0.4$. If we extrapolated the correlation function down to the small scales of interest here, we would expect the pair statistics to vary as $(1+z)^{0.6}$. Our results indicate a rate of evolution that is somewhat larger than this, though the difference may not be statistically significant.

Following the merger remnant analysis of the preceding chapter, we will attempt to interpret the implications of our results for galaxies at the present

epoch. We begin by using our earlier estimates of the local epoch merger fraction ($f_{\rm mg}$=0.011; § 3.9.2) and the merger timescale ($T_{\rm mg}$=0.5 Gyr; § 3.9.3). We now employ the estimates of merger rate evolution from this study. For simplicity, we take the merger rate to evolve as $(1+z)^2$. Using Equation 3.32, with lookback time computed using h=0.7 and q_0=0.5, we find that 13.2% of $M_B \leq -18$ galaxies at the present epoch have undergone a major merger since $z \sim 1$. This remnant fraction is twice as large as the value found assuming no evolution in the merger rate (§ 3.9.4). Even so, our result implies that the majority of bright ($M_B \leq -18$) galaxies at the present epoch have not undergone a major merger since $z \sim 1$.

Chapter 5

Galaxy Properties in CNOC2 Pairs

5.1 Introduction

In this chapter, we will analyze the properties of galaxies in close dynamical pairs. We will use the CNOC2 survey, for which we have amassed an extensive array of information on the spectral and photometric properties of galaxies with known redshifts. We wish to address two questions.

1) How do the properties of galaxies in close ($5\ h^{-1}$ kpc$\leq r_p \leq 20\ h^{-1}$ kpc) dynamical ($\Delta v \leq 500$ km/s) pairs compare with field galaxies in general?

2) Do the properties of paired galaxies vary with projected separation r_p? In particular, are there any signs of enhanced star formation at small separations?

To address these issues, we will identify a sample of close companions from the CNOC2 sample. We will compare these galaxies with a "control" sample of field galaxies that is subjected to the same redshift and luminosity selection effects as the companion sample. We will carry out a detailed

comparison of paired and field galaxies, with hopes of shedding new light on the questions raised above.

In Section 5.2, we provide an overview of the known properties of merging and interacting galaxies. A description of the CNOC2 data, along with photometric and spectroscopic measurements, is given in Section 5.3. We outline our method of selecting pair and control samples in Section 5.4. We then compare the properties of close (5 h^{-1} kpc$\leq r_p \leq$ 20 h^{-1} kpc) companions with galaxies in the control sample (§ 5.5), followed by an analysis of trends with r_p (§ 5.6). Results are discussed in Section 5.7. Where necessary, we assume a Hubble constant of 100 km s^{-1}Mpc^{-1} ($h = 1$) and q_0=0.5.

5.2 Background

The study of interacting and merging galaxies is a popular endeavour. Most of the work has consisted of detailed observational and theoretical studies of well-known nearby systems, such as the Antennae (NGC 4038/4039). While great progress has been made with this approach, it is inherently difficult to apply the results of these studies to galaxies in general. Part of the difficulty lies in the methods used to identify these samples. If interacting systems are selected based on subjective measures such as pair morphology, it is difficult to extend the results to other galaxies. In the past decade, some progress has been made, using the study of galaxies at moderate redshift ($z \sim$0.3). These studies tend to sample large numbers of galaxies, providing a reasonable cross-section of all galaxy types.

A number of studies of close galaxy pairs at moderate redshift have

attempted to measure the properties of galaxies in close pairs, and to compare these galaxies with the global field population. These studies began with Zepf and Koo (1989), and have since been extended to include redshift samples (e.g., Carlberg, Pritchet and Infante 1994, Yee and Ellingson 1995). The results of these studies were discussed in Chapter 2. Overall, galaxies in close pairs have been found to be similar to field galaxies. However, it is possible that these results are due to an inability to detect differences, rather than an actual absence of significant differences. Here, we outline some of the shortcomings of these studies, and describe steps we will take to alleviate some of these concerns.

The primary difficulty with published studies of close pair properties is the lack of redshift information available. Without redshifts for both members of each pair, many galaxies that fall in the pair sample will be unrelated foreground or background galaxies. This contamination is generally on the order of 50% at moderate redshift, and increases as one goes to higher redshift. Moreover, some of the remaining physical pairs are likely to be physically associated but non-merging systems. Another difficulty with the absence of redshifts is that one is limited to the study of observed properties (e.g., apparent magnitude) instead of intrinsic properties (e.g., absolute magnitude). Finally, without redshifts, one is limited to the study of close ($r_p \lesssim 20\ h^{-1}$ kpc) pairs, as optical contamination becomes increasingly problematic at larger separations.

Clearly, a lack of redshifts places significant limitations on one's ability to carry out a detailed comparison of paired and field galaxies. However, another important problem remains, even for simple flux-limited samples.

As we have outlined in Chapters 3 and 4, galaxies in pairs are subjected to different selection effects than field galaxies in general. This means that paired galaxies will have a redshift distribution that is skewed towards low redshift. This redshift-dependent effect complicates the comparison of paired and field galaxies, and has not been accounted for in any published pair studies.

In this chapter, we will address many of these issues. We will use the CNOC2 redshift survey, which is an order of magnitude larger than that of the largest redshift sample (CNOC1) previously used to study close pairs (Chapter 2 of this dissertation). The CNOC2 sample contains several additional properties for each galaxy, allowing us to extend earlier property analyses. We will restrict our analysis to dynamical pairs with $\Delta v \leq 500$ km/s, eliminating concerns about optical contamination and reducing the contribution of non-merging pairs. As we have redshifts for all of the galaxies under consideration, our analysis will deal only with intrinsic galaxy properties. Finally, we will address the issue of pair selection bias, by introducing a new technique for extracting a comparable sample of field galaxies.

5.3 Data

The CNOC2 Field Galaxy Redshift Survey consists of imaging and spectroscopic data obtained with the multi-object spectrograph (MOS) at the Canada-France-Hawaii Telescope (CFHT). These observations were described in detail in Section 4.2. Here, we will provide a brief overview of the photometric and spectroscopic quantities that will be used throughout this analy-

sis.

5.3.1 Properties Derived From Imaging Data

The primary information derived from the imaging data is 5-colour photometry, for all detected galaxies. This photometry was obtained using MOS in imaging mode, with Johnson UBV and Kron-Cousins $R_C I_C$ filters. The photometry goes considerably fainter than the spectroscopic sample, with approximate 5σ detection limits as follows : $U(23.0)$, $B(24.6)$, $V(24.0)$, $R_C(24.0)$, and $I_C(23.0)$. In order to avoid colour biases, we use the same aperture in all filters for each galaxy. This aperture is large enough to avoid significant problems associated with differences in the PSF for different filters.

By combining broad band fluxes with redshift, one can transform from apparent properties (flux and colours) to intrinsic properties (luminosity and rest-frame colours). The general expression for conversion from an observed flux, expressed as apparent magnitude m, to an intrinsic luminosity, expressed as absolute magnitude M, is given by

$$M = m - 25 - 5 \log d_L(z) - k - A, \tag{5.1}$$

where $d_L(z)$ is the luminosity distance at redshift z, k is the k-correction (see § 4.5.2), and A is the correction for extinction from the Milky Way. To promote consistency with earlier chapters, we will use the $B-$band as our preferred measure of galaxy luminosity. Rest-frame colours can be computed by finding the difference in absolute magnitude for any two passbands. Throughout this analysis, we will take $B - R$ to be representative of the

overall colour of each galaxy. This colour index relies on two of our most secure bandpasses, and spans a useful spectral regime for galaxies in our spectroscopic sample.

In order to make use of the full 5-colour photometry available, we fit model spectra to the photometry for each galaxy. This procedure was described in Section 4.5.2. After selecting the model spectral energy distribution (SED) that provides the best match to the photometry, we assign the galaxy an SED classification, denoted SedCl. This classification scheme spans the continuum of model spectra, with SedCl=0 for an elliptical galaxy, and SedCl=4 for an irregular galaxy. These classifications appear to be well correlated with measures derived independently from spectral cross correlation (see Yee, Ellingson, and Carlberg 1996).

5.3.2 Spectral Line Indices

The primary information provided by a galaxy spectrum is the redshift. However, a wealth of additional information may be present, even for spectra of relatively low dispersion. The CNOC2 spectra cover a rest frame wavelength range from approximately [OII]3727Å to the G−band ($\lambda \approx 4300$Å), for all galaxies in the redshift range $0.1 \leq z \leq 0.55$. The spectra have a dispersion of 3.45Å per pixel, corresponding to a spectral resolution of 16.5Å. A number of spectral line indices have been measured for CNOC2 galaxies (Morris et al. 1999), following the techniques outlined by Balogh et al. (1999). At present, line measurements are available for two of the four CNOC2 patches (0223+00 and 0920+37), and will be used in this analysis. Here, we give a brief summary for the line indices of interest. In each case, the precise

definition is shown with respect to a sample spectrum, in Figure 5.1.

Rest frame equivalent widths were measured for the [OII]3727Å emission line and the $H\delta$4103Å absorption line. These equivalent widths, denoted W_0(OII) and $W_0(H\delta)$, were measured using an automated procedure, by summing the observed flux above (W_0(OII)) and below ($W_0(H\delta)$) the continuum level of the spectrum. The continuum itself was estimated by fitting a straight line to the flux in the adjacent blue and red continuum regions. Note that W_0(OII) is negative when the line is in emission, and $W_0(H\delta)$ is positive in absorption.

The break strength at 4000Å, hereafter denoted D4000, is defined as the ratio of the flux in the red continuum to that in the blue continuum. The definition used here is much narrower than the standard definition of Hamilton (1985). This narrower definition allows for more appropriate uncertainty estimates and is less sensitive to reddening effects. D4000 is similar in nature to a broadband colour, in which the respective filters straddle the 4000Å break. In some respects, D4000 is more robust, since rest frame colours depend on k-corrections that are estimated from best-fit model spectra, while D4000 is measured directly from the spectrum. However, D4000 measurement uncertainties are generally larger than those for the corresponding broadband colours. It is also worth noting that galaxy spectra sample light from the central regions of the galaxy, while the broadband colours tend to sample a more extended region. This effect is not expected to be large, since the slit width (1.″5) samples a sizable region of diameter $\sim 4\ h^{-1}$ kpc at z=0.3.

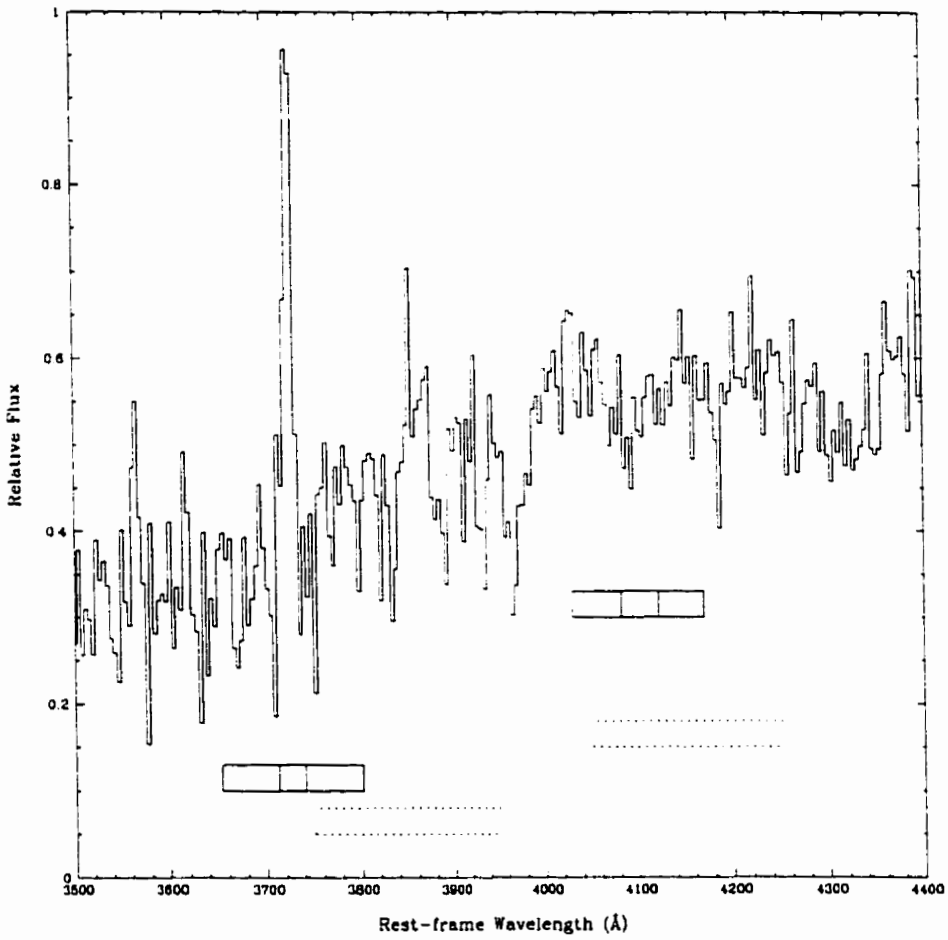

Figure 5.1: A sample CNOC2 spectrum is shown, in order to illustrate the precise definitions of W_0(OII), $H\delta$, and D4000. The solid boxes give W_0(OII) and $H\delta$ line and continuum regions, while dotted boxes denote the blue and red continuum used for measuring D4000. See also Figure 1 of (Morris et al. 1998).

5.4 Sample Selection

The primary goal of this analysis is to determine how interactions and mergers influence the properties of member galaxies. To achieve this objective, we identify a sample of galaxies with a relatively high probability of undergoing close encounters. We then proceed to identify a comparable sample of "field" galaxies. In both cases, we will select CNOC2 galaxies with $R_C \leq 21.5$ and $0.1 \leq z \leq 0.55$.

5.4.1 CNOC2 Companions

Our primary interest is in the properties of galaxies which are likely to be undergoing interactions or mergers. In Chapter 3, we demonstrated that companions with 5 h^{-1} kpc$\leq r_p \leq$ 20 h^{-1} kpc and $\Delta v \leq$ 500 km/s are ideal candidates. Thus, these close companions will be used for a detailed comparison with field galaxies. We also wish to examine trends in galaxy properties with pair separation. Due to the relatively small number of companions satisfying our close companion criteria, there is limited information within this sample itself. In addition, there are some clear examples of interacting galaxies with separations as large as $\sim$ 100 h^{-1} kpc(§ 3.7). Thus, to identify trends with r_p, we will extend the companion sample out to larger separations.

On physical scales of $r_p \sim 10\ h^{-1}$ kpc, the vast majority of close companions are found in pairs, rather than triples or higher-order N-tuples. However, as we go out to larger scales, this will no longer be true. That is, a given galaxy may be the companion of several different galaxies, at a range of sep-

arations. Thus, there are different ways we could proceed at this stage. We begin by finding all possible pairs in the survey, allowing both permutations. Therefore, any two galaxies (A and B) will contribute two pairs (AB and BA). A survey of N galaxies will thus yield $N(N-1)$ pairs. Each of these pairs has a host galaxy and a companion, and has a measurement of r_p and Δv associated with it. We will proceed by assigning r_p and Δv to the companions only. This gives us a list of $N(N-1)$ companions. From this list, we extract those with $\Delta v \leq 500$ km/s. We will consider companions with r_p ranging from 5 h^{-1} kpc to 400 h^{-1} kpc. With this approach, a given galaxy may appear several times in the sample, as the companion of several different galaxies.

5.4.2 Identification of a Comparable Sample of Field Galaxies

Now that we have a well-defined sample of companions, we need to identify a sample of field galaxies for comparison. Naively, one might think of simply using all remaining galaxies in the sample, or even to use the full sample (since close companions represent a small fraction of the full sample). However, owing to the presence of selection effects, this approach is not robust. The primary factor that must be taken into account is that the overall redshift distribution of field galaxies is determined by the selection function, while the distribution of galaxies in pairs depends on the *square* of the selection function. To picture this, consider the high redshift end of a redshift sample, where the sampling is sparse. Let p be the probability of acquiring a redshift for a random field galaxy in this regime. Now, consider a pair of galaxies

lying at the same redshift. The probability of acquiring redshifts for both members is p^2 (if only one redshift is obtained, the identified galaxy will be tagged as an isolated field galaxy). It follows that the redshift distribution of galaxies in pairs will be markedly different from the general field population. We note, however, that our pair sample is not subjected to the correlation function bias that results from selecting pairs using an angular separation criterion (Carlberg, Pritchet, and Infante 1994), due to our use of a projected physical separation criterion (made possible with redshift information).

Given that the overall redshift distribution of companions is different from that of the field sample, it is dangerous to make a direct comparison of galaxy properties in these two samples. If any property differences are detected, it is entirely possible that the differences will be due to the pair selection process, rather than any true intrinsic differences. There are a number of effects that could produce such false detections. First of all, the distribution of luminosities will be different in the field and paired samples, due to the flux-limited nature of this sample. Many galaxies properties are known to correlate with luminosity (see Silk and Wyse 1993 for a review). In addition, many observed galaxy properties change with redshift, due to selection effects such as k-corrections. The same is true for the measurement errors on these properties. Finally, even intrinsic galaxy properties are known to vary with redshift, due to the evolution of galaxies and galaxy populations. Clearly, significant differences in the redshift distributions of these samples may well lead to inferred differences in properties that have nothing to do with the true differences between field and paired galaxies.

We have established that paired galaxies are doomed to have different

redshift distributions than field galaxies. However, it is possible to minimize or completely remove any contribution from these well-understood selection effects. To compensate for this bias in selecting galaxies in pairs, we will use Monte Carlo simulations to generate a "control" sample of field galaxies that is subjected to the same pair selection effects. We begin by generating simulations that mimic the large-scale distribution of galaxies in the CNOC2 sample. Galaxies are distributed at random on the sky, filling the defined survey boundaries. We must then assign a redshift to each galaxy. In order to attain a redshift distribution that is similar to CNOC2, we smooth the observed CNOC2 redshift histogram, and fit a fifth order polynomial to this relation. This purely empirical approach has the advantage of sidestepping knowledge of the galaxy LF and redshift-dependent selection effects, such as those associated with spectroscopic incompleteness. We generate large numbers of galaxies, filling the volume encompassed by $0.1 \leq z \leq 0.55$. These simulations correctly reproduce the large scale distribution of galaxies in CNOC2.

On smaller scales along the line-of-sight, there will be differences between companions and galaxies in the control sample, due to density fluctuations within the sample. Pairs will be more likely to be found in regions of higher density, since pair selection depends on the square of the selection function. This is a complex issue, however, since dynamical pairs are less likely to be found in regions of higher velocity dispersion, typically associated with the densest regions. As this affects only the small scale distribution, there should not be a significant systematic offset in redshift between companions and field galaxies in the control sample. Therefore, we will ignore this effect

in the generation of the control sample, while cautioning that this must be taken into account when comparing redshift distributions in detail.

We now use these Monte Carlo simulations to extract a control sample of galaxies from the CNOC2 survey. As outlined earlier in this section, this control sample must be subjected to the same selection criteria as the sample of close companions. To generate our control sample, we randomly select "host" galaxies from the simulations. We then look for companions in the CNOC2 data. As with the real companions, we require $\Delta v \leq 500$ km/s. We also impose limits on r_p. However, the actual values of these limits are unimportant. That is, regardless of the restrictions on r_p, we will find a sample of galaxies that depends on the square of the selection function. We wish to generate a large control sample. However, as these companions are being chosen from the CNOC2 sample ($N \sim 5000$), there is a limited amount of information available. As a result, we impose $r_p \leq 500\ h^{-1}$ kpc, which yields a control sample that is comparable in size to the true field sample.

We now check to see if this procedure has been successful. We generate redshift histograms for the CNOC2 sample and the Monte Carlo simulations, and do the same for CNOC2 companions and the control sample. The resulting redshift distributions are plotted in Figure 5.2. Several important conclusions may be drawn from this plot. First, the overall redshift distribution for the Monte Carlo simulations (panel b) provides a good smoothed fit to the CNOC2 field sample, as desired. Secondly, the distribution of companions is found to be skewed towards low redshift. That is, when compared with the distribution of field galaxies, there is a deficit of pairs at high redshift, and (to a lesser extent) an excess at low redshift. This is true both

for companions (panel c) and the control sample (panel d). This skewing of companions is a consequence of the pair bias discussed above, and is precisely the effect we have set out to address. Finally, comparison of panels c and d indicates that CNOC2 companions and the control sample have similar redshift distributions, particularly at the low and high redshift ends of the sample. This agreement shows that, with the sample of CNOC2 companions generated using Monte Carlo simulations, we have obtained a control sample that is directly comparable to the real companions found with CNOC2 alone. This control sample of field galaxies will be used throughout the remainder of this analysis, and will be assumed to be free of bias due to pair-related redshift selection effects.

5.5 Differential Analysis of Close Companions and Field Galaxies

We are now ready to proceed with our comparison of close companions ($5\ h^{-1}$ kpc$\leq r_p \leq 20\ h^{-1}$ kpc) and field galaxies (from the control sample). We will focus on 7 key properties. Along with the fundamental properties of redshift (z), absolute magnitude (M_B), and rest-frame colour ($(B-R)_0$), we will consider SED classification (SedCl), break strength at 4000Å (D4000), [OII]3727Å equivalent width (W_0(OII)), and $H\delta$ equivalent width ($W_0(H\delta)$). All of these properties were described in Section 5.3. Rest-frame colour is closely related to SedCl and D4000, in that all three properties provide a measure of the relative contribution of light in the blue and red regions of the optical spectrum. We plot SedCl and D4000 versus colour in Figure 5.3.

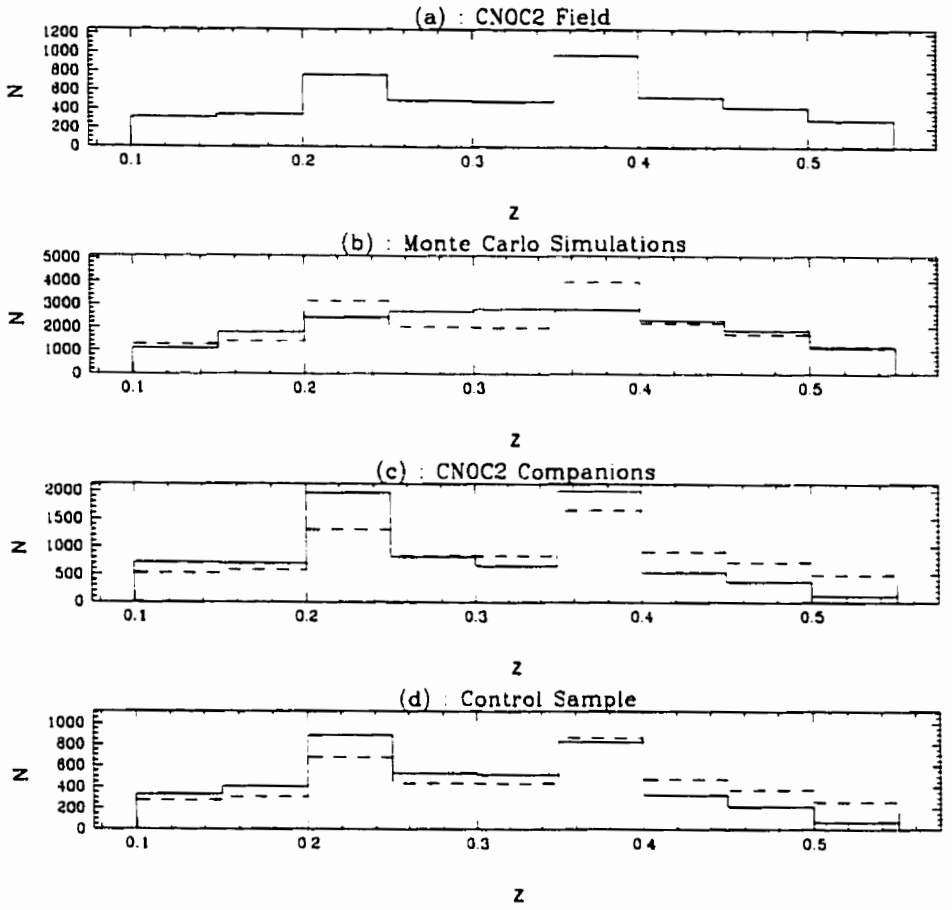

Figure 5.2: Redshift histograms are given for four different samples of galaxies. Histograms are normalized such that the area under each is equal. From top to bottom, the solid lines represent : (a) the CNOC2 field sample, consisting of all galaxies lying in the primary sample (the dashed line in panels (b)−(d) reproduces this histogram, scaled appropriately, providing a fixed frame of reference); (b) the Monte Carlo simulations, with distribution determined by synthetic $n(z)$ outlined in text; (c) CNOC2 companions ($r_p \leq 500\ h^{-1}$ kpc, $\Delta v \leq 500$ km/s); and (d) the control sample, generated by finding CNOC2 companions around host galaxies drawn at random from the Monte Carlo simulations.

While there is clearly some scatter, a clear correlation is seen in both cases. Large $(B-R)_0$, small SedCl, and large D4000 all signal a spectrum that is dominated by the light of old, red stars. Galaxies with properties at the other extreme exhibit an increased contribution from young, blue stars. Large (negative) W_0(OII) is indicative of an emission line spectrum, generally associated with current star formation activity. Large $W_0(H\delta)$ indicates a sizable contribution from A stars. This may be the result of a recent (not active) burst of star formation (e.g., Dressler and Gunn 1983), recently truncated star formation without a large initial burst (Newberry, Boroson, and Kirshner 1990, Abraham et al. 1996, Morris et al. 1998) or perhaps a dusty ongoing starburst (Poggianti et al. 1999).

5.5.1 Mean Properties

We begin by computing mean properties for galaxies in the two samples. We compute 1σ errors using the Jackknife technique (these errors are directly comparable to the error in the mean). The control sample is much larger than the companion sample; hence, the errors will be very small in comparison. We also perform Kolmogorov-Smirnov (K-S) tests to determine if there are significant differences in the distribution of properties between the two samples. The K-S test statistic given indicates the significance level for the hypothesis that the two data sets are drawn from the same distribution. A small significance level indicates that the two distributions have significantly different cumulative distribution functions. The mean properties of galaxies in the companions and control samples are presented in Table 5.1, along with the results of the K-S tests.

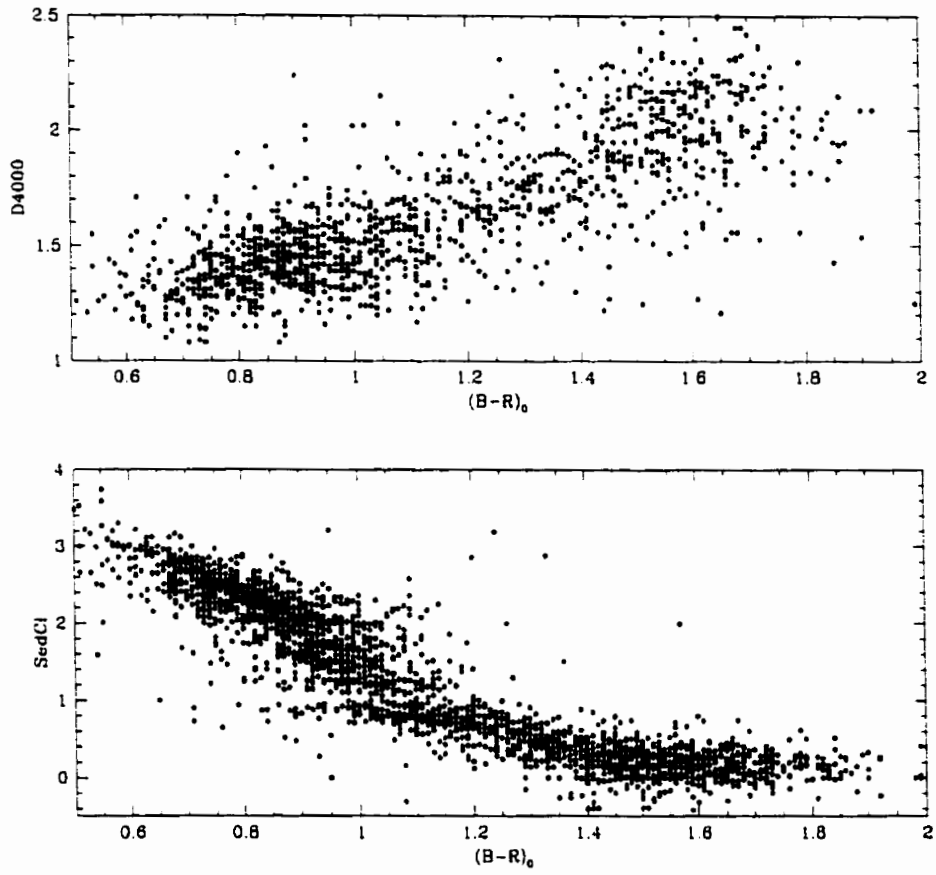

Figure 5.3: SED classification (SedCl) and the size of the 4000Å break (D4000) are plotted versus rest-frame $B - R$ colour. All galaxies shown have $R_C \leq 21.5$ and $0.1 \leq z \leq 0.55$.

Table 5.1: Mean Properties of Galaxies in Close Pairs

Property	N(pair)	N(control)	Mean(pair)	Mean(control)	K-S(%)
z	108	4115	0.301± 0.011	0.295± 0.002	11.0
M_B	108	4104	-19.01± 0.10	-18.78± 0.01	0.7
$(B-R)_0$	108	4113	1.18± 0.04	1.12± 0.01	5.4
SedCl	108	4097	1.12± 0.10	1.26± 0.02	8.5
D4000	56	2090	1.71± 0.05	1.63± 0.01	11.6
W_0(OII)	50	1984	-22.28± 3.40	-17.88± 0.47	40.2
$W_0(H\delta)$	62	2304	3.24± 0.47	3.50± 0.08	76.8

There are several important results to be gleaned from this table. First of all, the mean redshift of companions is consistent with that of the control sample. The K-S test indicates somewhat different cumulative redshift differences; however, this is to be expected, due to clustering that is present for companions but absent in the control sample. The fact that the mean redshifts are so similar provides additional confirmation that the two samples are selected in the same manner. It also assures us that any differences we might find between companions and field galaxies will not be attributable to systematic differences in redshift. That is, any redshift-dependent effects on properties, including spectroscopic selection effects, k-corrections, and luminosity evolution, will affect both samples to the same degree, to first order. This greatly simplifies the interpretation of our results.

Based on mean properties, close companions appear to be fairly similar to field galaxies from the control sample. Companions are on average 0.2 magnitudes brighter, with a difference detected at the 2σ level. We have confirmed that this difference is not due to small differences (e.g., due to clus-

tering) in the redshift distributions. $(B-R)_0$, SedCl, and D4000 all indicate that companions are of slightly earlier spectral type, at roughly the 1σ level. The relative size of this effect in these three indices is consistent with the correlations seen in Figure 5.3. Companions appear to have slightly stronger [OII] emission, though only at the 1σ level. Mean $W_0(H\delta)$ is slightly smaller for companions, but the difference is not statistically significant. Results from the K-S tests are consistent with these conclusions.

5.5.2 Histograms

While mean properties are useful, there is additional information available in the distribution of properties within each sample. We will present this information in the form of histograms. Figures 5.4–5.10 contain histograms for close companions (top panel) and field galaxies from the control sample (bottom panel), for the 7 properties under consideration (the remaining panels will be discussed in § 5.6). A direct comparison of close companions and the field is made easier by reproducing the control sample histogram in the companion plot, with the control sample normalized to the area under the companion histogram.

A number of interesting features are seen in these Figures. The redshift distributions in Figure 5.4 show that companions are more clustered than the control sample. That is, the distribution of companions is more peaked than the control sample. This is to be expected, as galaxies in the control sample are located at random locations along the line of sight, on small scales (on larger scales, their distribution is constrained to match the CNOC2 redshift distribution, as described in § 5.4.2). Close companions appear to be gener-

ally brighter (Figure 5.5) than field galaxies. Colour histograms (Figure 5.6) reveal an interesting result. There appears to be a clear excess of very red companions. There is also marginal evidence for an excess of very blue companions. Alternatively, this could be interpreted as a deficit of companions with normal colours. This effect will not be evident when comparing mean colours (though it will contribute to a low K-S significance level). A similar trend is seen in both SedCl (Figure 5.7) and D4000 (Figure 5.8), which are closely related to colour. Inspection of W_0(OII) histograms (Figure 5.9) reveals a consistent excess of companions with strong [OII]. Once again, however, there are signs of a small excess at the opposite extreme. The same effect is seen in the distribution of $W_0(H\delta)$(Figure 5.10).

5.5.3 Fractional Properties

In order to quantify these visual impressions, we will measure the fraction of galaxies with extreme properties. For example, when considering colour, we will determine what fraction of the sample is redder than $(B-R)_0$=1.5 (the "red fraction") and bluer than $(B-R)_0$=0.8 (the "blue fraction"). These limits must be chosen with care. This analysis will be most meaningful if we select limits that best separate normal galaxies from those that are more extreme in nature. However, this constraint must be balanced by the need to extract a subset that is large enough to yield reasonably small statistical errors. For a sample of N galaxies with a subset of m extreme galaxies, the fraction of extreme galaxies is given by

$$f = \frac{m}{N} \pm \frac{1}{N}\sqrt{\frac{m(N-m)}{(N-1)}}, \tag{5.2}$$

where errors are determined using the Jackknife technique. For small m, the relative error is roughly proportional to $m^{-1/2}$, which is similar to Poisson statistics. As a compromise between maximizing property extrema and minimizing statistical errors, we choose limits corresponding roughly to the 20th percentile of properties in the control sample. Finally, and most importantly, these limits must not be chosen with reference to the observed companion histograms, as there may be a tendency to choose limits that will best support our preliminary conclusions. Hence, we refer only to the control sample histogram when selecting these limits.

The minimum and maximum limits and the resulting property fractions are given in Table 5.2. Bright ($M_B < -19.6$) galaxies are found to be ~40% more common in the pair sample, and the excess is confirmed at the 2σ level. We also verify an excess of galaxies with early-type spectra. This effect is seen in $(B-R)_0$, SedCl, and D4000, all at the 2σ level, with an overabundance of $\sim 50\%$. In addition, these three properties all imply a small excess of galaxies with late-type spectra, though this effect is not statistically significant. Excesses are seen at both extremes for both W_0(OII) and $W_0(H\delta)$. The strongest effect is in the fraction of galaxies with W_0(OII)< -30Å, where a 2σ excess is seen, and close companions are 50% more common than field galaxies. Recalling that negative values of W_0(OII) denote emission, this indicates that companions are forming stars at a higher rate that field galaxies. This result is particularly intriguing in light of our earlier findings that companions are generally of earlier spectral type than field galaxies. As emission lines are usually less prevalent in early type galaxies, our [OII] result is in conflict with what would be expected on this basis alone.

Table 5.2: Fractional Properties of Galaxies in Close Pairs

Property	Criterion	N(pair)	N(control)	Frac(pair)	Frac(control)
M_B	< -19.6	108	4104	28.70± 4.37	20.08± 0.63
M_B	> -17.8	108	4104	12.96± 3.25	15.62± 0.57
$(B-R)_0$	< 0.8	108	4113	19.44± 3.83	17.26± 0.59
$(B-R)_0$	> 1.5	108	4113	30.56± 4.45	18.87± 0.61
SedCl	< 0.3	108	4097	29.63± 4.41	22.41± 0.65
SedCl	> 2.2	108	4097	24.07± 4.13	22.02± 0.65
D4000	< 1.4	56	2090	28.57± 6.09	25.26± 0.95
D4000	> 1.9	56	2090	32.14± 6.30	20.00± 0.88
W_0(OII)	< -30	50	1984	34.00± 6.77	22.08± 0.93
W_0(OII)	> -2	50	1984	22.00± 5.92	20.31± 0.90
$W_0(H\delta)$	< 1	62	2304	25.81± 5.60	22.01± 0.86
$W_0(H\delta)$	> 6	62	2304	24.19± 5.48	19.49± 0.83

5.6 Variation of Properties with Physical Separation

We have carried out a detailed comparison between the properties of close companions ($5\ h^{-1}$ kpc$\leq r_p \leq 20\ h^{-1}$ kpc) and field galaxies (from the control sample). We will now extend the companion sample to larger separations, in order to look for a connection between galaxy properties and pair separation. First, we sort companions according to separation, and place them in several bins of r_p, with separations spanning $5\ h^{-1}$ kpc$\leq r_p \leq 400\ h^{-1}$ kpc. These histograms are given in Figures 5.4–5.10.

At large separations, there are striking differences between companions and field galaxies. These companions are more clustered, are of earlier spectral type (based on $(B-R)_0$, SedCl, and D4000), and have smaller

W_0(OII) and $W_0(H\delta)$. They are also slightly brighter, though this effect is less pronounced. These effects are clearly seen at all separations in the range 20 h^{-1} kpc$< r_p <$ 400 h^{-1} kpc. While this is a strong effect, it is not unexpected. The well-known morphology-density relation (Dressler et al. 1980) has established that early type galaxies are more prevalent in regions of higher density. We remind the reader that companions may be associated with more than one host galaxy (§ 5.4.1). In dense regions such as clusters or groups, many companions will be found on scales of $\gtrsim$ 100 h^{-1} kpc. This is evident in Figure 5.4, where companions are more prevalent in the peaks of the redshift distribution. This effect is most evident on the largest scales, and appears to decrease in importance as one moves to smaller scales.

We will now focus our analysis on scales less than 100 h^{-1} kpc. These scales are the most relevant for studying galaxy interactions (see § 3.7). We have learned that companion properties are not field-like on scales of $\sim$ 100 h^{-1} kpc. We will now attempt to determine if galaxy properties change systematically as we approach the small scales ($r_p \sim$ 20 h^{-1} kpc) where galaxy interactions become important.

We begin by placing companions in bins of size 10 h^{-1} kpc, ranging from 0-100 h^{-1} kpc (note, however, that due to resolution effects, we find very few pairs with $r_p <$ 5 h^{-1} kpc). We compute the mean properties of companions in each bin, and present the results in Figure 5.11. In each case, mean properties are compared with the mean value for the field, derived from the control sample. We do the same for fractional properties, generating plots for properties below (Figure 5.12) and above (Figure 5.13) the limits given in Table 5.2.

These three plots contain a lot of information. Here, we attempt to summarize and interpret the most obvious trends. Overall, companions tend to become more field-like on smaller scales. That is, while companions at 50 h^{-1} kpc$\lesssim r_p \lesssim$ 100 h^{-1} kpc appear to be of earlier spectral type than field galaxies (as expected from the morphology-density relation), there is a general approach toward field properties, down to scales of $r_p \sim 10\ h^{-1}$ kpc. The strongest trends are seen for W_0(OII) and SedCl, which indicate an increased prevalence of strong [OII] emitters and late-type galaxies. There is also some evidence of bluer colours and stronger $H\delta$. The most significant differences are seen at 10 h^{-1} kpc$\lesssim r_p \lesssim$ 20 h^{-1} kpc, where the fraction of blue, late-type galaxies exceeds values found in the field itself. This effect is seen in W_0(OII), D4000, $(B-R)_0$, and SedCl. Surprisingly, this trend does not continue below 10 h^{-1} kpc; in fact, galaxies appear to become less field-like at these small separations.

5.7 Discussion

We have carried out a detailed comparison between galaxies in close pairs and the field, using the largest redshift sample currently available at moderate redshift. This study is limited to confirmed dynamical pairs, yielding a sample with greatly reduced contamination from unrelated or non-merging companions. We have carefully identified a control sample of field galaxies that is subjected to the same redshift-dependent selection effects as the pair sample. Our analysis focusses on the intrinsic properties of redshift, absolute magnitude, and rest-frame colour, along with photometric and spectroscopic

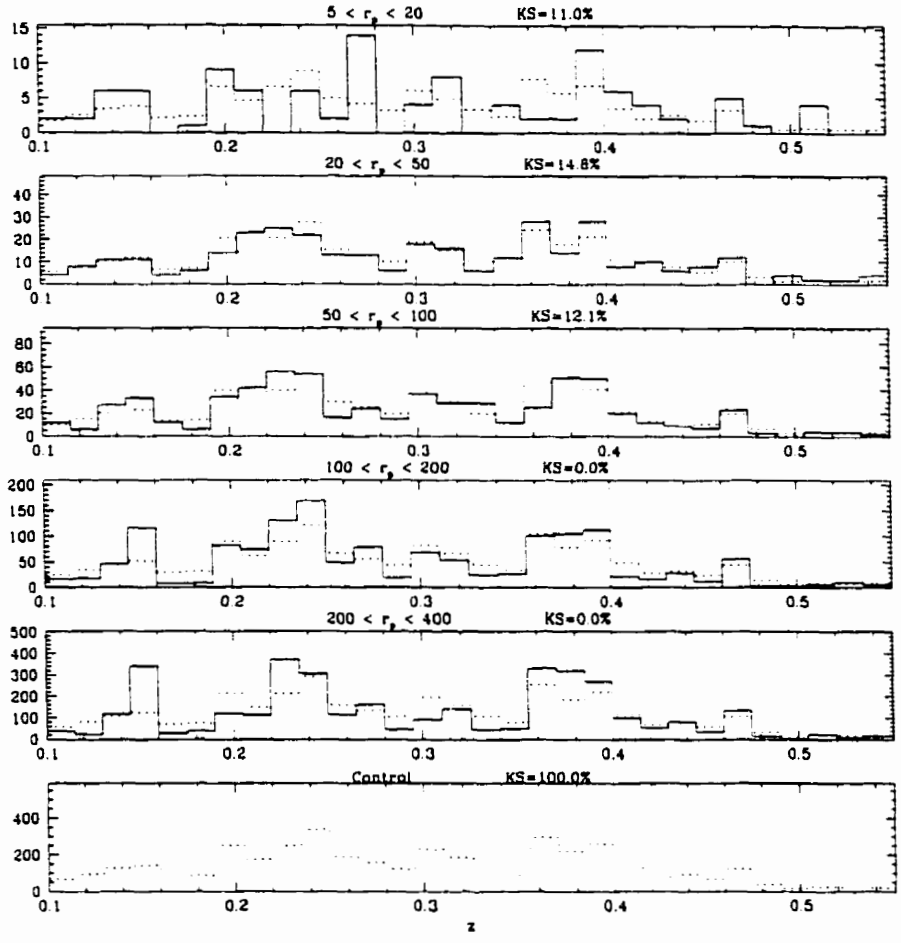

Figure 5.4: Redshift histograms are given for the control sample (bottom panel) and companions in several bins of projected separation r_p. Histograms are normalized such that the area under each is equal. The dashed line in each figure denotes the control sample. In each case, a K−S test was used to compare the observed distribution with that of the control sample. A small significance level indicates that the two samples have significantly different cumulative distribution functions.

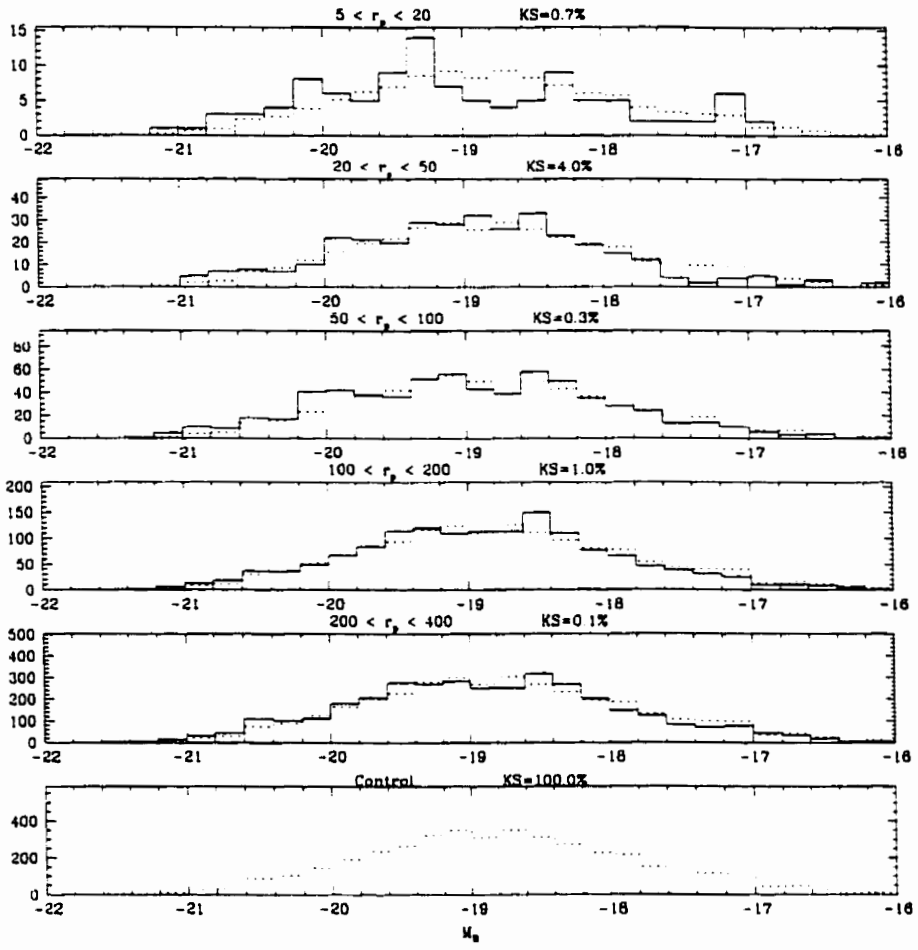

Figure 5.5: $B-$band absolute magnitude (M_B) histograms are given for the control sample (bottom panel) and companions in several bins of projected separation r_p. Histograms are normalized such that the area under each is equal. The dashed line in each figure denotes the control sample. In each case, a K$-$S test was used to compare the observed distribution with that of the control sample. A small significance level indicates that the two samples have significantly different cumulative distribution functions.

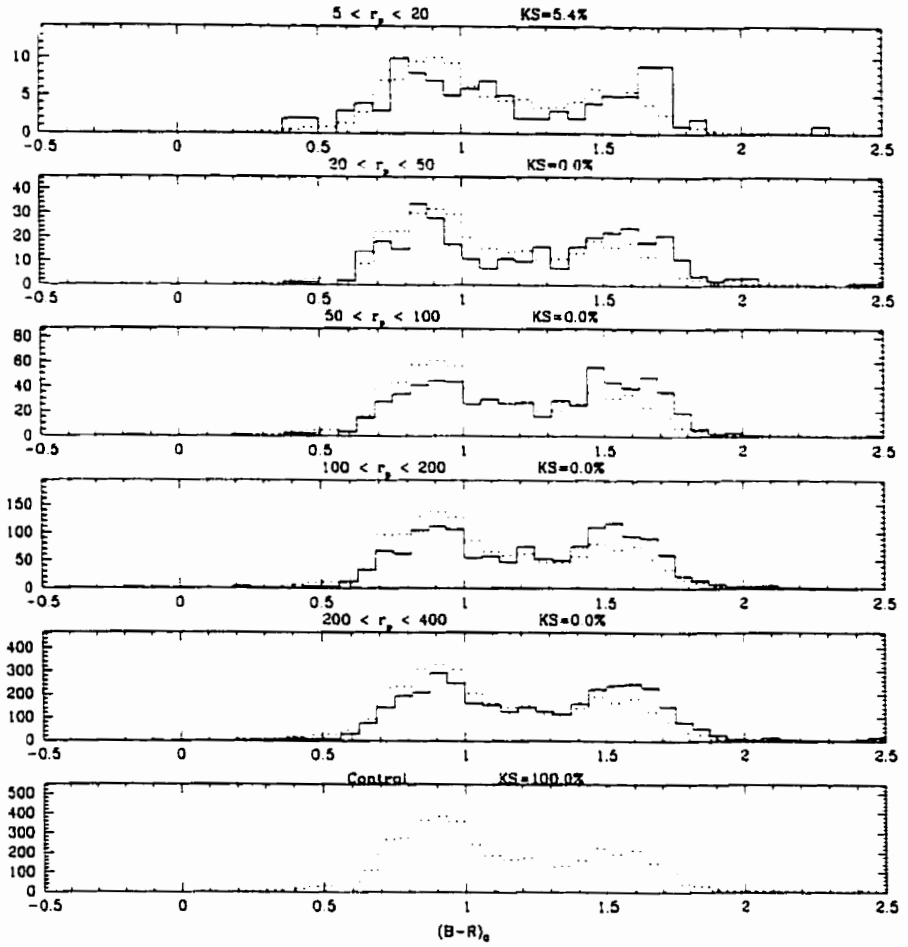

Figure 5.6: Rest-frame $B - R$ colour histograms are given for the control sample (bottom panel) and companions in several bins of projected separation r_p. Histograms are normalized such that the area under each is equal. The dashed line in each figure denotes the control sample. In each case, a K−S test was used to compare the observed distribution with that of the control sample. A small significance level indicates that the two samples have significantly different cumulative distribution functions.

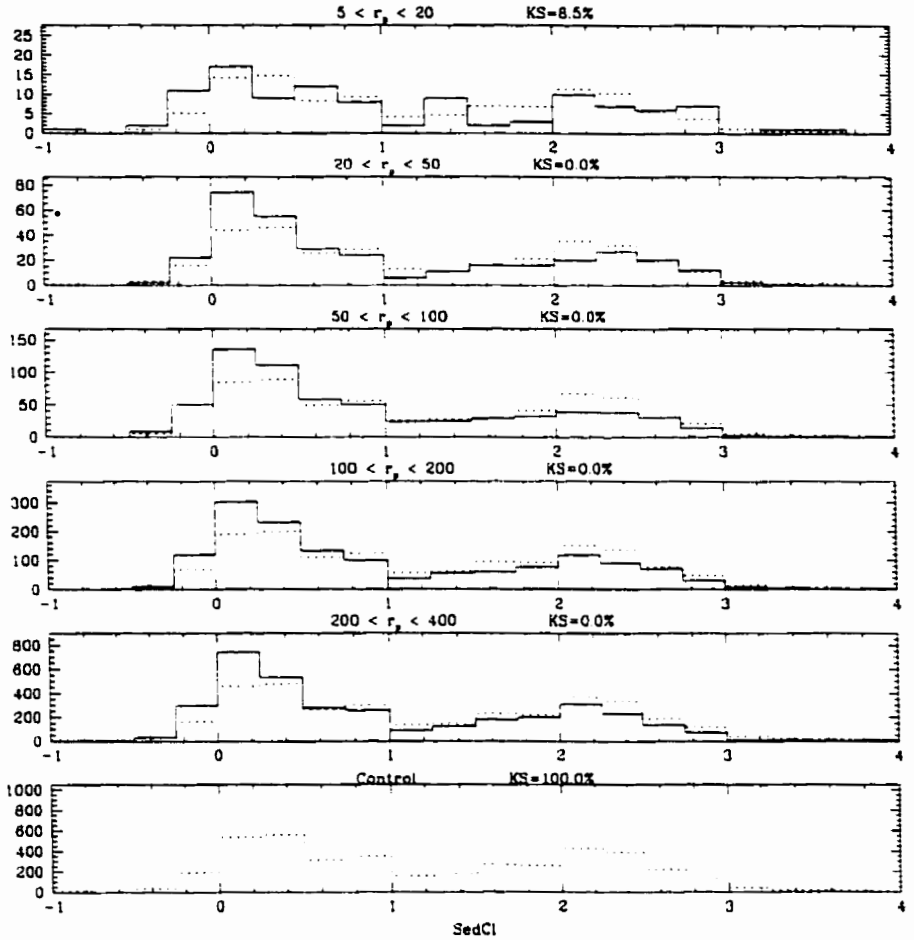

Figure 5.7: SED classification histograms are given for the control sample (bottom panel) and companions in several bins of projected separation r_p. Histograms are normalized such that the area under each is equal. The dashed line in each figure denotes the control sample. In each case, a K−S test was used to compare the observed distribution with that of the control sample. A small significance level indicates that the two samples have significantly different cumulative distribution functions.

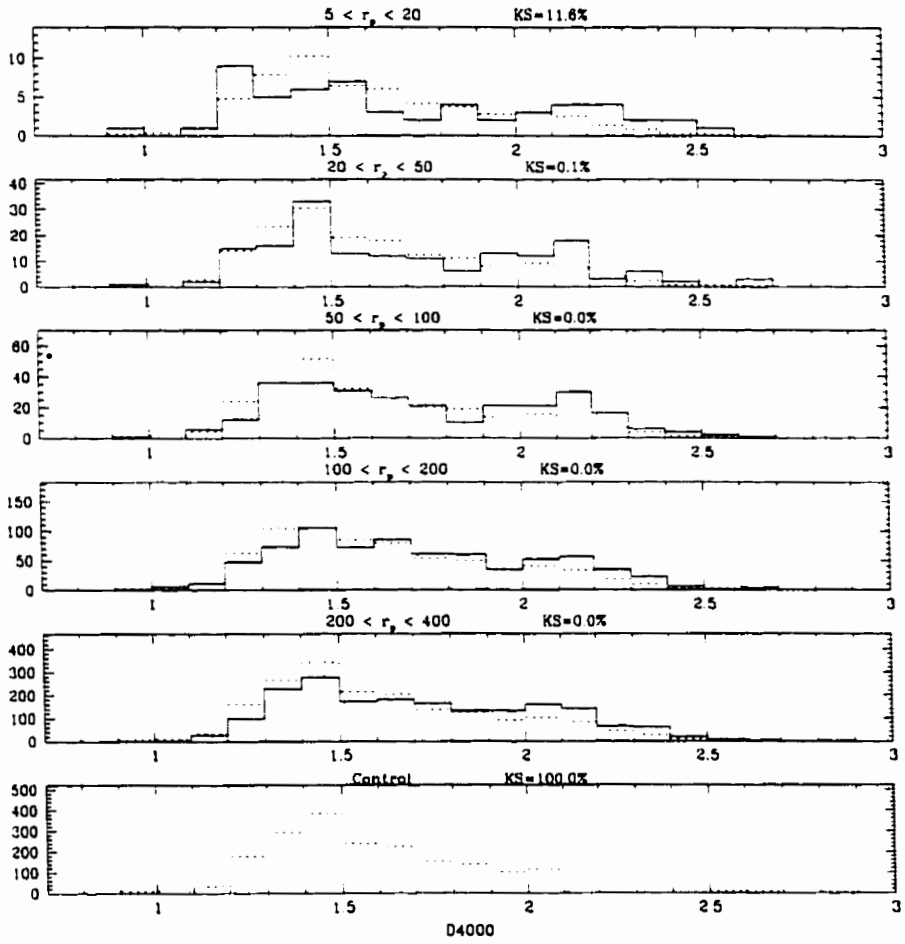

Figure 5.8: D4000 histograms are given for the control sample (bottom panel) and companions in several bins of projected separation r_p. Histograms are normalized such that the area under each is equal. The dashed line in each figure denotes the control sample. In each case, a K−S test was used to compare the observed distribution with that of the control sample. A small significance level indicates that the two samples have significantly different cumulative distribution functions.

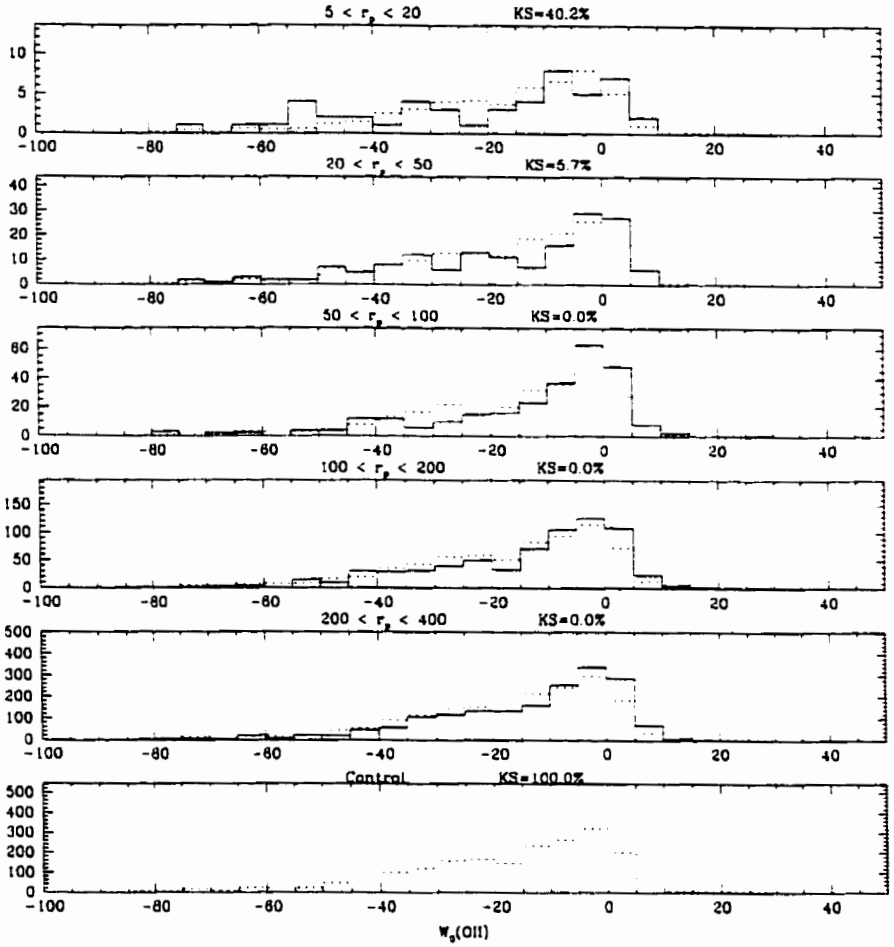

Figure 5.9: W_0(OII) histograms are given for the control sample (bottom panel) and companions in several bins of projected separation r_p. Histograms are normalized such that the area under each is equal. The dashed line in each figure denotes the control sample. In each case, a K−S test was used to compare the observed distribution with that of the control sample. A small significance level indicates that the two samples have significantly different cumulative distribution functions.

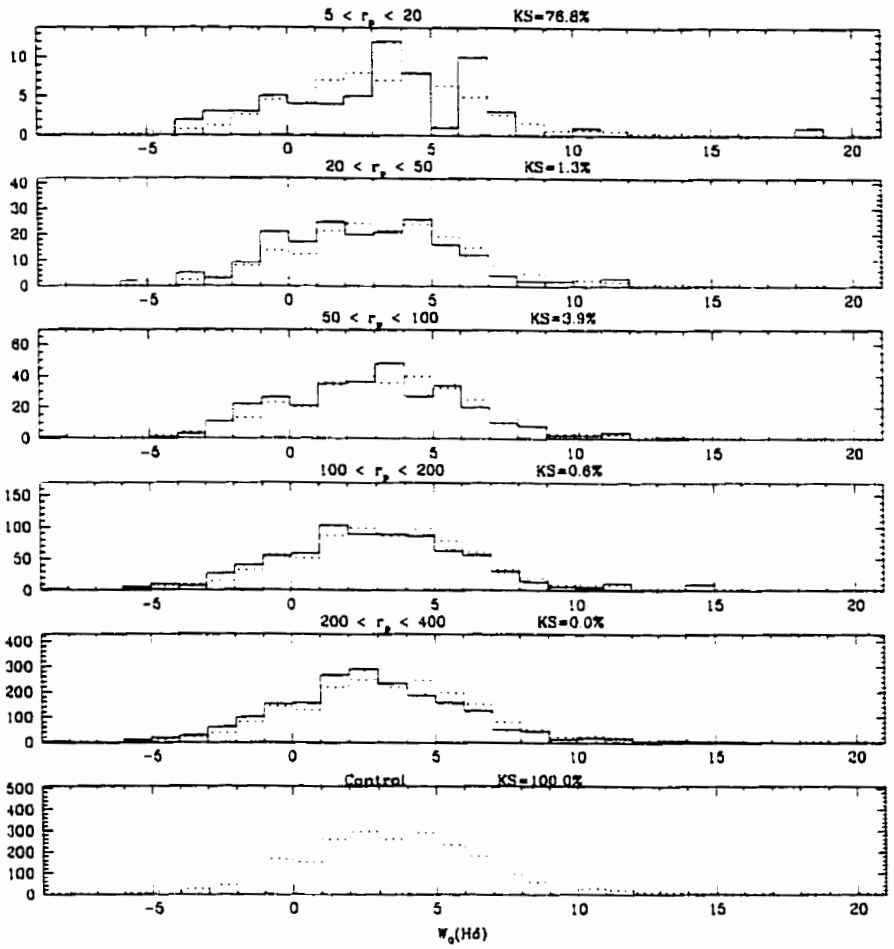

Figure 5.10: $W_0(H\delta)$ histograms are given for the control sample (bottom panel) and companions in several bins of projected separation r_p. Histograms are normalized such that the area under each is equal. The dashed line in each figure denotes the control sample. In each case, a K−S test was used to compare the observed distribution with that of the control sample. A small significance level indicates that the two samples have significantly different cumulative distribution functions.

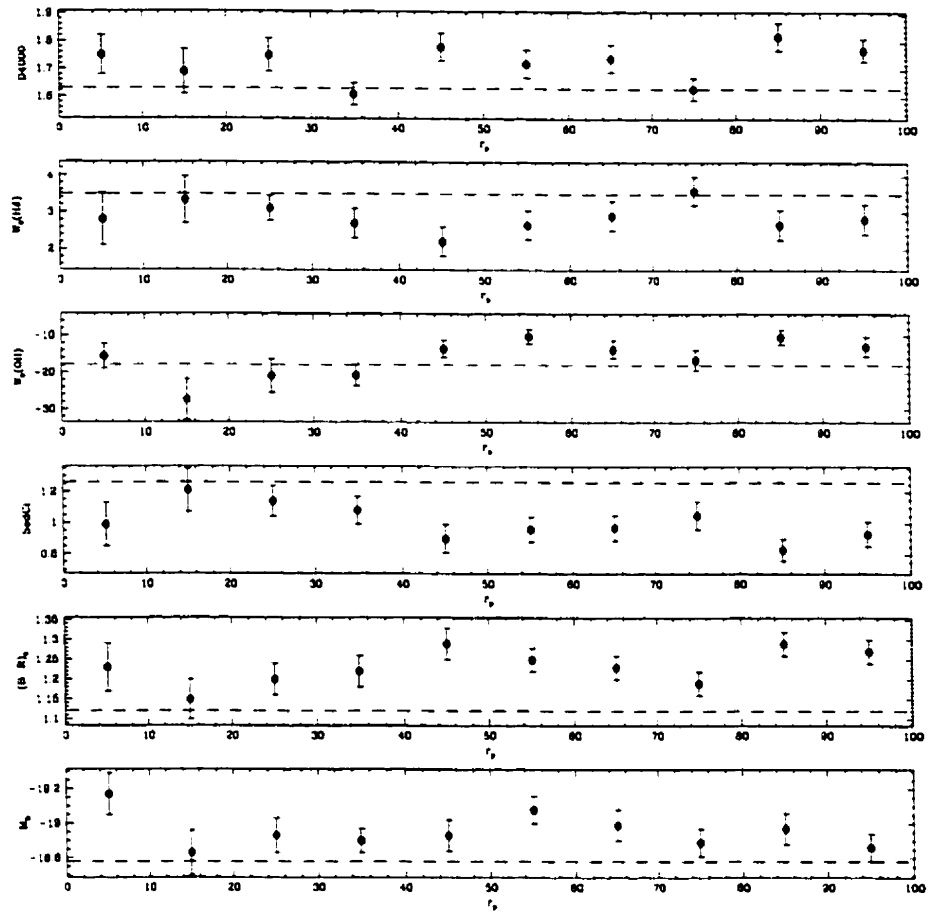

Figure 5.11: Mean properties of companions are computed as a function of projected physical separation (r_p). Errors are computed using the Jackknife technique, and are essentially equivalent to the 1σ error in the mean. Quantities computed are (bottom to top) : $B-$band absolute magnitude (M_B), rest-frame $B-R$ colour ($(B-R)_0$), SED classification (SedCl), [OII]3727Å equivalent width (W_0(OII)), $H\delta$ equivalent width ($W_0(H\delta)$), and the size of the 4000Å break (D4000). Dashed lines indicate mean properties for field galaxies, derived from the control sample.

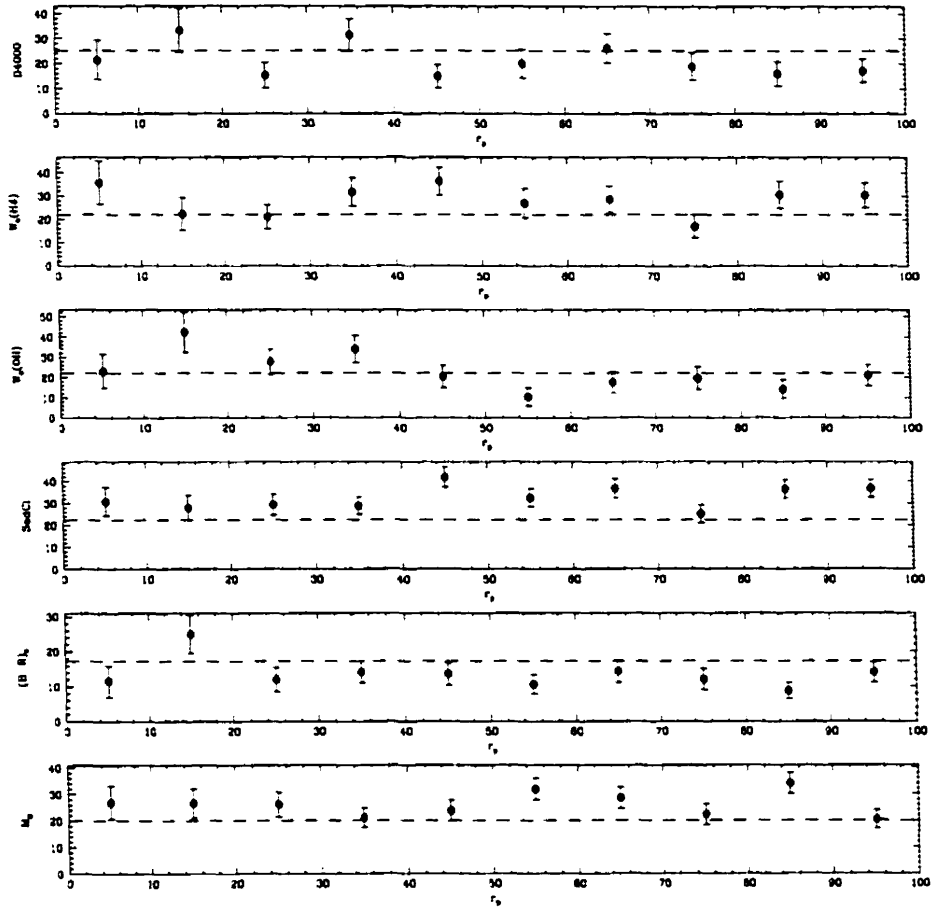

Figure 5.12: The fraction of galaxies *below* the lower threshold given in Table 5.2 is computed as a function of projected physical separation (r_p). Errors are computed using the Jackknife technique. Quantities computed are (bottom to top) : fraction with $M_B < -19.8$, fraction with $(B-R)_0 < 0.8$, fraction with SedCl < 0.2, fraction with W_0(OII)< -40Å, fraction with $W_0(H\delta) < 0$Å, and fraction with D4000 < 1.35. Dashed lines indicate the corresponding fractions for field galaxies, derived from the control sample.

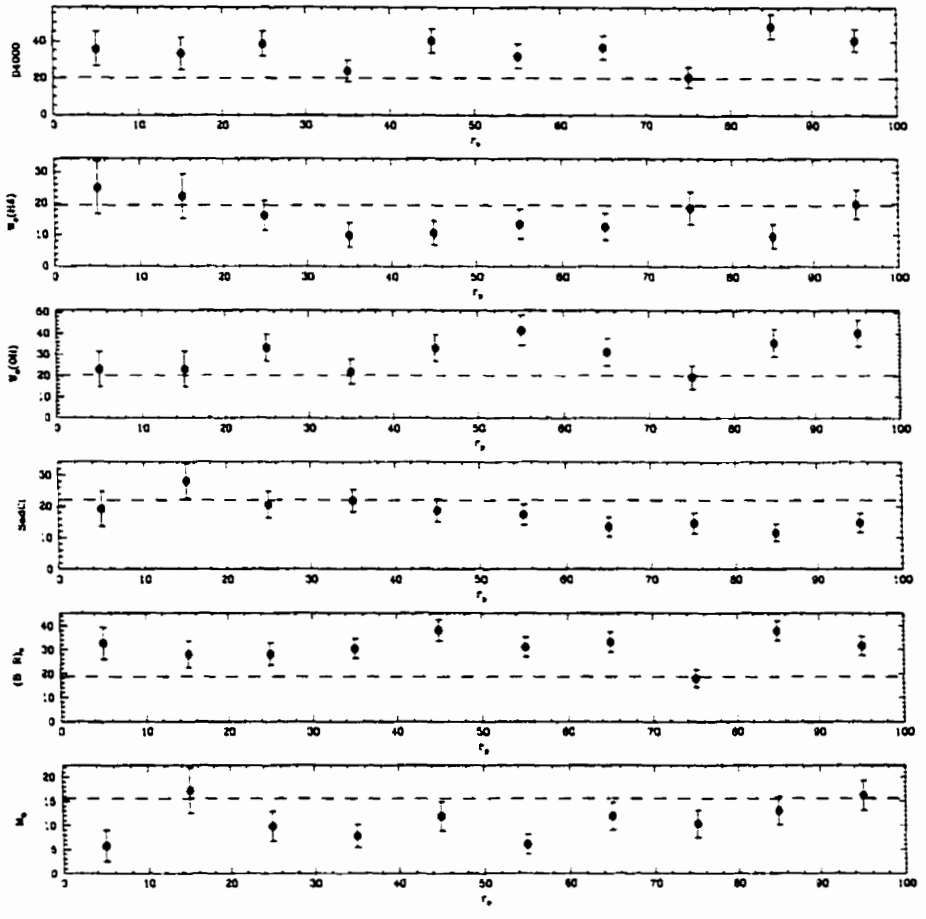

Figure 5.13: The fraction of galaxies *above* the upper threshold given in Table 5.2 is computed as a function of projected physical separation (r_p). Errors are computed using the Jackknife technique. Quantities computed are (bottom to top) : fraction with $M_B > -17.5$, fraction with $(B-R)_0 > 1.6$, fraction with SedCl > 2.3, fraction with W_0(OII)> 0Å, fraction with $W_0(H\delta)$> 7Å, and fraction with D4000 > 2.00. Dashed lines indicate the corresponding fractions for field galaxies, derived from the control sample.

measures of galaxy type and line strength.

Overall, close (5 h^{-1} kpc$\leq r_p \leq$ 20 h^{-1} kpc) companions are found to have properties that are fairly similar to field galaxies chosen from the control sample. However, there are some interesting differences in detail. Mean properties indicate that close companions are of slightly earlier spectral type, though with enhanced [OII] emission. However, close inspection of the distribution of these properties indicates a greater spread in the properties of companions, with an increased prevalence often seen at both extremes. This is most apparent in the measurement of spectral indices [OII] and $H\delta$. This may indicate that galaxies in pairs have a more complex recent star formation history than their counterparts in the field (cf. Larson and Tinsley 1978).

We have extended the study of companions to larger separations, yielding the first moderate$-z$ study of companion properties as a function of pair separation. At projected separations of $r_p \gtrsim 50\ h^{-1}$ kpc, companions appear to follow the morphology-density relation seen on scales typical of groups or poor clusters ($r_p \sim 300\ h^{-1}$ kpc). On smaller scales, there is a general return to field properties. This is most evident with [OII] and SedCl, for which properties eventually surpass those in the field. The strongest effects are seen at 10 h^{-1} kpc$\leq r_p \leq$ 20 h^{-1} kpc, though they do not continue to smaller separations.

There are a number of possible interpretations of our results. The tendency for galaxies in close pairs to be of somewhat earlier spectral type than field galaxies may indicate that the morphology-density relation is at work for at least some of these companions. This would not be surprising, since pairs are more likely to be found in regions that are at least somewhat

overdense. The preferred environment for low velocity pairs may be loose groups, where the density is reasonably high, and yet the velocity dispersion is low enough to allow galaxy interactions to be effective (see Section 1.2.2). The morphology-density relation is well established in rich clusters (Dressler 1980), but has also been extended to loose groups (Postman and Geller 1984).

We have found evidence that at least some close pairs have properties indicative of atypical ongoing or recent star formation. The strongest evidence for this effect comes from the strength of [OII] emission, which is more prevalent than for field galaxies. This may be indicative of interaction-induced star formation. The combination of strong [OII] and redder-than-average colours for some close companions may hint at the existence of a population of merging systems, reddened by the presence of dust. Significant amounts of dust may contribute to increased scatter in many of the observed properties of galaxies in pairs.

There are several ways to improve on these results. First, high quality imaging would allow us to determine which of these moderate$-z$ pairs are undergoing interactions. While some of these pairs do exhibit signs of interactions, our MOS images suffer from a lack of resolution. At present, the Hubble Space Telescope provides the best available means for alleviating this problem. We have been awarded 72 orbits of *HST* time to obtain high resolution images of these CNOC2 close pairs. Secondly, it is unclear how important dust is in these systems. This issue becomes increasingly important as one probes to higher redshift. This information is essential if we are to determine how the optical properties of galaxies in pairs are affected by dust. Thirdly, more information on the large scale environment of close

pairs would allow us to distinguish between competing explanations for the observed properties of galaxies in our companion sample. In particular, measurements of local density and the identification of galaxy groups would help in identifying the preferred neighbourhoods of interacting galaxies. Finally, larger redshift samples would allow us to investigate property differences as a function of galaxy type and luminosity. This is particularly important if we are to understand the relative contributions of major and minor mergers.

Chapter 6

Conclusions

6.1 Summary of New Results

We have developed new techniques for relating the statistics of close galaxy pairs to the galaxy merger and accretion rates. The first statistic, denoted N_C, gives the number of close $M \leq M_2$ companions per galaxy, where M_2 is some specified limiting absolute magnitude. Given companions that are likely to merge within $\lesssim 1$ Gyr, N_C is directly proportional to the instantaneous galaxy merger rate. The second statistic, denoted L_C, gives the total luminosity in close $M \leq M_2$ companions per galaxy, and is proportional to the accretion rate. Beginning from first principles, we have outlined the relationship between these statistics and the galaxy luminosity function and correlation function, facilitating the interpretation of these pair statistics with respect to measurements of the global distribution of galaxies on larger physical scales.

We have uncovered a serious conceptual problem inherent in earlier measures of close pair statistics. While the traditional close pair fraction has been

treated as a measurement of galaxy clustering, it is in fact equally dependent on the mean density of galaxies in the sample. As a result, the pair fraction is intimately connected to the minimum luminosity or mass of the sample in question. Moreover, the pair fraction will be adversely affected by all selection effects that alter the apparent density of the sample, including the imposition of a flux limit. Our new statistics have been designed with these biases in mind. Due to the pairwise nature of our techniques, it is relatively straightforward to measure and correct for biases related to the flux limit or completeness of galaxy redshift surveys. We have introduced weighting schemes to account for these effects, and have demonstrated the success of this approach using Monte Carlo simulations.

Using these techniques, we have measured N_C and L_C for the large, well-defined SSRS2 ($z \sim 0$) and CNOC2 ($0.1 \leq z \leq 0.55$) redshift surveys. Close companions are required to have $5\ h^{-1}$ kpc $\leq r_p \leq 20\ h^{-1}$ kpc and $\Delta v \leq 500$ km/s. At least half of the SSRS2 systems satisfying these criteria exhibit clear signs of interactions on DSS images. For SSRS2, we find $N_c(M_B \leq -18) = 0.0227 \pm 0.0054$ and $L_c(M_B \leq -18) = 0.0235 \pm 0.0061 \times 10^{10}\ h^2 L_\odot$ at z=0.016. For CNOC2, we find $N_c(M_B \leq -18) = 0.0342 \pm 0.0077$ and $L_c(M_B \leq -18) = 0.0367 \pm 0.0093 \times 10^{10}\ h^2 L_\odot$ at z=0.271. From these measurements, we infer evolution in the merger rate going as $(1+z)^{1.83\pm1.47}$, and an accretion rate evolution of $(1+z)^{1.99\pm1.62}$. These results are based on a much more solid foundation than were results from earlier studies of close pairs, due to the specification of M_2 and correction for density-related selection effects. In addition, this is the first study relying exclusively on dynamically–confirmed pairs, thereby eliminating optical contamination and

narrowing the focus to the low-velocity pairs most likely to be undergoing mergers.

Finally, we have carried out a detailed analysis of galaxy properties for CNOC2 close pairs, comparing close companions with field galaxies and with companions at larger separations. Close companions are found to be of slightly earlier spectral type than field galaxies drawn from a carefully selected control sample. There is some evidence for a larger spread in the properties of close companions, perhaps implying that these galaxies have had a more complex star formation history than field galaxies. Companions at larger separations exhibit properties attributable to the morphology-density relation, due to the higher density neighbourhoods prevalent on these larger scales. This difference decreases on small scales, with close companions becoming increasingly field-like down to scales of $r_p \sim 10\ h^{-1}$ kpc. Companions with $10\ h^{-1}$ kpc$\leq r_p \leq 20\ h^{-1}$ kpc have the strongest [OII] emission of all, hinting at a significant contribution from interaction-induced star formation.

6.2 The Contribution of Mergers to Galaxy Evolution

Measurements of pair statistics at low and moderate redshift provide two key ingredients needed in determining the overall importance of mergers in the recent history of galaxies and galaxy populations. A conclusive answer will require secure estimates of the merger timescale in the individual systems under consideration here. However, using reasonable assumptions, we have estimated the cumulative effect of mergers as a function of redshift. By ex-

trapolating our measure of merger rate evolution ($(1+z)^2$) to higher redshift, we conclude that $\sim$ 13% of present epoch galaxies brighter than $M_B=-18$ have undergone major mergers since $z \sim 1$. This estimate is uncertain by at least a factor of 2; nevertheless, it indicates that most galaxies probably have not been transformed by major mergers in the last two-thirds of the history of the universe.

One of the most important lessons from this dissertation is the realization that the merger rate depends on the limiting absolute magnitude (or mass) of the sample of galaxies under consideration. This has important implications regarding our interpretation of the importance of mergers. The conclusions in the preceding paragraph apply strictly to galaxies brighter than $M_B=-18$. Probing fainter will increase the fraction of galaxies undergoing mergers, thereby giving added importance to mergers. For example, if we choose $M_2(B)=-17$, the present epoch remnant fraction increases from $\sim$ 13% to $\sim$ 24%. The SSRS2 and CNOC redshift surveys used in this dissertation sample primarily bright (L_*) galaxies, and therefore do not provide much information on the density and clustering properties of intrinsically faint galaxies. Therefore, our measurements do not rule out a significant and perhaps dominant role for merging in the evolution of low luminosity galaxies, whether in the form of accretion onto brighter galaxies or self-merging with other faint galaxies.

6.3 Future Work

In this dissertation, we have carefully accounted for a number of biases that affect the measurement of pair statistics. The most uncertain of these is the correction for luminosity evolution. This effect is quite strong in the optical part of the spectrum. The correction was quite significant at the very modest mean redshift of z=0.27; clearly, this will become increasingly troublesome at higher redshifts. The ideal method of combating this effect is to use a spectral regime which is less sensitive to luminosity evolution. To do this, one should probe rest-frame wavelengths at which old stellar populations dominate, rather than those in which bright young stars contribute a large fraction of the light. The near-infrared part of the spectrum satisfies this criterion. In particular, the $K-$band (λ=2.2μm) is well suited to the task. Furthermore, k-corrections are less of an issue at these wavelengths, making it easier to select a fair sample of all galaxy types. Measurements of luminosity in this regime will be more closely related to total galaxy mass, as desired.

By computing pair statistics in the near-infrared, it will be possible to reduce the level of uncertainty in the moderate redshift pair statistics presented in Chapter 4. Moreover, it will allow pair statistics to be computed in a reliable manner out to redshifts of $z \sim 1-2$. These measurements will benefit from superior leverage in redshift evolution. Moreover, if pair statistics increase with redshift, as claimed in this work, an improved yield of close companions can be expected. This high redshift regime is of great interest, as there are many indications that it coincides with a peak in the rate of cosmic star formation, perhaps signalling the epoch at which most

galaxies were first assembled.

The redshift surveys used in this dissertation are well-suited to the study of relatively bright ($\sim L_*$) galaxies. However, there is mounting evidence that evolution may be stronger for galaxies of lower luminosities. With larger and deeper samples, it will be possible to apply pair statistics to fainter galaxies, and to measure the merger and accretion rates as a function of luminosity. This should help to establish the importance of minor mergers, along with equal mass mergers of faint galaxies. These systems may prove to be an important and perhaps even dominant contributor to merger-driven galaxy evolution.

We have used the optical properties of galaxies in close pairs in an attempt to detect differences associated with galaxy-galaxy interactions and mergers. However, the optical part of the spectrum may be strongly affected by the presence of dust. It is unclear exactly how this will affect the observed properties of paired galaxies. To minimize this uncertainty, it is preferable to acquire data in spectral regions that are less sensitive to dust. The near-infrared regime is the optimal choice in this respect. There is another important effect related to the presence of dust. After absorbing visible light, this energy may be re-emitted at mid- and far-infrared wavelengths. In fact, in the most extreme cases, galaxies emit the bulk of their energy in this regime (Sanders and Mirabel 1996). Therefore, observations at these wavelengths would be of great benefit in ascertaining the importance of dust in interacting and merging systems.

Bibliography

Abraham, R. G., Smecker-Hane, T. A., Hutchings, J. B., Carlberg, R. G., Yee, H. K. C., Ellingson, E., Morris, S., Oke, J. B., and Rigler, M.: 1996, *Astrophys. J.* **471**, 694

Alonso, M. V., da Costa, L. N., Latham, D. W., Pellegrini, P. S., and Milone, A. E.: 1994, *Astron. J.* **108**, 1987

Alonso, M. V., da Costa, L. N., Pellegrini, P. S., and Kurtz, M. J.: 1993, *Astron. J.* **106**, 676

Arp, H.: 1966, *Astrophys. J. Supp.* **14**, 1

Arp, H. C. and Madore, B. F.: 1987, *Catalog of Southern Peculiar Galaxies and Associations*, Cambridge University Press

Bahcall, J. N., Kirhakos, S., Saxe, D. H., and Schneider, D. P.: 1997, *Astrophys. J.* **479**, 642

Bahcall, S. R. and Tremaine, S.: 1988, **326**, 1

Balogh, M. L., Morris, S. L., Yee, H. K. C., Carlberg, R., and Ellingson, E.: 1999, *Preprint*

Barnes, J., Hernquist, L., and Schweizer, F.: 1991, *Scientific American* **265**, 40

Barnes, J. E.: 1988, *Astrophys. J.* **331**, 699

Barnes, J. E. and Hernquist, L.: 1992, *Annual Review of Astronomy and Astrophysics* **30**, 705

Barton, E. J., Bromley, B. C., and Geller, M. J.: 1998, *Astrophys. J. Lett.* **511**, 25

Benoist, C., Maurogordato, S., da Costa, L. N., Cappi, A., and Schaeffer, R.: 1996, *Astrophys. J.* **472**, 452

Binney, J. and Tremaine, S.: 1987, *Galactic Dynamics*, Princeton University Press : Princeton

Broadhurst, T. J., Ellis, R. S., and Glazebrook, K.: 1992, *Nature* **355**, 55

Broadhurst, T. J., Ellis, R. S., and Shanks, T.: 1988, *M.N.R.A.S.* **235**, 827

Burkey, J. M., Keel, W. C., Windhorst, R. A., and Franklin, B. E.: 1994, *Astrophys. J. Lett.* **429**, 13

Carlberg, R. G.: 1990, *Astrophys. J. Lett.* **359**, 1

Carlberg, R. G.: 1995, *Galaxies in the Young Universe*, Springer-Verlag, Berlin (ed. H. Hippelein, K. Meisenheimer, and H. J. Roser)

Carlberg, R. G.: 1999, *The Formation of Bulges*, Cambridge University Press

Carlberg, R. G. and Charlot, S.: 1992, *Astrophys. J.* **397**, 5

Carlberg, R. G., Pritchet, C. J., and Infante, L.: 1994, *Astrophys. J.* **435**, 540

Carlberg, R. G., Yee, H. K. C., Ellingson, E., Abraham, R., Gravel, P., Morris, S., and Pritchet, C. J.: 1996, *Astrophys. J.* **462**, 32

Carlberg, R. G., Yee, H. K. C., Morris, S. L., Lin, H., Sawicki, M., Wirth, G., Patton, D., Shepherd, C. W., Ellingson, E., Schade, D., Pritchet, C. J., and Hartwick, F. D. A.: 1998, in *Wide Field Surveys in Cosmology, 14th*

IAP meeting held May 26-30, 1998, Paris. Publisher: Editions Frontieres. ISBN: 2-8 6332-241-9, p. 143., pp 143+

Chandrasekhar, S.: 1943, *Astrophys. J.* **97**, 255

Charlton, J. C. and Salpeter, E. E.: 1991, *Astrophys. J.* **375**, 517

Coleman, G. D., Wu, C. C., and Weedman, D. W.: 1980, *Astrophys. J. Supp.* **43**, 393

Colless, M., Ellis, R. S., Broadhurst, T. J., Taylor, K., and Peterson, B. A.: 1993, *M.N.R.A.S.* **261**, 19

Colless, M., Ellis, R. S., Taylor, K., and Hook, R. N.: 1990, *M.N.R.A.S.* **244**, 408

Couch, W. J. and Sharples, R. M.: 1987, *M.N.R.A.S.* **229**, 423

Courteau, S. and van den Bergh, S.: 1999, *Astron. J.* in press

da Costa, L. N., Willmer, C. N. A., Pellegrini, P. S., Chaves, O. L., Rité, C., Maia, M. A. G., Geller, M. J., Latham, D. W., Kurtz, M. J., Huchra, J. P., Ramella, M., Fairall, A. P., Smith, C., and Lípari, S.: 1998, *Astron. J.* **116**, 1

Davis, M. and Peebles, P. J. E.: 1983, *Astrophys. J.* **267**, 465

Dressler, A.: 1980, *Astrophys. J.* **236**, 351

Dressler, A. and Gunn, J. E.: 1983, *Astrophys. J.* **270**, 7

Driver, S. P., Windhorst, R. A., and Griffiths, R. E.: 1995, *Astrophys. J.* **453**, 48

Dubinski, J., Mihos, J. C., and Hernquist, L.: 1999, *Astrophys. J.* submitted

Efron, B.: 1981, *Biometrika* **68**, 589

Efron, B. and Tibshirani, R.: 1986, *Statistical Science* **1**, 54

Ellingson, E. and Yee, H. K. C.: 1994, *Astrophys. J. Supp.* **92**, 33

Ellis, R. S.: 1997, *Annual Review of Astronomy and Astrophysics* **35**, 389

Fèvre, O. L., Abraham, R., Lilly, S. J., Ellis, R. S., Brinchmann, J., Tresse, L., Colless, M., Crampton, D., Galzebrook, K., Hammer, F., and Broadhurst, J.: 1999, *M.N.R.A.S.* submitted

Frei, Z. and Gunn, J. E.: 1994, *Astron. J.* **108**, 1476

Fukugita, M., Shimasaku, K., and Ichikawa, T.: 1995, **107**, 945

Glazebrook, K., Ellis, R., Santiago, B., and Griffiths, R.: 1995, *M.N.R.A.S.* **275**, 19

Griffiths, R. E., Casertano, S., Ratnatunga, K. U., Neuschaeffer, L. W., Ellis, R. S., Gilmore, G. F., Glazebrook, K., Santiago, B., Huchra, J. P., Windhorst, R. A., Pascarelle, S. M., Green, R. F., Illingworth, G. D., Koo, D. C., Bershady, M. A., Forbes, D. A., Phillips, A. C., Green, R. F., and Tyson, J. A.: 1994, *Astrophys. J. Lett.* **435**, 19

Hamilton, D.: 1985, *Astrophys. J.* **297**, 371

Heckman, T. M.: 1983, *Astrophys. J.* **268**, 628

Hibbard, J. E. and van Gorkom, J. H.: 1996, *Astron. J.* **111**, 655

Hickson, P.: 1982, *Astrophys. J.* **255**, 382

Holmberg, E.: 1937, *Lund. Ann.* **6**, 1

Infante, L. and Pritchet, C. J.: 1995, *Astrophys. J.* **439**, 565

Karachentsev, I.: 1972, *Comm. Spec. Ap. Obs., USSR* **8**, 1

Kennicutt, R. C., Keel, W. C., van der Hulst, J. M., Hummel, E., and Roettiger, K. A.: 1987, *Astron. J.* **93**, 1011

King, C. and Ellis, R. S.: Astrophys. J., *1985* **288**, 456

Koo, D. C. and Kron, R. G.: 1992, *Annual Review of Astronomy and Astrophysics* **30**, 613

Larson, R. B. and Tinsley, B. M.: 1978, *Astrophys. J.* **219**, 46

Lilly, S. J., LeFèvre, O. L., Hammer, F., and Crampton, D.: 1996, *Astrophys. J. Lett.* **460**, 1

Lilly, S. J., Tresse, L., Hammer, F., Crampton, D., and LeFèvre, O.: 1995, *Astrophys. J.* **455**, 108

Lin, H., Yee, H. K. C., Carlberg, R. G., and Ellingson, E.: 1997, *Astrophys. J.* **475**, 494

Lin, H., Yee, H. K. C., Carlberg, R. G., Morris, S. L., Sawicki, M., Patton, D. R., Wirth, G. D., and Shepherd, C. W.: 1999, *Astrophys. J.* In Press

Liu, C. T. and Kennicutt, R. C.: 1995, *Astrophys. J.* **450**, 547

Lonsdale, C. J., Hacking, P. B., Conrow, T. P., and Rowan-Robinson, M.: 1990, *Astrophys. J.* **358**, 60

Loveday, J., Maddux, S. J., Efstathiou, G., and Peterson, B. A.: 1995, *Astrophys. J.* **442**, 457

Madau, P., Pozzetti, L., and Dickinson, M.: 1998, *Astrophys. J.* **498**, 106

Marzke, R. O., da Costa, L. N., Pellegrini, P. S., Willmer, C. N. A., and Geller, M. J.: 1998, *Astrophys. J.* **503**, 617

Mihos, J. C.: 1995, *Astrophys. J. Lett.* **438**, 75

Mihos, J. C. and Hernquist, L.: 1994, *Astrophys. J. Lett.* **425**, 13

Mihos, J. C. and Hernquist, L.: 1996, *Astrophys. J.* **464**, 641

Morris, S. L., Carlberg, R. G., Yee, H. K. C., Lin, H., Patton, D. R., Pritchet, C. J., Sawicki, M., Shepherd, C. W., and Wirth, G. D.: 1999, *in preparation*

Morris, S. L., Hutchings, J. B., Carlberg, R. G., Yee, H. K. C., , Ellingson, E., Balogh, M. L., Abraham, R. G., and Smecker-Hane, T. A.: 1998,

Astrophys. J. **507**, 84

Neuschaefer, L. W., Ratnatunga, K. U., Griffiths, R. E., Casertano, S., and Im, M.: 1995, *Astrophys. J.* **453**, 559

Newberry, M. V., Boroson, T. A., and Kirshner, R. P.: 1990, *Astrophys. J.* **350**, 585

Nilson, P.: 1973, *Uppsala General Catalog of Galaxies*, Royal Society of Sciences of Uppsala : Uppsala

Patton, D. R., Pritchet, C. J., Yee, H. K. C., Ellingson, E., and Carlberg, R. G.: 1997, *Astrophys. J.* **475**, 29

Peebles, P. J. E.: 1980, *The Large Scale Structure of the Universe*, Princeton University Press : Princeton

Peletier, R. F., Davies, R. L., Illingworth, G. D., Davis, L. E., and Cawson, M. C.: 1990, *Astron. J.* **100**, 1091

Poggianti, B. M., Smail, I., Dressler, A., Couch, W. J., Barger, A. J., Butcher, H., Ellis, R. S., and Oemler, A.: 1999

Postman, M. and Geller, M. J.: 1984, *Astrophys. J.* **281**, 95

Roberts, M. S. and Haynes, M. P.: 1994, *Annual Review of Astronomy and Astrophysics* **32**, 115

Rocca-Volmerange, B. and Guiderdoni, B.: 1990, *M.N.R.A.S.* **247**, 166

Sanders, D. B. and Mirabel, I. F.: 1996, *Annual Review of Astronomy and Astrophysics* **34**, 749

Schechter, P.: 1976, *Astrophys. J.* **203**, 297

Schweitzer, F.: 1982, *Astrophys. J.* **252**, 455

Sebok, W. L.: 1986, *Astrophys. J. Supp.* **62**, 301

Silk, J. and Wyse, R. F. G.: 1993, *Physics Reports* **231**, 293

Silva, D. R. and Bothun, G. D.: 1995, *American Astronomical Society Meeting.* **187**, 83

Toomre, A.: 1977, *Evolution of Galaxies and Stellar Populations*, New Haven : Yale Obs. (ed. B.M. Tinsley and R.B. Larson)

Toomre, A. and Toomre, J.: 1972, *Astrophys. J.* **179**, 623

Tyson, J. A.: 1988, *Astron. J.* **96**, 1

Vogeley, M. S.: 1993, *Ph.D. thesis*, Harvard University

Williams, R. E., Blacker, B., Dickinson, M., Dixon, W. V., Ferguson, H. C., Fruchter, A. S., Giavalisco, M., Gilliland, R. L., Heyer, I., Katsanis, R., Levay, Z., Lucas, R. A., McElroy, D. B., Petro, L., Postman, M., Adorf, H., and Hook, R.: 1996, *Astron. J.* **112**, 1335

Willmer, C. N. A., da Costa, L. N., and Pellegrini, P. S.: 1998, *Astron. J.* **115**, 869

Windhorst, R. A., Burstein, D., Mathis, D. F., Neuschaefer, L. W., Bertola, F., Buson, L. M., Koo, D. C., Matthews, K., Barthel, P. D., and Chambers, K. C.: 1991, *Astrophys. J.* **380**, 362

Windhorst, R. A., Fomalont, E. B., Kellermann, K. I., Partridge, R. B., Richards, E., Franklin, B. E., Pascarelle, S. M., and Griffiths, R. E.: 1995, *Nature* **375**, 471

Woods, D., Fahlman, G. G., and Richer, H. B.: 1995, *Astrophys. J.* **454**, 32

Xu, C. and Sulentic, J. W.: 1991, *Astrophys. J.* **374**, 407

Yee, H. K. C.: 1991, **103**, 396

Yee, H. K. C., Carlberg, R. G., and Morris, S. L.: 1999, *in preparation*

Yee, H. K. C. and Ellingson, E.: 1995, *Astrophys. J.* **445**, 37

Yee, H. K. C., Ellingson, E., and Carlberg, R. G.: 1996, *Astrophys. J. Supp.*

102, 269

Yee, H. K. C., Sawicki, M. J., Carlberg, R. G., Lin, H., Morris, S. L., Patton, D. R., Wirth, G. D., Shepherd, C. W., Ellingson, E., Schade, D., and Marzke, R.: 1997, *Proceedings of IAU Joint Discussion 11, Redshift Surveys in the 21st Century*

Zabludoff, A. I., Zaritsky, D., Lin, H., Tucker, D., Hashimoto, Y., Shectman, S. A., Oemler, A., and Kirshner, R. P.: 1996, *Astrophys. J.* **466**, 104

Zepf, S. E. and Koo, D. C.: 1989, *Astrophys. J.* **337**, 34

Glossary

AGB: Asymptotic Giant Branch.

AGN: Active Galactic Nuclei.

CDM: Cold Dark Matter.

CF: Correlation Function.

CFHT: Canada-France-Hawaii Telescope.

CNOC: Canadian Network for Observational Cosmology.

CNOC1: The CNOC Cluster Redshift Survey.

CNOC2: The CNOC Field Galaxy Redshift Survey.

D4000: Break strength at 4000Å.

DSS: Digitized Sky Survey.

E/S0: Elliptical (E) or lenticular (S0) morphological classification.

EW: Equivalent width.

FWHM: Full width at half-maximum.

Gunn gr**:** Refers to photometry in the Gunn g (green:5200Å) and r (red:6700Å) filters.

Gyr: Gigayear (10^9 years).

h: Parameterizes the Hubble constant, such that H_0=100h km s^{-1}Mpc^{-1}.

HST: Hubble Space Telescope.

IRAS: Infrared Astronomy Satellite.

kpc: kiloparsec (10^3 parsec).

LF: Luminosity Function.

MOS: The CFHT multi-object spectrograph.

Mpc: Megaparsec (10^6 parsec).

parsec: Distance at which one Astronomical Unit (AU) subtends 1″ on the sky. Equal to 3.26 light years.

PSF: Point Spread Function.

q_0: The cosmological deceleration parameter.

SED: Spectral Energy Distribution.

SedCl: Spectral Energy Distribution Classification.

SSRS2: Second Southern Sky Redshift Survey.

$UBVR_CI_C$: Refers to photometry using Ultraviolet (Johnson U:3650Å), Blue (Johnson B:4400Å), Visual (Johnson V:5500Å), Red (Kron-Cousins R_C:6500Å) and Infrared (Kron-Cousins I_C:8300 Å) filters.

UGC: Uppsala General Catalog of Galaxies.

ULIRG: Ultra-luminous infrared galaxy.

WFPC2: Wide Field Planetary Camera 2 (HST).